Development of a novel experimental methodology for characterizing low and high temperature solid, fuel-based deposits on metallic walls

Louise Ganeau

Thèse de doctorat

NNT : 2021UPAST115

Development of a novel experimental methodology for characterizing low and high temperature solid, fuel-based deposits on metallic walls

Thèse de doctorat de l'Université Paris-Saclay et de l'Université de Duisburg-Essen

École doctorale n° 579
Sciences Mécaniques et Energétiques, Matériaux et Géosciences (SMEMAG)
Spécialité de doctorat : Energétique

Unité de recherche : Mobilité et Systèmes à l'IFP Energies Nouvelles (Rueil-Malmaison, FRANCE)

Thèse présentée et soutenue à l'Université de Duisbourg-Essen le 18 novembre 2021 par

Louise GANEAU

Composition du Jury

Pascale DESGROUX Professeur, Université de Lille (PC2A)	Présidente et Rapporteure
Raul PAYRI Professeur, Université Polytechnique de Valence (CMT)	Rapporteur & Examinateur
Sebastian KAISER Professeur, Université de Duisbourg-Essen (IVG)	Examinateur
Christophe LAUX Professeur, Université de Paris-Saclay (EMC2)	Examinateur
Gilles BRUNEAUX Docteur, HDR, IFP Energies Nouvelles	Co-Directeur de thèse
Christof SCHULZ Professeur, Docteur, Université de Duisbourg-Essen (IVG)	Co-Directeur de thèse

ÉCOLE DOCTORALE
Sciences mécaniques et énergétiques, matériaux et géosciences (SMEMAG)

Titre : Développement d'une nouvelle méthode de caractérisation de dépôts haute et basse température sur parois métalliques

Mots clés : dépôts moteurs, moteur essence, injection directe

Résumé : Dans le cadre de cette thèse, une nouvelle méthode est présentée afin d'étudier la formation des dépôts dans la chambre de combustion des moteurs essences. En effet, le processus de formation des dépôts n'est pas bien compris et il n'y a pas ou peu d'expériences permettant d'étudier in situ. L'objectif de la thèse est donc premièrement de proposer une méthodologie afin de comprendre le processus de formation des dépôts, et deuxièmement de la mettre en application afin d'étudier l'impact de différents facteurs sur la formation des dépôts. Cette méthodologie est basée sur la séparation de deux chemins de formations de dépôt : le chemin de formation par un film liquide et le chemin de formation par les suies.

Une première étude est menée avec des expériences sont réalisées avec des appareils pour générer des dépôts de référence pour chacun des chemins de formation de dépôt. Ces dépôts sont analysés par microscopie électronique et spectroscopie infrarouge et Raman afin de déterminer les propriétés physiques et chimiques des dépôts de référence. A partir de cette caractérisation, les propriétés identifiées pour les dépôts de références sont retrouvées dans les dépôts formés sur des pistons dans une chambre de combustion d'un moteur essence.

La deuxième étude porte sur des essais in situ avec l'utilisation d'une caméra rapide afin de de comprendre les mécanismes de formation des dépôts. De même, elle est basée sur la séparation des chemins de formation des dépôts. L'étude des mécanismes du chemin de formation du film liquide montre que la formation des dépôts est liée à la durée de vie du film liquide sur la surface du piston : en s'évaporant lentement, le film liquide réside longtemps sur la surface et le dépôt peut se former. Pour l'étude des mécanismes du chemin de suie, deux mécanismes de transport sont responsables du dépôt de suies sur la surface : la thermophorèse et la turbulence.

La dernière étude de la thèse porte sur l'impact de la condition de la surface sur la formation des dépôts.

Les conditions étudiées sont la température de la surface, la rugosité et les matériaux transparents. Seule la température de la surface a un impact signifiant sur la quantité de dépôt. Le faible impact des matériaux transparents sur la formation des dépôts pourra rendre possible dans de futures études l'utilisation de diagnostics optiques pour étudier in situ la formation des dépôts.

Maison du doctorat de l'Université Paris-Saclay
2ème étage aile ouest, Ecole normale supérieure Paris-Saclay
4 avenue des Sciences,
91190 Gif sur Yvette, France

ÉCOLE DOCTORALE
Sciences mécaniques et énergétiques, matériaux et géosciences (SMEMAG)

Title : Development of a novel experimental methodology for characterizing low and high temperature solid, fuel-based deposits on metallic walls

Keywords : engine deposits, gasoline engine, direct injection

Abstract : Within the framework of this thesis, a new method is presented to study the formation of deposits in the combustion chamber of gasoline engines. The process of deposit formation is not well under-stood and there are no or few experiments that study the process in situ. The objective of the thesis is therefore first to propose a methodology to understand the process of deposit formation, and second to apply it to study the impact of different factors on the formation of deposits. This methodol-ogy is based on the separation of two deposit formation paths: the liquid-film path and the soot path.

A first study is conducted with devices to generate reference deposits for each of the deposit formation paths. These deposits are analyzed by electron microscopy and infrared and Raman spectroscopy to determine the physical and chemical properties of the reference deposits. Based on this char-acterization, the properties identified for the reference deposits are found in deposits formed piston deposits in a combustion chamber of a gasoline engine.

A second study concerns in situ experiments with the use of a high-speed camera to understand the mechanisms of deposit formation. Similarly, it is based on the separation of deposit formation paths. The study of the mechanisms of the liquid-film path shows that the formation of deposits is linked to the lifetime of the liquid film on the piston surface: By evaporating slowly, the liquid film resides for a long time on the surface and deposits can form. For the study of the mechanisms of the soot path, two transport mechanisms are responsible for the soot deposit on the surface: Thermophoresis and turbulence.

The last study of the thesis deals with the impact of the surface condition on the formation of de-posits. The conditions studied are surface temperature, roughness, and material. Only the surface temperature has a significant impact on the quantity of deposit. The low impact of transparent mate-rials (silica and sapphire vs. aluminum) on the formation of deposits may make it possible in future studies to use optical diagnostics to study the formation of deposits in situ.

Maison du doctorat de l'Université Paris-Saclay
2ème étage aile ouest, Ecole normale supérieure Paris-Saclay
4 avenue des Sciences,
91190 Gif sur Yvette, France

université PARIS-SACLAY
ÉCOLE DOCTORALE
Sciences mécaniques et énergétiques, matériaux et géosciences (SMEMAG)

Titel : Entwicklung einer neuen experimentellen Methodik zur Charakterisierung von festen, brennstoffbasierten Ablagerungen auf metallischen Wänden bei niedrigen und hohen Temperaturen

Schlüsselwörter : Motorablagerungen, Ottomotor, Direkteinspritzung

Zusammenfassung : In dieser Arbeit wird eine neue Methode zur Untersuchung der Bildung von Ablagerungen in der Brennkammer von Benzinmotoren vorgestellt. Der Prozess der Ablagerungsbildung ist bisher nicht gut verstanden und es gibt nur wenige oder gar keine Experimente, mit denen man die Bildung von Ablagerungen in situ studieren kann. Das Ziel der Dissertation ist daher erstens, eine Methodik vor-zuschlagen, um den Prozess der Bildung von Ablagerungen zu verstehen, und zweitens, sie anzu-wenden, um die Auswirkungen verschiedener Faktoren auf die Bildung von Ablagerungen zu unter-suchen. Diese Methodik basiert auf der Trennung von zwei Ablagerungsbildungspfaden: Dem Flüs-sigfilmbildungspfad und dem Rußbildungspfad.
In einer ersten Studie wurden Geräten zur Erzeugung von Referenzablagerungen für jeden der Abla-gerungswege durchgeführt. Diese Ablagerungen werden durch Elektronenmikroskopie sowie Infra-rot- und Raman-Spektroskopie analysiert, um die physikalischen und chemischen Eigenschaften der Referenzablagerungen zu bestimmen. Basierend auf dieser Charakterisierung werden die für die Re-ferenzablagerungen identifizierten Eigenschaften in Ablagerungen zugeordnet, die sich auf Kolben in der Brennkammer eines Benzinmotors gebildet haben.
Eine zweite Studie fokussiert auf In-situ-Versuche mit Hilfe einer Hochgeschwindigkeitskamera, um die Mechanismen der Ablagerungsbildung durch Beobachtung im laufenden Motor zu verstehen. In ähnlicher Weise basiert es auf der Trennung der Ablagerungswege. Die Untersuchung der Mecha-nismen des Weges der Flüssigkeitsfilmbildung zeigt, dass die Ablagerungsbildung mit der Lebens-dauer des Flüssigkeitsfilms auf der Kolbenoberfläche zusammenhängt: Durch langsames Verdamp-fen bleibt der Flüssigkeitsfilm lange Zeit auf der Oberfläche und die Ablagerung kann sich bilden. Für die Untersuchung der Mechanismen des Rußpfades sind zwei Transportmechanismen für die Ablagerung von Ruß auf der Oberfläche verantwortlich: Thermophorese und Turbulenz.
Der letzte Aspekt der Arbeit befasst sich mit dem Einfluss der Oberflächenbeschaffenheit auf die Bildung von Ablagerungen. Die untersuchten Bedingungen sind Oberflächentemperatur, Rauigkeit und transparente Materialien. Nur die Oberflächentemperatur hat einen signifikanten Einfluss auf die Menge der Ablagerung. Der geringe Einfluss transparenter Materialien auf die Ablagerungsbil-dung könnte es in zukünftigen Studien ermöglichen, die Ablagerungsbildung in situ mithilfe opti-scher Diagnostik zu untersuchen.

Maison du doctorat de l'Université Paris-Saclay
2ème étage aile ouest, Ecole normale supérieure Paris-Saclay
4 avenue des Sciences,
91190 Gif sur Yvette, France

Development of a novel experimental methodology for characterizing low and high temperature solid, fuel-based deposits on metallic walls

Der Fakultät für Ingenieurwissenschaften, Abteilung Maschinenbau und Verfahrenstechnik der

Universität Duisburg-Essen

zur Erlangung des akademischen Grades

einer

Doktorin der Ingenieurwissenschaften

Dr.-Ing.

vorgelegte Dissertation

von

Louise Ganeau

Le Mans, FRANCE

Gutachter: Univ.-Prof. Dr. rer. nat. Christof Schulz

Ing., Dr., HdR,Gilles Bruneaux

Tag der Einreichung : 18/11/2021

REMERCIEMENTS

My first thanks go to the members of my thesis jury, Professor Pascal Desgroux, Professor Sebastian Kaiser, Professor Christophe Laux, Professor Raul Payri. I thank them for their interest in my work, and for the expertise they brought to its evaluation.

Le travail présenté dans ce manuscrit a été mené en cotutelle entre l'université de Duisburg-Essen et l'université de Paris-Saclay. Il a été financé et réalisé à l'Institut Français du Pétrole et des Energies Nouvelles.

Je voudrais remercier tout d'abord Christof Schulz, mon directeur de thèse de l'université de Duisburg et Gilles Bruneaux, mon directeur de thèse de l'université de Paris Saclay, pour leurs précieux conseils.

Je souhaiterai par ailleurs remercier Stéphane Henriot et Richard Tilagone pour leur accueil dans la direction Mobilité et Systèmes de l'IFP Energies Nouvelles, et Julian Kashdan dans son département.

Je souhaiterais particulièrement remercier Maira Alves Fortunato et Guillaume Pilla. Je suis très reconnaissante pour leur soutien sans faille pendant ces années de thèse. J'ai beaucoup appris avec eux. Merci Guillaume pour ta grande disponibilité et tes nombreux conseils pendant la rédaction de la thèse.

Je tiens également à remercier tous les techniciens sans qui je n'aurais pas eu ces résultats à présenter : merci à Thomas Collazo, Francis Lenglet, Vincent Ricordeau, pour les beaux dépôts moteurs, merci à Jérôme Chérel pour toute l'organisation des essais, merci à l'équipe de microscopie de Solaize et en particulier, à Hedwige Marmet, Florent Moreau et Anne-Lise Taleb pour leur temps passé à explorer mes dépôts, merci également à Julien Labaume et Pascal Herault pour leurs analyses chimiques.

J'ai une pensée particulière pour mon collègue de bureau, Duy avec qui j'ai passé mes années de thèse. Ce fut toujours un plaisir d'échanger ensemble. J'ai également une pensée pour tous mes autres collègues thésards, Andreas, Edouard, Hassan, Abhijit, Kamal, Julien, Alexis, Mathieu, Antoine, Benoît, Maxime, Fabien ainsi que tous les autres collègues de la direction.

Merci aussi à l'association de football de l'IFP Energies Nouvelles pour son accueil chaleureux dans l'équipe. Merci Clément et Samir pour votre confiance dans mes arbitrages du samedi où j'ai appris la règle obscure du hors-jeu…

Mes derniers remerciements vont à ma famille qui m'a soutenu pendant toutes mes études, et à mes amis qui m'ont encouragé jusqu'au bout. Et enfin je souhaite remercier mon compagnon, Valentin, qui a toujours été là dans les moments difficiles.

CONTENT

SYMBOLS

I	Luminescence intensity
p_{atm}	Atmospheric pressure
Φ	Fuel/air equivalency ratio
Ra	Roughness arithmetic mean
t	Time
$T_{Cooling\ water}$	Engine cooling water temperature
T_{Final}	Final piston surface temperature
$T_{Initial}$	Initial piston surface temperature
T_L	Leidenfrost temperature
T_N	Nukiyama temperature
T_{2min}	Surface temperature of the sapphire piston after 2 minutes
τ	Decay rate of the luminescence intensity

ACRONYMS

CAD	Crank angle degree
CAD BTDC	Crank angle degree before top dead center
CO_2	Carbon dioxide
FTIR-ATR	Fourier transform infrared spectroscopy – attenuated total reflectance
GHG	Greenhouse gas(es)
LPG	Liquid petroleum gas
MIP	Mean indicated pressure
NO_2	Nitrous oxide
NO_x	Nitrogen oxides
PM	Particulate matter
PT	Phosphor thermometry
SEM-EDS	Scanning electron microscopy – energy-dispersive spectroscopy
SI	Spark ignition
TDC	Top dead center
uHC	Unburned hydrocarbons

1 INTRODUCTION

1.1 Motivation

As an example of the actions needed to mitigate the effect of greenhouse gas emissions on global warming, the EU has recently launched ambitious targets to reduce CO_2 emissions by at least 55% by 2030 compared to 1990 [1]. A quarter of Europe's greenhouse gas (GHG) emissions has their origin from the transport sector and, in 2014, the EU has indicated that road transport alone accounts for more than 70% of all GHG emissions of the overall transportation sector [2]. Given this data, the transportation industry is committed to the continued reduction of all possible sources of GHG such as CO_2, NO_X, and N_2O. In this context, automobile manufacturers have developed new engine technologies to reduce fuel consumption, GHG, and pollutants emissions including new engine designs (e.g. downsizing), and new injection strategies (e.g. gasoline direct injection, multi-pilot injections). Despite their advantages, these new technologies have created significant constraints for fuels, namely operating conditions under high pressure and temperature [3–5]. In parallel with the advances in engine technology, the fuels' suppliers have also developed new fuel formulations and introduced a larger variety of biofuels in the market. Biofuels have a chemical composition and physical properties that, while complying with international fuel quality standards, may have chemical and physical differences from conventional fossil fuels [6, 7]. Both trends, new engine technology and new (bio)fuels, have been pointed out as the major source of deposits observed in different parts of the engines such as combustion chamber, injector holes, valves, and pumps [8, 9]. In spark-ignition engines, the deposits observed in the combustion chamber is problematic since it can form an insulating layer on the walls of the combustion chamber [10, 11]. This will increase the temperature locally and lead to unwanted combustion, thus degrading the engine performance. In addition, the deposits can also adsorb unburned hydrocarbons (uHC) and release them during the expansion phase, and so increasing GHG and pollutant emissions [12]. The use of additives antioxidants and/or detergents in fuels are some of the strategies adopted by the industrials to eliminate or, at least, to reduce the deposits formed in combustion chambers. But additives are prone to chemical and thermal degradation in the fuel system, which can make them ineffective or even contribute to deposits formation [13]. Therefore, other solutions must be addressed. For this, it is necessary to understand the mechanisms and the main parameters leading to deposits formation.

Many studies are available on the formation of deposits in the fuel system of vehicles (e.g., tank, fuel lines, injector, and holes) [14–17]. However, the deposits formation process at these locations is not representative of combustion chamber conditions in terms of pressure, temperature, and soot presence. The literature available about deposits in combustion chambers are mainly focused on *ex-situ* deposits analysis and aiming to determine their chemical composition [18]. These *ex-situ* studies have shown that the formation of deposits is a complex process that presents different physical and chemical characteristics depending on the operating conditions such as the injection time [19]. The deposits obtained is formed rather by the contribution of soot, by the contribution of liquid fuel, or rather by the contribution of engine oil [20, 21]. Nonetheless, the parameters that play a role in the mechanisms of deposits formation are still poorly understood, in particular, the synergy that could exist between fuel injection and soot formation on the deposits observed on pistons and combustion chamber walls. Moreover, the formation of deposits in a real engine is a long process. Thus, *ex-situ* chemical characterizations of the deposits require a large sample mass and thus long engine experiments (~100h). These industrial processes of deposits formation in real engines are mostly used to evaluate the properties of fuels to form deposits but are not used to perform fundamental studies on their formation mechanisms. There is no

established experimental methodology to study the mechanisms of deposits formation in the combustion chamber of engine.

1.2 Scope and outline of the work

The objective of this work is to develop such a methodology and use it to provide a better understanding of the deposits formation process. The methodology is based on laboratory controlled reference deposits that reproduce the engine deposits from liquid-film and soot. The impact of engine oil in the formation of deposits is not considered in this work. The data from the physicochemical characterization of these reference deposits allow the identification of the engine parameters promoting the formation of engine deposits related to the liquid-film path or the soot path. This methodology is then applied to the understanding of deposits formation mechanisms throughout the engine cycles for the liquid-film path and the soot path. The work is performed in single-cylinder direct injection research engines with optical access. The characterizations of the deposits is performed using ex-situ analysis such as electronic microscopy and in-situ diagnostics such as direct visualization by a high-speed camera.

The manuscript first presents a review of the literature on the existence of deposits in the combustion chamber of spark-ignition engines (Chapter 2). The experimental means are then described in a third chapter with the presentation of the deposits formation devices and the *ex-situ* and *in-situ* analysis techniques used. Chapter 4 introduces the new methodology for studying engine deposits based on the formation of reference deposits. Chapter 5 describes the *in-situ* investigation of engine deposits formation mechanisms for the liquid-film path and the soot path. From two engine experiments, different possible scenarios of the deposits formation mechanisms are presented. The last chapter (Chapter 6) of this thesis is devoted to the study of the effect of different engine parameters on deposits formation.

2 DEPOSITS IN SPARK IGNITION ENGINES

This chapter aims to present the state of the art in understanding the formation of deposits in the combustion chamber of gasoline engines. The idea is to determine the properties and characteristics of the deposits as well as to identify the relevant analytical techniques to study the mechanisms of deposits formation. There is a lot of research published on deposits in Diesel engines but significantly less on gasoline engines. For this reason, some sections of this chapter are based on Diesel engine cases. First, the location and consequences of deposits formation within the combustion chamber are presented. The objective is to determine, which parts of the combustion chamber are the most critical and will be the focus of this thesis. Second, different existing assumptions of deposits formation mechanisms are explained. Third, the factors leading to the formation of deposits, such as fuel properties, surface temperature, and engine operating parameters, are identified, and fourthly, the chemical and physical properties of the deposits, such as morphology or chemical composition, are identified.

Many additional studies on deposits formation resulted from petrochemistry research, mostly in the context of effects that are relevant during fuel storage, and distribution in tanks and pipes. One important aspect of this thesis is to translate methodological approaches from this community to analyze and interpret in-cylinder deposits.

2.1 Deposits fuel production and handling

Once crude oil is extracted from the rock, it is refined and stored before being distributed to petrol stations. During this storage phase, the refined fuel will start to degrade slowly. This degradation is due to autoxidation reactions that occur in three different stages [22]. Autoxidation designates the degradation of organic compounds at low temperatures (<300 °C) in the presence of oxygen. The first stage of this phenomena is the initiation phase that corresponds to the abstraction of hydrogen atoms from the hydrocarbon compounds and the formation of free radicals. This initiation is sensitive to temperature, the presence of oxygen or impurities in the fuel, the specific fuel composition, especially the presence of unsaturated compounds. The second step called propagation corresponds to the formation of hydroperoxides that then further react towards oxidation products. The last stage is the termination, where free radicals recombine to form stable oxidation products corresponding to deposits. During storage in the distribution system, autoxidation is rather slow because the fuel is stored in a controlled environment. Once the fuel is brought to a vehicle tank, autoxidation reactions are faster because the fuel is subjected to the variable ambient environment. Also, during vehicle operation, fuel flows through the fuel system where pressure and temperature are higher than in the tank, increasing autoxidation reactions and a faster formation of the deposits than for the storage. Figure 1 shows the dependence of jet fuel oxidation to temperature [23]. A similar degradation is observed for any product containing hydrocarbons. It can be seen oxidation increases above 150 °C.

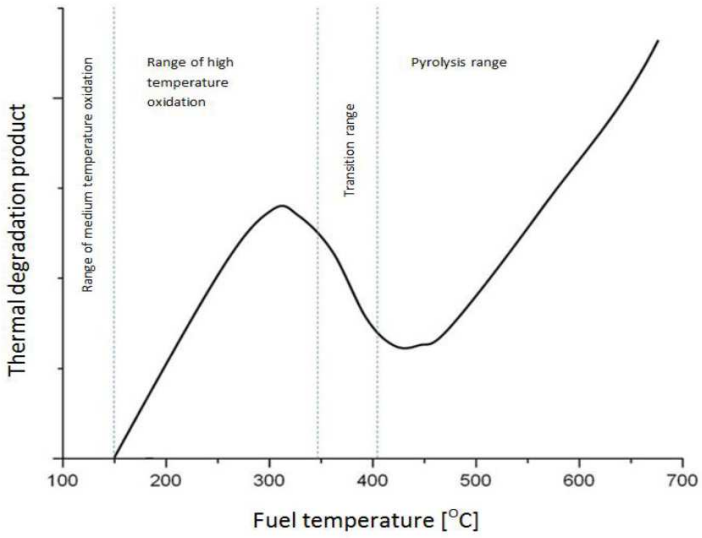

Figure 1: Jet fuel thermal degradation temperature range [23].

Above 400 °C, a different thermal degradation mechanism takes place, which is pyrolysis. In engine applications, this process is more likely to occur in or near the combustion chamber, where the temperature is much higher due to combustion. However, the mechanisms taking place inside the combustion chamber are not clear and are the subject of this thesis. Figure 2 summarizes the various existing interactions from storage to vehicle operation. The deposits resulting from autoxidation can cause different failure events: They can clog the fuel filter, the fuel pump, and the return rail leading to failures of the fuel system.

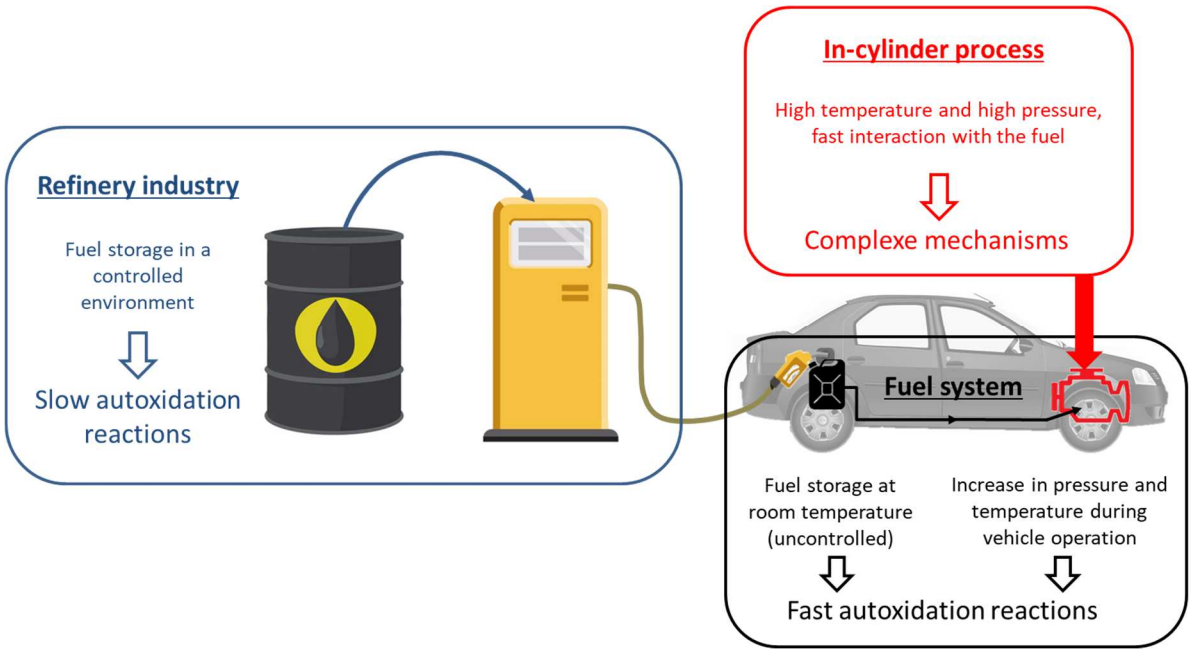

Figure 2: Various interactions between the fuel and its environment, from the refining industry to the operation of the vehicle.

2.2 Location of deposits in the combustion chamber and consequences on the engine operation

2.2.1 Injector nozzle

Deposits can form inside the injection holes and on the nozzle surfaces as shown in Figure 3 [24]. The deposits can clog the injector holes, potentially changing the spray pattern resulting in larger droplets and thus poorer mixture formation [25, 26]. This deterioration of the spray pattern has several consequences on combustion behavior. It can contribute to the formation of rich zones in the fuel/air mixture that promotes knocking or pre-ignition [25]. The inhomogeneous fuel/air mixture can also increase unburned hydrocarbon and CO emissions. By modifying the shape of the spray pattern, the spray angle can be reduced, and the penetration of the spray can be increased, which promotes wetting of the walls and leads to emissions of particulates and hydrocarbons [26].

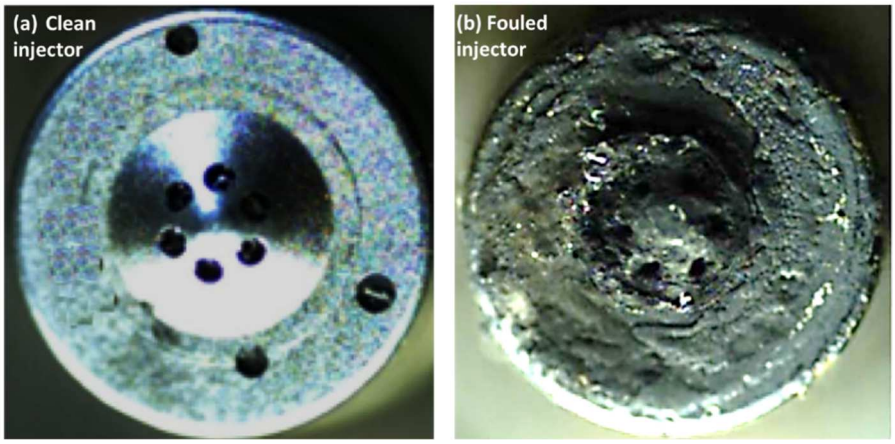

Figure 3: Example of deposit on injector tip from a gasoline engine [24]

A possible mechanism explaining the formation of deposits on the injector nozzle has been proposed by Caprotti et al [27]. This mechanism is described in four steps. First, after the nozzle is closed after the injector has delivered fuel, residual liquid fuel may remain stored in the injection holes. Second, this fuel expands during the expansion stroke and causes a film of liquid fuel to form at the injector nozzle. Third, the high temperature of the nozzle surface induces evaporation of the more volatile fuel components. The heavier fraction of the fuel remains in the nozzle and fuel degradation occurs, resulting in sticky deposits. Fourth, soot, unburned hydrocarbons, and lubricant components accumulate on the surface of the deposit. After each nozzle closure, the process starts again, and the deposit develops on the injector nozzle [28].

2.2.2 Spark plug

Deposits can also form at the spark plug. The deposits that may contain elemental carbon, can act as an electrical conductor and thus change the spark discharge characteristics. The change in spark discharge characteristics can cause degradation of combustion initiation, misfiring, and short circuits [29]. Figure 4 shows an example of a deposit formed on the spark plug in the form of carbon filaments. Spark-plug deposits may form when the engine is started, regardless of the ambient temperature. When the vehicle is operated in a warm or temperate climate, the spark plug reaches a self-cleaning temperature of approximately 400°C where the deposit burns off and is no longer a problem. The formation of deposits on the spark plug is, therefore, more problematic in cold climates with extended warm-up times, which can lead to a build-up of deposits [30]. In this case, one of the solutions to limit ignition failures due to

deposit formation on the spark plug is the application of high voltage to the spark plug when misfiring is detected [29, 31]. To avoid melting the center electrode with the high voltage, automobile manufacturers now use precious metals such as nickel, platinum, or iridium for the center electrode to increase the service life and improve the ignition efficacy of spark plugs [32].

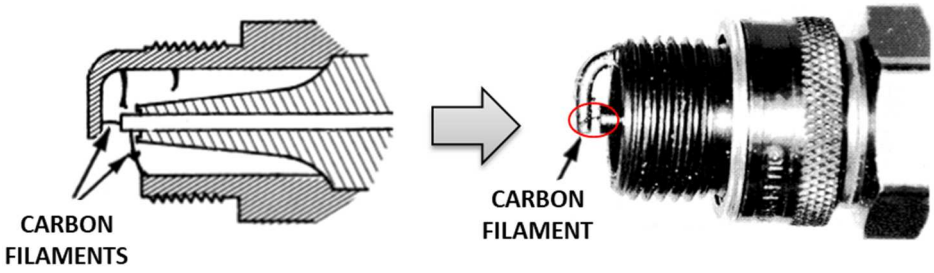

Figure 4: Sketch and photo of a spark plug with fouling caused by carbon filaments [29].

2.2.3 Intake valves

Intake valves can also suffer from deposit formation. Figure 5 compares a clean intake valve to a dirty valve recovered from a spark-ignition gasoline engine with a port fuel injector [33]. Deposits on intake valves mainly affect gasoline engines operating with a port fuel injection system. This is related to the position of the intake valve with the fuel injection system. Fuel can wet the rear side of the intake valve, which contributes to the formation of deposits. Deposits on the intake valves can change the gas flow into the engine, which affects the mixture formation inside the combustion chamber and leads to a reduction in engine power [34]. To remedy these deposits, fuels with detergent additives are generally used [35].

Figure 5: Comparison of a clean intake valve and a fouled intake valve [33].

2.2.4 Combustion chamber walls

Deposits can also form on the combustion chamber wall: The piston top in Figure 6, the cylinder liner and head cylinder in Figure 7 [36]. Because deposits can be porous, they can absorb unburned hydrocarbons and particulate matter and then release them during the expansion stroke contributing to increased emissions of unburned hydrocarbons and particulate matter [12, 37].

40 km/h (50h) 70 km/h (50h) 140 km/h (50h)

Figure 6: Piston deposits formed after 50 h for different operating conditions in a direct-injection spark-ignition engine [36].

Figure 7: Enlarged image of cylinder-head deposits [38].

Figure 8 illustrates the effect of combustion chamber deposits on the increase of unburned hydrocarbon emissions from the exhaust of a four-cylinder spark-ignition engine [39]. These emissions were measured using a rapid-response flame ionization detector at the exhaust valves during the exhaust phase of the combustion cycle. The red and blue curves correspond respectively to the emissions measured with a clean engine and an engine with deposits after 60 hours of engine operation. The comparison only covers the two peaks around 540 and 645°CA. The authors attributed the increase in unburned hydrocarbon emissions to the desorption of fuel in the deposits that were previously absorbed by the deposits. Another consequence related to the formation of deposits on the combustion chamber walls is the reduction of the heat flux through the combustion chamber wall due to the insulating thermal properties of the deposits. This leads to an increase in the temperature of the gases in the chamber and thus to an increase in NO_x emissions [28].

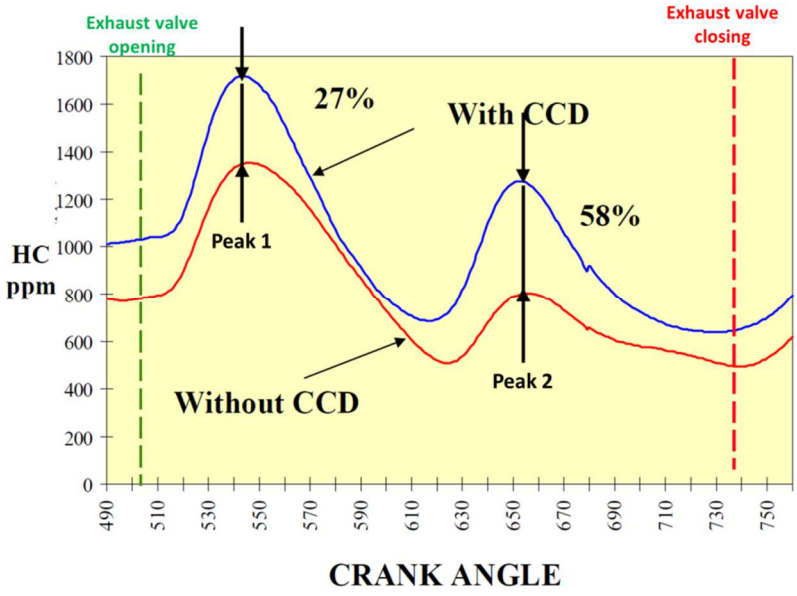

Figure 8: Comparison of unburned hydrocarbon emissions with and without combustion chamber deposits (CCD) [39].

The thermal properties of deposits on combustion chamber walls can also lead to surface ignition [10, 11, 40]. Surface ignition corresponds to auto-ignition of a fuel/air charge due to hot spots, here caused by the high temperature of the deposit layer. This effect leads to an increase in the required octane number [41]. Hosogi et al. have studied the effect of carbon deposition on knocking by implementing a method that enabled the generation of deposits with controlled thickness. A deposit with a thickness of about 150 µm was formed on the walls of the combustion chamber using an oil drip device mounted on the intake manifold of a gasoline engine. The authors were able to attribute low-speed pre-ignition phenomena (LSPI) to the presence of deposits in a small super-charged gasoline engine. The mechanism involved in LSPI by deposition is as follows: The deposits that are formed in the combustion process can lift off and wander within the combustion chamber. During combustion, the temperature rises, and the deposit begins to oxidize. If the deposits are not fully oxidized, they may remain incandescent until the next cycle (Figure 9) and then ignite the mixture [42].

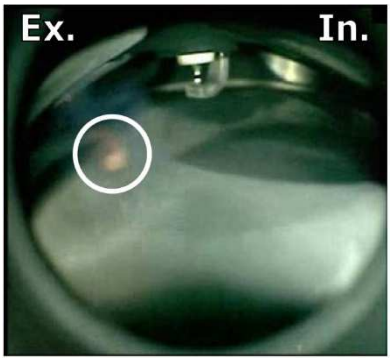

Figure 9: In-cylinder visualization of incandescent deposits leading to local ignition [42].

2.2.5 Conclusions on the location and consequences of engine deposits

The main consequence of in-cylinder deposits are combustion degradation. It can affect the fuel/air mixture by altering the pattern of the injector nozzle holes and by disrupting the airflow during intake due to deposits on the intake valves. Its thermal properties can also create hot zones leading to auto-

ignition. Deposits can also cause ignition failures by altering the spark characteristics. All these consequences on combustion can damage the engine, increase fuel consumption, and pollutant emission. Therefore, it is important to understand how deposits form to avoid or limit their formation.

2.3 Deposits formation hypotheses

2.3.1 Deposits mechanisms

The mechanisms of deposits formation in gasoline engines are poorly documented. There are two main mechanisms of deposist formation described in literature.

In 1993, Lepperhoff and Houben proposed a two-phase deposits formation mechanism [25]. The first phase is the induction phase that corresponds to the formation of a liquid fuel film due to the condensation of high-boiling hydrocarbons on the combustion chamber walls. Soot particles formed during combustion can then be trapped in this thin layer. The liquid film and the trapped particles constitute the first layer in contact with the walls of the combustion chamber. The second phase, called the growth phase, corresponds to the development of deposits formed by the aggregation of particles and the condensation of the fuel. During these two phases, additional chemical reactions take place in the deposits, such as pyrolysis or polymerization due to the high temperature of the combustion chamber walls and the long residence time of the deposits.

Daly et al. proposed a five-step mechanism involving the formation of two deposition zones as shown in Figure 10 [43]. The first step is the initiation of deposits formation corresponding to the condensation of oil and fuel on the walls of the combustion chamber forming a liquid film. The second step corresponds to reactions between the molecules inside the liquid film leading to the formation of a lacquer-like deposit. These reactions lead to condensation reactions of the oxidation products and addition/substitution reactions lead to the polymerization of the heaviest (mostly the aromatic) fuel compounds [44]. The third step is the thermal degradation of the surface of the deposits due to combustion. These 3 steps describe the formation of the Zone 2 deposits in Figure 10. The fourth step corresponds to the initiation of zone 1 deposits, which repeats the previous steps and corresponds to the growth of the deposits. The fifth step is the steady-state phase of the deposit, which reaches a limiting thickness due to the opposition of the formation and removal mechanisms.

The observation of a limiting thickness of the deposits has been documented in the literature [19, 43, 45]. Lepperhoff and Houben propose three different mechanisms leading to the removal of deposits [20]. The first mechanism leading to the removal of the deposits is physical. It is the evaporation and desorption of volatile components present on the surface of the deposits when the temperature rises or the mechanical washing of the deposits by the liquid fuel. The second mechanism, described as mechanical by the authors, corresponds to the abrasion of the deposits by aerodynamic forces. It also corresponds to the rupture of the deposits by shear forces induced by temperature differences in the deposits. The third mechanism of deposits removal is chemical. In this case, hot gases or hot walls of the combustion chamber under an oxygen-rich atmosphere contribute to oxidizing the soot and hydrocarbons contained in the deposits at 200 and 500 °C, respectively.

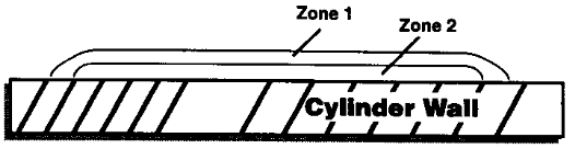

Figure 10: Proposed mechanism for combustion chamber deposits formation [43].

The previous mechanisms consist of a temporal description of the deposits formation process. Two important factors in the formation of the deposits were identified: the formation of a liquid film due to the condensation of the fuel and the deposition of soot on the walls of the combustion chamber. Here, these processes are presented by splitting the mechanisms of deposits formation into two distinct pathways: the liquid-film pathway and the soot pathway.

2.3.2 Liquid-film-path mechanism

As described above, the liquid-film-path mechanism has two main steps: The formation of a liquid film on the combustion chamber wall and its thermal degradation leading to a solid deposit. The first step is important because it initiates the formation of the deposit. The liquid film can form in two different ways: First, the liquid film can be formed simply by the condensation of the heaviest fuel components [46]. Second, spray impact on the combustion chamber wall (usually the liner or piston) can lead to the formation of liquid films. Its formation rate and its lifetime depends on several parameters such as injection pressure, injection phase, duration, and wall temperature [47]. During the last step, thermal degradation and reactions lead to the formation of a solid deposit.

2.3.3 Soot-path mechanism

The soot-path mechanism corresponds to the deposition of soot on the combustion chamber wall. Several authors in literature focused their work on the wall deposition of small particles in an engine. Thus, thermophoresis was identified as a phenomena possibly leading to soot deposition [48–50]. Thermophoresis is a transport mechanism that occurs in a temperature gradient [51]. In the warm regions, the particles are subject to collisions more frequently than in the cold regions. The disparity in momentum induces a thermophoresis force that causes the particles to move towards the cold surface (Figure 11).

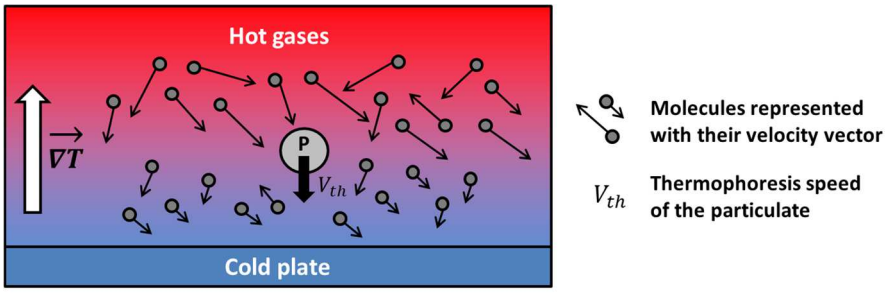

Figure 11: Particle P subjected to thermophoretic forces directed against the temperature gradient.

Inertial deposition explains the deposition of particles from gas stream. Close to walls, the gas can undergo acceleration that change the direction of the flow. Depending on the shape and diameter of the particles, their velocity may be different from that of the gas. This critical velocity is called exhaust velocity and may cause the particle not to follow the new direction of the gas flow. Two cases are depending on the type of flow. On one hand, in a laminar flow, the formation of an exhaust velocity

may be due to the presence of an obstacle or the deflection of the flow line, such as a curved pipe for example. On the other hand, in case of turbulence, the particles will follow the turbulent vortices, and depending on the particles characteristics (size, weight), they can be ejected from the vortices [52]. In both cases, the presence of a solid surface in front of the flow can lead to a deposition if the inertia of the particles is important, as shown in Figure 12 (case 1: impact). Two other mechanisms are shown in Figure 12 also exist. These are diffusion (case 2), which occurs when the mass of the particles is very low, and Brownian motion controls the trajectory of the particles [53]. As a result, the particles move randomly and may encounter an obstacle and settle on it. The second case is sedimentation, which is the result of the action of the force of gravity on heavy particles.

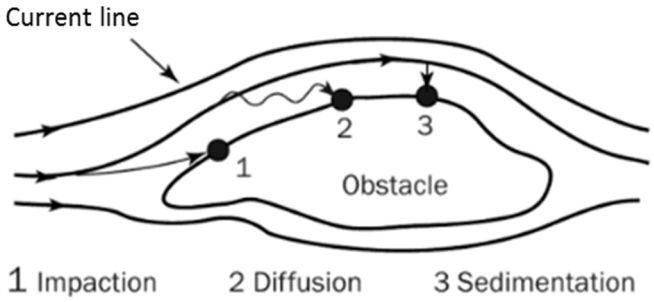

Figure 12: Schematics of the formation of deposits for a laminar flow in presence of an obstacle [52].

2.4 Factors leading to deposits formation

2.4.1 Fuel and additives and components in gasoline

Aromatic fuel compounds strongly contribute to deposits formation [54, 55]. It has been shown that increasing the number of alkyl substituents in aromatics promotes deposits formation in the combustion chamber [19, 56]. Cheng measured an increase in the mass of the deposits formed on the cylinder as the length of the alkyl chains attached to the benzene ring of the fuel increased [19]. The author attributed this increase to the high boiling point of long-chain alkyl substituted aromatics. In the same study, Cheng investigated the effect of increased alkyl chain locations on the benzene ring and showed that there is also a correlation between the boiling point of the molecules and the mass of the deposits formed. According to the work of Uehara et al., the high-boiling compounds do not evaporate in the combustion chamber and form a liquid film layer on the wall leading to deposits formation [56].

Olefins can act as boosters for deposits formation [55, 56]. Due to their low thermal stability they can contribute to deposits formation at low temperature by autoxidation and at high temperature by pyrolysis.

Oxygenates: The removal of additives such as lead from gasoline has led to the use of oxygenated compounds to increase the octane number. Compounds such as ethanol, methyl tert-butyl ether (MTBE), ethyl tert-butyl ether (ETBE), or tert-amyl methyl ether (TAME) are now used. Experiments have been carried out to determine the effect of oxygenated compounds on the formation of deposits in injectors. Ashida et al. experimented the effect of various fuels with oxygenates such as MTBE and ethanol on

the loss of injector fuel flow attributed to deposits formation. They found that their effect was not significant because mixtures of MTBE (fuel 9) and ethanol (fuel 10) had little deposition compared to fuel 2, which contained no oxygenates but alkylates (Figure 13)[1] [54].

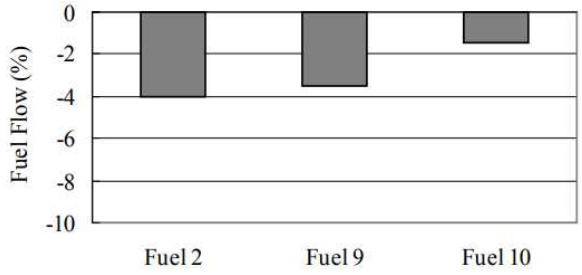

Figure 13: Effect of oxygenated compound in fuel flow of injector nozzle [54].

Studies have shown that increasing the concentration of ethanol in gasoline results in reduced deposits on the injector nozzle [10, 57, 58]. Figure 14 illustrates this effect where different photos of the spray pattern, injector nozzle, and nozzle holes were taken after a 10-hour direct injection experiment for different ethanol content in gasoline [57]. Without ethanol (E0), deposits appear to cover almost the entire nozzle hole. As the concentration of ethanol increases, the presence of deposits decreases. There are almost no deposits with 100 % ethanol (E100). The authors attribute this effect to lower sulfur and aromatic content as the fuel contains more ethanol.

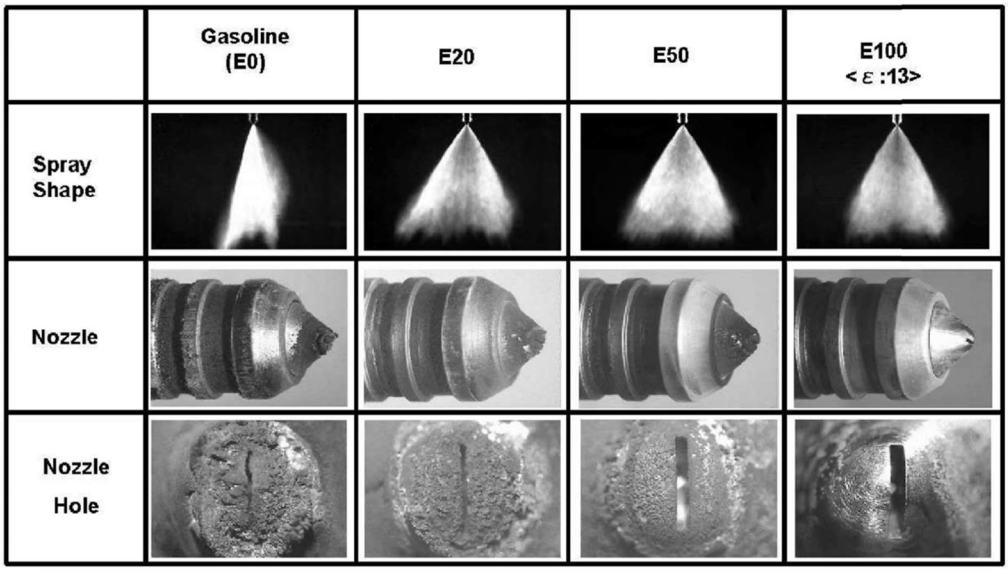

Figure 14: Comparison of spray shapes, nozzles, and nozzle holes after a 10-h durability experiment using various ethanol blends [57].

Octane boosters: Fuel additives can also lead to the formation of deposits. Nagano et al. investigated the effect of three additives on deposits formation: 4-tert-butyltoluene (TBT), n-methyl-aniline (NMA), and 2-methyl-1,5-pentanediamine (MPD) [13]. Their role is to increase the octane number of the fuel. To study the trend of these additives to contribute to deposits formation, experiments were carried out in a spark-ignition engine. The results show that the deposits layer formed from TBT and NMA mixtures is four times thicker than the deposits formed from the base fuel. Figure 15 shows that the deposits are

[1] Alkylate: Substance with additional alkyl groups

visually darker when additives are used, especially with the MPD mixture, which has a black deposit covering the entire surface. The engine experiment with this MPD mixture had to be stopped because it caused the piston rings to stick together in a very short time. The author hypothesized that polar substances due to the presence of amino groups in the additives led to increased deposits formation. It is also important to note that all three additives have high boiling points: this was also observed in Cheng's work on the negative effects of high-boiling substances on deposits [19].

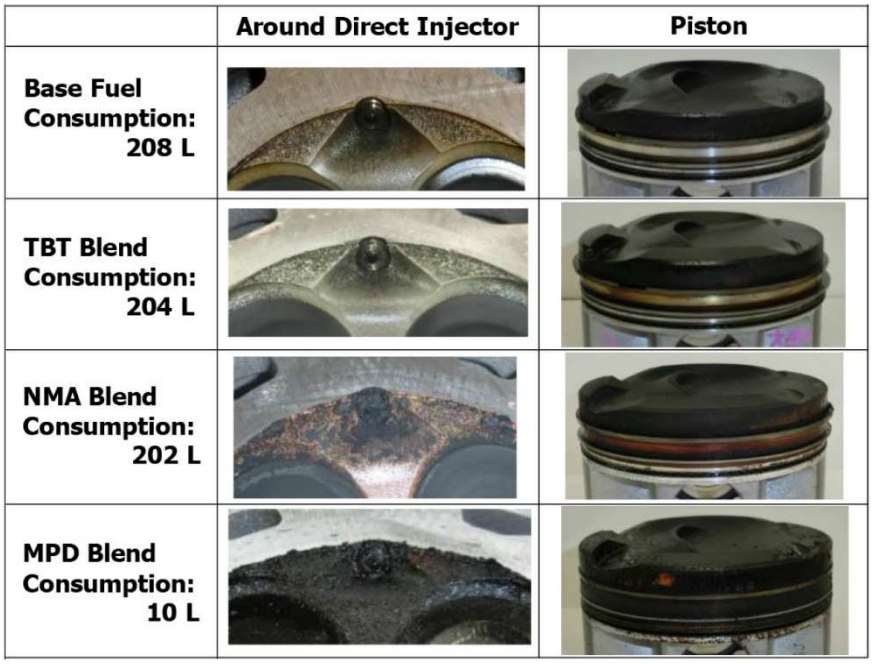

Figure 15: Comparison of deposits at the injector and on the piston for various octane-boosting additives [13].

Detergents: Some detergents can prevent or limit the formation of deposits but can also contribute to their formation if incorrectly dosed [54, 56, 59]. Polyisobutylene amine (PIBA) prevents the formation of deposits in the injector, but its dosage should be limited as it may contribute to the formation of deposits in the combustion chamber [54]. The work of Ramadhas et al. shows the impact of detergents on deposits in the combustion chamber [56]. In engine experiments, they found that the minimum deposits mass was obtained with fuel without additives compared to fuel with detergents. According to the authors, these detergents are sensitive to high temperatures in the combustion chamber and decompose, contributing to fuel degradation and deposits formation.

2.4.2 Fuel and additives and components in Diesel fuel

Fatty acid methyl esters (FAME) are derived from the transesterification of fatty acids from vegetable oil and are used as a bio-Diesel fuel. FAME can oxidize due to various factors and can lead to the formation of deposits in the fuel system. Their role in the formation of deposits in the combustion chamber has not yet been shown. However, studies have shown a greater presence of deposits at the nose of the injector when using biodiesel. Autoxidation is supported by the presence of unsaturated bonds, their location, the presence of metals or other trace elements that could act as oxidation initiators [60], temperature, dissolved oxygen in the liquid fuel [8], soak time, and evaporation temperature [61, 62]. Several authors have pointed out that FAME films in the fuel system have a longer lifetime, resulting in a stronger coking effect [8, 63–65]. FAME may also contain impurities such as metals or glyceride generated during refining and lead to the formation of deposits [61]. Biodiesel fuels are also more sensitive to oxidation stability and may form sediments when fuel aging products polymerize [61, 66].

2.4.3 Fuel impurities

Metals and insoluble salts: Research has shown that zinc contributes to the formation of deposits on injector nozzles, but the mechanism involved is unknown [67–70]. It is present in additives to improve lubrication such as anti-wear, corrosion inhibition, and anti-oxidation. Figure 16 illustrates the effect of zinc on the formation of deposits on the injector nozzle [71]. Three levels of zinc were experimented with a diesel engine operating at full load at 1200 rpm for 6 h. The higher the zinc content, the greater the loss of fuel flow. The loss of fuel flow is due to the formation of deposits that block the holes in the injector nozzle. The presence of zinc in lubricating oil also contributes to the formation of deposits in the combustion chamber [72].

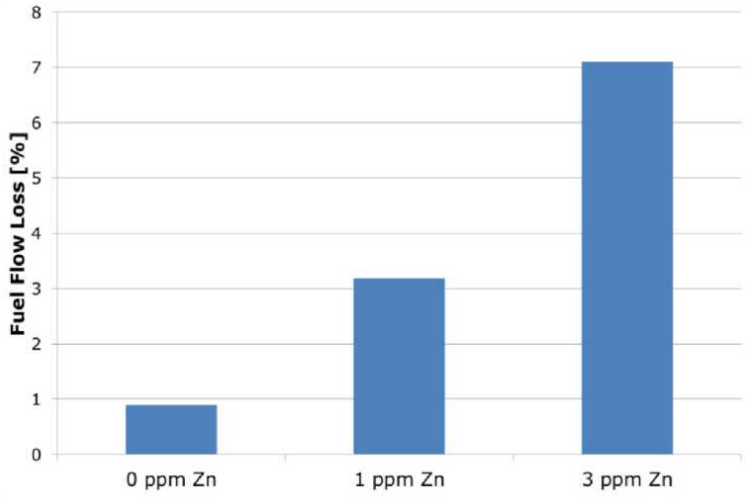

Figure 16: Effect of zinc concentration on injector deposits formation in a base fuel with 10% rapeseed methyl ester (B10) [71].

Other elements, such as copper, calcium, or iron also accelerate the formation of deposits on the injector nozzle [71]. Metallic elements from lubricants, additives, or fuel impurities such as Fe, Ca, Mg, Na, and K and insoluble salts have been found in the composition of injector deposits, but the mechanisms involved in the formation of deposits are not well identified [55].

Sulphur: Several studies have been conducted to understand the impact of sulfur on deposition formation [54]. At low sulfur concentrations (<310 ppm), there is no consensus on its impact on injector deposits, whereas at high sulfur concentrations (>500 ppm) there is an agreement that sulfur increases the formation of deposits [55].

2.4.4 Lubricant oil

Studies determining the composition of the deposits formed in the piston grooves of a Diesel engine show that the deposits originate from the thermal degradation of the lubricant. They found that temperature and metals in the oil influence oil degradation [73]. Calcium present in lubricating oil has also been found in the deposits and is therefore assumed to be involved in the process of deposits formation [74].

2.4.5 Surface temperature

The temperature of the combustion chamber wall surface is an important factor in the formation of deposits. The work of Nakic et al. has established a relationship between the amount of deposits formed

on the cylinder surface and its temperature. They raised the surface temperature of the piston (using a ceramic wafer) and observed that the thickness of the deposits decreased. (Figure 17) [75]. They also noticed that the morphology and composition of the deposits strongly depends on the temperature.

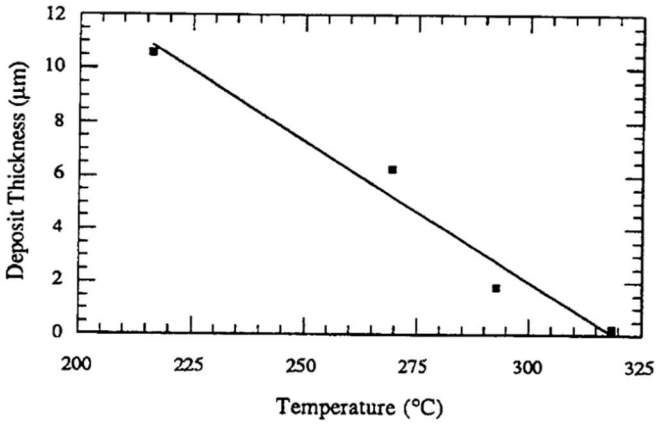

Figure 17: Dependence of the average deposits thickness on the piston temperature [75].

Cheng's work has also shown the effect of surface temperature on the mass of deposits formed on four sampling probes using a dedicated petrol engine (Figure 19a) [19]. To study the effect of surface temperature he made the temperature of the coolant from 20 to 95 °C. After each experiment, he weighed the deposits formed on the sample probes. He found that the weight of the deposits decreased with the temperature of the coolant (Figure 19b). Assuming that the coolant only affects the wall surface temperature, they concluded that a higher surface temperature reduces deposits formation by limiting the formation of liquid films through condensation.

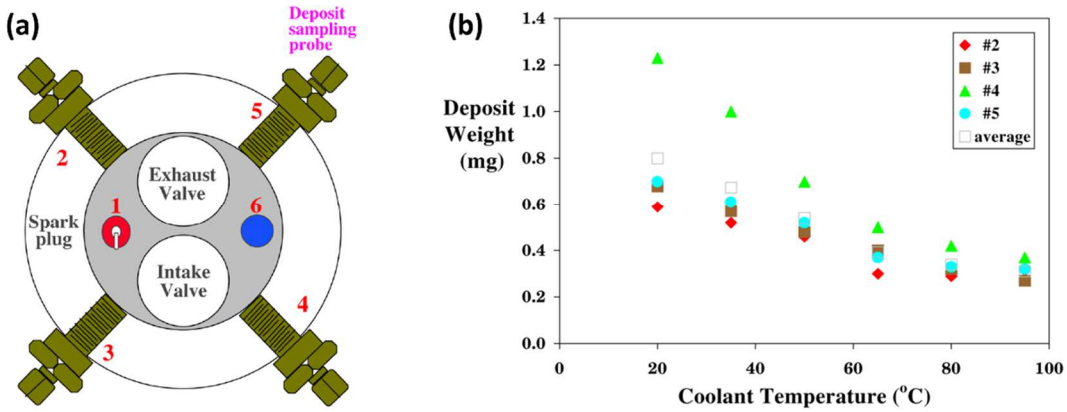

Figure 18: (a) Schematics of an engine insert for holding the sampling probes. (b) Effect of the cooling water temperature on the weight of the deposits at four sampling locations [19].

To study the effect of surface temperature on deposits formation in a non-combustion environment, Furuhata et al. set up an experiment to investigate the deposits-forming processes of a liquid fuel on a hot plate [76]. They observed that the amount of mass deposition decreases with increasing temperature (Figure 19). The authors showed that there is a strong correlation between the amount of deposits formed and the amount of liquid fuel evaporated from the plate. They also studied the effect of plate roughness on the deposits and found fewer deposits formed on a smooth plate. This result shows that surface conditions can have an impact on the formation of deposits.

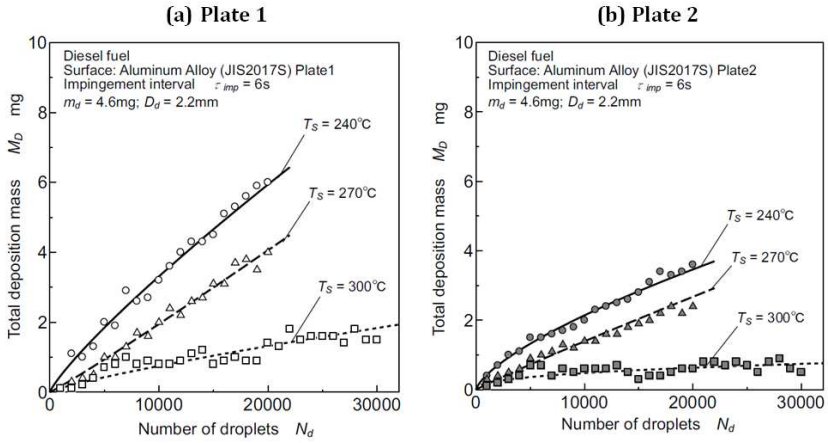

Figure 19: Diesel fuel deposits formed on heated aluminum alloy plates. (a) Rough plate (b) smooth plate [76].

Arifin's thesis work also focused on the effect of surface temperature on a liquid fuel film using a hot plate [64]. To clarify the observations of Furuhata et al., he found that the formation of deposits is minimal when the plate is close to the temperature corresponding to the shortest fuel evaporation time. According to Furuhata et al., in the combustion chamber of an engine, the deposits formed from a fuel film also undergoes significant carbonization due to the high flame temperature. The deposits can also oxidize and thus decrease in thickness.

2.4.6 Influence of engine operating conditions

The fuel/air equivalency ratio ϕ has a significant effect on combustion chamber deposits. Cheng studied the effect of ϕ on combustion chamber deposits in a single-cylinder spark-ignition engine [19]. He recovered and weighed at the end of each 2-h experiment the deposits formed on the four probes samples positioned in the cylinder. The minimum mass of deposits was obtained for ϕ = 1.1 while it increases when ϕ was greater or less than 1.1 (Figure 20). For rich mixtures, he observed that the deposits are mainly black in color and mainly consisted of carbon. He assumed that deposits formed under fuel-rich conditions are related to the formation of soot. For fuel-lean mixtures, the mechanism is not well identified. Cheng supposes that low gas temperatures and the oxygen concentration have an impact on the formation of the deposits. The work of Noma et al. also underlined that the minimum mass of deposits is obtained under stoichiometric conditions [36].

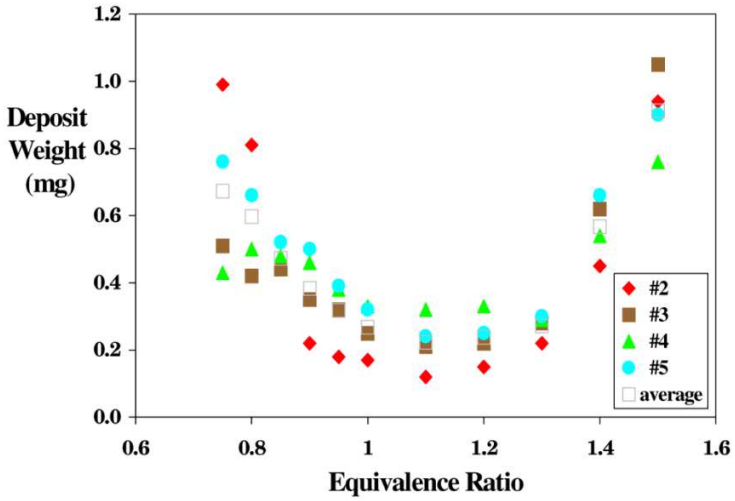

Figure 20: Effect of the fuel/air equivalent ratio ϕ on deposits formation at four sampling locations [19].

Spark advance: Cheng studied the influence of spark advance on the mass of deposits formed in a research gasoline engine (Figure 21) [19]. He placed four sampling probes at different locations in the cylinder and measured the deposits mass formed after each experiment (Figure 18a). He found that the spark advance had a limited impact on the mass of the deposits formed. However, he observes an effect of the location of the sampling probes on the mass of the deposits formed. The maximum deposits mass was obtained for sampling probes located near the exhaust and the minimum deposits mass was obtained for sampling probes located near the ignition zone. The authors assume that it is the gas phase that is involved in the formation of the deposits by influencing the condensation of liquid fuel: Probes located near the ignition zone are subject to high gas temperatures that will limit fuel condensation on the wall; probes located on the exhaust side are exposed to lower surface temperatures and therefore to a higher risk of fuel condensation.

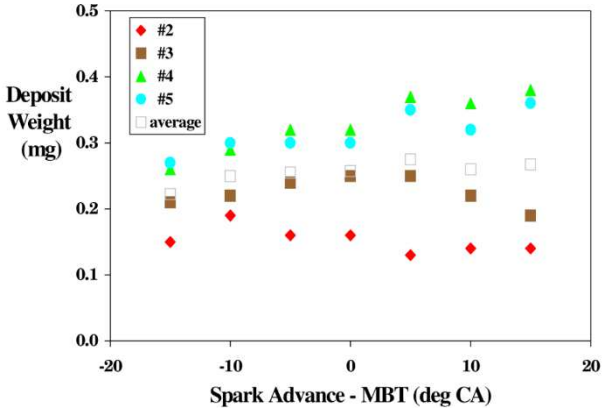

Figure 21: Effect of spark advance on deposits formation at four sampling sites [19].

Engine load: Cheng also studied the effect of manifold pressure using the same sampling method [19]. By increasing the inlet pressure by 0.4 and 0.65 bar the mass of the deposits decreases (Figure 22). When the manifold pressure reaches 0.65 bar, the weight of the deposits increases. He does not explain these observations.

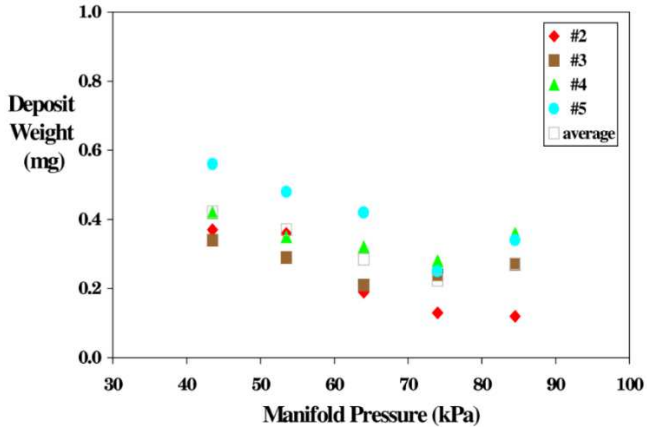

Figure 22: Effect of manifold pressure on deposits formation at four sampling sites [19].

The engine load also has an impact on the formation of deposits in the combustion chamber [19, 77]. Oh et al. conducted experiments with a gasoline engine for 75 h at different loads. They alternated high and low engine loads at different frequencies. As the engine load increases, the mass of deposits decreases relative to low engine load conditions (Figure 23). Their interpretation of these results is that the temperature is higher with high load and leads to thermal decomposition of the deposits.

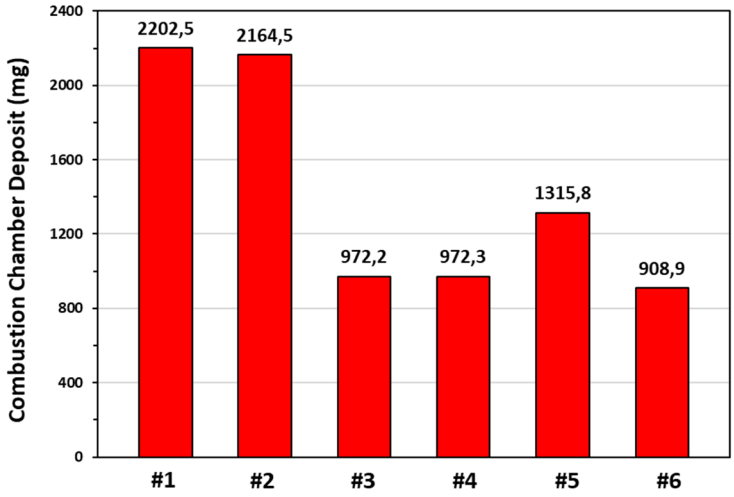

Figure 23: Mass of combustion chamber deposits (piston top and cylinder head) for various engine load conditions [77].

Exhaust gas recirculation (EGR) is a strategy of redirecting part of the exhaust gases to the intake manifold. It reduces NO_x emissions by diluting the fresh gas, thereby reducing the combustion temperature. This strategy is commonly used for diesel engines and is beginning to be studied for spark-ignition engines. Singh et al. investigated the influence of EGR on deposits formation in an air-cooled, direct-injection, two-cylinder Diesel engine [78]. Figure 24 compares photos of the piston and cylinder head surfaces 25 % EGR and without EGR operation. The difference is noticeable, there is a black layer covering the entire piston surface in the case with 25 % EGR as opposed to the case without EGR. EGR, therefore, contributes to the formation of deposits by increasing the amount of soot settling on the walls of the combustion chamber. Due to the dilution of the fresh gas by the exhaust gas, the temperature inside the combustion chamber decreases. This decrease in temperature reduces the oxidation of the soot and thus increases the amount of soot deposited on the walls of the combustion chamber.

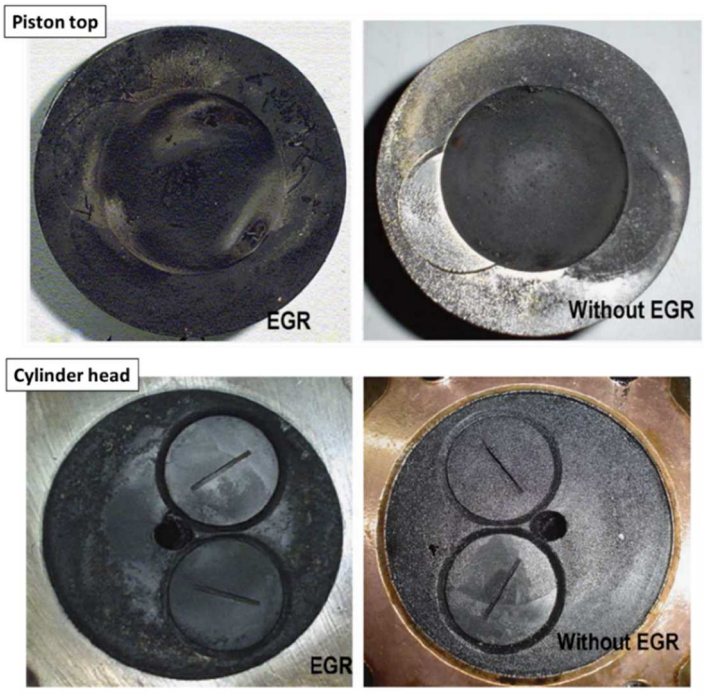

Figure 24: Soot deposit on the piston (top) and the cylinder head (bottom) after 96 h of engine operation with and without EGR operation [78].

2.5 Deposits properties

The main objectives of this section are to identify the properties of the deposits as a function of their location in the combustion chamber and engine operating parameters. Another objective is to identify the techniques used to characterize the deposits properties. The most interesting techniques for thesis work are discussed in the conclusion of this section.

2.5.1 Deposits structure

2.5.1.1 Macroscopic structure

The first interesting feature of the deposits is that they can have a different color according to different parameters [19]. For example, Cheng observed that when the fuel/air equivalence ratio is higher than 1.3, the deposits have a black color (Figure 25). Below this value, the deposits are yellow or brown. According to the same study, the cooling temperature also influences the color: The deposits are black for a temperature below 50°C and above 50°C, the deposit tends more towards brown. Cheng also noted a change in color depending on the manifold pressure. The deposits turn brown to black as the manifold pressure increases from 43.5 to 84.5 kPa. This interesting property may indicate a particular formation process that will lead to a black or lighter color. These engine parameters are not the only ones that influence the color of the deposits, additives can also change the color of the deposits [38, 79]. Figure 26 shows the deposits formed on a cylinder head of a spark ignition direct injection engine running on two different fuels. The presence of additives changes the color of the deposits, which have white areas.

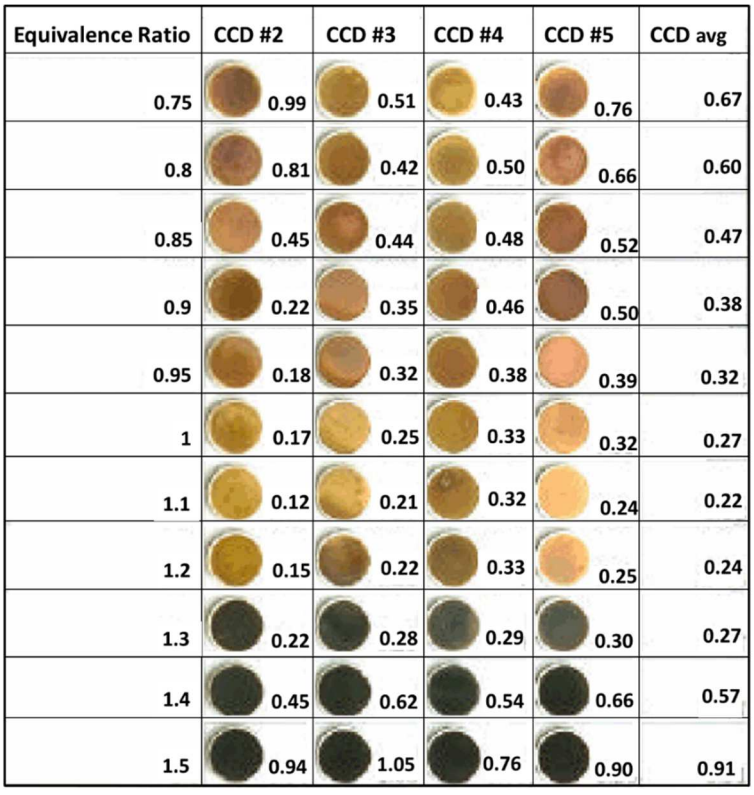

Figure 25: Samples from different locations in the cylinder for different fuel/air ratios [19].

Different surface conditions of the deposits were observed. They can have a shiny appearance when the combustion chamber wall temperature is low [19]. This appearance is attributed to a liquid state of the

deposits due to the slow evaporation of the liquid fuel. Diaby et al. also observed an oily appearance of the deposit attributed to a high volatile organic content composition [21]. Conversely, they observed dry-looking deposits corresponding to a low volatile organic matter content. The deposits may have cracks resulting from exposure to high temperatures, as shown in Figure 26b. The deposits may also be subject to spalling, as shown in Figure 27 [80]. The authors attributed the spalling to increased valve leakage ratings and engine starting problems.

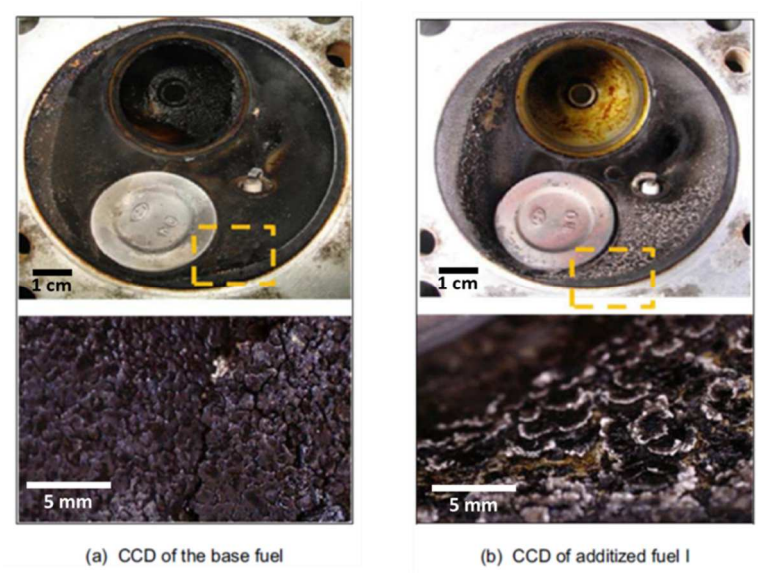

Figure 26: Enlarged image of cylinder-head deposits after operation with base fuel and additive-containing fuel [38].

Figure 27: Piston with deposits flaking [80].

2.5.1.2 Microscopic structure

There are few studies that determine the deposits morphology and those existing focus mainly on injector nozzle deposits. However, these studies have revealed several types of morphologies depending on the engine operating parameters. This section classifies these morphologies into three categories: liquid and sooty, which have already been defined by Cheng, and smooth [19].

Liquid-like appearance: The liquid-like appearance corresponds to the observation of a spherical structure that can turn into a droplet when the cooling temperature decreases [19]. This morphology seems to also depend on the fuel composition as it appears when detergent additives are used.

Soot-like appearance: The deposits may have a soot-like morphology corresponding to the observation of a black deposit [19]. This morphology appears for a rich mixture when a lot of soot is formed. This is confirmed by the observation of aggregates of spherical particles typical of soot on injector nozzles (Figure 28) [12, 81, 82]. Another hypothesis put forward is that the spherical deposits are formed in the liquid phase, then deposited on the tip and finally aggregated into a dense cluster [19, 61, 82].

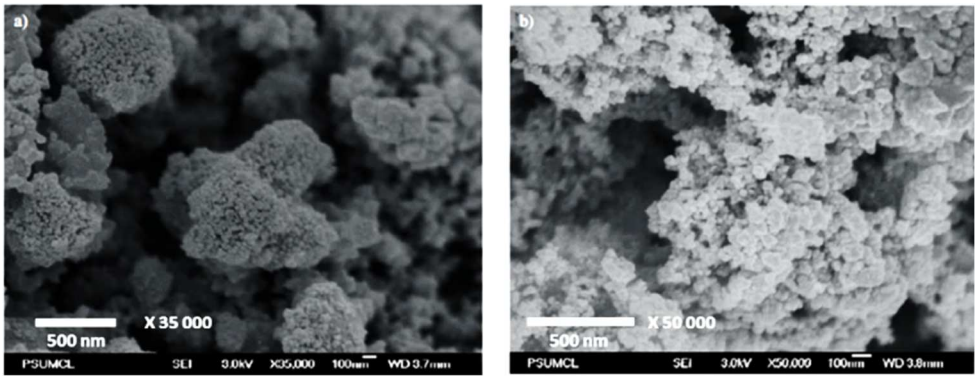

Figure 28: Field-emission scanning electron microscopy (FESEM) of deposits formed on a high-pressure injector nozzle [82].

Smooth appearance: Esaki observed a flat deposits morphology formed on the inlet valve [83]. Rounthwaite also described a smooth, flat layer morphology observed on deposits formed inside a diesel injector nozzle hole [84]. Figure 29 is an electron micrograph of the deposits formed on the first ring of a piston [21]. The deposits have a flat surface with some cracks. This morphology is attributed to the mechanical polishing of the moving ring.

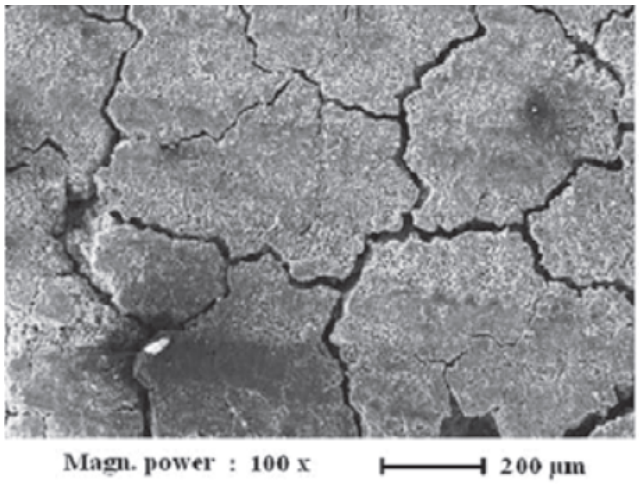

Figure 29: Microscopic image of the first ring deposits [21].

To determine the structure of the deposits, Nagano carried out a transverse observation of the deposits formed on a piston [13]. Different layers are observed on the deposits by scanning electron microscopy (SEM, Figure 30a). This observation supports the theory of layer deposition formation developed by Lepperhoff and Daly. Elemental analysis by Electron Dispersive X-ray Spectroscopy (EDX) (Figure 30b) of the same study shows that the deposits originates from oil, fuel, and soot.

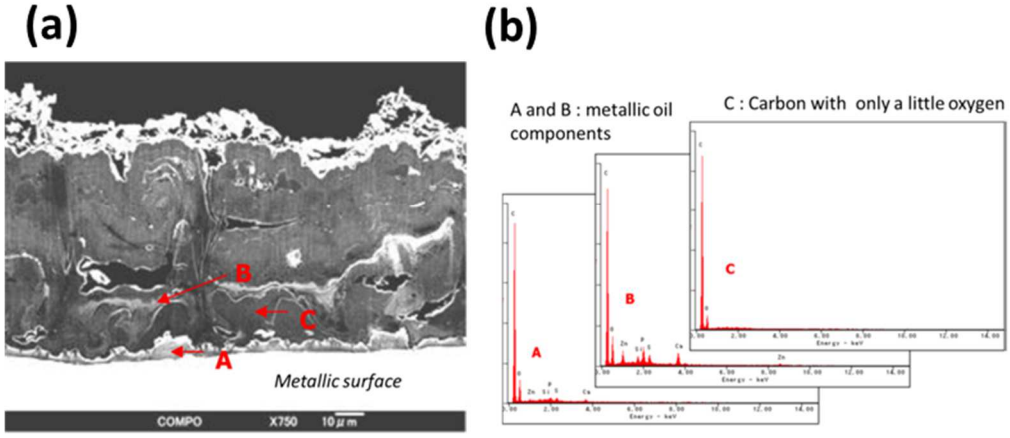

Figure 30: (a) SEM image of the cross-section of deposits from the piston surface
(b) EDX spectrum at three locations marked in (a) [13].

2.5.1.3 Porosity

Deposits porosity studies provide information on the ability of deposits to absorb fuel during the intake stroke and release it during the exhaust stroke [12, 79, 85, 86]. Initial work on this topic was conducted by Zerda et al. who characterized the pore size[2] of deposits recovered from the cylinders of a spark-ignition engine [79]. The methodology implemented was gas sorption with CO_2 and N_2 coupled with a numerical method. CO_2 and N_2 sorption is used to characterize micropores (size below 2 nm) and mesopores (between 2 and 50 nm) respectively. The cylindrical deposits analyzed have micropores of about 0.3, 0.5, and 0.8 nm and mesopores of about 5 and 35 nm wide (Figure 31). This study concluded that porosity depends on fuel compounds, lubricant additives, and temperature.

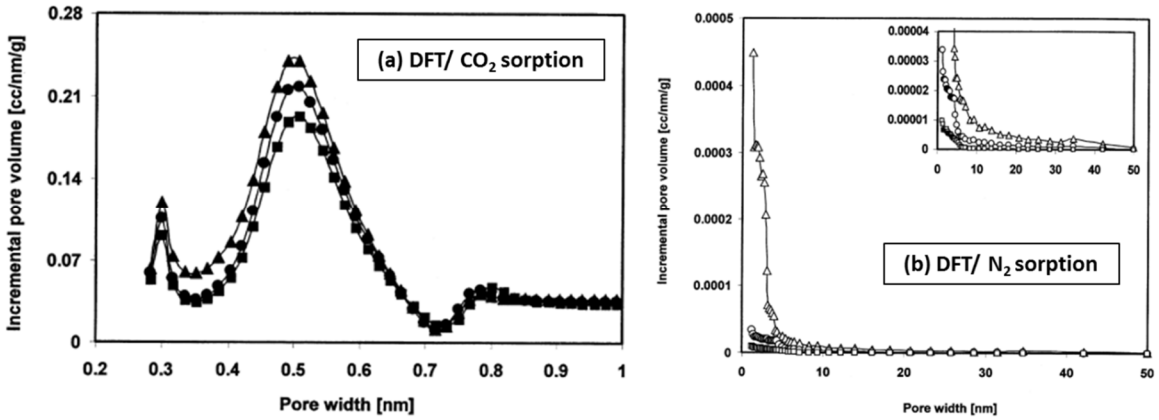

Figure 31: Pore size distribution of the engine deposits. Triangles: cylinder head, Circles: piston top, Squares: intake valves) [79].

2.5.2 Thermal properties of the deposits

Several studies have shown that deposits can form an insulating layer on the walls of the combustion chamber. In Ref. [28], it was established that the heat flux decreases by 40 % with a 10-µm thick deposits compared to clean walls. This leads to an increase in the gas temperature in the combustion chamber and results in increased NO_x emissions and knock [87]. Several studies have focused on determining the

[2] The pore size corresponds to the distance between two opposite walls of a pore of a sample. It can be calculated by porosimetry that measures the absorption of a gas by the sample.

thermal properties of the deposit such as thermal diffusivity and thermal conductivity [11, 40, 41, 88–91]. The thermal conductivity of the deposits is very low compared to that of aluminum, respectively <1 W/m K and 231 W/m K at 293 K [92]. This explains the thermal insulation effect of the deposits. An interesting method has been implemented based on the measurement of the thermal properties of the deposits. By measuring the surface temperature of the deposits and using a mathematical approach based on the solution of the 1D thermal equation, its thickness can be determined [41].

2.5.3 Chemical composition of deposits

Studies have shown that engine deposits are composed of fuel, oil, and soot [20, 43]. Nagano et al. determined the composition of deposits formed on different parts of the combustion chamber and with different fuels by thermogravimetric analyses [13]. This technique was used to determine the oil (oil and oil additives, oxidized organic products, and residual components) and fuel (volatile components, soot) content of the deposits. In the case of the piston head and cylinder head, the deposits are mainly composed of oil by-products (oxidized organic products and residual components) and soot. For the intake valves, the deposits consist mainly of oil and their by-products, with a lower soot content than for the combustion chamber deposits. They attribute this difference to a dripping effect of the oil towards the bottom of the valve.

The EDX analysis revealed the presence of inorganic components from the lubricating oil. Concentrations of zinc, calcium, and phosphorus were found to be four times higher in the deposits on the piston head than on the cylinder head [13]. Energy-dispersive spectroscopy (EDS[3]) analysis of the deposits from different parts of the combustion chamber showed a similar elemental composition (Figure 32). The deposits is mainly composed of carbon and oxygen, with traces of S, Al, Cu, Ca, and Zn attributed to lubricating oil, detergents, and corrosion inhibitors [93].

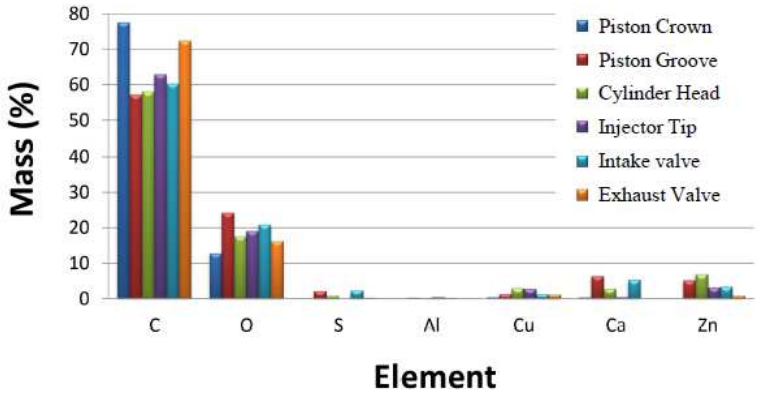

Figure 32: Elemental composition of deposits from a direct injection Diesel engine working with B50 (standard Diesel fuel with 50% of biodiesel) [93].

2.5.4 Conclusions on deposits properties

Different analysis techniques have been described in this section. These techniques were first based on macroscopic observations involving the color and surface state of the deposits. It showed that the appearance of the deposits is related to the engine operating parameters. Thus, it is possible to adjust the engine parameters to obtain a specific type of deposits. Electron microscopy has shown that it is suitable for the characterization of the deposits morphology and for distinguishing the deposits corresponding to

[3] EDS/EDX: EDS and EDX are two analytical techniques for determining the elemental composition of a sample. While EDS analyzes backscattered electrons emitted by the source, EDX analyzes the photon emission caused by X-rays.

the liquid-film and the soot path. Nevertheless, few studies have provided information on the characterization of the morphology of deposits, particularly for deposits that form on the walls of combustion chambers. Various chemical analyses enabled to characterize the composition of the deposits. The elemental composition provided by EDS and EDX showed that the deposits are mainly composed of carbon and oxygen. It is important to note that this elemental analysis technique does not detect the presence of hydrogen [94]. Other elements were found corresponding to oil and fuel impurities. The porosimetry study of the deposits allows the pore size and number distribution of the pores to be determined. However, there is not yet a study to link the porosity of the deposits with unburned hydrocarbon emissions. Another useful technique is thermogravimetry, which makes it possible to quantify the components of the deposits. However, this is a destructive technique and requires a large amount of deposits.

2.6 Conclusions

Engine deposits can form at various locations in the combustion chamber. They contribute to degraded combustion and increased pollutant emissions, which can lead to increased fuel consumption and reduced engine power. Different hypotheses of deposits formation mechanisms have been described in the literature involving the formation of a liquid film on the surface and the deposition of soot formed during combustion that is deposited on the surface of the combustion chamber or the liquid fuel film formed. Several factors have been identified as contributing to the formation of deposits. First, certain fuel properties may be predominant factors such as the presence of certain additives or the presence of high boiling point species. Surface temperature is also an important factor in the formation of deposits. Engine parameters, such as the presence of exhaust-gas recirculation (EGR), fuel type, fuel/air equivalence ratio influence the formation of deposits. Various analysis techniques were identified in the literature review. Microscopic observation was identified as a non-destructive analysis technique to determine the morphology of engine deposits. Elemental analysis coupled with electron microscopy is of interest to identify the elements present in the deposits, which are mainly carbon and oxygen. Techniques such as porosimetry and thermogravimetry are promising for characterizing the deposits but are destructive.

Several important parameters influence the formation of deposits. These include engine operating conditions, combustion chamber wall surface temperature and, fuel properties. Other physical phenomena are involved, such as the physics of the spray during injection or the aerodynamics inside the cylinder. To better understand, how these parameters and phenomena affect the formation of deposits, it is relevant to use methods for *in situ* analyses. Therefore, an optical engine seems appropriate for this thesis. As an optical engine does not use lubricating oil, fuel- and combustion-based deposits formation can be separated from other factors. This thesis focuses on conventional gasoline fuel to limit the effects of fuel properties. The thesis is built in three research topics:

- The first topic of this thesis (Chapter 4) analyzes macroscopically deposits formed at different locations in the combustion chamber to determine their similarities or differences according to engine operating parameters. A methodology to identify the origins of the deposits is presented to determine whether the liquid-film or the soot path is dominant. Two devices will be used to form reference deposits from these two pathways and the reference deposits will be compared with deposits gained from the engine combustion chamber. The objective is to evaluate the applicability of the reference deposits as a model for the engine deposits.
- The second topic of the thesis (Chapter 5) describes the study of the mechanisms of deposits formation. This study is motivated by the lack of a real-time experimental method in research

to study the mechanisms of deposits formation. This study is therefore based on the use of *in situ* analysis by direct visualization, analysis of the particle distribution with a particle analyzer, and the use of the previous method to distinguish the deposition pathways and quantify their contribution.

- The third and last topic of this thesis (Chapter 6) is devoted to the study of parametric variations on deposits formation. The effect of surface temperature will be studied by direct visualization. The effect of roughness on deposits formation will also be evaluated. And to document and help the implementation of optical diagnostics to measure the properties of deposits, the effect of transparent materials on the formation of deposits will be studied.

3 LABORATORY EXPERIMENTS AND ANALYSIS FOR DEPOSITS FORMATION

This chapter describes the experimental devices and means of analysis used during the thesis work. First, the experimental devices allowing to form reference deposits are presented. Then, the *ex situ* and *in situ* analytical means that enable the evaluation of the physical and chemical properties of the deposits, as well as to identify the possible formation of deposits, are presented.

3.1 Laboratory experiments for deposits formation

3.1.1 Microcoking device

The objective of the microcoking device is to form deposits from a liquid film in a controlled environment. These deposits will then be used as a reference for the liquid-film path mechanism.

Working principle: The microcoking device was first developed by Chevron to determine the thermal stability of engine lubricants according to standard protocol GFC L-027-T-97 [72]. It enables forming deposits from fuel thermal degradation at high temperature in a static mode on an aluminum plate. As illustrated in Figure 33a, it consists of an aluminum alloy plate (1) where deposits are formed in a bowl (2) and of a resistive heater (3). The aluminum plate has holes for the introduction of thermocouples (4). The temperature is controlled with a proportional integral derivative (PID) controller (5). It can be set between room temperature and 300 °C.

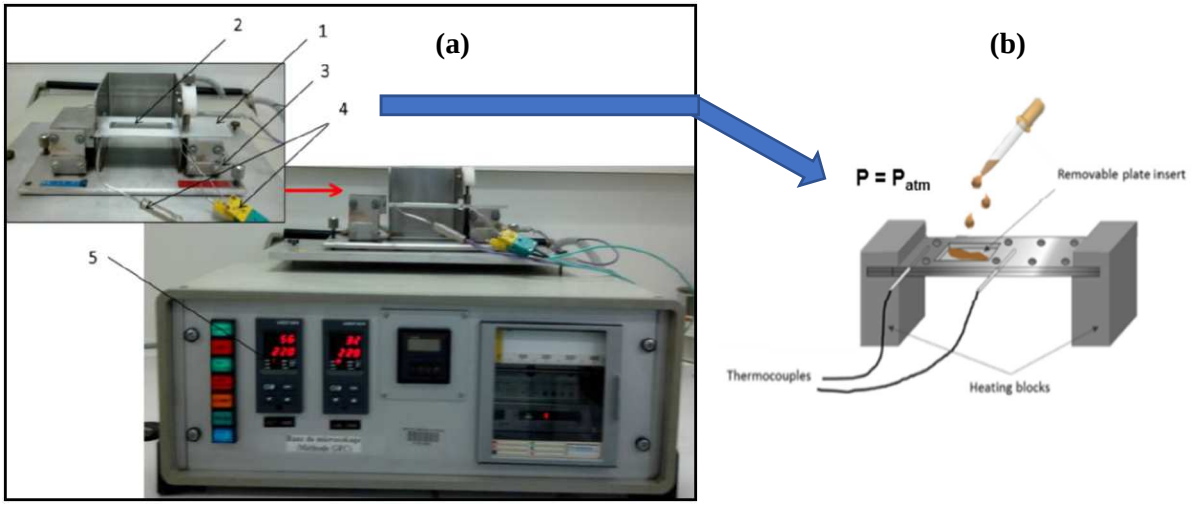

Figure 33: (a) Photo and (b) schematics of the microcoking device.

Deposit formation protocol: 4 ml of the fuel of interest is deposited in the bowl. The temperature is then increased from room temperature to 100 °C with a rate of 5 °C/min. The temperature is then kept constant at 100°C for 15 min. The total duration of the test is 30 minutes. At the end of the test, the plate is removed and is let to cool and settle for 6 h. Figure 34 presents the temperature evolution of the plate during deposits formation tests. These tests are realized with the same materials as the ones that will be used in the optical engine: aluminum, steel, quartz, and sapphire. All plates present a similar roughness

with a *Ra*[4] of 1.2 µm. The thickness of the plate is 2 mm and supposedly thin enough to consider the temperature evolution is identical for every experiment.

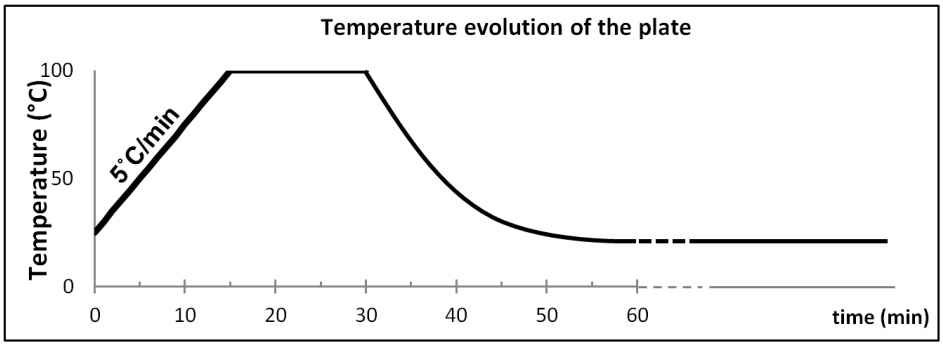

Figure 34: Temperature variation of the plate during deposits formation.

3.1.2 Soot generator

A soot generator was used to form engine-representative particles that were deposited on a plate to form a reference for the soot-path mechanism deposits.

Working principle: The soot generating device is called CAST (Combustion Aerosol Standard). It enables the formation of calibrated soot with known and reproducible properties. The principle consists in quenching a premixed sooting flame with N_2 gas (Figure 35). The soot formed follows the flow of the combustion and diluting gases and can be deposited on a plate placed at the exhaust. The size of the soot particles is determined by adjusting the flow rates of air, fuel gas, and N_2. A parametric study has been carried out to find the optimal flow rates to obtain maximum soot deposition on the plate in the shortest possible time. The CAST used in this study is configured to operate with Diesel fuel. A study has shown the similarity between soot from petrol and Diesel engine exhaust from a microscopic point of view (similar morphology and size in the tens of nanometers) [96]. There may be some difference in the composition of diesel and petrol soot due to oil impurities and metals related to engine wear. CAST will not affect the composition of soot by these impurities. Soot formed with the CAST is therefore assumed to be representative of gasoline soot.

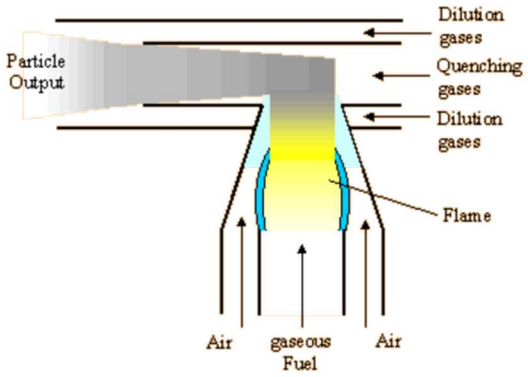

Figure 35: Schematics of the CAST soot generator [97].

Deposits formation protocol: A heated aluminum plate placed at the CAST exhaust as shown in Figure 36, at a distance of 3 cm to recover the maximum amount of soot. The temperature of the plate is set at 80 °C. The flow rate values of the different gases are shown in Table 1. The soot generator is activated once the plate is at 80 °C. Then the test starts for a duration of 15 min. After 15 min, the CAST is

[4] *Ra* corresponds to the value of the arithmetic mean deviation of the profile from the mean line [95].

stopped. Then the soot-covered plate remains at 80 °C for 15 min. At the end of the test, the plate is removed and cools down naturally to room temperature.

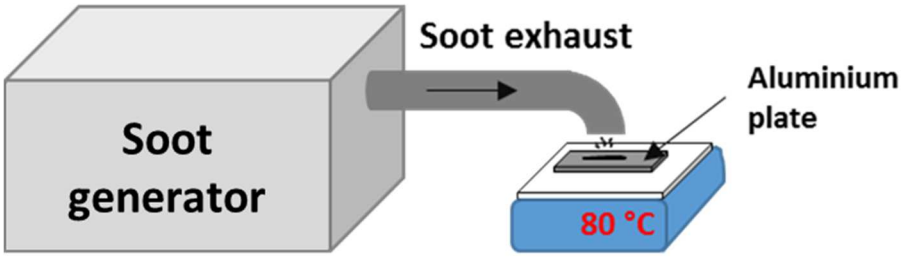

Figure 36: Schematics of the set-up.

Table 1: Gas flows for operation of the CAST soot generator.

Oxygen dilution with air	Liquid Diesel fuel	Dilution gases	Air
3	70 ml/min	3 ml/min	100 ml/min

3.1.3 Smoke meter

A smoke meter was used to collect soot from the exhaust of an engine on a paper filter to use as a second reference of soot deposits.

Working principle: The engine exhaust gases first pass through a dryer to remove moisture. Then it passes through a paper filter (filter area in Figure 37) where soot is trapped. The conventional use of this device is to measure the soot content in the engine exhaust.

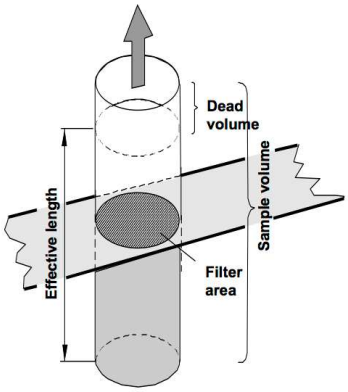

Figure 37: Soot collection principle of AVL smoke meter [98].

Deposits formation protocol: The smoke meter was used at the exhaust of a conventional single-cylinder spark-ignition direct-injection engine operated with E10 fuel. The black disc on to the soot collection paper filter presented in Figure 38 corresponds to soot filtered from 1 l of gas sampled at the exhaust during 30 s.

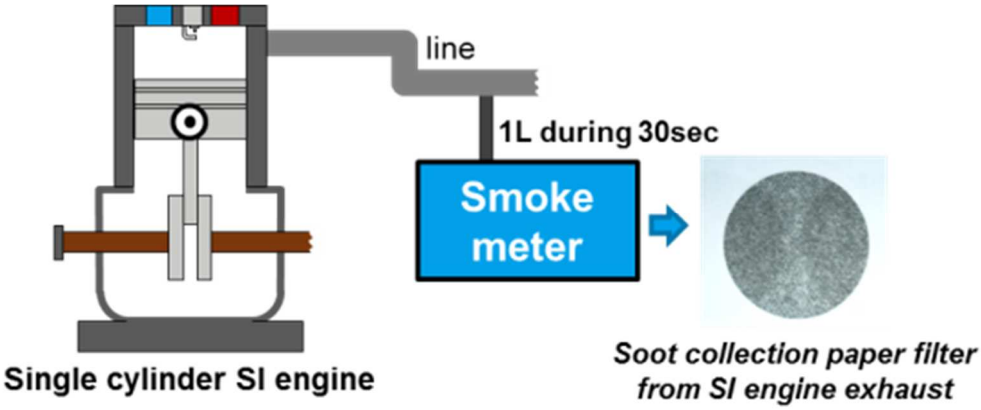

Figure 38: Schematics of the experiment for the recovery of soot from a gasoline engine by a smoke meter.

3.1.4 Engines

To study deposits formation in representative engine conditions, two optically-accessible single-cylinder direct-injection gasoline engine was used during the thesis. Optical engines are a good compromise between engine representativeness and given flexibility in configuration and *in situ* accessibility.

3.1.4.1 400 cm^3 engine experiment to recover engine deposits

Engine specifications: The engine used is a single-cylinder, direct-injection, spark-ignition engine. It is optically accessible and is coupled to a chassis dynamometer to adjust the engine load (Figure 39). The engine is equipped with various pressure and temperature sensors. Figure 40 shows the engine schematics and Table 2 shows the engine specifications. The intake valve, 20 mm bowl rim, injector, and piston insert can be easily removed for *ex situ* surface analysis.

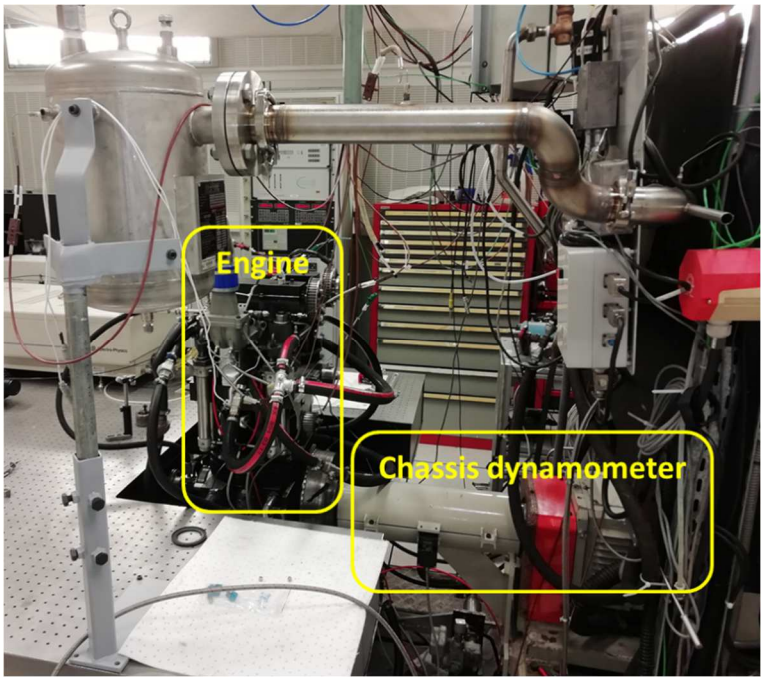

Figure 39: Optically-accessible engine mounted on the test bench.

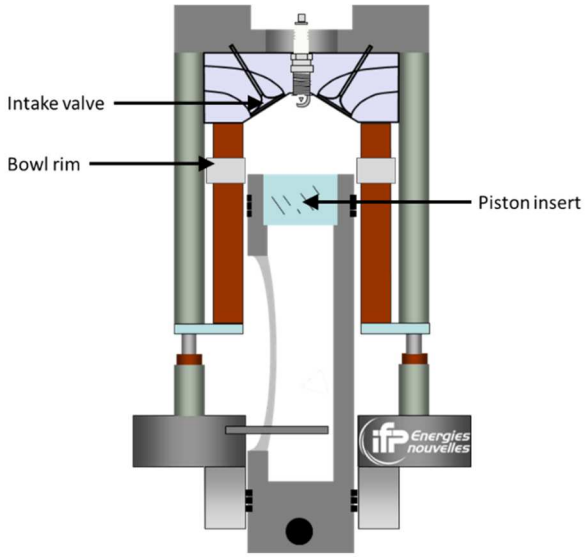

Figure 40: Schematics of the single-cylinder spark-ignition direct-injection engine.

Table 2: Engine specifications

Piston displacement	400 cm^3
Bore	77 mm
Stroke	85.8 mm
Compression ratio	10
Engine speed	1200 rpm
MIP	4.5 bar
Injector	Bosch HDEV 5.2 6-hole
Injection pressure	200 bar
Excess air ratio	1.0

To study the formation of deposits on the cylinder liner, a bowl-rim is inserted between the liner and the cylinder head (Figure 41). This bowl-rim consists of three inserts that can be removed and analyzed after engine operation. Their location is described in Figure 42. It allows testing of different materials that will not have a significant impact on combustion due to the small size of the inserts. The optical engine has a standard engine base with a piston lifter. The overall configuration has a dry segmentation[5].

[5] Dry segmentation: It avoids the use of oil in the cylinder that could lead to signal interference when performing optical measurements such as laser-induced fluorescence.

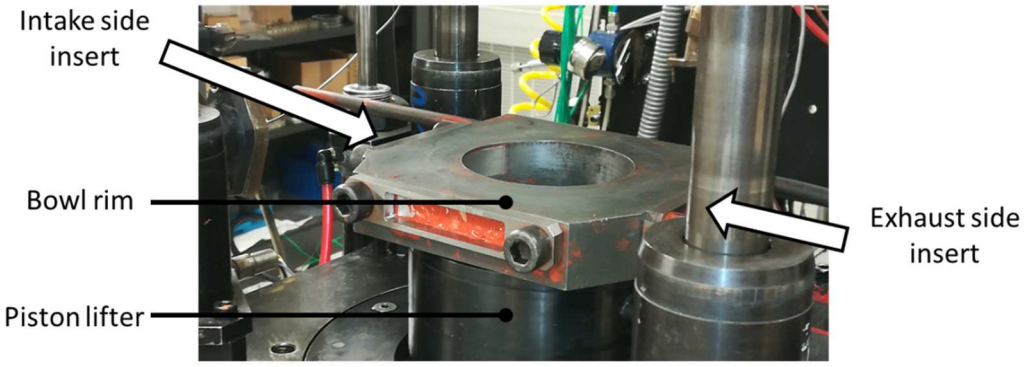

Figure 41: Image of the position of the bowl rim on the engine.

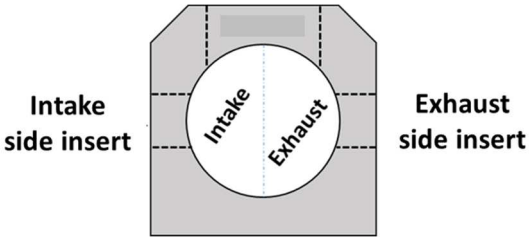

Figure 42: Bowl rim with the insert location

Deposits formation protocol: Before each engine test, a special precaution is taken to clean with acetone the surfaces of interest (piston top, injector nose, valves, bowl-rim inserts). The other parts of the combustion chamber are also cleaned to avoid increased emissions or the creation of hot spots due to deposits formed during previous tests. The engine runs on conventional E10 fuel. Engine tests for forming deposits in the combustion chamber are carried out at 1200 rpm with a mean indicative pressure (MIP) set at 4.5 bar. Different engine control parameters are modified according to the tests. The cooling-water temperature of the cylinder and cylinder head is varied between 20 and 90 °C. The start of injection is also modified to generate different types of interactions between the spray and the wall. Details of the operating parameters are given below, along with the results. Different deposits locations in the combustion chamber were studied: injector nozzle, intake valves, piston top and cylinder walls with removable cylinder inserts. Each of these parts was sampled at the end of each test.

3.1.4.2 462 cm^3 engine experiment to study in situ deposits formation

The objectives of using this specific engine are to generate a data base of piston deposits for different engine operating parameters and to apply *in situ* diagnostics.

Engine specifications: The engine is an optically accessible single-cylinder spark-ignition direct-injection operated with E10 fuel as for the first campaign (Figure 43). One of the specificity of this engine is that one of the exhaust valves was replaced by an optical access Figure 44. A port-fuel injection (PFI) system is also implemented at the intake valve admission to enable homogeneous combustion. The engine specifications are presented in Table 3.

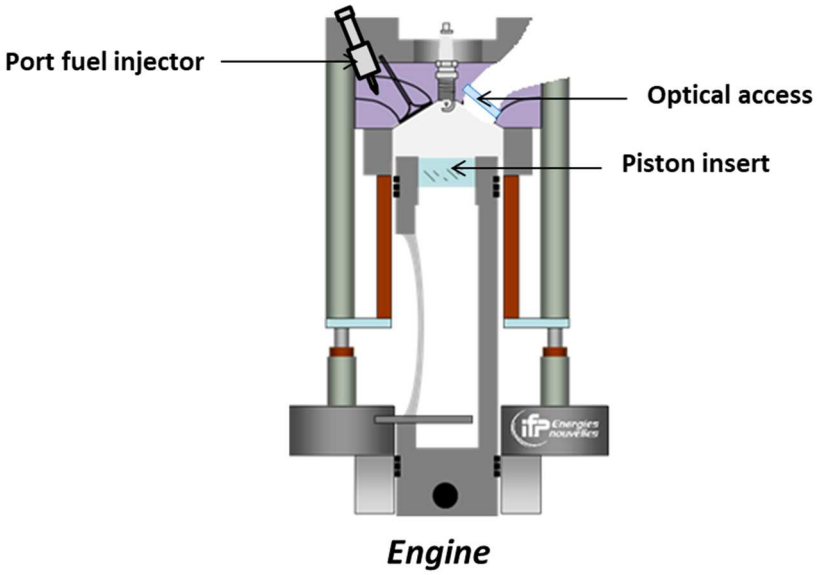

Figure 43: Schematics of the optically-accessible single-cylinder spark-ignition direct-injection engine with port fuel injection.

Table 3: Engine specifications

Piston displacement	461.95 cm^3
Bore	82.7 mm
Stroke	86 mm
Compression ratio	11.5
Engine speed	1200 rpm
PMI	4.5 bar
Injector	Bosch HDEV 5.1 6-hole
Injection pressure	200 bar
Excess air ratio	1.0

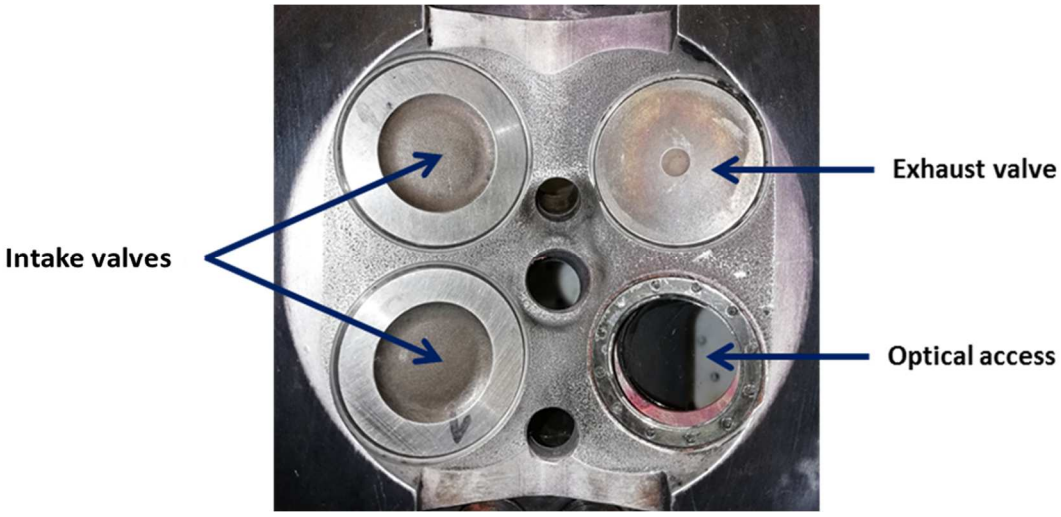

Figure 44: Bottom view of the cylinder head exhibit the sapphire window in place of an exhaust valve.

The engine is operated at 1200 rpm for a MIP set at 4.5 bar. The cylinder and the cylinder head are cooled by water. Only the piston is sampled at the end of the engine tests. For these tests, the same cleaning protocol is applied than for the 400 cm^3 engine.

Engine warm-up injection strategy: To study the formation of deposits in a stable environment, a specific engine warm-up strategy has been implemented. It aims to start deposits formation tests with a hot engine to avoid deposits formation during the first combustions. This strategy consists of running the engine for 2 min in PFI. This 2-min duration was chosen based on a study that showed that after 1 min, the engine begins to reach a stabilized temperature [99]. In this thesis, 2 min are set to ensure a stable temperature before the deposits formation test. This warm-up strategy is used for two cooling water temperatures: 20 and 90 °C. At the end of the tests, no deposition was observed with the naked eye. After this heating phase, the injection mode switches to direct injection and the deposits formation test starts. This change of injection strategy is manual and takes 2 s during which there is no injection. This avoids overlapping injection modes that would lead to rich combustion.

3.2 Analysis of deposits formed in the combustion chamber

In this section, the techniques used to analyze the deposits after engine operation are presented. First, scanning electron microscopy (SEM) was used to characterize the deposits morphology and combined with energy-dispersive spectroscopy (EDS) providing information on the elementary composition of the deposits. Fourier-transform infrared spectroscopy (FTIR) was then used to get specific information on organic molecules. Finally, Raman spectroscopy was used to retrieve information on molecular structure a composition.

3.2.1 SEM-EDS: Morphology and elementary composition analysis

The SEM-EDS consists of an electron gun that focuses an electron beam on the sample. The interaction between the emitted electrons and the elements of the sample modify the electron behavior. Two types of electrons are detected (Figure 45). The first ones are the backscattered electrons which are very sensitive to the atomic number of the atoms. The heavier the nucleus of the atoms in the sample, the more backscattered electrons are detected. In this way, it is possible to determine the constituent elements of the sample. This analysis is called EDS. The second ones are called secondary electrons and are very sensitive to irregularities, even small ones, and therefore to the topography of the surface. This analysis, called SEM, therefore gives information on the morphology of the sample.

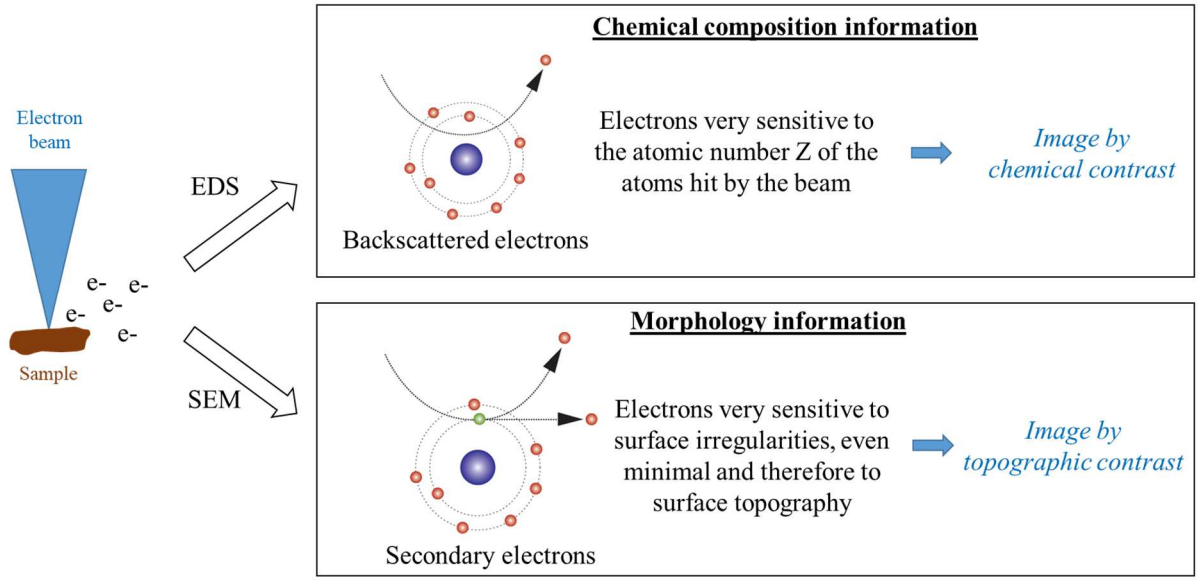

Figure 45: Overview of the electron interactions with the sample.

In this work, two microscopes are used to characterize the morphology of the deposits: A Nova nano SEM, FEI, and a Supra 40, Zeiss. The first allows observations to be made on metallic surfaces. The second allows observations on transparent materials. For each microscope, the electron beam energy is adjusted to obtain the sharpest image. Two detectors are used: the secondary detector for morphological observations and the primary detector for the analysis of elemental composition.

- Nova nano SEM specifications: this SEM-EDS device allows to obtain microscopic images with a magnification from 35× to 1,000,000×. Depending on the electron acceleration voltage applied to the sample it provides images with a resolution from 0.8 to 4.0 nm.
- Supra 40, Zeiss specifications: this SEM-EDS device allows to obtain microscopic images with a magnification from 12× to 900,000×. Depending on the electron acceleration voltage applied to the sample it provides images with a resolution from 1.3 to 5.0 nm.

3.2.2 FTIR-ATR

Working principle: The Fourier-transform infrared-attenuated total reflectance (FTIR-ATR) spectrometer enables the identification of organic molecules. The sample is in contact with a crystal as illustrated in Figure 46. The internal reflection at the crystal surface creates an evanescent wave that penetrates the sample for ~1 µm. The attenuated infrared beam is then detected and analyzed. The amount of light absorbed by a sample is measured as a function of wavelength.

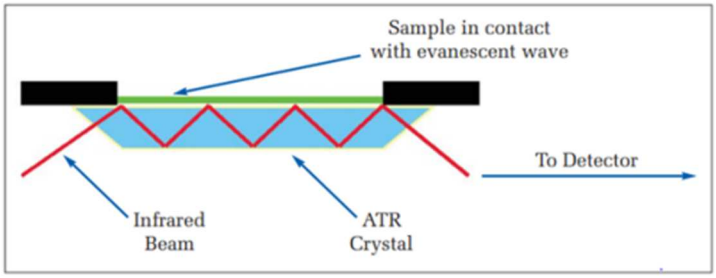

Figure 46: Working principle of FTIR-ATR [100].

Analysis protocol: The device used is a Vertex70 from Bruker. This spectrometer can acquire infrared spectra from 50 to 6000 cm^{-1}. The spectral resolution provided by the device is 4 cm^{-1}. The amount of light absorbed by the deposits is measured here as a function of wavelength from 400 to 4000 cm^{-1}. The results of this analysis are spectrums of transmittance or absorption according to the wavelength. Each FTIR-ATR spectrum corresponds to an average of 100 scans of the sample using air as reference. All the spectra were obtained at room temperature.

Post-processing: The spectrometer provides infrared absorption of the deposits. The absorption bands of the sample revealed by the FTIR-ATR analysis are compared with data from the literature as in Table 4 [61]. The objective is to find characteristic bands corresponding to specific chemical functions present in the sample.

Table 4: Chemical functions and associated FTIR peak intensities [61].

Category		Wavenumber / cm^{-1}	Intensity	Assignment
Carboxylic acid		3400 – 2500	Strong	O-H
		1350 – 1450	Medium	O-H
		1740 – 1660	Strong	C=O
		1320 – 1210	Strong	C-O
Aldehyde	Aliphatic	1650 – 1740	Strong	C=O
		1650 – 1725	Strong	C=O
	Aromatic	2720 – 2820	Medium	C-H of CHO
Ketone	Aliphatic	1650 – 1740	Strong	C=O
		1070 – 1220	Medium	C=O
	Aromatic	1650 – 1725	Strong	C=O
		1210 – 1325	Medium	C=O
Ester		1730 – 1750	Strong	C=O
		1300 – 1000	Strong	C-O
Alcohol	RCH_2OH	3600	Variable	O-H (free)
		3400	Strong	O-H (bonded)
		1000 – 1080	Strong	C-O
	R_2CHOH	3600	Variable	O-H (free)
		3400	Strong	O-H (bonded)
		1050 – 1160	Strong	C-O
	R_3COH and ArOH (phenol)	3600	Variable	O-H (free)
		3400	Strong	O-H (bonded)
		1110 – 1220	Strong	C-O
Alkane		2850 – 3000	Strong	C-H stretching
		1450 – 1470	Strong	C-H stretching
		1370 – 1380	Strong	$CH_2 – CH_3$ twist
		720 – 725	Medium	$CH_2 – CH_3$ twist
Alkene	Cis-RCH=CHR	3010 – 3020	Weak	=C-H stretching
		1660	Weak	C=C stretching
		675 – 725	Medium	C-H
	Trans-RCH=CHR	3010 – 3020	Weak	=C-H stretching
		1660	Weak	C=C stretching
		970	Strong	C-H

3.2.3 Raman scattering

This complementary technique to the FTIR-ATR spectroscopy provides information on the molecular composition and structure of the deposit.

Working principle: Raman spectroscopy is based on the inelastic interaction of light with a sample. This interaction generates molecular vibrations characteristic of a molecule. When the light is applied to the sample, two type of Raman scattering signals are emitted: the Stokes signal and the anti-Stokes signal. The resulting Raman spectra analyzed here use only Stokes Raman scattering. The position of peaks and bands in the spectrum in the spectrum indicates the frequency of vibrational modes corresponding to a specific molecule or crystal structure.

Analysis protocol: The device used is a Renishaw inVia Raman microscope. This Raman spectrometer is coupled with a He-Ne laser (λ = 632 nm). It is equipped with four objective lenses with 5×, 20×, 50× and 100× magnification. The microscope optics were used to focus the excitation laser beam onto the sample and to collect the backscattered light. The instrument was calibrated with measurements on pure silicon with a strong isolated signal at 520 cm^{-1}. For each deposits sample, the optimal laser power was first determined. With the optimal power found, the deposits were then analyzed at different locations. The analysis was repeated twice for the same area.

Post processing: From the Raman spectra, the peaks and band positions observed are compared with data from the literature. This provides information on the molecular composition of the deposits. Other information can characterize deposits such as the peaks ratio intensity and the full width at half maximum (FWHM). Work realized on carbonaceous material such as Diesel soot has linked these parameters with the graphitization level of the carbon [101]. Figure 47 presents the Raman spectrum of Diesel soot illustrating the different parameters which can be calculated.

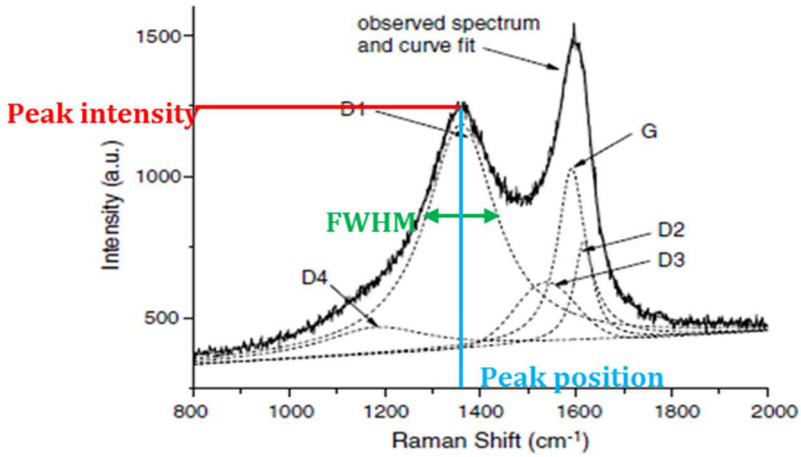

Figure 47: Raman spectrum of Diesel soot with curve fit
based on the expected bands for carbonaceous structures [101].

3.3 In-cylinder experiments

This section presents the analysis techniques for characterizing the processes taking place inside the combustion chamber.

3.3.1 Phosphor thermometry

Working principle: The objective of phosphor thermometry (PT) is to measure the temporal variation of the piston surface temperature during the experiments. PT is a non-intrusive temperature measurement technique. It consists of the determination of the decay rate of a laser signal sent on a phosphor layer applied onto the surface of interest. This decay rate depends on the temperature. Figure 48 presents the principle of the technique. For a given temperature, the intensity decays exponentially following Eq. 1.

This technique was implemented on the engine using a Nd:YAG laser at 355 nm. The laser repetition frequency was 10 Hz thus allowing to perform one temperature measurement per cycle.

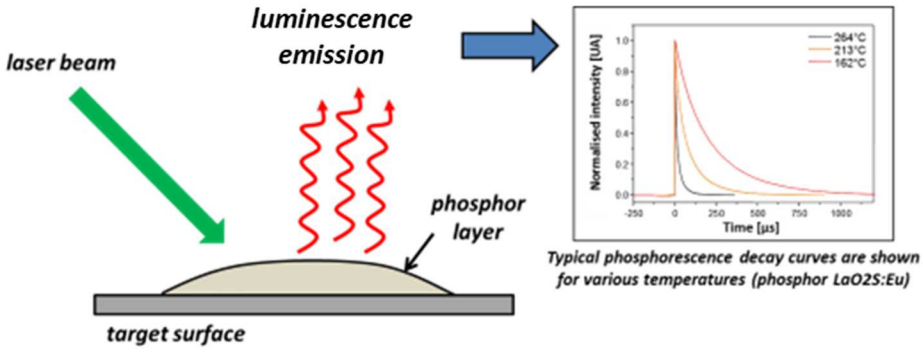

Figure 48: Principle of the technique.

$$I = I_0 \exp\left(\frac{-t}{\tau}\right) \qquad \text{(Eq. 1)}$$

Measurement protocol: Different phosphors are available to perform PT. The choice of a phosphor depends on its temperature sensitivity and its characteristic emission wavelength. Figure 49 presents the temperature sensitivity of the luminescence lifetime of several phosphors.

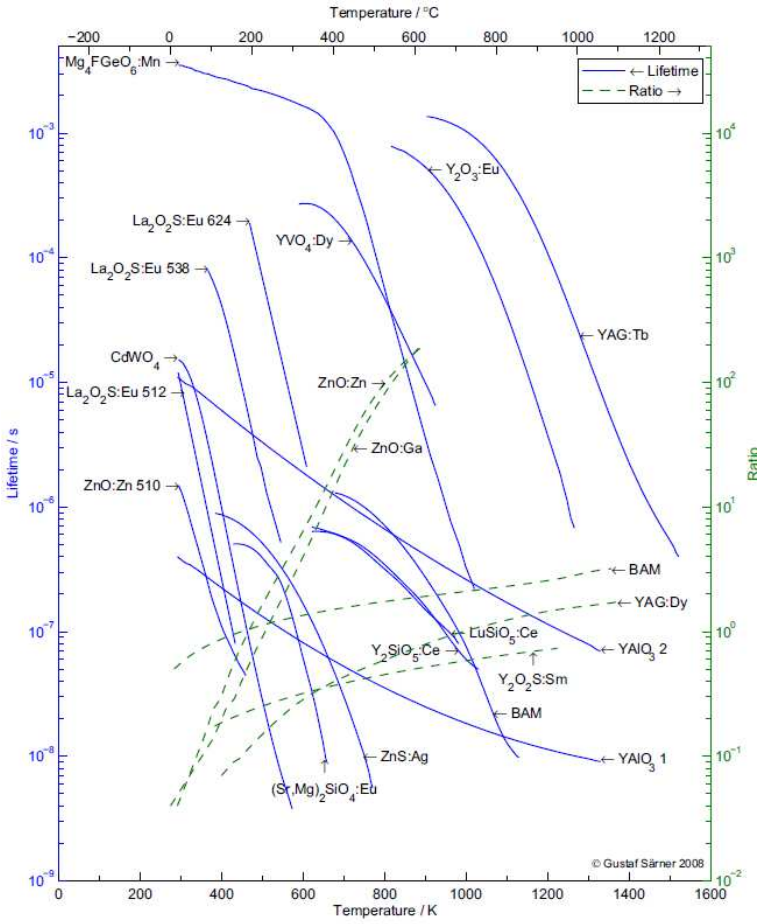

Figure 49: Temperature sensitivity of the luminescence lifetime (blue, left axis and the intensity ratio (green, right axis) for various phosphors [102].

The literature review has shown the combustion chamber wall temperature ranges between 420 and 470 K [103]. Therefore, the phosphor chosen is europium-activated lanthanum oxysulfide (La_2O_2S:Eu) with an emission peak at 538 nm. Figure 50 presents the different temperature sensitivity of La_2O_2S:Eu for different emissions peaks (512, 538, and 624 nm) provided by that phosphor.

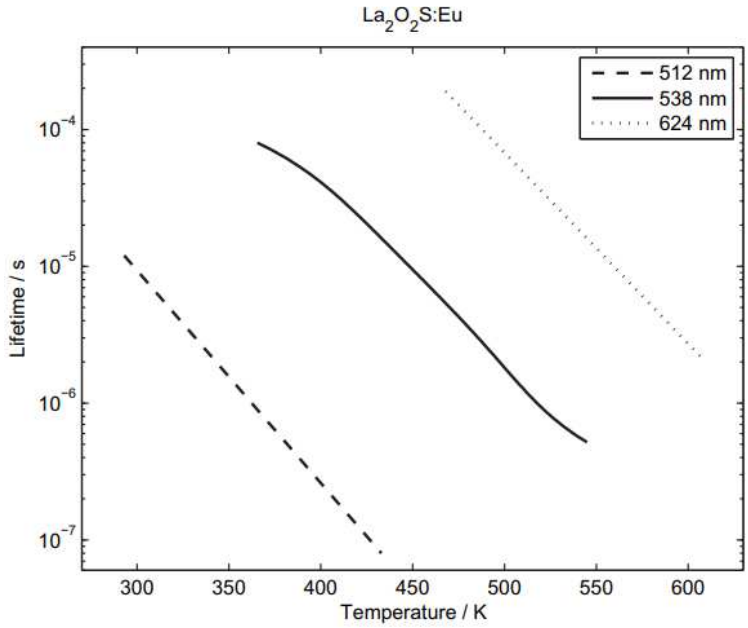

Figure 50: Temperature sensitivity of La_2O_2S:Eu phosphor for different emissions [102].

Calibration: To retrieve temperature from the measured light emission, a specific calibration matching the engine setup is required. In this work, it was realized with a heated plate on which a layer of the phosphor has been applied. The phosphor is mixed with a binder to obtain a great adhesion of the phosphor on the plate. The mixture corresponds to one-part phosphor to 20 parts binder. The mixture is then applied homogenously on the plate. The thickness of the mixture is estimated at 100 µm. The layer is supposed to be thin enough to be equal to the plate temperature. An optical fiber assembly is used to focus the laser beam on the phosphor layer and to recover the emitted laser signal (Figure 51). The Nd:YAG laser passes through an optical fiber. At the exit of the optical fiber, the beam is focused on the phosphor layer with a converging lens. The optical fiber is a multi-core technology allowing to both emit and recover signals (Figure 52). Thus, the luminescence emissions are recovered with the same optical fiber assembly and measured with a photomultiplier Hamamatsu H6780. For each temperature, the luminescence emission of the phosphor from 100 laser pulses is acquired. Then post-processing of these signals is carried out to obtain the corresponding decay rate. The temperature of the plate is varied between 105 and 261 °C. The resulting calibration curve is presented in Figure 53.

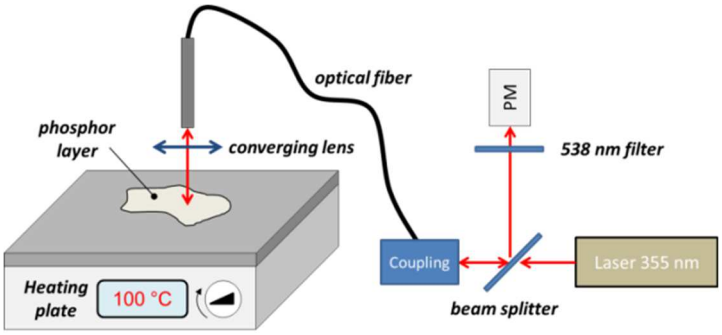

Figure 51: Schematics of the experimental set-up for calibration.

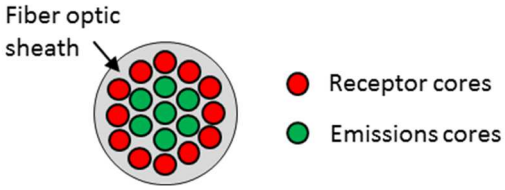

Figure 52: Schematics of the optical fiber cores disposition within the sheath.

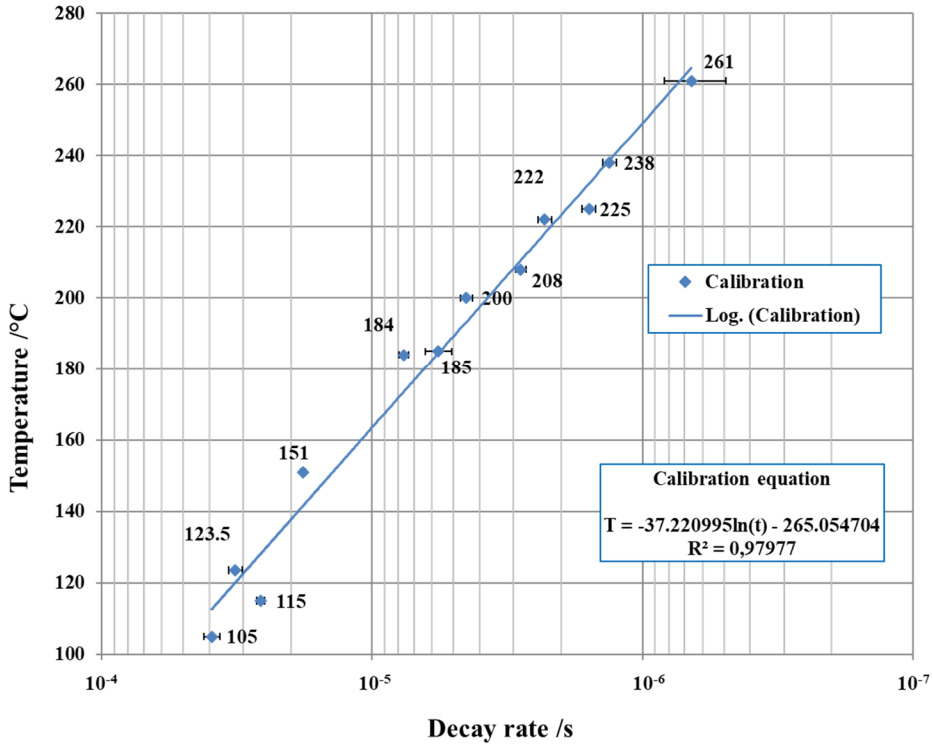

Figure 53: Calibration curve of the temperature with the decay rate of the luminescence emission.

The calibration equation from the calibration is presented in Eq. 2. It will be used to obtain the corresponding temperature from piston surface temperature measurement during engine experiments.

$$T\ /°\mathrm{C} = -37.221 \ln(\tau) - 265.055 \qquad \text{(Eq. 2)}$$

Engine setup: The motor configuration assembly is shown in Figure 54. The photomultiplier gain is set with a control voltage of 220 mV and the laser is set with a power of 21.5 mJ. The oscilloscope parameters are set to acquire 100 curves of 25 000 points. This corresponds to an acquisition averaged over

10 s. As the duration of the experiments is several minutes, the temperature evolution over 10 s is considered constant. The calibers are set at 20 µs per division and 50 mV per division for all acquisitions.

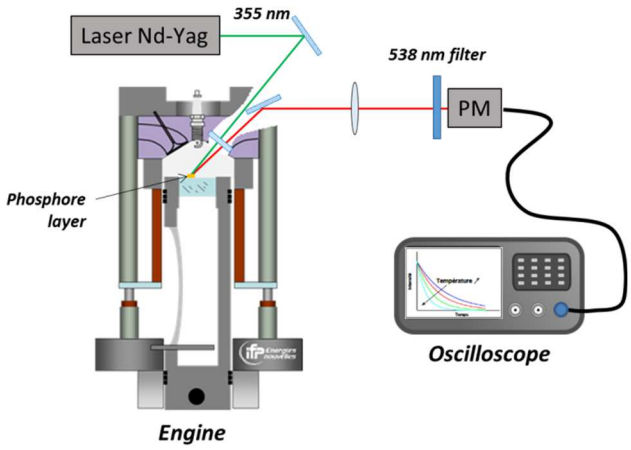

Figure 54: Schematics of the of the set-up of the measurement of the temperature of the piston surface by phosphor thermometry.

In the experiments, the cooling water temperature is set at 20 °C. The injection and ignition parameters are shown in Table 5. The engine is started in PFI to avoid the formation of deposits on the piston that could cover the phosphorus layer and lead to misinterpretation of the surface temperature. The laser is then triggered at the top dead center corresponding to the valve overlap. Acquisitions are carried out every 2 min during the experiment which lasts 10 min. The time evolution of the piston surface temperature is thus obtained from the measurement points averaged over 10 s every 2 min. Post-processing of the experiment results gives the surface temperature (see Appendix).

Table 5: Engine operating parameters for phosphor thermometry measurements.

PFI parameters			Ignition	
Injection pressure / bar	Injection phasing / °	T_{inj} Main / µs	Ignition phasing /°	Load time / µs
3	280	6000	347	4500

3.3.2 High-repetition-rate visualization

The objective is to record videos of deposits forming in real-time for different engine operating conditions and to identify combustion-related phenomena occurring inside the combustion chamber, such as liquid-films or incandescent soot.

Setup: A camera coupled with an endoscope is set on the optical access replacing one of the two exhaust valves in Figure 55. The endoscope gives a full vision of the piston surface when it is at the bottom dead center. The high-repetition-rate camera is a Photron Fastacam Mini Ax. The acquisition frequency is set at 4 kHz, and chip resolution is 640 × 608 pixels.

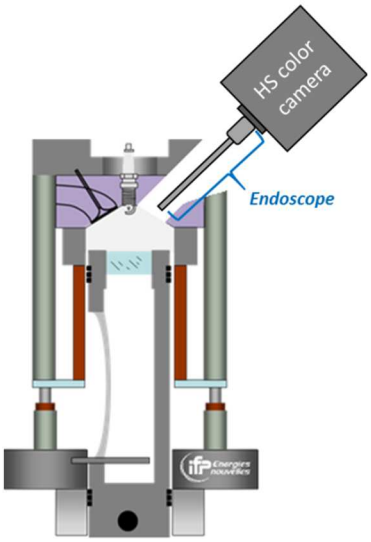

Figure 55: Engine with the high-repetition-rate camera and endoscope.

Methodologies: Two acquisition strategies were used:

- The first is to acquire the first 125 cycles of the engine experiment. The objective is to observe the phenomena related to the formation of the deposits occurring at the start of the experiment.
- The second consists of acquiring one cycle every 75 cycles for the duration of the experiment, i.e., for 10 min. The objective here is to observe the formation of the deposits throughout the experiment.

3.3.3 Particle analyzer

Set up: A DMS 500 from Cambustion was implemented at the exhaust of the engine to characterize engine soot emissions. This device characterizes the size distribution from 5 nm to 1 µm and determine the number of particulates from engine exhaust. A sampling flange with an internal thickness of 8 mm, as shown in Figure 56, is inserted inside the exhaust line one meter away from the exhaust collector.

Figure 56: Sampling probe

For each experiment, dilution ratios are set to avoid particle saturation of the DMS 500. A first dilution ratio is already set to 5 by the manufacturer for all engine experiments. A second dilution ratio is then set by the operator according to the signal obtained during the experiment. This second dilution ratio is determined during preliminary experiments. If the signal is low, the second dilution ratio shall be maintained at 1. If the signal is outside the measuring range, it shall be increased to between 12 and 500.

Analysis: Two different types of information are extracted from the results of the experiments with the DMS 500. The first gives an overview of the particle size distribution over the entire engine experiment (Figure 57). It shows whether the particle size distribution changes during engine operation. For example, in Figure 57, there is an increase in the number of particles between 10 and 100 nm during the first 100 seconds. Then the distribution is fairly constant during the rest of the experiment.

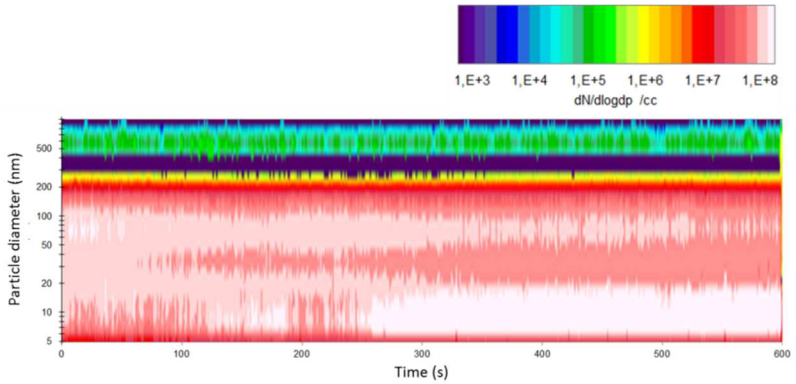

Figure 57: Contour plot of the soot particle-size distribution of the experiment 2.

The second piece of information is the size spectral density corresponding to the particle distribution for a time range chosen over the engine experiment. It allows identifying the distributions corresponding to nucleation or accumulation mode. Nucleation mode corresponds to the particles formed from the vapor phase of unburned fuel to a solid phase. This formation occurs in the fuel-rich region at elevated temperatures. Accumulation mode corresponds to the last phase in the soot life process. It follows the steps of coalescence and surface growth of the nucleated particles and corresponds to the agglomeration of single particulates into a chain of particles as presented in Figure 58 [104].

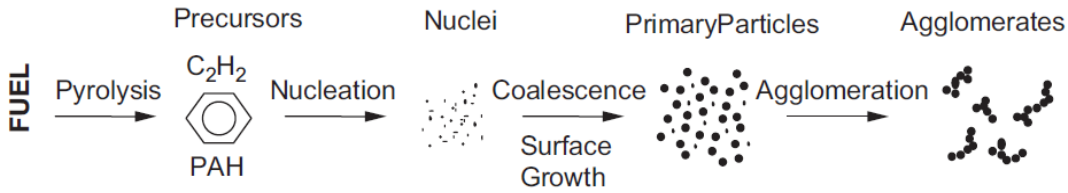

Figure 58: Schematics of soot formation from partially-burned fuel compounds to solid agglomerates [104].

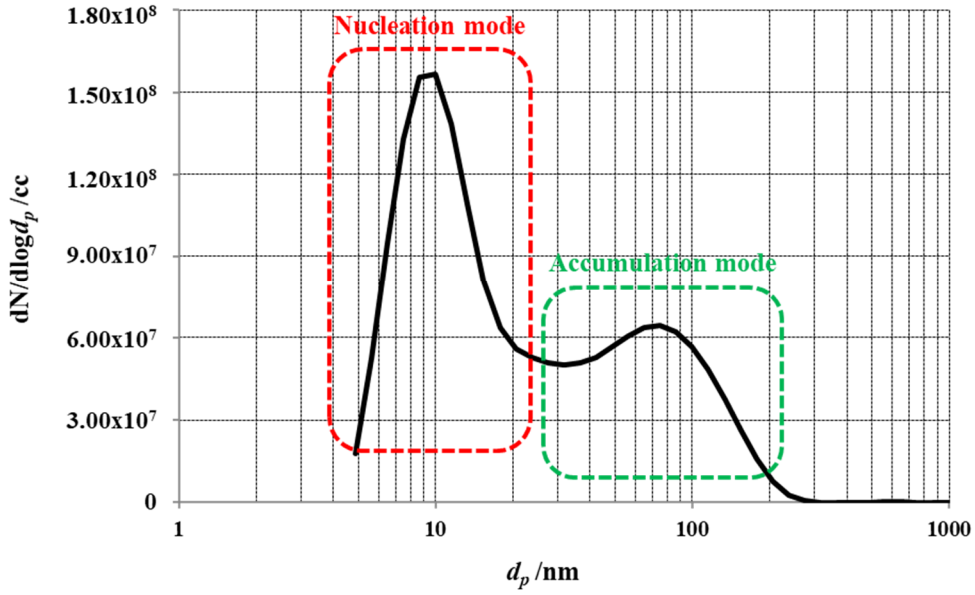

Figure 59: Particle-size distribution of soot sampled for 10 min.

4 ESTABLISHMENT OF THE METHODOLOGY TO STUDY ENGINE DEPOSITS

The objective of this chapter is to define and evaluate a method for distinguishing and quantifying the different pathways of deposits formation in engines, i.e., the liquid film path and the soot path. This method is based on the *ex situ* analysis of reference and engine deposits. First, the reference deposits are analyzed to determine their physical and chemical properties with a special interest in macroscopic and microscopic analysis. Then, the deposits from different engine experiments are analyzed macroscopically and microscopically. The objective is to determine the effect of different engine parameters on the properties of the deposits. The first parameter studied is the effect of the location inside the combustion chamber on the properties of the deposits. The purpose is to identify the most relevant combustion chamber part for further investigation. The second parameter investigated is the impact of the geometry of two engines on the properties of the deposits to determine the possibility to study the deposits independently of the engine geometry. The third and final parameter is the determination of the effect of injection timing on the deposits properties. The properties of these deposits formed from different injection timing are compared with reference deposits. The most promising deposits are then chemically analyzed and compared with the reference deposits to determine the usefulness of these chemical analysis techniques in identifying the deposits formation pathways.

4.1 Analysis of reference deposits

4.1.1 Matrix

Table 6 presents the devices used to form reference deposits, and the methods to analyze them. Deposits formation and sampling protocols are presented in Chapter 2.

Table 6: Reference deposits formation devices and the analytical methods

Deposit pathway	Device	Element sampled	Analysis methods
Liquid-film path	Microcoking device	Aluminum plate	SEM-EDS, FTIR-ATR, Raman
Soot path	Soot generator	Aluminum plate	Raman
	Gasoline engine	Paper filter from a smoke meter	SEM-EDS, FTIR-ATR

4.1.2 Macroscopic analysis

The macroscopic analysis of the reference deposits presented here will focus on the visual aspect of the deposits. Color will be of primary interest, but texture and shape will also be considered.

The liquid-film path reference deposit was obtained by using the microcoking device. This type of deposit forms corresponds to a transparent varnish on the surface of the aluminum plate. It has a shiny appearance, a smooth surface, and adheres to the surface. It can hardly be removed by scraping or even when using solvents such as with an acetone.

Two strategies were used to obtain deposit corresponding to the soot-path mechanism. The first consists of recovering soot from the exhaust of a gasoline engine using a smoke meter to determine the typical morphology of soot from a gasoline engine. The second is to form calibrated soot with a soot generator that is deposited on an aluminum plate for chemical analysis. The deposit formed with the soot generator and the gasoline engine are both black. The texture observed is rough and appears granular to the touch.

The soot path deposit formed with the soot generator on the aluminum plate can be removed easily by wiping the plate with a tissue.

These macroscopic observations show a significant difference in color, texture and adhesion with the aluminum plate between the liquid-film path deposit and the soot path deposit. These macroscopic differences could give a first indication on the type of deposit, i.e., liquid-film-path deposit or soot-path deposit.

4.1.3 Microscopic analysis

Microscopic analysis is used to determine the morphology of the deposits. This analysis is carried out by SEM-EDS to characterize the structure of the deposit from the millimeter to the sub-micrometer scale. The method distinguishes the topography of the deposit to determine their surface structure.

The liquid-film-path reference deposit formed by the microcoking device presents an extended smooth surface delimited in red in Figure 60. The morphology of the aluminum plate and some traces of smaller spherical deposits with an average diameter > 200 nm are dispersed over the surface.

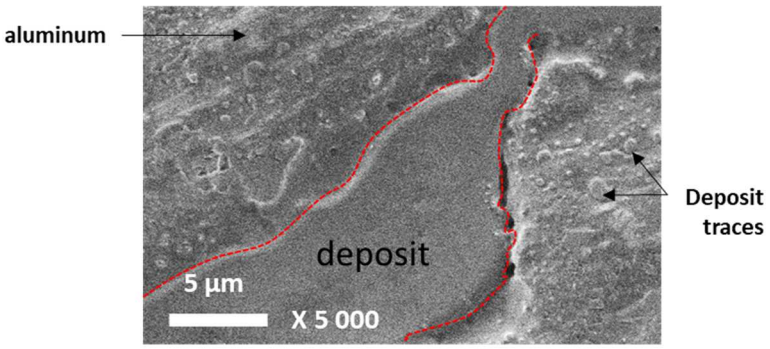

Figure 60: SEM image of reference liquid-film-path deposit formed on an aluminum plate with the microcoking device.

The soot-path reference deposit recovered from a smoke meter set at the exhaust of a gasoline engine is related to a granular morphology presenting particulates agglomerated in Figure 61. The average diameter of deposited particles is < 100nm.

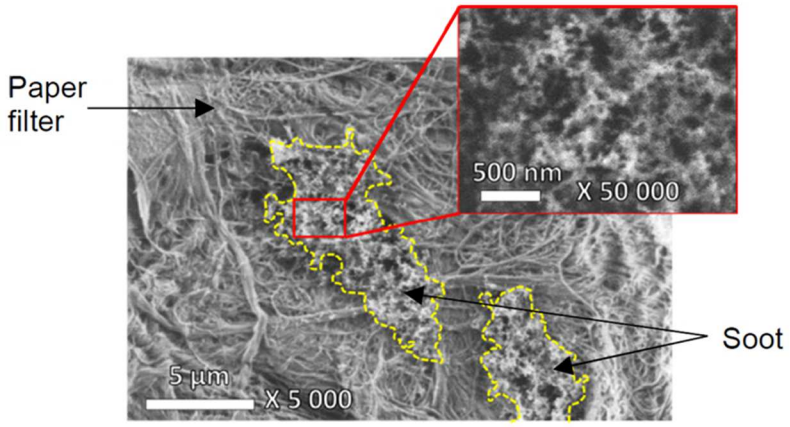

Figure 61: SEM image of soot-path deposit on a paper filter collected with a smoke meter from the exhaust of a SI engine; magnified 5000 times and 50,000 times.

The liquid-film-path and soot-path reference deposits show very distinct strucure. The liquid-film-path deposit morphology corresponds to a smooth surface with dispersed particles (diameters 0.2–1 µm). The

soot-path deposit shows granular particles with an average diameter below 100 nm forming large aggregates. These characteristic morphologies, if encountered when analyzing engine deposits, could help to identify the origin of engine deposits by determining which pathways are involved.

4.1.4 Chemical analyses

Two types of chemical analyses are carried out to characterize the reference deposits. They consist of two spectrometric techniques, the first is based on the study of the infrared absorption signal and the other on the study of the Raman signal. These two complementary methods will identify the specific chemical characteristics of each of the reference deposits. The analyses are carried out on the deposits formed on the aluminum plates, i.e., the deposit formed with the microcoking apparatus and the deposit formed with the soot generator.

4.1.4.1 Infrared absorption spectroscopy

The analysis of the infrared spectra of the deposits is carried out by a FTIR-ATR spectrometer. The operating principle is described in chapter 2. This analysis will identify the chemical functions of the two reference deposits. The objective is to identify absorption bands or peaks that are different between both reference deposits and thus, to identify their presence in the engine deposits.

Figure 62 shows the infrared spectra of the analysis of the reference liquid-film path deposit formed with the microcoking device. A broad –OH absorption band in the 3500–3000 cm^{-1} range is observed. A multi-peak absorption feature in the –C–H bonds region (2950–2800 cm^{-1}) is present. The infrared spectrum shows a C=O peak around 1730 cm^{-1} and a broad –OH band in the 3500–3000 cm^{-1}.

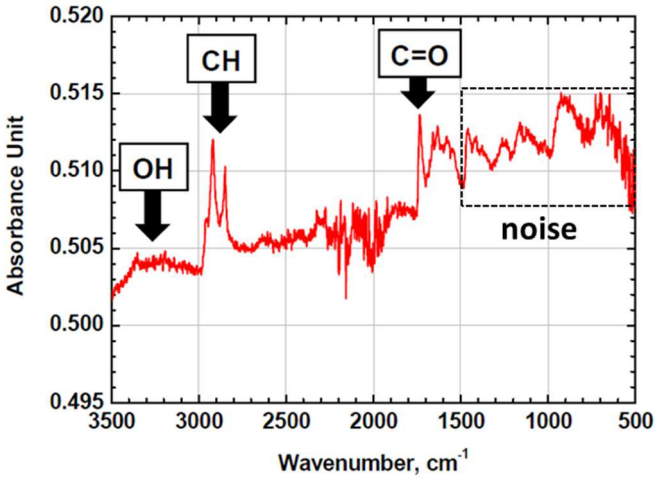

Figure 62: FTIR-ATR absorption spectra of liquid-film path deposit formed on aluminum plate with the microcoking device.

The infrared spectrum of the soot reference deposit is presented in Figure 63. As for the liquid-film path deposit, a broad –OH absorption band is observed in the 3500–3000 cm^{-1} range. In this range, there is the presence of a sharp peak centered at 3300 cm^{-1} with a shoulder at 3250 cm^{-1}. A single peak absorption feature is observed in the –C–H-bond region. There is a specific absorption in the 1500–1000 cm^{-1} range related to aromatic bonds.

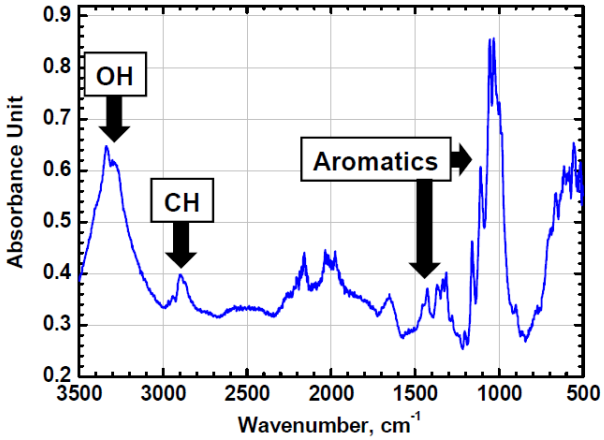

Figure 63: IR absorption spectra of soot path deposit sampled from a paper filter from a smoke meter at the exhaust of SI engine.

The differences observed for the –OH and –C–H regions of the spectra are not significant, especially considering that these deposits are reference cases obtained in the laboratory under well-controlled conditions. It is difficult to identify specific characteristics that would enable to distinguish the formation pathways when analyzing engine deposit obtained under real conditions.

The band around 1730 cm^{-1} corresponding to –C=O group is a specific absorption band of the liquid-film path deposit, but the signal is weak and noisy. Engine experiments are needed to conclude if these regions of the spectra could be used to distinguish both deposit formation pathway and to conclude on this methodology.

4.1.4.2 Raman spectroscopy

The analysis of the Raman spectra also aims to determine the specific chemical features of the reference deposits. The bibliography has already highlighted the existence of two G and D bands at 1350 and 1600 cm^{-1} in the Raman signal of soot, which are characteristic of the presence of carbon. The analysis will focus on the determination of the intensity, the FWHM of these two peaks between 800 and 2000 cm^{-1} of the two reference deposits. The objective is also to identify the existence of other zones of the Raman signals specific to each of the two deposits.

Figure 64 shows the Raman signal of the liquid-film path deposit. The signal observed cannot be interpreted due to noise related to the low quantity of deposit combined with interference from fluorescence of the sample.

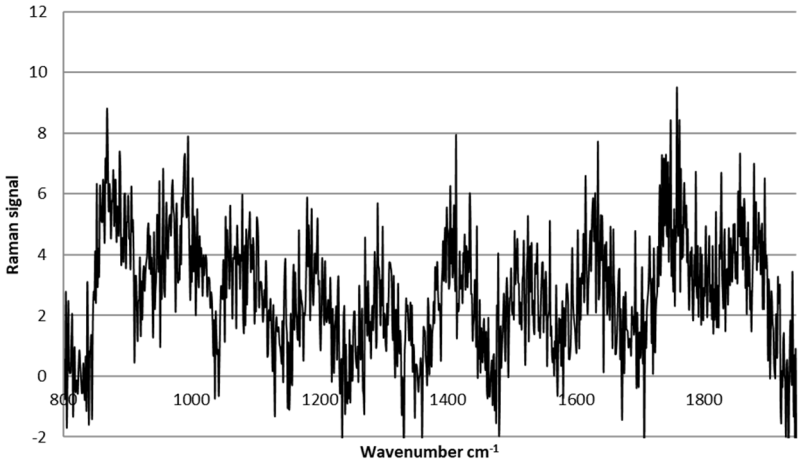

Figure 64: Raman signal (affected by strong fluorescence interference) of liquid-film path deposit formed on an aluminum plate with the microcoking device.

The Raman signal of the soot-path reference deposit is presented in Figure 65. The two characteristic peaks related to carbonaceous material defined in the chapter 3 are observed. The D peak at 1350 cm^{-1} and the G peak at 1604 cm^{-1}. The ratio of the value of the intensity of the peak G over the intensity of the peak D is 1.15. The FWHM of the two peaks is 121 and 68 cm^{-1} respectively.

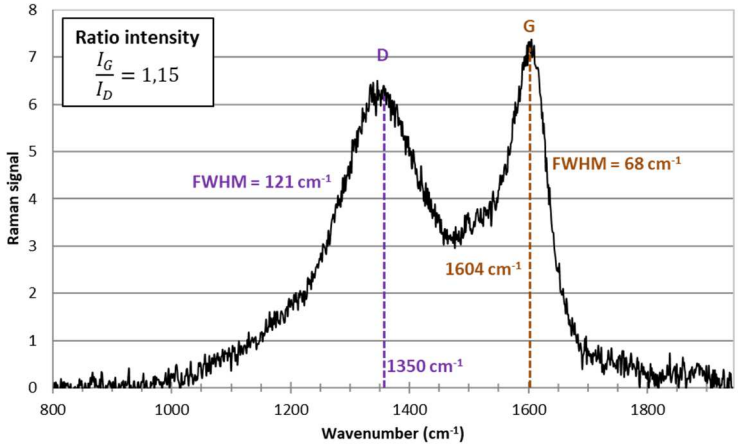

Figure 65: Raman signal of soot path deposit sampled from a paper filter of a smoke meter at the exhaust of a SI engine.

The Raman signal for the liquid-film path therefore cannot provide information on the presence of liquid-film path in engine deposit. Regarding the analysis of the soot-path mechanism, two characteristic peaks corresponding to the structure of carbon at 1350 and 1600 cm^{-1} were identified as indicative. Analysis will be carried out on the engine deposit to determine the capacity of the technique to identify the presence of the G and D peaks.

In the literature, it has been shown that analysis of the value of the D/G and FWHM ratios of the G and D bands indicates the degree of graphitization of carbonaceous materials. These analyses will be carried out on engine deposits in order to determine a possible trend [101].

4.1.5 Conclusions on the reference deposits characteristics

Macroscopic and microscopic analyses allowed to characterize the two reference deposits. They have highlighted significant differences that will help to distinguish between the deposits from the liquid-film

path and the soot path in engine deposits. The liquid-film path deposit is characterized by a transparent, shiny and smooth appearance. At the microscopic level its morphology is also characterized by a smooth surface which includes large areas of around 15 µm but also small traces with a diameter of around 200 nm. The soot path deposit has a black, matt appearance. Its morphology observed by microscopy corresponds to agglomerates of particles with a diameter of about 100 nm.

The infrared spectra analysis enabled the identification of the infrared absorption bands and peaks of the two types of deposit. However, several of these absorption zones are present in the two reference deposits which will complicate their attribution in engine deposits analysis. The Raman spectra analysis provided interesting results for the soot path deposit but not for the liquid-film path deposit. This method will then not allow to distinguish the reference deposits in the engine deposits. However, the observation of the G and D peaks in the engine deposits will confirm the presence of soot path deposit and their analysis may show trends.

Firstly, the analyses of engine deposits will be based on macroscopic and microscopic analyses which are two promising techniques. Secondly, the relevance of the chemical analyses based on the study of infrared spectra and Raman signals will be discussed at the end of the chapter.

4.2 Influence of the sampling location in the combustion chamber on deposits visual appearance and morphology

In this section an engine experiment is carried out to study the impact of the sampling location on the visual appearance and morphology of the deposit. For each engine part sampled, the analysis will focus on the color, texture and surface condition of the deposits. Then, the morphology will be observed by microscopy to identify the structures present and describe the existing morphologies.

4.2.1 Engine experiment description and analysis of the different sampling location deposits formed with the 400 cm^3 engine

The engine experiment is carried out with the 400 cm^3 engine described in Chapter 2. The injection time is set at 60 CAD BTDC, the water-cooling temperature at 20 °C and the test duration at 10 min. Three locations of interest were chosen to sample deposits: Intake side of the cylinder, injector nozzle and piston surface. Each sample is analyzed following the protocol established for the reference deposits studied in previous section, i.e., macroscopic and microscopic analysis. Representative results are presented in Figure 66.

The macroscopic analysis shows that the deposit formed on the intake side insert has a black color and its texture is matt (Figure 66a). The appearance of the deposit is homogeneous over the entire surface of the intake side insert and it is possible to observe the aluminum surface underneath the deposit layer. Observation by the SEM-EDS microscopic system of the deposit at the intake side insert reveals different information about its morphology depending on the level of magnification. Observations of the order of a hundred to ten microns show a flat surface with the presence of structures similar to big grains of the order of 10 µm. Below the micrometer, the big grains and the flat surface have a similar morphology corresponding to a mixture of particles with smooth surfaces and holes. The results of the macroscopic analysis are similar to those of the reference soot path deposit. Also, the presence of particles and smooth surfaces morphologies were respectively observed in the reference deposits corresponding to the soot path and the liquid-film path.

The injector nozzle also has a black and matt visual appearance (Figure 66b). Microscopic observations show the presence of flat surfaces and big grains ranging from 5 to 15 µm. At submicron scales, the morphology is similar between the flat surface and the big grains. As with the insert, it corresponds to smooth surfaces, particles and holes. The visual aspect of the injector nozzle deposit is similar to the reference soot path deposit and these morphologies were observed in both reference deposits microscopic observations.

A black deposit with a matt appearance covers the piston surface (Figure 66c), except for six light areas. These areas form a pattern that can be related to the sprays from the six holes of the injector. To establish the morphology of the piston surface two different types of areas are defined. The corresponding black and lights areas are separately analyzed. On a scale of about ten microns, the deposit in the light areas appears to be made up of large structures of the order of 10 µm which sometimes meet and form grooves. Below the micrometer, these large structures appear as clusters of particles with an average diameter below 100 nm. The grooves are composed of smooth surfaces and particles. For the black zone, the deposit is uniformly composed of a layer of particles. The morphology of the light areas seems to correspond to the liquid-film path and the soot path deposits. The morphology of the black zone seems to correspond to the soot path deposit only. The black area has a similar appearance and morphology to the reference soot path deposit. The light areas deposit has an appearance like the reference liquid-film path deposit. The morphologies of these zones have the same characteristics as the two reference deposits with smooth surfaces and particles.

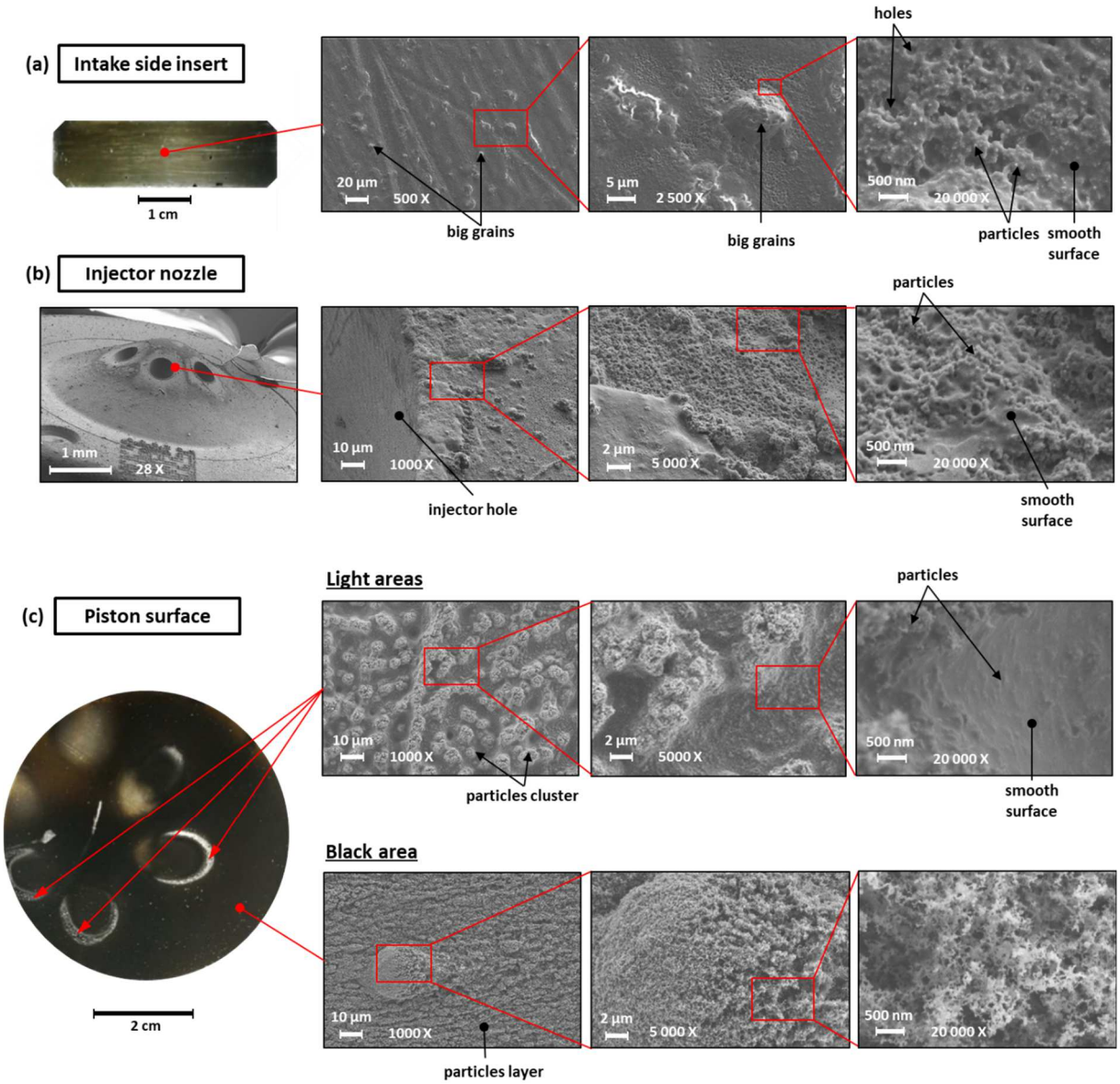

Figure 66: Microscopic observations of deposits on different sections of the combustion chamber from experiment 2 with the 400 cm^3 engine. (a) Intake side insert, (b) injector nozzle, (c) piston surface.

4.2.2 Conclusions on the influence of the sampling location in the combustion chamber on deposits visual appearance and morphology

Macroscopically, the deposits formed at the intake side insert and at the injector nozzle have similar appearances with a black color and a matt texture. Their morphology is also similar which are both formed from particles and smooth surfaces. Therefore, it appears that there is no significant difference in the effect of the sampling location on the visual appearance and morphology between the intake-side insert and the nozzle injector.

The piston seems to be the most interesting sampling location. Indeed, the surface of the piston shows visual differences from the other two sampling locations with the existence of a pattern with six light areas and one black area. For the morphology, the light areas present a smooth surface and particles morphologies. The particles form cluster of the order of 10 µm. The black area morphology presents a uniform layer of particles with an average diameter under 100 nm. These macroscopic and microscopic

characteristics are comparable to the characteristics of the reference deposits, which involve very distinct mechanisms.

4.3 Influence of the engine geometry on deposits visual appearance and morphology

This section investigates the effect of engine geometry on the visual appearance and morphology of the piston deposits. The objective is to determine the possibility of using two different engines operating under similar operating conditions to form identical deposits. A new piston deposit is formed with the 462 cm^3 engine under the same operating conditions as the piston deposit formed with the 400 cm^3 engine presented in the previous section. This deposit is then analyzed macroscopically and microscopically. The results obtained with the 462 cm^3 engine are compared with the results obtained with the 400 cm^3 engine.

4.3.1 Engine experiment description and analysis of the piston deposit formed with the 462 cm^3 engine

The engine experiment is carried out with the 462 cm^3 engine described in Chapter 2. As for the piston deposit formed with the 400 cm^3 engine presented in the previous section, the engine parameters set for the 462 cm^3 engine are the same: the injection timing is set at 60 CAD BTDC, the water-cooling temperature at 20 °C and the test duration at 10 min. The piston deposit is analyzed following the protocol established for the reference deposits studied in previous section, i.e., macroscopic and microscopic analysis. Representative results are presented in Figure 67.

Macroscopic observations show two distinct deposit areas: A black area and six light areas. The black area covers almost the entire piston. It presents a black color with a matt texture. The six-light area form a pattern that can be related to the spray from the six holes of the injector. These initial observations show a great similarity with the observations of the macroscopic analysis of the piston deposits formed with the 400 cm^3 engine. The same pattern and the same two areas of deposits identified in the previous section are found.

For the light areas, the morphology observed at a scale of about 10 µm consists of structures that are 5 µm wide with the presence of smooth surface. In comparison with the piston deposit of the 400 cm^3 engine, the same morphologies are observed with the 462 cm^3 engine. Here, the black area consists of a homogeneous layer of particles with a diameter of less than 100 nm. The same morphology is found in the black area of the deposit formed with the 400 cm^3engine.

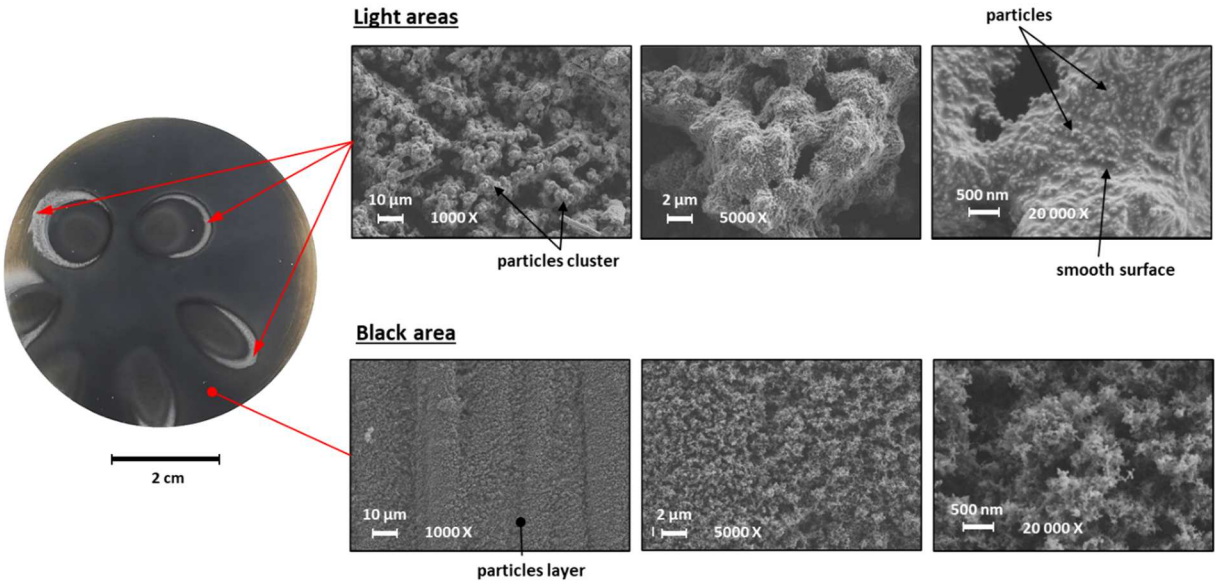

Figure 67 : Comparison of macroscopic and microscopic images of the deposits formed with the 462 cm^3 engine B

(late injection case at cold-start condition).

4.3.2 Conclusion

In conclusion, the geometry of the two engines does not have a significant impact on deposit formation. Indeed, the same morphologies are observed with some differences in the size of their structures. These differences are considered insignificant in this study and are related to measurement repeatability biases. Then, the analyses of deposits formed with the same parametric variations but with different engine geometry can be compared.

4.4 Influence of the injection timing on deposits visual appearance and morphology

This section looks at the effect of injection timing on piston deposit formation. Indeed, by modifying injection timing, the air/fuel mixing duration and the distance between the nozzle and the piston surface will also be modified. These two factors could impact the appearance and morphology of the deposits. The objective is first to determine which phasing produces the most deposit, and then to identify the injection timing that will allow the separate study of liquid-film path and soot path deposits. The analysis of the deposits will focus on visual and macroscopic observations. The deposits will be then analyzed by FTIR-ATR and Raman spectrometry to conclude on the usefulness of these two methods in the identification of the liquid-film path and soot path.

4.4.1 Description of the engine experiments

Table 6 describes the experiments of deposit formation realized for different injection timing. Three cases are studied. The first consists of a standard injection to limit the formation of liquid film and soot. This experiment lasts 120 min to obtain a sufficient amount of deposit for the analyses. The second case is an early injection timing where the mixing duration is longer to limit soot formation, and the distance between the piston and the nozzle is the shortest to encourage the formation of a liquid fuel film. The

third case is the late injection timing, already studied in the previous section, to limit the mixing time and encourage soot formation. For early and late injection cases, both experiments last 10 min. At the end of each experiment, the piston is sampled, and the deposit is analyzed first by SEM-EDS. The piston deposits are then analyzed by FTIR-ATR and Raman spectroscopy measurements.

Tableau 1: Deposits formation engine experiments and their parametric variations

Experiment name	Engine	$T_{cooling\ water}$ /°C	Injection timing /CAD before TDC	Test duration /min
Standard injection	400 cm^3	20	260	120
Early injection	462 cm^3	20	360	10
Late injection	462 cm^3	20	60	10

4.4.2 Macroscopic and microscopic analyses

Before analyzing the deposits resulting from the various engine experiments, a deposit-free surface is presented in Figure 68. The surface of the aluminum piston has a metallic grey appearance with shiny aspect. The surface is not smooth, it has circular machining marks all over the surface corresponding to a measured roughness of *Ra* = 1.2 µm. These machining marks are also visible by microscopic analysis. They can be clearly distinguished in ranges between 1 and10 µm in Figure 69. These images will serve as reference image to discriminate deposits morphologies from raw piston surface.

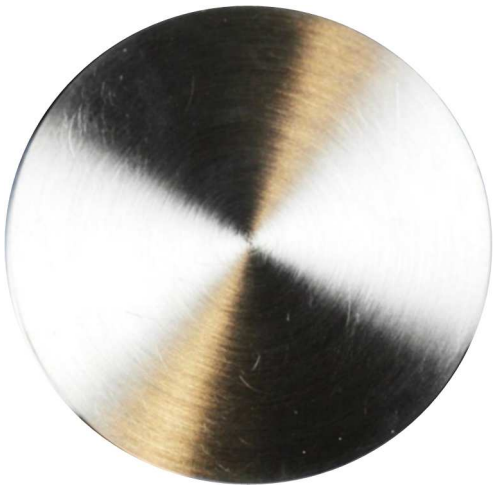

Figure 68: Surface of a clean piston.

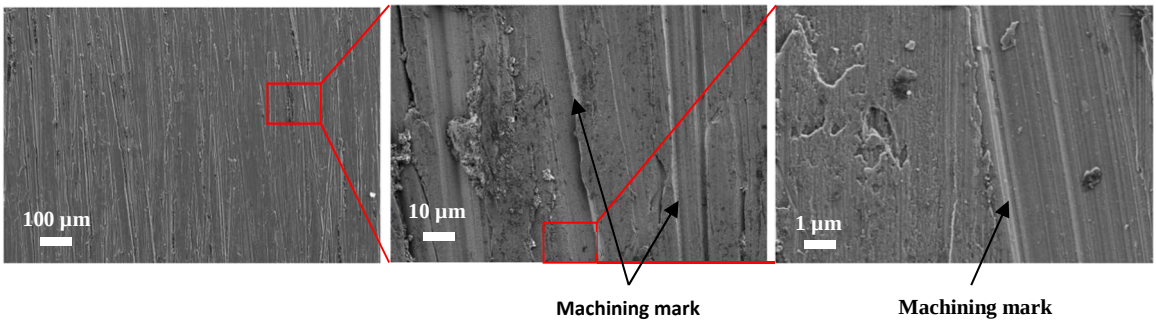

Figure 69: SEM images of the surface of a deposit-free piston.

The piston deposit formed at the end of the standard injection case is presented in Figure 70. The color of the piston surface remains almost entirely metallic grey, but it looks more matt than the free-deposit piston. The piston also presents a black deposit area covering 20 % of the piston surface and a deposit forming a black circular arc.

The microscopic analysis of the grey surface shows machining marks and particles with an average diameter of less than 100 nm. The microscopic observations of the black deposit show that this deposit corresponds to a layer of particles with an average diameter of less than 100 nm that are much more frequent in numbers than the metallic grey deposit. It is not possible to distinguish the machining marks at scales smaller than 2 µm. This indicates that the deposit is thicker. The deposit forming the black circular arc has a smooth surface and presents additional particles.

The smooth surface morphology characterizing the liquid-film-path reference deposit is observed on a very small surface of the piston. Particles corresponding to the soot path reference deposit are observed on all the piston surface with different concentrations. The standard injection strategy limits the formation on both the liquid-film path deposit and the soot path deposit. Indeed, by injecting fuel at 260 CAD BTDC, the impact of the spray is very limited. This engine setting corresponds to a standard operation optimized to obtain the least amount of exhaust emissions. In the context of this work, this operating point is not interesting because it does not favor deposit formation.

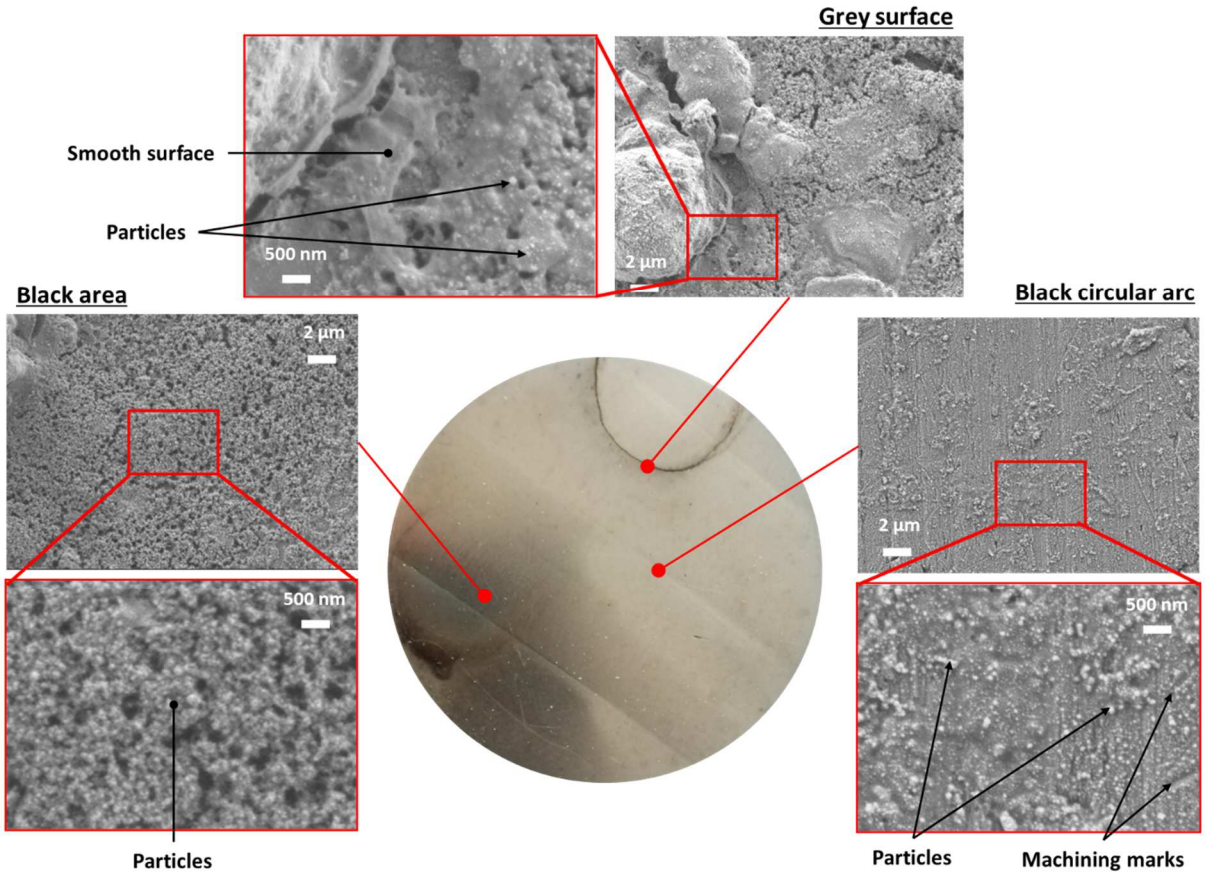

Figure 70: Macroscopic observations by SEM-EDS of the experiment 7 standard injection case.

The piston deposit formed during the early injection case is presented in Figure 71. The piston has a deposit in the shape of a flower with 6 petals. These can be related to the six sprays of the injector nozzle. These petals have different colors and textures identified in five different zones. These zones are called

“black area”, “black area periphery”, “brown area”, “spray impact periphery” and “spray impact core”. The black area has a black color and a matt appearance. The black area periphery consists of black fringes. The brown area has a brown color with a matt appearance. The spray impact periphery is black with an iridescent appearance. The spray impact core has a metallic grey color with a matt appearance. All these areas have a smooth texture except for some areas of the black area which present some cracks.

The microscopic analysis shows that all these zones have a smooth surface morphology. This morphology has been found in the reference deposit formed with the microcoking which is attributed to the liquid-film path. A granular morphology is also observed with the presence of particles of an average size inferior to 100 nm. This specific morphology was observed in the reference deposit formed with the gasoline engine which is attributed to the soot path. The spray impact core presents a different morphology with a grainy surface. Nevertheless, it could correspond to a mixture of deposits formed from the liquid-film path and the soot path. Compared to the standard injection case, the early injection strategy appears then to greatly favor the liquid-film-path mechanism.

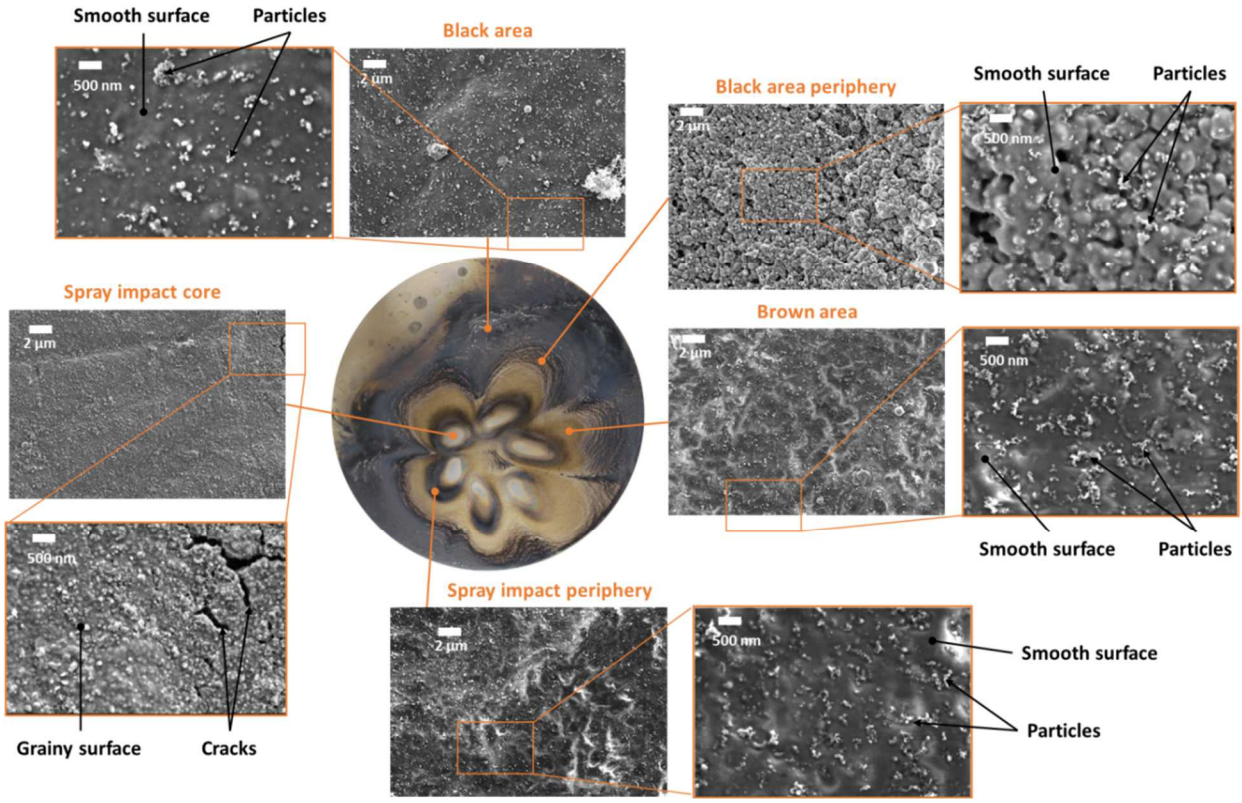

Figure 71: Macroscopic observation by SEM-EDS of early injection case (experiment 4).

The piston corresponding to the late injection case in Figure 72. Here, the different deposit areas are presented in more details. As seen before, the piston presents a surface almost entirely covered with a black color deposit with a matt texture. The piston deposit has a pattern with six light areas related to the six spray cones generated by the injector. Three areas are identified. First, the black area corresponds to the black deposit area on the periphery of the piston. The second area corresponds to the spray impingement. It consists in six light areas and six impact areas associated with each of the six spray impacts. The last area is the middle spray area located at the central area of the piston.

The morphology of the black area and the spray middle area is composed of a layer of particles with a diameter inferior to 100 nm corresponding to the soot path mechanism. The impact area also shows the

presence of particles but at a scale of 2 µm the particles group together in structures of the order of 2 µm in diameter. The comparison with the early injection case shows a stronger contribution from the soot-path mechanism which validates the late injection strategy set to limit the air/fuel mixture time and promoting rich zones, suitable to soot formation. The clear area is the only zone where a smooth layer morphology is observed with the presence of particles. Nevertheless, if a smooth layer cannot be directly observed for the other zones, the presence of a pattern like the injection scheme tends to exhibit that the liquid film mechanism could be present as well.

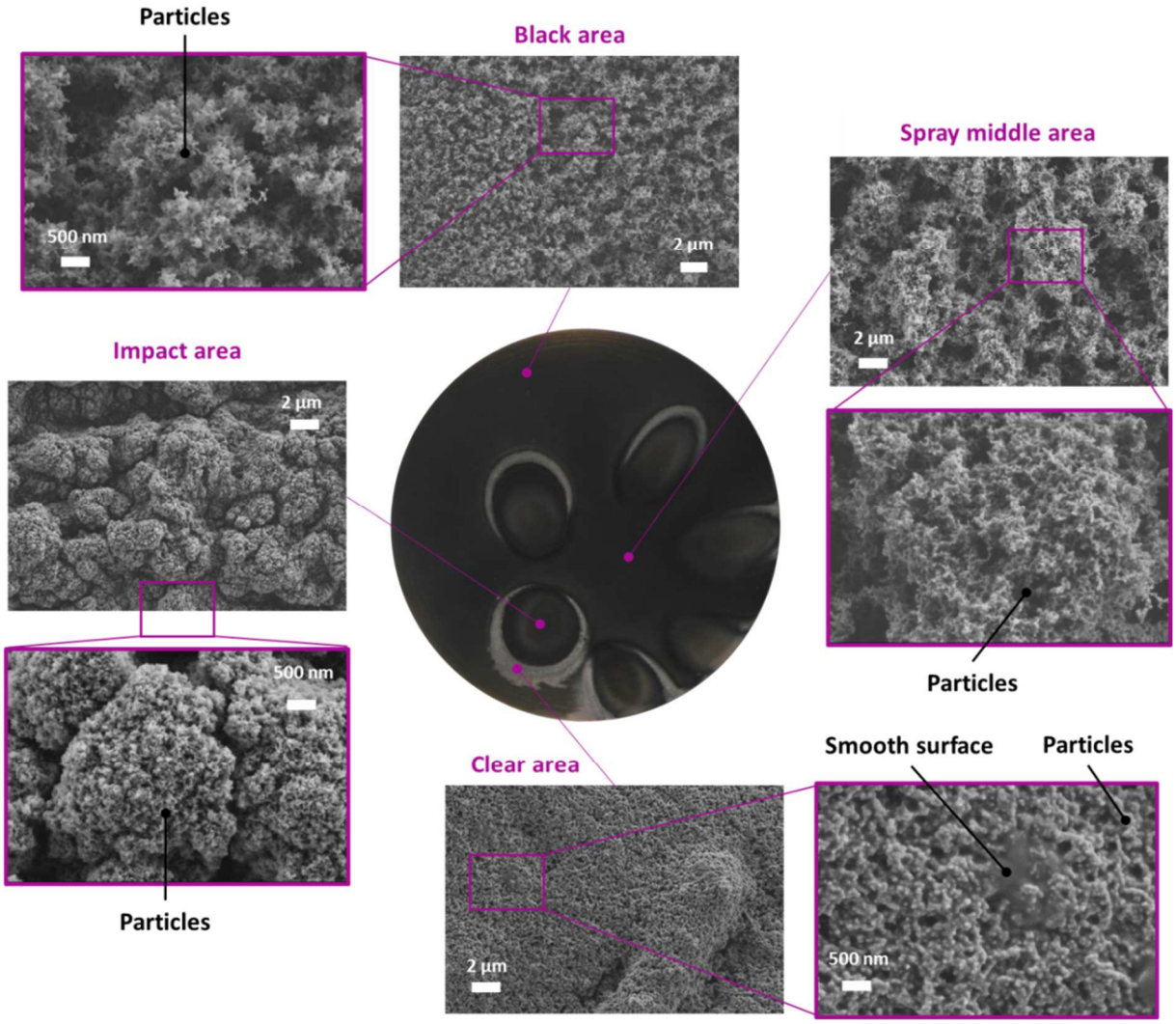

Figure 72: Macroscopic observation by SEM-EDS of late injection case (experiment 5).

4.4.3 Conclusions on the influence of the injection timing on deposits visual appearance and morphology

Morphological analysis of the piston deposits shows the presence of smooth surfaces and particles. In comparison with the reference morphologies, these deposits are associated with both the liquid film path and the soot path mechanism. Early injection and late injection present both deposit pathways but in different proportion. Early injection promotes the liquid-film path deposit and the late injection promotes the soot-path deposit. This result is coherent because early injection causes spray impingement that can favor the formation of a liquid film and the late injection leads to a short mixing time resulting in rich zones thus promoting soot formation. Therefore, the microcoking device and the smoke meter seem to

reproduce the morphology of the engine deposit pathways. Compared to these two piston deposits obtained in 10 min, the deposit formed with standard injection during 120 min shows very few deposits. Therefore, this injection case will not be studied further in the rest of the study. Another conclusion is that, although both mechanisms seem to be involved, the chosen engine operation parameters each favors one mechanism.

4.5 Determination of the usefulness of FTIR-ATR and Raman spectroscopy to characterize engine deposits chemical properties

This section aims to determine the possibility of identifying the chemical signatures characterizing reference engine deposits by FTIR-ATR and Raman spectroscopy analysis. The analyses are carried out on both early and late injection piston deposits. For each analysis, the results are compared with those of the laboratory reference deposits.

4.5.1 Infrared spectroscopy analysis

Deposits obtained from the engine experiments were analyzed and compared to the ones obtained with the microcoking device and the soot sampled with the smoke meter. Infrared spectroscopic analyses were carried out on the black area deposits for both injection cases because the other zones did not provide sufficient material for the measurement.

The signals obtained of the piston deposit for early and late injection cases are compared with the liquid-film path reference deposit (formed with the microcoking device) in Figure 73. The same multi-peak absorption corresponding to the –C–H bonds as well as the broad –OH band region are found for the engine deposits and the liquid-film path reference deposit. This result shows the presence of a liquid-film path deposit in the engine deposit. Both engine deposit cases show a spectrum with strong noise.

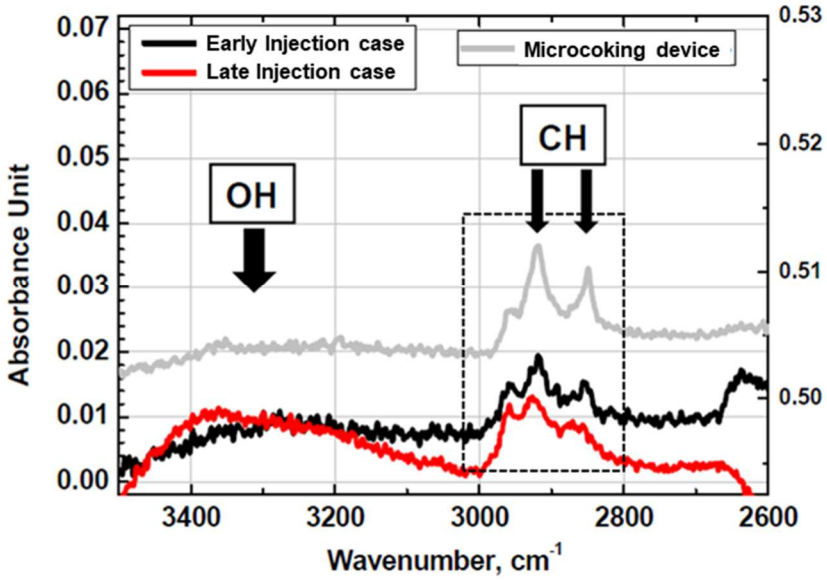

Figure 73: IR absorption spectra for engine deposits and liquid-film path deposit formed with the microcoking device.

The infrared absorption spectra measured from engine deposits are compared with those determined from the soot-path deposit formed from the smoke meter (Figure 74). Typical absorption features of

aromatics identified on the soot IR spectrum are weak but not completely absent. Probably a larger amount of sample is necessary to obtain a better signal.

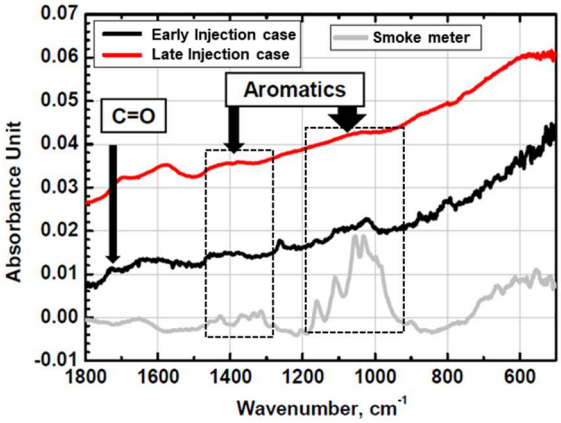

Figure 74: IR absorption spectra for engine deposits and soot-path reference deposit.

The FTIR-ATR spectra of deposits obtained with the microcoking device and the smoke meter show typical absorption features that can be distinguished and related to the two formation paths. Comparison with spectra measured on engine deposits show that these features can be identified. The –CH bond feature with multiple peaks, representative of aliphatic components, as well as the carbonyl function -C=O appears as a good tracer for material generated via the liquid-film-path mechanism. Moreover, because the FTIR spectrum of the reference soot deposit presents an absorption feature with a single peak in the same region, this part of the spectrum contains information suitable to identify the source of the deposit. Nevertheless, the FTIR technique appears to require larger amounts of deposit to provide measurements with less noise to enable the identification absorption bands indicating the presence of aromatics that are the typical footprint of soot.

4.5.2 Raman spectroscopy analysis

Raman spectroscopy analysis was carried out on the piston deposits formed at early and late injection timing. The analysis was performed on the different deposit areas identified for the two pistons. The results of the Raman such as peak positions and peak intensities were then compared with the ones from the reference soot-path deposit.

Figure 75 shows the six areas analyzed by Raman spectroscopy materialized by green dots. No interpretable signal was obtained for zones Z_4, Z_5 and Z_6. Zones Z_1, Z_2 and Z_3 show two peaks D and G around 1390 and 1610 cm^{-1} characteristic of carbonaceous materials. The peak ratio values of the D and G peaks are similar for the three zones with an average value of 1.65. There is some discrepancy in the FWHM values attributed to signal noise, making it difficult to determine the FWHM value. These two peaks are also identified in the soot reference deposit, although the soot reference deposit present a lower peak value at 1.15.

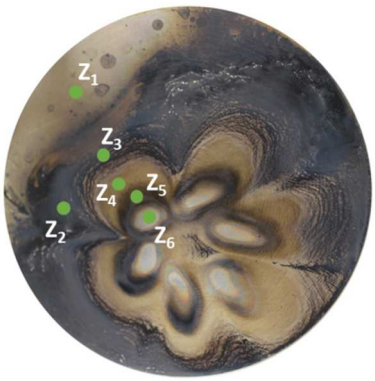

Figure 75 : Location of the Raman analysis zones Z_n (green dots) for the early injection case.

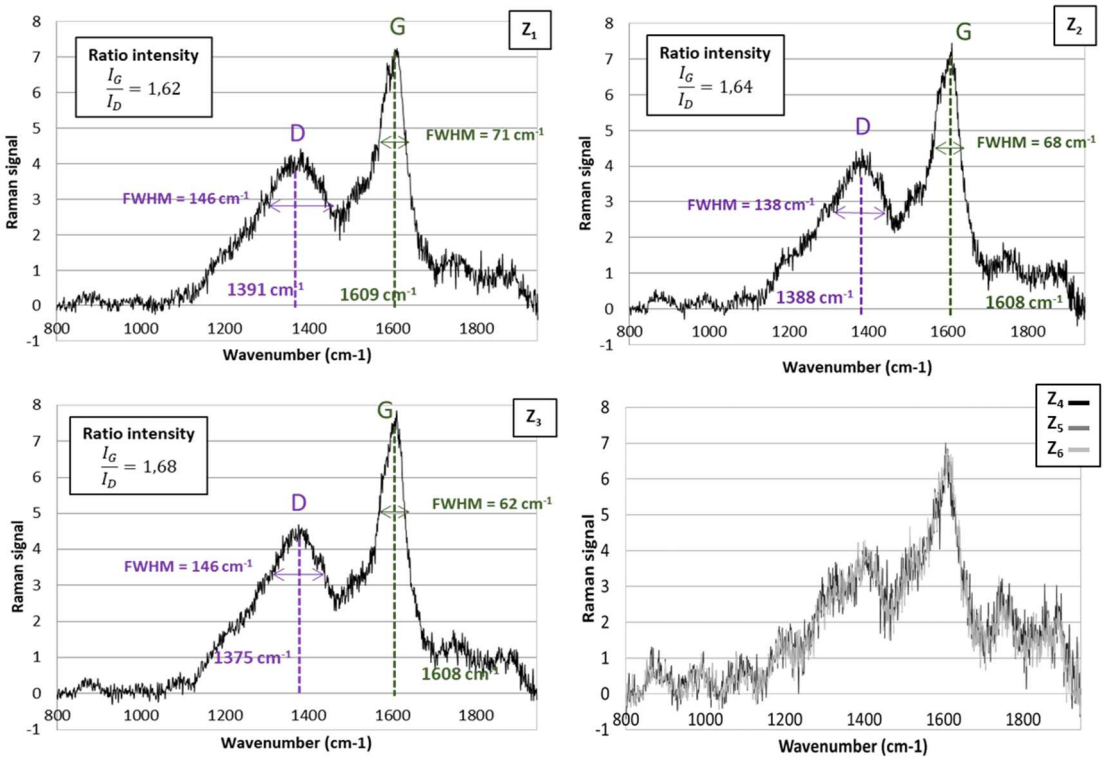

Figure 76 : Raman signal of zones $Z_{1\to6}$ for piston deposits from early injection experiment.

For the late-injection case, Figure 77 shows the location of the Raman measurements on piston top surface with the green dots. No interpretable signal was obtained for the zone Z_1 and Z_2. This is due to a signal saturation which was not possible to avoid. The two peaks D and G characteristic of carbonaceous materials are also identified around 1350 and 1600 cm^{-1}. However, the high signal-to-noise ratio for zone 3 makes it difficult to determine the exact position of the peaks and therefore makes the FWHM values of the two peaks uncertain. The Raman signal for zone 4, on the other hand, has a low signal-to-noise ratio. The value of the peak intensity ratio is 1.53 and the FWHM values of peaks D and G are 121 and 68 cm^{-1}, respectively. These values are different from those of the reference soot deposit.

Figure 77 : Location of the Raman measurement zones Z_n (green dots) for the late injection experiment.

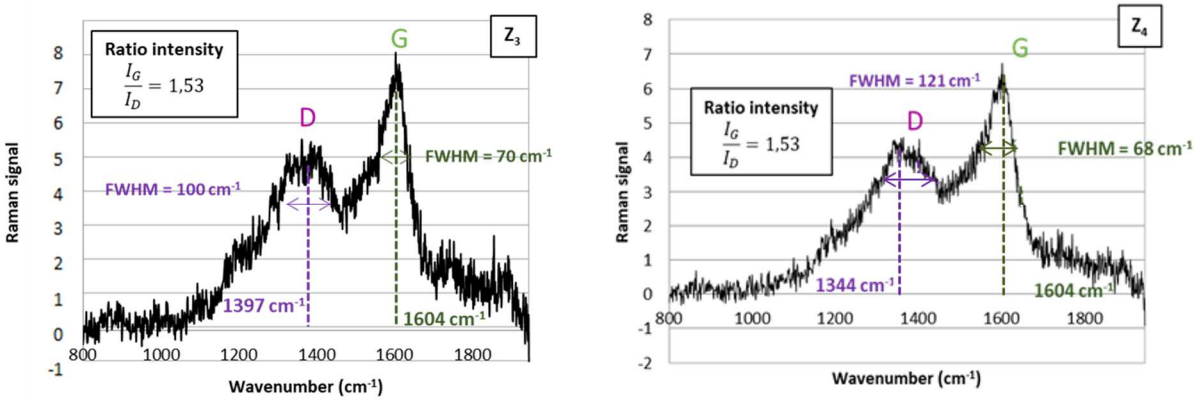

Figure 78: Raman signal of zones Z_3 et Z_4 for piston deposits from the late injection case experiment.

4.5.3 Conclusions on the usefulness of FTIR-ATR and Raman spectroscopy to characterize engine deposits chemical properties

Figure 79 shows the peak ratio of the different zones of the analyzed deposits. Given the measurement uncertainty presented by an error bar, there is no significant difference between the case of early and late injection, whereas the microscope showed significant differences in the morphology of the engine deposits that seem to indicate different deposit origins. Also, the peak ratio value for the reference soot-path deposit is 1.15, which is much lower than the peak ratio of the engine deposit in the late injection case of zone 1 which is equal to 1.6, even with both presenting a similar morphology. This technique does not make it possible to dissociate the mechanisms of the liquid-film path and the soot path in motor deposits and therefore does not help to identify the mechanisms responsible for the formation of the deposit. In addition, the line width of the Raman signals cannot be interpreted because of the important noise of the measures.

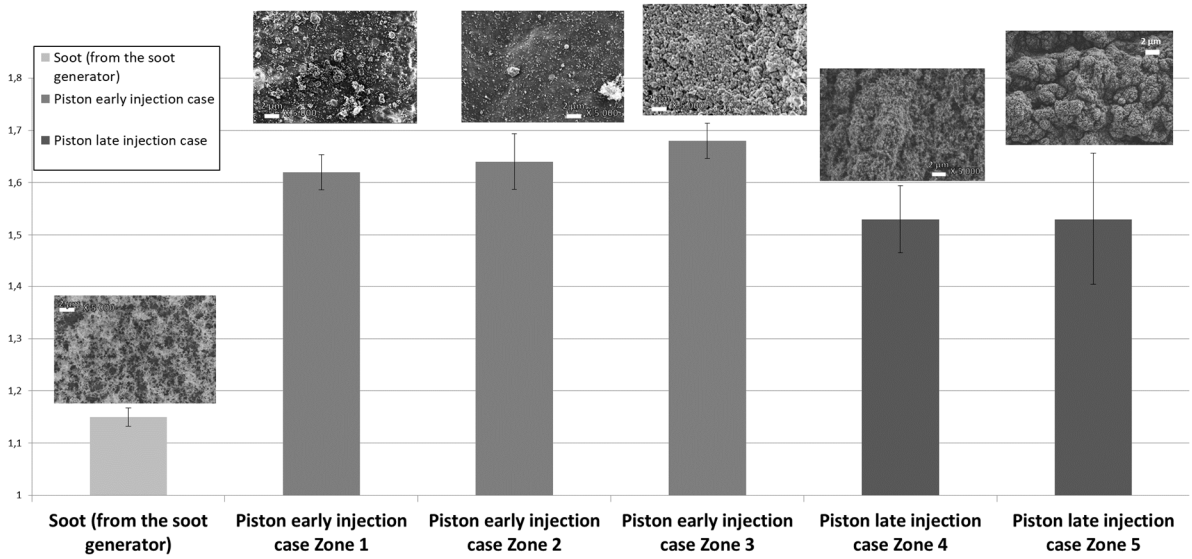

Figure 79 : Peak ratios I_D/I_G of the soot reference deposit and the piston deposits zones for the early and late injection cases.

4.6 Conclusions on the methodology to study engine deposits

The characteristics of the reference deposits were determined macroscopically and microscopically. The reference deposit corresponding to the liquid film path has a transparent color and a glossy appearance with a smooth surface morphology. The deposit corresponding to the soot path has a black color and a matt appearance with a particle morphology.

The deposits formed for different engine parameters were analyzed using the same methodology. The results showed that the location in the combustion chamber has no significant impact on the appearance and morphology of the deposits. The piston deposit has a particular pattern attributed to the impact of the spray on the surface. This area of the combustion chamber is selected in the rest of the study. Then, the effect of engine geometry on the deposits was studied. This study showed that the deposits can be studied independently of the two engines used in the study. Finally, different engine experiments were carried out to form deposits on the pistons for three different injection timing. Two injection timing were chosen: the first is early injection at 360 CAD BTDC which forms deposits with a morphology essentially corresponding to the path of the liquid film; the second is the late injection at 60 CAD BTDC which contributes largely to the deposit formation with a morphology corresponding to the soot path. These two injection timings will enable the study of the mechanisms of both deposit formation pathway.

In addition to macroscopic and microscopic analyses, FTIR-ATR and Raman spectroscopic analyses were evaluated. The objective was to determine the ability of these techniques to identify chemical signatures corresponding to reference engine deposits. FTIR-ATR spectroscopy made it possible to identify the presence of a deposit formed from the liquid film path for early and late injection cases, but not for the soot path. The technique does not provide information on the proportion of deposit for each pathway. The use of FTIR-ATR spectroscopy is then excluded for the following work performed during this thesis. For the Raman analysis, no information could be extracted for the reference deposit for the liquid film pathway and no correlation was found between the morphology and the information derived from the peak analysis. Therefore, the technique does not allow a correlation between carbon structure and morphology. The use of Raman spectroscopy is hence also excluded hereafter. The method used to determine the origin of engine deposits provides only qualitative information.

5 ENGINE DEPOSITS FORMATION MECHANISMS

The objective of this chapter is to provide an understanding on engine deposit formation mechanisms. The strategy is to isolate the two deposit formation pathways to study their mechanisms separately. The early injection condition is used to study the mechanisms of liquid-film path formation and late injection to study the mechanisms of soot path formation. The mechanisms identified for each of the formation pathways are then compared for each of the injection strategies. Firstly, the operating conditions and the type of analysis performed are presented. The study is then divided in two sub-sections: the first concerns the liquid-film path and for the second the soot-path mechanism. In a third section the mechanisms are compared with each other. The conclusions present the deposit formation scenarios deduced from the previous analyses.

5.1 Description of engine experiments

The experiments are carried out with the 462-cm^3 engine described in chapter 3 that is equipped with optical access to enable high-speed imaging of the piston surface. Table 7 presents the parametric variations for two injection strategies. For the early injection timing strategy, experiments under two conditions were carried out with different initial piston surface temperatures. The objective is to characterize the behavior of the liquid film as a function of surface temperature to highlight the physical mechanisms in the liquid film. The first experiment starts at a piston temperature of 20 °C to represent cold-start conditions, called “cold-start case”. The second experiment begins after a 2-minute preheating of the engine through operation with port fuel injection (PFI), called “warm-start case” (see chapter 3). At the end of the warm-up phase, the piston surface temperature is 133 °C. At this time, PFI is switched off and the 10-minute experiment with direct fuel injection (DI) starts. For the late DI injection timing case, the experiment starts with an initial piston temperature of 20°C corresponding to the cold-start case.

Table 7: Table of engine experiments with the 462 cm^3 engine

Injection strategy	Start condition	Injection phasing /CAD BTDC	Injection duration /ms	Ignition phasing /CAD BTDC	Initial piston surface temperature /°C	Expriment duration /min
Early injection	Cold start case	360	1.85	13	20	10
	Warm start case	360	1.85	13	133	10
Late injection	Cold start case	60	1.85	13	20	10

The temporal variation of the piston surface temperature are shown in Figure 80. The temperatures were measured by phosphor thermometry (see Chapter 3). Two characteristic phases 1 and 2 are observed and defined as: Phase 1 corresponds to the first two minutes of the experiment, when the difference between the piston temperature in the two cases is greatest, while Phase 2 starts at 2 min and continues until the end of the experiment. It corresponds to the moment when the two temperature profiles start to converge and reach a similar final temperature at the end of the experiment.

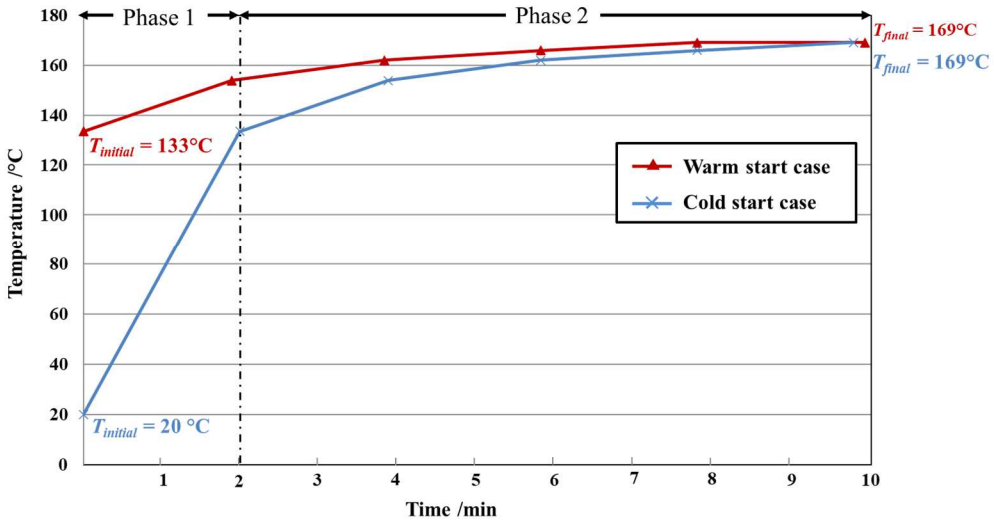

Figure 80: Variation of the piston surface temperature during engine experiment for cold and warm start.

For each experiment, two types of analysis are carried out. First, an *in situ* analysis is carried out during the experiment which consists of using the high-speed camera to observe the deposit formation and the phenomena occurring in the combustion chamber such as near wall combustion or liquid films. In the exhaust gases, particle-size distributions were measured with a DMS 500. This analysis enables the correlation of particulate emissions with the presence of soot-related deposits. After the end of the experiment, the piston surfaces are analyzed *ex situ* using the methods described in the previous chapter.

5.2 Contribution of the liquid-film path mechanism to deposits formation

The piston deposits formed in the cold start and the warm start cases at early injection are first analyzed to study the liquid-film path mechanism. This section will focus on establishing a correlation between the presence of a liquid film and the deposit formation. The piston deposits are compared using macroscopic, microscopic, and *in situ* analyses of the piston samples. The observed deposits corresponding to the soot-path are deliberately not considered in this section and are the subject of the following section.

5.2.1 Macroscopic analysis

Figure 81 displays macroscopic images of the piston deposits formed at cold- and warm-start conditions for early injection. Characteristic deposit patterns are observed on the piston surfaces (Figure 81). There are two zones: An inner zone corresponding to the impact core of the spray and an outer zone corresponding to the rest of the piston surface. They are described separately in the following paragraphs.

The inner zone is similar for both pistons. It corresponds to a central pattern composed of six zones (marked in red in Figure 81). Each zone consists of a light core and a dark outline called the spray impact core and the spray impact periphery, respectively. Since these areas correspond to the impact points of the liquid spray, it seems reasonable to link this central pattern to the formation of a liquid film during the experiment.

The outer zone is the entire area between the red contour and the edge of the piston in Figure 81. This area exhibits differences between the warm- and cold-start cases. In the former, the outer zone corresponds to a brown area with brown marks marked in yellow (Figure 81). In the latter, several zones

exist: Starting from the spray impact zone towards the piston edges, a first brown area is observed surrounded by a black area (marked in yellow). These two zones are surround by deposits forming black wave patterns, thereafter called “black area periphery”. This particular pattern indicates a forward or backward movement mechanism that will leave fringes of black deposits. The black area deposits and the peripheral black fringe pattern are not present in the warm start case. It may indicate that the so-called “black deposits” only form when the piston temperature is low, here during the warm-up phase of the engine.

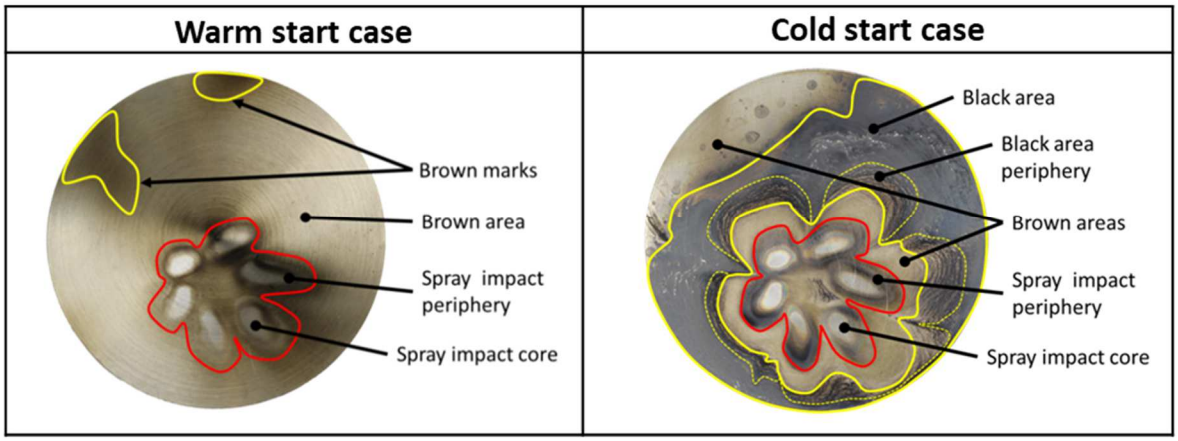

Figure 81: Piston deposits for the warm- and cold-start case with the different areas identified.

In conclusion, two different phenomena are observed for the two zones. The first is related to the impact of the spray on the piston surface, which leads to the formation of deposits in the inner zone that are not temperature-dependent. The second phenomenon corresponds to the mechanism that will form the outer zone.

5.2.2 Microscopic analysis

Figure 82 shows the four deposit zones identified during the macroscopic analysis: Brown area, brown marks, spray impact periphery, and spray impact core). These zones are analyzed and compared with the cold-start case deposit presented in section 4.4.2 (Figure 71).

When observed with a spatial resolution of about 2 µm, the brown area looks almost homogeneous. With a resolution of about 500 nm, a smooth surface covered with scattered particles whose average size is less than 100 nm in diameter is observed. Brown marks have a morphology similar to the brown area with the presence of a smooth surface covered by particles that are less scattered and whose average diameter is also below 100 nm. The darker appearance of these areas is probably related to the higher density of particle. The spray impact periphery also includes the presence of smooth surfaces and particles. The number density of these particles is between the brown area and brown marks ones. Their average diameter size is also less than 100 nm. The morphologies of the liquid-film path and soot path deposits are both found in these three deposit zones indicating that the related mechanisms are involved. A granular morphology is observed in the spray impact core with the presence of cracks. The latter are probably due to a high thermal stress caused by the high temperature in the combustion chamber.

Comparing with the cold-start case in Figure 71, even if a large difference is observed on the macroscopic scale with the existence of the black area in the cold case, many similarities are observed on the microscopic scale. In both cold- and warm-start cases, the spray impact periphery, spray impact core, located in the same places on the piston, present a deposit similar in appearance and morphology. The

brown area of the warm-start case is located where the brown area and the black area are located in the cold-start case, and similar morphologies characterized by a smooth surface covered by particles are observed. These results show that probably the same processes are involved despite the differences in temporal variation of the temperature and the difference observed on the macroscopic scale. Deposit related to the soot path are also observed but not analyzed in this section that concerns mechanisms related to the liquid-film path only, they will be studied later in chapter. To better understand the formation processes of the different zones, the analysis will continue with the *in situ* analysis of the deposit formation, with particular attention to the impact of the spray on the piston surface.

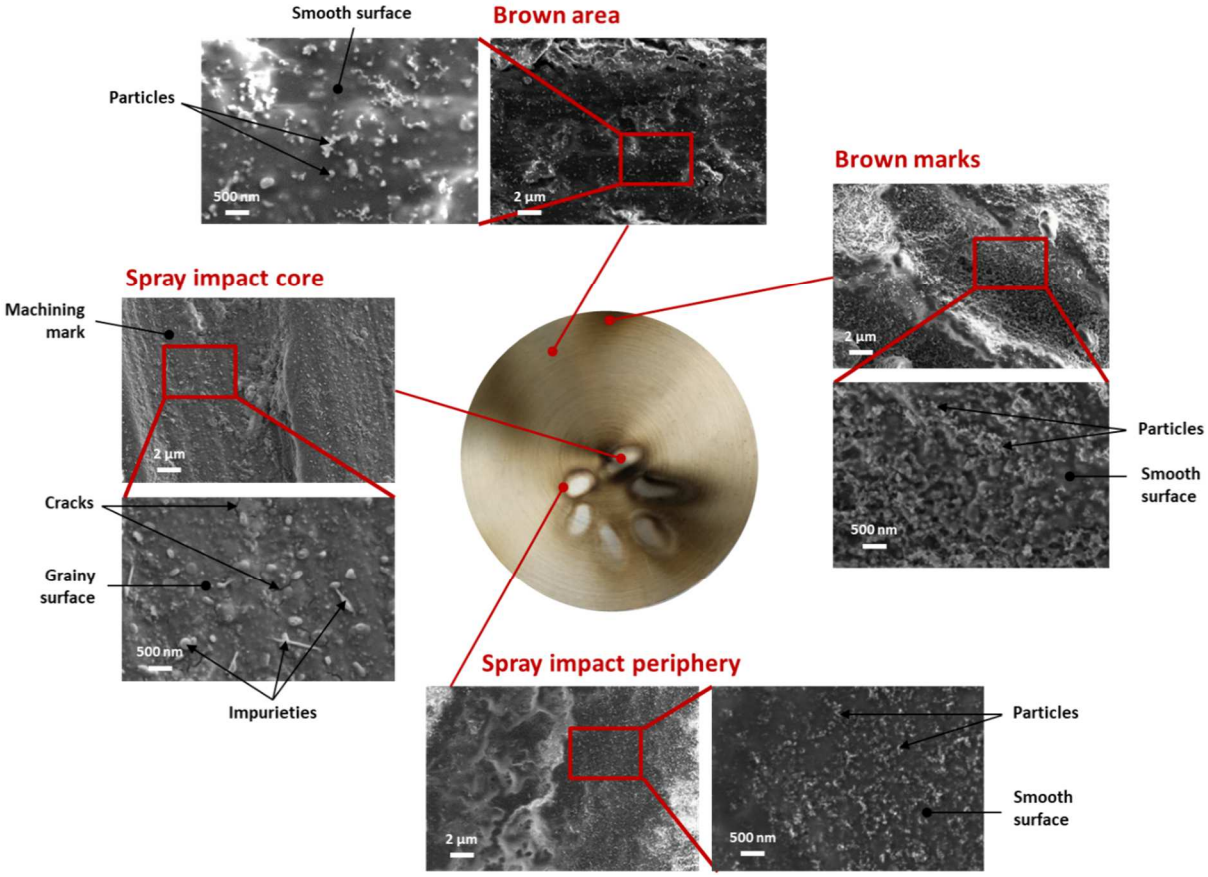

Figure 82: SEM images of the piston deposit areas obtained in the early injection cold start experiment.

5.2.3 *In situ* analysis

5.2.3.1 Visualization of the formation of liquid films

In the early injection condition, the fuel is injected at top dead center, when the distance between the piston and the injector nozzle is shortest. At this distance, the spray hits the surface of the piston. This impact of the spray can lead to the formation of a liquid film. Depending on several parameters including injection angle, injection pressure, amount of fuel injected or temperature of the piston surface, the liquid film formed is transported along the piston surface. This phenomenon is called “liquid-film spreading”. It is possible to distinguish two areas on the piston related to the impact of the spray: The spray impact area and the liquid film spreading area as illustrated in Figure 83. The spreading length is defined as the

distance between the periphery of the spray impact area and the liquid-film spreading periphery. This length varies according to the parameters mentioned above.

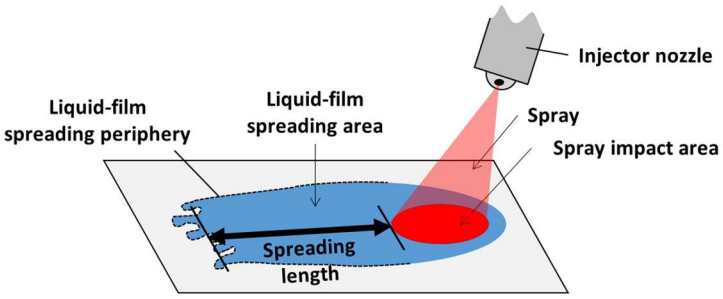

Figure 83: Schematics of liquid-film spreading resulting from spray impact for a single spray cone.

The high-speed camera is used in these experiments to observe deposit formation on the piston surface, the liquid film, and combustion. However, the optical access is progressively obstructed during deposit formation with obstruction rates varying according to the operating conditions, making visualization of the combustion chamber and piston impossible after some time. In the cold-start case, it was possible to image the piston for around six minutes. In the warm-start case, window fouling is slower, and it was possible to observe the piston until the end of the experiment.

Liquid-film spreading is identified on the images by visual inspection of the appearance of the reflections, where these are characteristic of a liquid flow. In the cold-start case, a liquid-film spreading is observed during the first two minutes of the experiment. During the first 75 cycles, the liquid film accumulates, and the spreading length increases until reaching the edge of the piston. After 100 cycles, the spreading length decreases until the moment when it is no longer possible to observe the liquid film because of optical access obstruction, six minutes after the start of the experiment. Figure 84 shows this liquid-film spreading from the first injection of the first cycle. The comparison between the diameter of the liquid-film area from the first cycle in Figure 84 and the pattern of the deposit obtained at the end of the experiment shows a correspondence between the presence of liquid film and the formation of the deposit. Figure 85 shows the evolution of spreading length and black area length over time. The black area length is defined as the distance between the first appearance of the black area at the outer edge of the film and its progression towards the spray impact (see illustration in Figure 84) These data were collected by eyes inspection of the images and are therefore purely qualitative. However, they clearly show that while the spreading length decreases, the black area length increases.

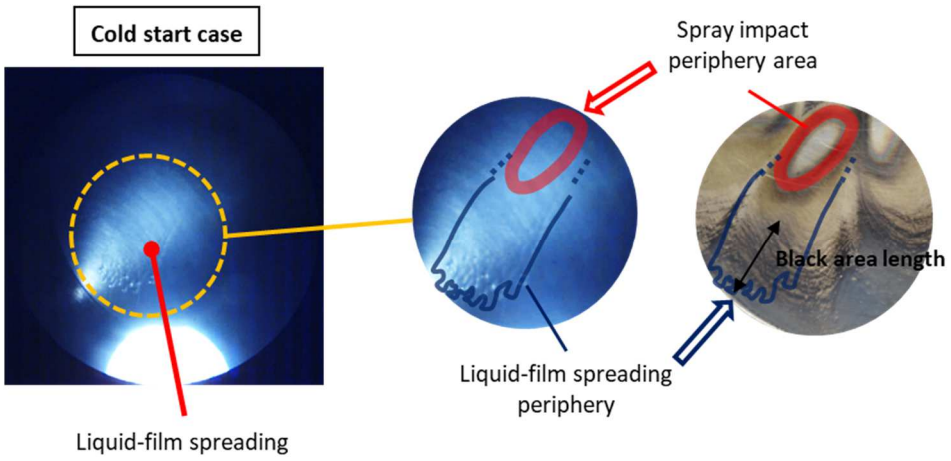

Figure 84: High-speed images obtained by *in situ* visualization of the piston top surface for the cold start case at 288 CAD during the first cycle of the engine experiment, and corresponding zone of the piston samples.

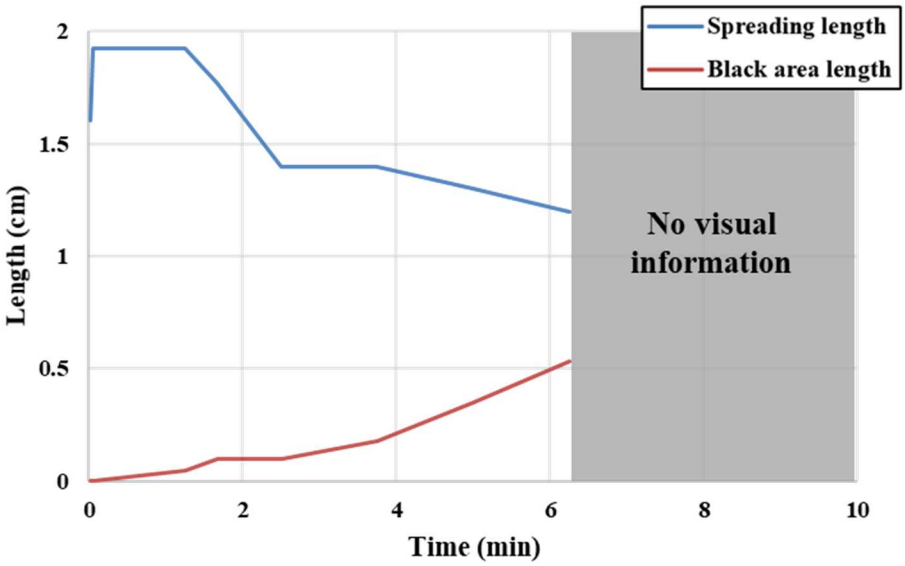

Figure 85: Spreading length and black area length evolution with time.

In the warm-start case, using the same acquisition parameters as for the cold start, no liquid-film spreading is observed in the *in situ* visualization experiments (Figure 86). Similarly, there is no black zone deposit. We can therefore assume a correlation between the black deposit and the existence of liquid spreading.

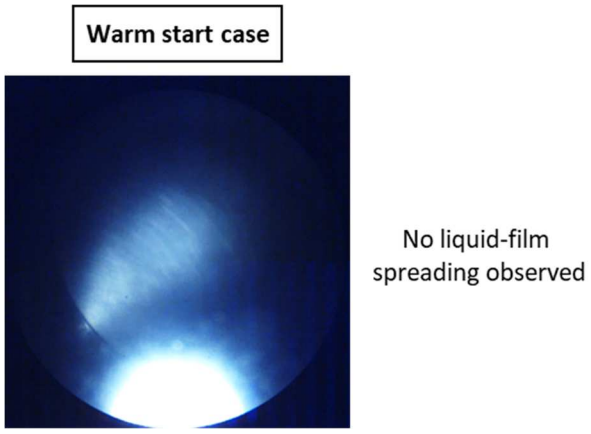

Figure 86: Image obtain by direct visualization with the high-speed camera of the piston top surface for the warm start case at 288 CAD during the first cycle of the engine experiment.

5.2.3.2 Visualization of the formation of deposits

In order to analyze the dynamics of deposit formation, Figure 87 compares *in situ* images of the piston surface acquired during the initial phase (Phase 1), when the temperature difference in piston temperature between both operating cases is significant. It also shows *ex situ* images of the piston surface sampled after the tests, both for warm- and cold-start cases. Phase 1 lasts about 2 minutes and although images acquired for 2 min were used in this analysis, only images acquired at 45 s after the start of the experiments are shown in the figure because due to the obstruction of the optical ports, the quality of the images obtained at 2 minutes is significantly lower than those obtained at 45 s. The comparison in Figure 87 shows that for both warm- and cold-start cases, the deposit observed at 45 s are similar to the ones observed on the piston sampled after the test, showing that these deposit very probably form in the initial phase of the experiments when the piston is still cold, and that little change occurs at later times when the piston is warm. The images in Figure 87 also highlight the differences between the warm- and cold-start case. While similar deposit are observed in the inner zone where the deposit corresponds to the spray impact zone, significant differences are observed in the outer zone. The black area deposit is observed in the cold-start case, but not in the warm-start case. These results indicate that the deposit formation in the inner zone is not very sensitive to the piston surface temperature while the black deposit in the outer zone is more sensitive to the piston surface temperature.

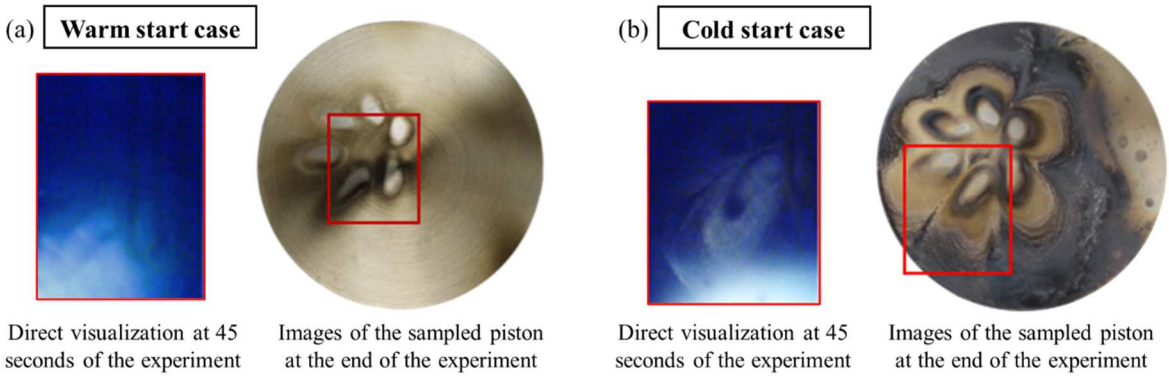

Figure 87: Images obtained by direct visualization of the piston surfaces at 45 s and images obtained after the experiment when the pistons were sampled at 10 min.

In summary, the analysis has identified two different mechanisms related to the injection: A direct spray impact creating a liquid film and consecutively a deposit, followed by the liquid spreading phenomena forming a black deposit. Also, while the former seems to be not very sensitive to piston surface temperature, the latter is. Therefore, the following parameters appear essential to understand the formation of deposit by a liquid-film and will be studied in more detail in the following section:

- The effect of the piston surface temperature on liquid-film evaporation
- The local cooling of the piston due to spray impingement
- The variation of the thickness of the liquid film

5.2.4 Parameters affecting the liquid film

5.2.4.1 Effect of piston surface temperature on liquid-film evaporation

The dynamic evolution of a liquid film as a function of the surface temperature is described by the Nukiyama theory [105]. It characterizes the behavior of liquid droplets as a function of surface temperature for a single-component fuel. The resulting Nukiyama curve shows the dependence of the lifetime of a liquid fuel droplet on the surface temperature and thus provides information on the evaporation rate of a fuel at a given temperature. This curve can also be applied to liquid fuel films to simulate their thermal behavior on the walls of the combustion chamber [106].

The objective of this section is to locate the conditions related to the cold-start and warm-start experiments on the Nukiyama curve to understand the evaporation rate of the liquid films during the experiments. After presenting the Nukiyama curve and its underlying regimes, the effect of pressure is investigated. As the in-cylinder pressure in an engine varies it is important to know how it impacts the evaporation of the liquid film. Then, the E10 substitute fuel called RFG is introduced. The Nukiyama curve of this fuel is used to determine, which evaporation regimes the cold- and warm-start cases correspond to.

According to Nukiyama, four regimes describe the evaporation process of a liquid film on a surface (Figure 88). Regime I (liquid-film evaporation) corresponds to a surface temperature below the saturation temperature (T_{sat}) of the liquid. In this case, the lifetime of the liquid film decreases linearly with the surface temperature and corresponds to slow evaporation of the liquid film. Regime II (nucleate boiling) is between the saturation temperature and the Nukiyama temperature (T_N) and corresponds to the formation of isolated bubbles in the liquid film. In this regime, the lifetime of the liquid film continues to decrease until it reaches the Nukiyama temperature, which is the temperature at which the liquid film lifetime is the shortest. At this temperature, bubbles continuously form in the liquid film. Regime III (transition boiling) is between the Nukiyama temperature and the Leidenfrost temperature (T_L) and shows an increase in the lifetime of the liquid film with increasing temperature. This is due to the fact that the liquid film boils and decomposes into bubbles which take time to evaporate. Regime IV (film boiling) starts at the Leidenfrost temperature T_L and corresponds to the boiling of the liquid film. When the temperature of the plate reaches T_L, evaporation is slowed down because the film is not continuous anymore, it is composed of droplet clouds levitating above the plate due to the presence of an insulating gas layer separating them from the surface. Heat transfer is therefore reduced. Above T_L, the evaporation rate increases with surface temperature.

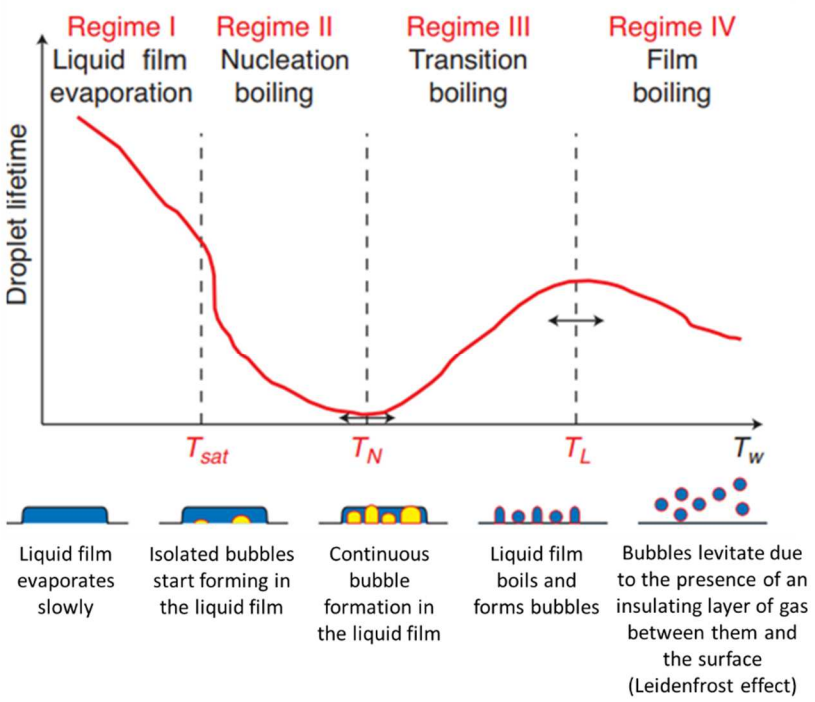

Figure 88: Nukiyama curve of the droplet lifetime vs. surface temperature for a single-component liquid [106].

Another parameter influencing the evaporation process described above is pressure. Figure 89 shows the effect of pressure on the liquid-film lifetime of iso-octane. The first part of the Nukiyama curve corresponds to a linear decrease in the liquid-film lifetime. With increasing pressure, this part of the curve is shifted to higher temperatures and thus displays an increase in evaporation time. For example, for a surface temperature of 100 °C, at atmospheric pressure (101 kPa) the evaporation time of a liquid film is about 5 s whereas it is about 11 s for a higher pressure of 717 kPa. The Nukiyama temperature (T_N) and the Leidenfrost temperature (T_L) increase with pressure. Finally, the part of the curve corresponding to Regime IV, i.e., for temperatures above T_L, faces a decrease in the lifetime of the liquid film. For example, for a temperature of 300 °C, the lifetime of the liquid film is 5 s at atmospheric pressure and for a pressure of 717 kPa, the lifetime drops to 0.5 s. These trends in the evolution of the Nukiyama curve with pressure will allow a more accurate characterization of the thermal behavior of liquid films of E10 fuel for both cold- and warm-start cases.

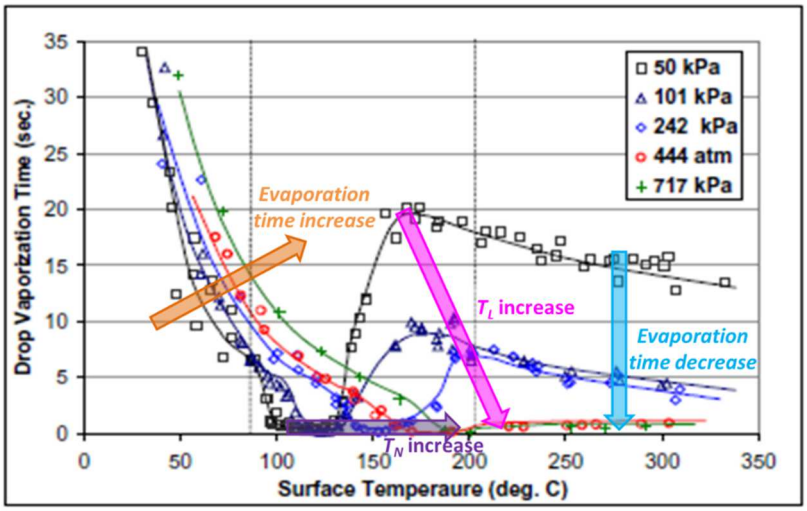

Figure 89: Nukiyama curves of iso-octane for different pressures [107].

The Nukiyama curves presented so far applies to single-component liquids only. Some studies exist to characterize the behavior of multi-component liquids, but none are available for the E10 fuel used in this thesis [107]. Nevertheless, some data is available for the Reformulated Gasoline (RFG) fuel. The choice of RFG fuel as a substitute for the description of E10 is based on the similar distillation curves of the two fuels. As the Nukiyama curve is related to the evaporation of the fuel, it seems appropriate to use a substitute for E10 fuel with similar evaporation properties such as RFG. The composition of both fuels is presented inTable 8 [108]. The temperatures of the evaporated fractions at 50 °C (T50) and 90 °C (T90) of the distillation curves of the two fuels appear to be similar. The T50 and T90 temperatures of E10 fuel were measured at 90 and 146.5 °C respectively. The RFG fuel has a T50 between 88 and 99 °C and a T90 between 138 and 149 °C. The differences observed between the two fuels in terms of aromatic, olefin, benzene and oxygen content will not be considered in the following analysis.

Table 8: Specifications of RFG and E10 fuels [108].

Fuels specifications	RFG	E10
Aromatic /v.%	18 – 20	25 – 32
Olefins /v.%	3.0 – 5.0	6 – 13
Sulfur /ppm	15 – 25	≥ 10
Benzene /v.%	0.5 – 1.0	≥ 10
T50 /°C	88 – 99	90
T90 /°C	138 - 149	146.5
Oxygen wt %	1.8 – 2.2	3.3 – 3.7

Figure 90 displays the Nukiyama curve for the RFG fuel at atmospheric pressure. The temperature ranges of the piston surfaces during the cold start and warm start experiments are indicated as color boxes. For the cold start case, during Phase 1, the liquid film is in the linear part of the curve where the evaporation rate increases linearly with surface temperature. At atmospheric pressure, Phase 2 is in both Regime II and III. Considering the effect of increasing pressure in the combustion chamber, it is assumed that Phase 2 is also in the linear part of the curve at pressures relevant to engine conditions. This result means that during the cold start case experiment, the liquid film evaporates faster and faster during the experiment as the surface temperature increases with time.

For the warm-start case, Phase 1 is at the end of Regime II and Phase 2 is at the beginning of Regime III. However, due to the effect of pressure, it is assumed that the liquid film during the experiment is at the end of the linear part of the curve corresponding to Regime II. Compared to the cold start case, the warm start case has a much faster evaporation speed during the test. These results appear to be consistent with the previous *in situ* analysis. Indeed, for the cold start case, it is possible to observe the liquid-film spreading at the beginning of the experiment. Then, as the surface temperature increases, the length of the liquid-film spreading decreases . For the warm-start case, no spreading is observed because the liquid film is in a fast evaporation mode compared to the cold-start case.

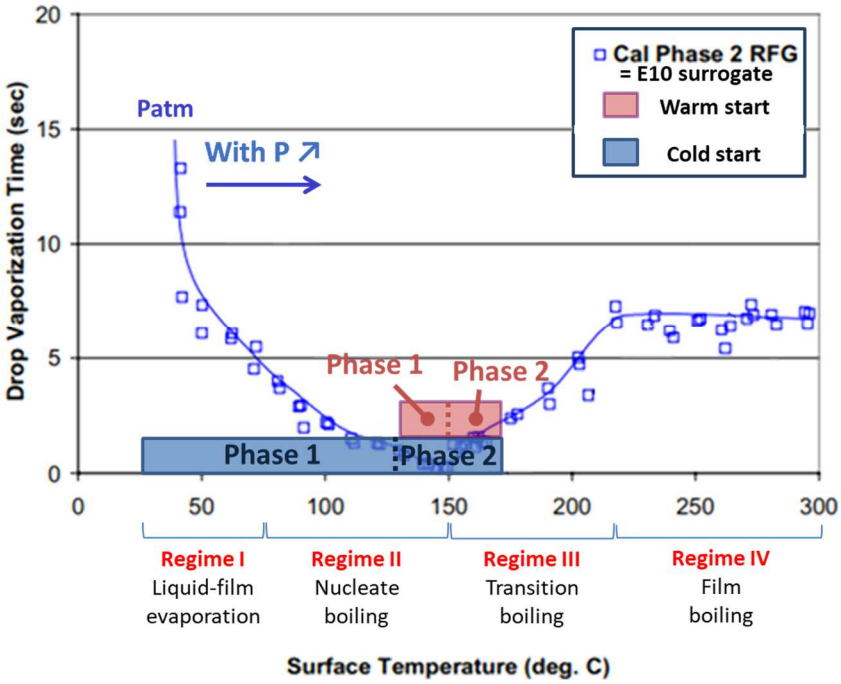

Figure 90: Nukiyama curve for RGF fuel at atmospheric pressure [107].

For the cold-start case, as seen above, the spreading of the liquid film seems to coincide with the black deposit. It can be assumed that the outer zone of the deposits on the piston surfaces is conditioned by the presence of liquid-film spreading whose evaporation rate depends on the surface temperature. Fast evaporation means that the liquid-film does not have time to form a deposit. However, it has been observed that the inner zone corresponding to the impact zone of the liquid film, is formed at both low and high temperatures.. The liquid film formed in this zone does not seem to follow the thermal behavior described by the Nukiyama curve The following sections aim to understand the formation of deposits by investigating other factors in the literature that may affect the evaporation time of the liquid film.

5.2.4.2 Variation of the thickness of the liquid film

The Nukiyama curve of a fuel is obtained by measuring the surface temperature-dependent evaporation time of fuel drops deposited on the surface with the same diameter, i.e., drops with the same volume. Thus, for an inhomogeneous thickness of a liquid film, it can be assumed that the evaporation time is not the same in the liquid film due to different volume of fuel to be evaporated. Kaiser et al. and Pan et al. measured the liquid-film thicknesses of fuel from the impact of a spray on a surface [109, 110]. Their measurements revealed zones of liquid fuel accumulation in the liquid film.

Kaiser et al. measured the liquid-film thicknesses on a piston in an optical access spark ignition engine with a direct injector by laser-induced fluorescence (LIF) [109]. The liquid film in their work shows spreading. Its size is of the order of 30 mm long by 20 mm wide for a spray impact corresponding to a single-hole injector. These dimensions are comparable to those obtained in this thesis work with the formation of a liquid film of 25 mm long and 13 mm wide (Figure 92). Also, the measurement conditions of the Kaiser et al. paper are similar to the conditions of the engine experiments performed in this work with 200 bar injection at 360 CAD BTDC. They found that the liquid-film thickness increases from the center to the periphery of the liquid film, i.e., the liquid film accumulates at the periphery of the liquid

film where it reaches a maximum thickness of 40 µm (Figure 91). At the center (impact core of the spray), the thickness is minimal. This information is now used to analyze the cold start case experiment. In this experiment it was shown by direct visualization that with increasing surface temperature the length of the spreading of the liquid film decreases. Thus, the periphery of the film, corresponding to a liquid fuel accumulation, moves closer to the center of the piston. Direct visualization also showed that the black area progresses from the edge towards the center of the piston and that this displacement correlates with the decrease in the length of the liquid-film spreading. Therefore, these results seem to show that the black area deposit forms at the periphery of the liquid film, where the accumulation of liquid fuel takes the longest time to evaporate. It can be assumed that the liquid-film path deposit forms when the evaporation speed of the liquid film is slow.

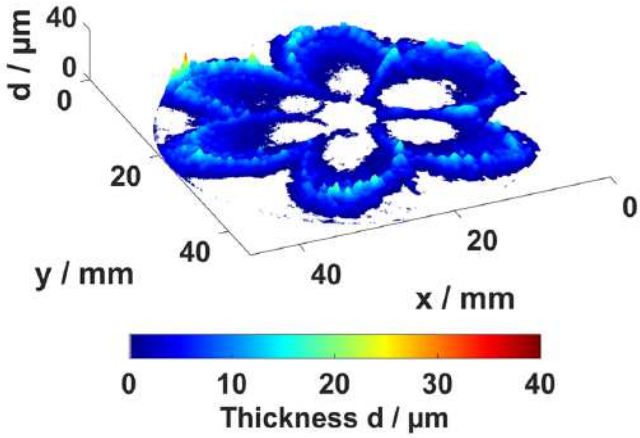

Figure 91: Thickness of the liquid film formed on a piston surface as measured by laser-induced fluorescence imaging (LIF). Image taken at 300 CAD BTDC, injection of liquid fuel at 200 bar at 360 CAD BTDC [109].

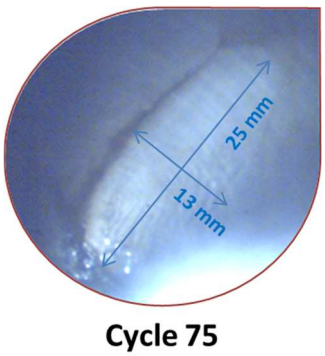

Figure 92: Direct visualization of the piston surface with a liquid-film with its size at 20 s of the experiment.

The work of Pan et al. showed a liquid-film accumulation at the periphery of the spray impact [110]. The size of the liquid film presented in this work is 15 mm wide and 25 mm long. This size is comparable to the liquid films observed for the cold start case experiment which are 13 mm wide and 25 mm long. The temperature delta between the fuel and the plate is about 3 °C. This temperature difference is similar to the initial condition of the cold start case experiment with a temperature difference between the piston surface and the fuel of 0 °C (piston surface and fuel are at atmospheric temperature).

The work of Pan et al. shows that the liquid film can accumulate also at the periphery of the spray impact, marked in red in Figure 93, in addition to the periphery of the liquid film, marked in white. Pan et al. observed, as did Kaiser et al., a minimum thickness at the center of the spray impact. *Ex situ*

analysis of the piston from the cold start experiment revealed by SEM-EDS a higher density of deposit at the periphery of the spray impact than at the spray core area (Figure 94). This result was obtained by atomic density mapping of the deposit (see section 3.2.1).

According to the work of Pan et al., the periphery of the spray impact seems to correspond to a zone of accumulation of the liquid film, while the spray core area corresponds to a very thin zone of the liquid film. The formation of the deposit is thus favored at the periphery of the spray impact, which presents an accumulation of liquid film that takes longer to evaporate.

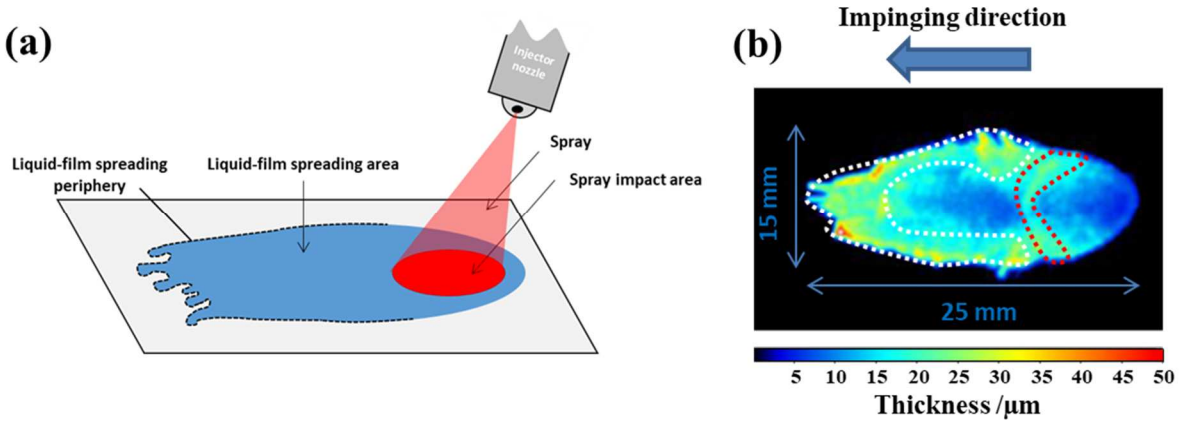

Figure 93: (a) Schematics of liquid-film spreading resulting from spray impact for a single spray cone, (b) LIF image of a liquid film of fuel injected at a temperature of –18°C on a plate cooled at –15°C [110].

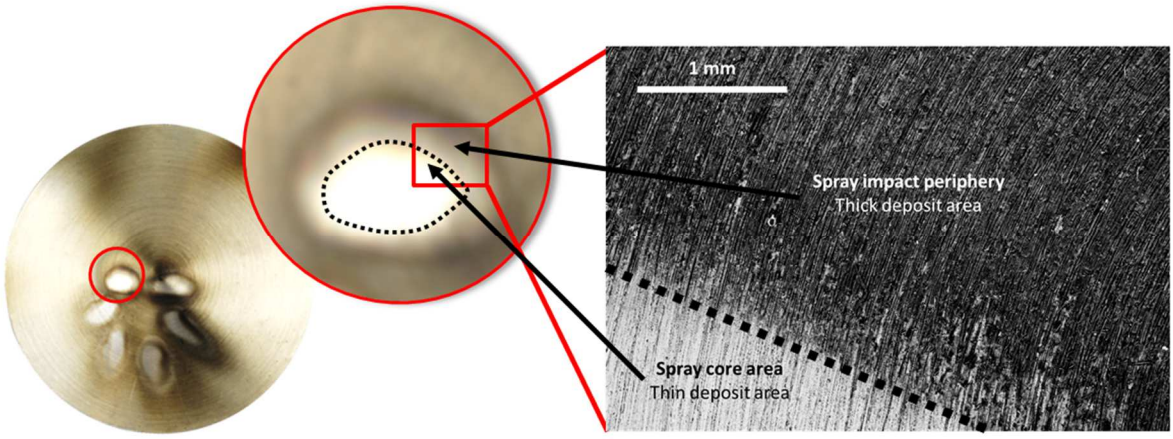

Figure 94: Atomic density mapping of the spray impact of the warm start case piston deposit taken by SEM-EDS.

5.2.4.3 Local cooling of the piston due to spray impingement

According to Nukiyama's theory, the rapid evaporation speed of the liquid film in the inner zone does not explain the presence of a deposit in this zone. To explain the deposit formation in the inner zone for the warm start case, the effect of the spray impact on the piston temperature is studied in this section.

A study conducted by Contino et al. showed that the impact of a spray on a surface leads to local cooling [111]. Contino et al. used infrared thermography measurements to obtain a 2D temperature map of the impacted surface as shown in Figure 95. In their study iso-octane is injected at 20 °C onto a plate at 93 °C. This temperature difference is close to the temperature difference of this work for the warm start case with a temperature difference observed between the piston surface with a temperature above 133 °C and a fuel temperature of 30 °C in the warm-start case. The authors observe a temperature gradient of the liquid film that has spread over the surface. The spray impact zone is the most cooled and is up to 18 °C lower than the initial plate temperature of 93 °C. This result means that for the warm-start case, the spray impact area is cooler than the rest of the piston. When the piston surface temperature is high relative to the fuel temperature, as in the warm-start case, the spray impact can cool the local surface temperature at the impact. This can lead to slower evaporation of the liquid film at the spray impact area, explaining the formation of deposits on this zone.

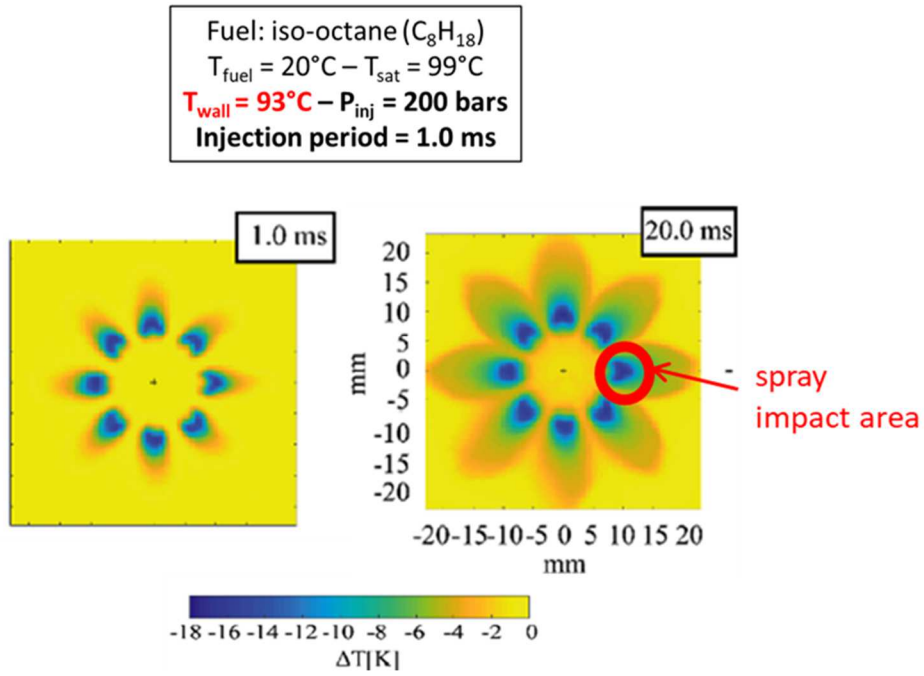

Figure 95: Temperature map obtained by IR thermography of a GDI spray impacting on a heated thin foil [111].

5.2.5 Synthesis of the mechanisms of deposit formation by the liquid-film path

Ex situ and *in situ* analyses of the two early injection deposit formation experiments compared to literature data have revealed mechanisms explaining the deposit formation by the liquid-film path.

During injection, the impact of the spray on the piston surface leads to the formation of a liquid film. From this liquid film two zones are distinguished: The spreading area and the spray impact area.

The first zone corresponds to the spreading of the liquid film that forms in the outer zone of the piston surface. The outer zone depends on the surface temperature. At high temperatures, the liquid film evaporates quickly, and the formation of deposits is limited. For the warm-start case, no spreading is observed

with the high-speed camera. However, microscopic analysis of the outer zone showed the presence of a deposit relative to the liquid-film path. It is likely that the liquid spread out but evaporated immediately, not allowing the formation of a thick layer of deposit compared to the black area observed for the cold-start case. For the cold start case, a spreading is clearly observed. Its path decreases as the piston surface temperature increases, and the black-area deposit is formed at the periphery of the liquid film, which moves towards the center of the piston. *In situ* visualization showed that the black area forms from the edge of the piston and progresses towards the center over several cycles (Figure 15). This may explain the presence of fringes in the black area, presented in section 5.2.1, which appear increasingly spaced in the direction of the piston center (Figure 96).

Figure 96: Visualization of the piston surface after different numbers of cycles for the cold-start case.

The brown areas observed on the external zones of the piston surfaces for both operating conditions correspond to the areas where the fuel evaporates rapidly which explains the presence of a thinner layer of deposit than for the black area observed for the cold-start case. In addition, brown marks were identified on the outer zone for the warm-start case, more precisely at the periphery of the piston. These marks are darker than the rest of the brown area and indicates a greater thickness of deposit. Their morphology indicates the involvement of a mechanism linked to the liquid film but the results presented in this chapter do not explain their presence.

The second zone corresponds to the liquid film formed in the inner zone of the piston. Two distinct liquid film areas are identified here: The spray impact core area and the spray impact periphery. The literature has shown that the liquid film has a minimum thickness at the spray core area and shows an accumulation of liquid fuel at the spray impact periphery. In addition, SEM-EDS analysis has shown a lower deposit density at the spray core area than at the spray impact periphery. This is attributed to rapid evaporation from the spray core area leading to limited deposit formation and slower evaporation at the spray impact periphery leading to deposit formation.

5.3 Contribution of the soot-path mechanism to deposits formation

In this section, the mechanisms leading to the soot-path deposit on the piston surface are studied. The study is based on the results obtained in the late injection experiment which favors soot formation. First, the different mechanisms of soot-path deposit formation in an engine are presented. Then, the contributions of these mechanisms at engine conditions are evaluated. For this purpose, the results of the *in situ* visualization and the measurement of the size and number distribution of the exhaust particles are compared with the data from the literature on aerosol transport and deposition mechanisms. Finally, the mechanisms involved in the deposition of soot on the walls of engine combustion chambers are proposed.

5.3.1 Soot transport mechanisms in engine

Different mechanisms are described in the literature to explain the soot deposit on the walls of the combustion chamber. The work of Suhre et al. investigated the possible mechanisms leading to soot deposition on the wall of a combustion chamber of a direct injection Diesel engine [3]. Since particles are subject to the action of several transport mechanisms, Suhre et al. proposed to weigh the action of these mechanism to determine the predominant ones. They first listed the possible deposition mechanisms:

- Thermophoresis, presented in section 1.4.1, is the movement of particles in a gas from the hot to the cold regions induced by a temperature gradient. The temperature difference between the cooled walls and the hot combustion gases induces a steep temperature gradient that generates thermophoresis forces on the soot particles directed towards the wall.
- Electrophoresis is the motion of particles carrying unbalanced charges in an electric field. According to Suhre et al., a net positive charge may exist on soot particles due to thermal ionization. The electric field thus carries the particles to the (electrically neutral) walls of the combustion chamber.
- Gravitational sedimentation is the deposition of particles on a surface under the action of gravity. This parameter depends on the mass of the particles. The impact of sedimentation on particles is usually represented graphically as a function of the particle diameter.
- Inertial deposition occurs when a particle caught in a turbulent flow is ejected from a vortex onto a surface due to its inertia. This mechanism can occur in a combustion chamber depending on the mass to aerodynamic drag ratio of the soot particles. If this ratio is large compared to the turbulence intensity, the particles can be eject from a vortex in the flow towards the combustion chamber wall.
- Brownian diffusion describes the behavior of a particle suspended in a fluid that interacts with the molecules of the fluid. These interactions lead to a random movement of the particles in the fluid. This mechanism transports particles only within the laminar sublayer but not preferentially towards the surface.

The authors did a numerical study where they analyzed the relative impact of these processes. They did not take into account gravitational sedimentation in their study as they considered the particle mass too low and the time scale involved too short to induce significant effects compared to the other forces. According to their calculations, electrophoresis and Brownian motion have a weak influence compared to thermophoresis. Also, they suppose that inertial deposition is unlikely because according to their calculation it can only occur in a very thin laminar layer on the order of about 30 nm. However, the results obtained by Boggs et al. show that inertial deposition is a possible in the cylinder [103].

In this work, the effects of electrophoresis and Brownian diffusion are neglected. The effects of thermophoresis, gravitational sedimentation, and inertial deposition are considered. To judge the relative contribution of these mechanisms, the results of real time particle-size measurements with the DMS 500 are used.

5.3.2 Soot transport mechanisms

5.3.2.1 Evaluation of the effect of gravitational sedimentation on soot transport to the combustion chamber walls

The particle size distribution was measured in the exhaust at each second of the late-injection experiment with the DMS 500 (Chapter 3). Figure 97 shows the temporal variation of the particle-size distribution,

which is mostly invariant over time. Therefore, it is possible to average the number and size distribution of the particles. Figure 98 shows the average particle-size distribution for the experiments, which is bimodal. The first peak, centered at 10 nm and ranging from 8 to 15 nm corresponds to the primary particles. The second peak, centered at 100 nm and ranging from 15 to 300 nm, corresponds to agglomerated soot. On the graph, a slight shoulder between 15 and 20 nm is observed. The number density of agglomerated soot particles is much lower than that of primary soot particles with 5.30×10^{6} cm^{-3} at 10 nm compared to 5.00×10^{8} cm^{-3} at 100 nm.

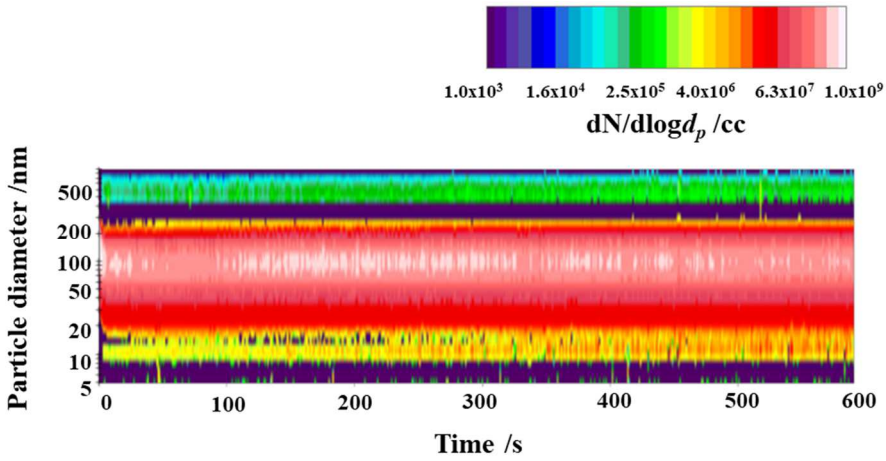

Figure 97: Temporal evolution of particulate size distribution for the late injection experiment case.

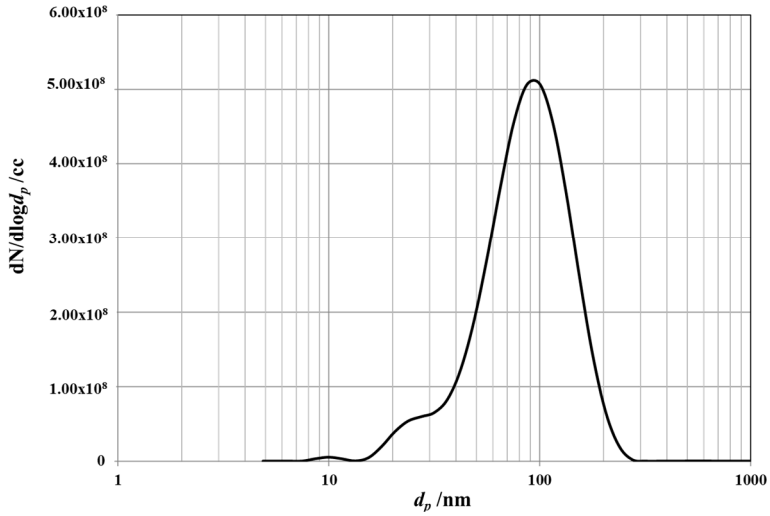

Figure 98: Particle-size distribution averaged over the 10 minutes for the late-injection experiments.

The study of Suhre et al. showed that one can assume that gravitational sedimentation is negligible for soot particles in the presence of turbulence inside the combustion chamber [50]. Our analysis will therefore focus on the case of a laminar flow, which may also exist near the combustion chamber walls[50]. Therefore, we estimate the deposition of particles by gravitational sedimentation in a duct with a laminar flow in the presence of a temperature gradient. The duct configuration is chosen because it is comparable to a semi-infinite horizontal plane, the diameter of the particles being much smaller than that of the duct.

It is therefore comparable to the combustion chamber of an internal combustion engine, with walls separated by a distance very large compared to the particle size. In order to use results available in the literature, we consider NaCl particles whose physical properties are similar to those of soot particles [51, 112]. To determine at which temperature gradient the gravitational sedimentation becomes negligible, Figure 99 shows the thermophoretic forces for different temperature gradients and the limit at which gravitational sedimentation becomes more important than thermophoresis. If the thermophoretic force is less than 100 N/kg, gravity governs the particle transport. The data obtained on the particle size distribution of soot particles in the late injection case experiment are shown in red on the graph. The soot particles measured at the exhaust are smaller than 1 µm and the temperature gradient in an engine is about 1000 K/cm at 0.5 mm from the wall, therefore the analysis of the graph shows that the thermophoretic force is well above 100 N/kg [113]. It is therefore possible to neglect the effect of gravitational sedimentation compared to that of thermophoresis.

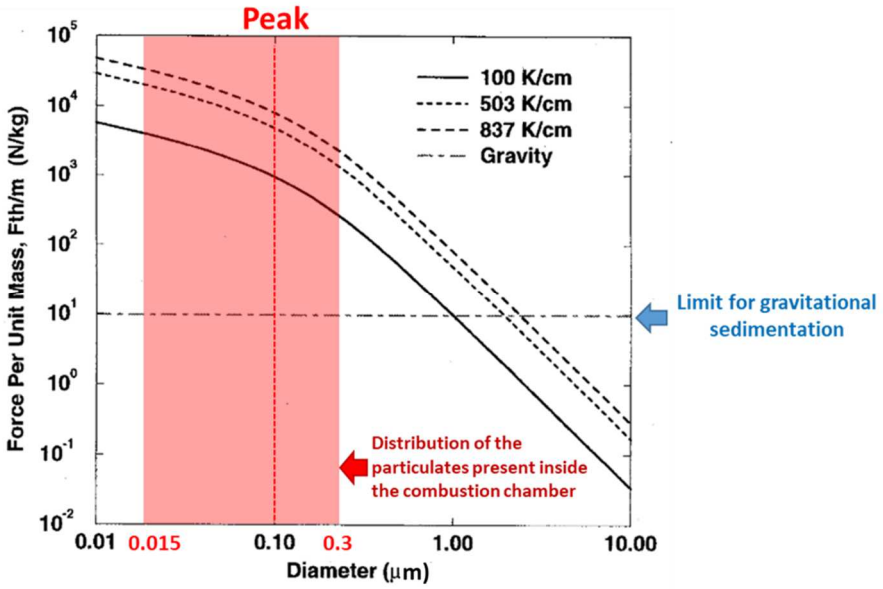

Figure 99: Figure adapted from work by Chunhong He and Goodarz Ahmadi comparing thermophoretic force and gravity for NaCl particles at different temperature gradients (simulation) in a laminar duct flow [114]. The distribution of the particle size obtained from the engine measurement are added to the original curve in the form of a red box.

5.3.2.2 Effect of thermophoresis on soot transport to the combustion chamber walls

As discussed above, the thermophoretic force is induced by a temperature gradient. Figure 100, taken from the work of Fan et al., shows near-wall temperature profiles at the cylinder head for different crank angle degrees [113]. These temperature profiles were obtained by numerical simulation of a spark-ignition direct-injection engine. Their study shows that the temperature gradient becomes significant for a wall distance of about 500 µm. Thus, beyond this characteristic distance, the temperature gradient becomes negligible. Figure 101 shows theoretically the evolution of the temperature gradient as a function of the distance to the wall. From a minimum distance from the wall, δ_{min}, the temperature gradient becomes zero and soot transport by thermophoresis does not exist. On the other hand, as one moves closer to the wall, the temperature gradient increases and so does the force of thermophoresis.

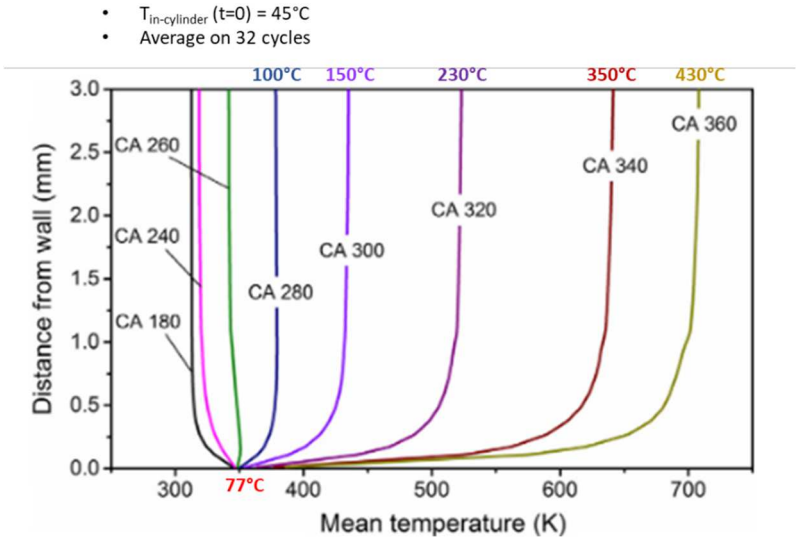

Figure 100: Near-wall temperature profile during compression of a SIDI engine from numerical simulations [113].

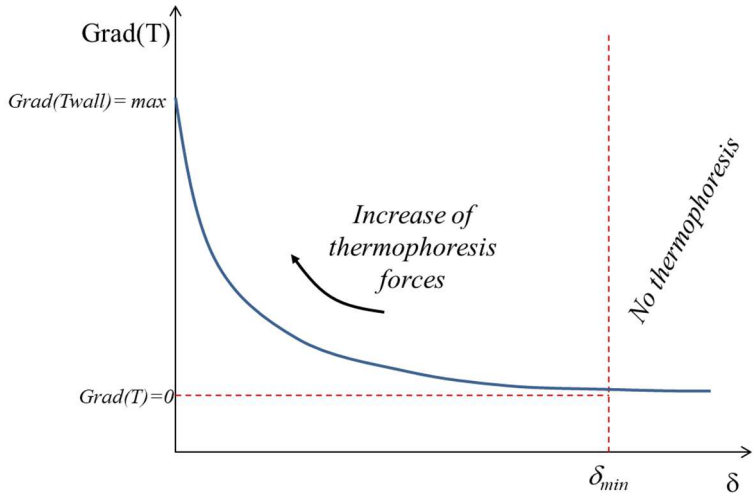

Figure 101: Dependence of the temperature gradient on the distance from the wall.

In the case of the late-injection experiment, orange light emission attributed to soot formed in rich areas near the wall was observed (Figure 102). In the first image (at 315 CAD), the spray impacts the piston surface. Then in the second image (at 367 CAD), the flame front is observed. Finally, at 376 CAD, it is possible to observe emission that is attributed to soot [115] that originates from rich combustion in zones with rich fuel/air mixtures as a result of the evaporation of the liquid film. The distance between the soot formation area and the wall is unknown. It can be assumed that since the soot was formed near the liquid film, it is located near the wall where the temperature gradients are highest. In this case, it seems consistent to assume that thermophoresis plays an important role in the transport of soot particle onto the piston surface.

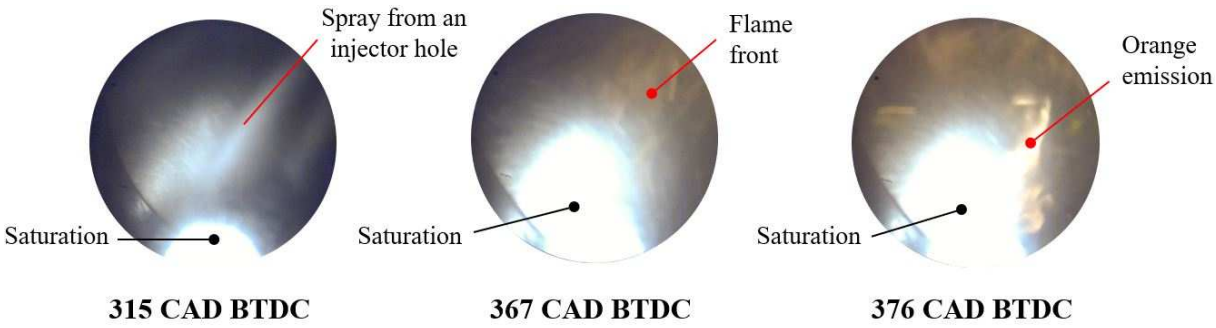

Figure 102: *In situ* visualization at 367 CAD of the first cycle of the late injection experiment. At 376 CAD, orange emission attributed to soot formed in rich areas near the wall is observed.

5.3.2.3 Effect of inertial deposition on soot transport to the combustion chamber walls

Ma et al. developed a model by numerical simulation to predict the near-wall boundary layer behavior [116]. In their research, they calculated the Reynolds number as a function of the piston displacement and the bore diameter. Figure 103 shows the temporal variation of the Reynolds number over the cycle for two different engine speeds. Although this calculation is probably oversimplified (it neglects the tumble breakdown process that generates significant turbulence at top dead center), it gives a rough estimate useful for our analysis. The graph shows that during the operation of an engine, the turbulence intensity varies with the position of the piston. According to the model, there is almost no turbulence when the piston is at top which is debatable and bottom dead center. Figure 22 shows that after injection and ignition the Reynolds number is high during the expansion stroke, thus it is possible that inertial deposition of soot particles happens.

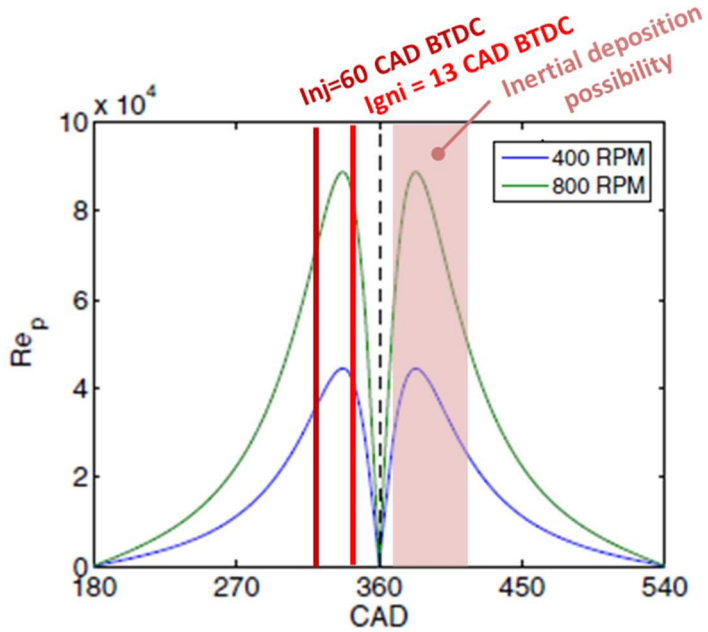

Figure 103 : Mean piston Reynolds number variation at the wall; adapted from Ma et al. [116].

5.3.3 Discussion on the mechanisms of soot deposition

Figure 104 shows the different soot deposit paths that may happen in the combustion chamber. Once formed, the soot is transported by the flow. Depending on the Reynolds number of the flow, i.e., the

intensity of the turbulence, different mechanisms will drive the transport of soot particles. If the turbulence is weak and the soot is close to the wall where there is a temperature gradient, thermophoresis is very likely to transport the soot towards the wall. If the turbulence is strong, as in the case of the expansion stroke, several possibilities are considered. If the soot has a low aerodynamic mass-to-drag ratio compared to the turbulence intensity, it will probably continue to follow the flow to the exhaust. If the soot has a high aerodynamic mass-to-drag ratio, it can be ejected from a vortex due to its inertia. In this case, if the soot hits a wall of the combustion chamber, it is likely to be deposited there; this is the inertial deposition mechanism.

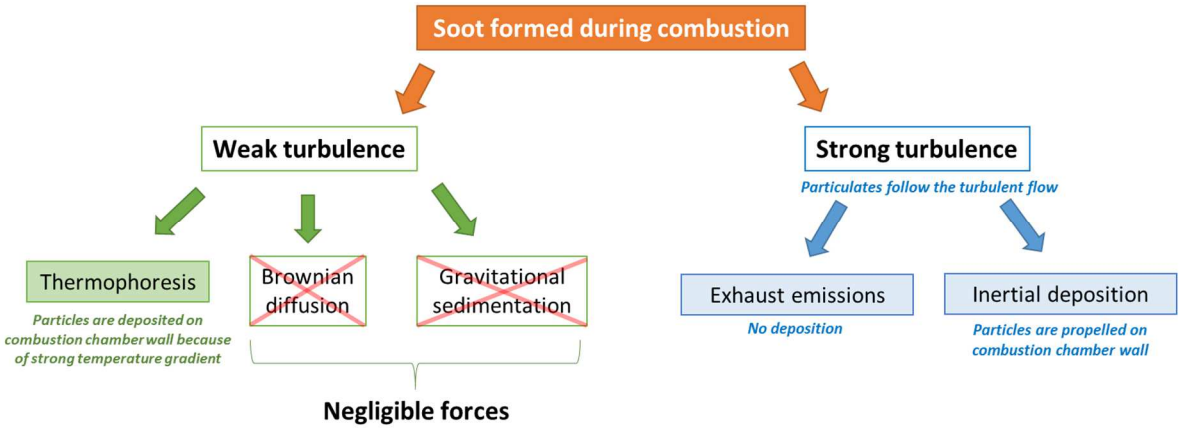

Figure 104: Schematics of the mechanisms leading to the deposition of soot in the combustion chamber.

5.4 Cross examination of the contribution of both liquid-film- and soot-path mechanisms to engine deposits

The mechanisms involved in the liquid-film- or soot-path deposit formation were identified separately by analyzing the piston deposits formed at early and late injection. In this section, the joint contribution of both mechanisms is presented and discussed.

5.4.1 Contribution of the soot path mechanism to deposits formation with the early-injection strategy

In the early-injection case, in addition to the presence of the liquid-film-path deposit, microscopic observation revealed the presence of soot-path deposits for both cold and warm start cases. Figure 105 shows the microscopic images obtained by SEM of the deposits formed for the two early injection cases and the late injection case at the same locations on the three pistons. It can be seen that the amount of soot is much higher in the late-injection case than in the two early-injection cases. The objective is now to understand whether the soot observed in the early injection cases followed the same formation and deposition mechanisms as in the late injection case.

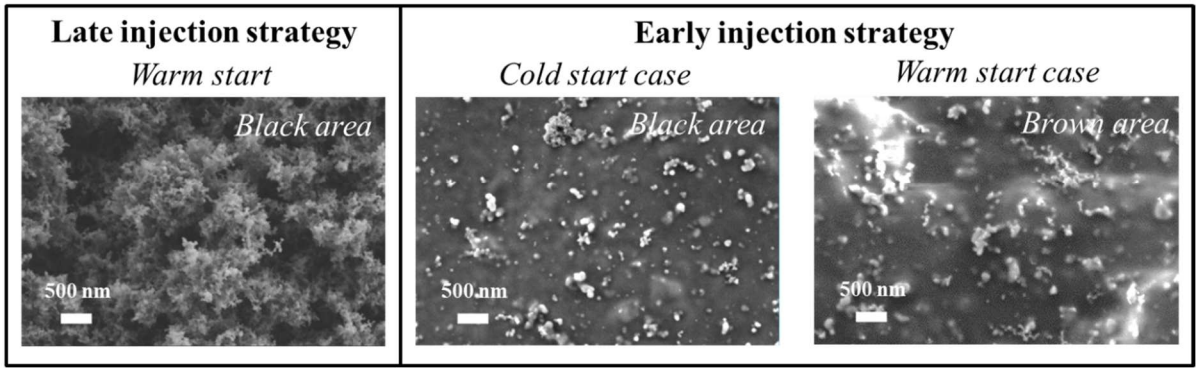

Figure 105: SEM images of the deposits for the experiments with the late- and the early-injection strategy for the cold- and warm-start cases.

Figure 106 shows the size and number distribution of the exhaust particles during the cold-injection case experiment. The distribution shows two distinct phases. In the first minute of the experiment, small primary particles and strong emission of large particles with comparably small agglomerate sizes are seen. After one minute, both the primary particles and the agglomerates become larger and no further changes are observed until the end of the experiment. Figure 107 shows the particle-size distribution of the early injection cold start experiment, averaged over the first minute, and averaged over the following nine minutes. The particle-size distribution of the late-injection experiment is also shown. The averaged distribution of the first minute of the early injection experiment is similar to the distribution of the late injection experiment. In the first minute of the early-injection experiment, the particles show a peak at 133 nm for 4.00×10^{8} cm^{-3} and the late injection shows a peak at 100 nm for 5.00×10^{8} cm^{-3}. The previous section showed that the formation of large agglomerate particles led to the formation of soot-path deposits formed by thermophoresis and inertial deposition. The soot-path mechanism is therefore compatible with the cold-start early-injection case during the first minute. Furthermore, according to these results in the early-injection case, soot is deposited only during the first minute. Therefore, there is less soot deposited for the early injection experiment compared to the late injection experiment. The macroscopic observations are therefore consistent with the DMS 500 data.

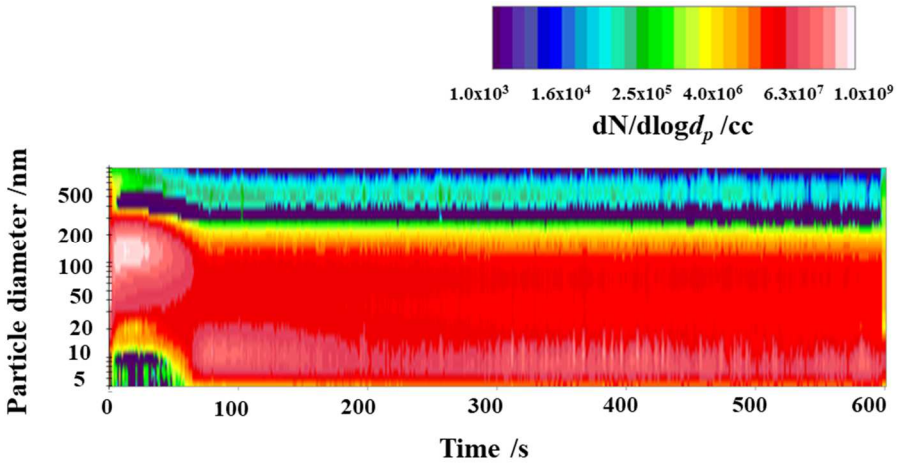

Figure 106: Variation of the particulate-size distribution during the early-injection cold-start case experiment for a sequence of engine cycles.

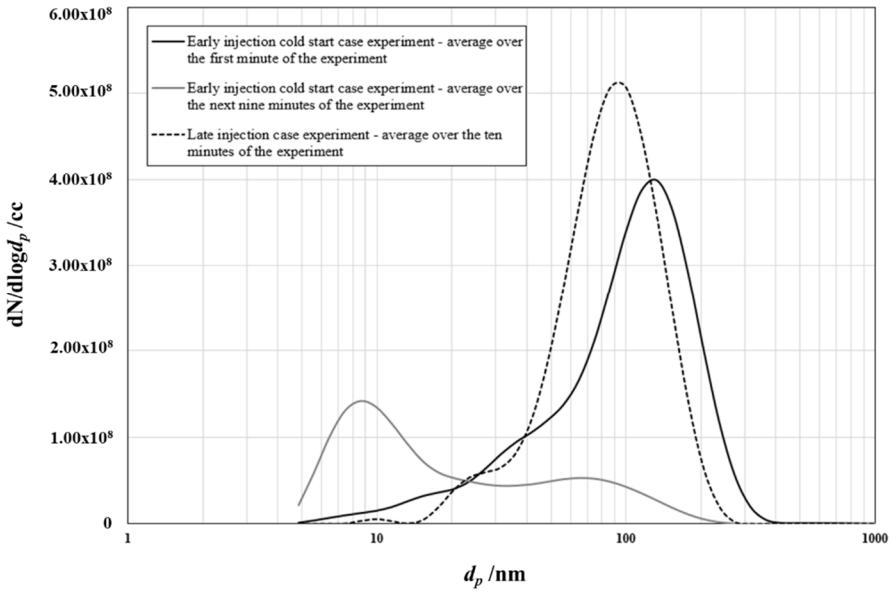

Figure 107: Particle-size distribution for the early-injection cold-start case and the late-injection experiments.

Figure 108 shows the distribution of particle size and number for the early-injection warm-start case. The distribution is rather homogeneous during the experiment. The graph in Figure 99 shows the particle-size distribution averaged over the duration of the experiment of the early injection warm-start case. In the bimodal distribution, both primary particles and agglomerates are visible. The primary particle mode dominates with a peak at 9 nm for 1.55×10^{8} cm^{-3}. The agglomeration mode presents a peak at 75 nm with a number density of 6.50×10^{7} cm^{-3}. In comparison, the graph displays the particle-size distribution of the late-injection case. The quantity and size of the particles are not very important for the early-injection warm-start case compared to the late-injection case. This result is consistent with the macroscopic and microscopic observations of the early-injection warm-start case, which show very little deposit corresponding to the soot path.

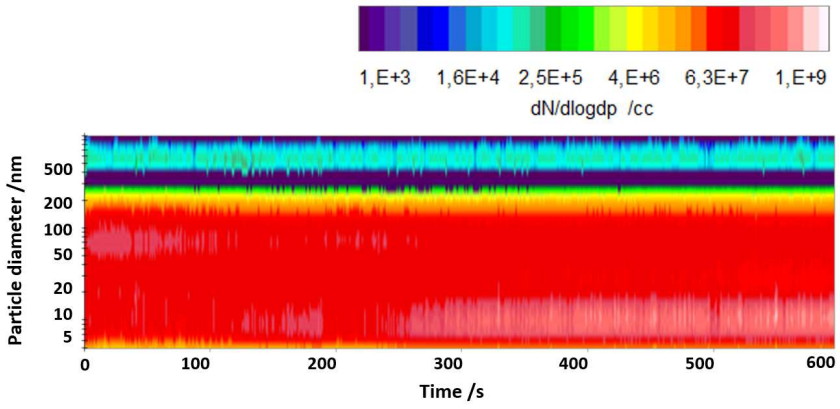

Figure 108: Variation of the particulate-size distribution during the early-injection warm-start case experiment for a sequence of engine cycles.

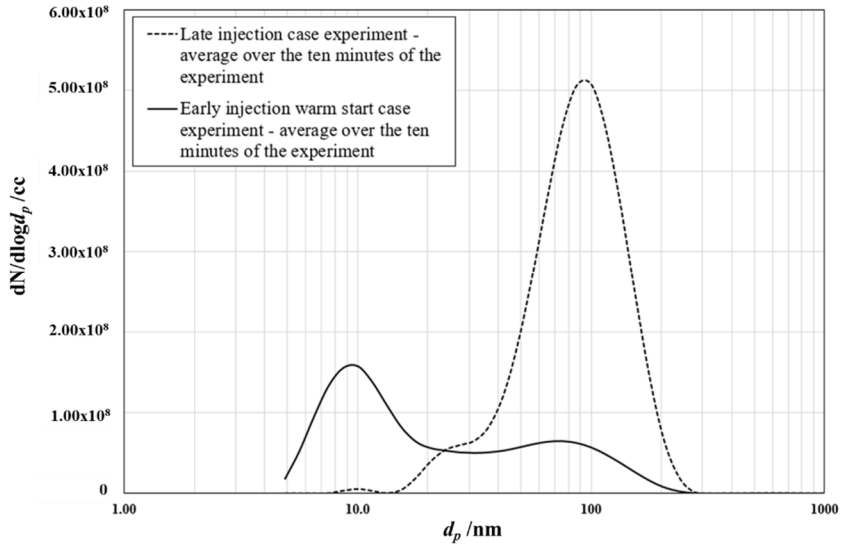

Figure 109: Particle-size distribution for the early-injection warm-start case and the late injection experiments.

In conclusion, the presence of large amounts of soot agglomerates during the first minute of the early-injection cold-start case showed a strong contribution of the soot-path mechanism in the initial phase of the experiment. The observation of little deposit corresponding to the soot path for both early-injection cases correlates with the short duration of exposure of the piston surface to soot or the low amount of agglomerated soot mode.

5.4.2 Contribution of the liquid-film path mechanism to deposits formation with the late injection case

Figure 110 shows the SEM microscopic analysis of the different deposit zones identified for the late injection strategy. The black area, spray center area, and impact area all show a layer of soot. The clear area is the only area where it is possible to observe the deposit corresponding to the liquid-film path. The objective is now to verify whether deposit formation mechanisms corresponding to the liquid-film path are compatible with the late injection case.

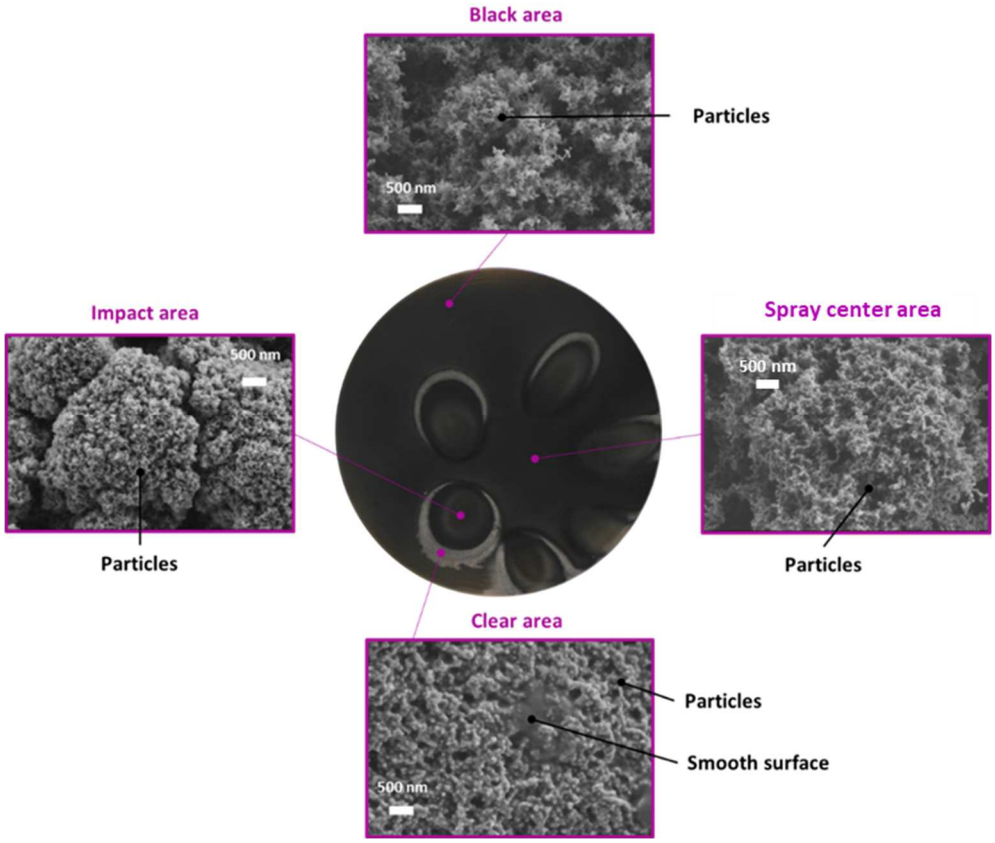

Figure 110: SEM images of the piston deposits for the late-injection case.

Macroscopic comparison of the deposits formed for the late-injection and the early-injection cases shows a similar pattern with six areas related to the six-cone spray impact. In addition, the high temperature of the piston surface (initial temperature of 133 °C) limited the formation of a liquid film, which explains the low deposit related to the liquid-film path. In conclusion, the liquid-film-path mechanism is compatible with the late-injection case.

5.4.3 Overall process involving the contribution of the liquid-film path and soot path mechanisms

The objective of this section is to propose an overall mechanism of deposit formation involving the liquid-film-path and the soot-path mechanisms.

Figure 111 shows the contribution of liquid film to deposit formation. At the time of injection, a small distance between the piston and the injector nozzle can lead to the impact of the spray (1). This impact leads to the formation of a liquid film, which can spread over the surface of the piston and which can lead to the formation of accumulation zones (2). From this liquid film, two areas can be distinguished, the spray-impact and the spreading area. Fuel in these areas evaporates at different rates depending on the film thickness and the surface temperature.

At high temperatures, the spreading evaporates very quickly, which limits the formation of deposits (3). The fuel in the spray-impact area evaporates slower than in the spreading zone because the spray impact causes local cooling (4). In the spray-impact area, two others areas are distinguished, the spray-impact periphery and the spray-impact core. Fuel in the spray-impact periphery, which is an accumulation area, evaporates slowly and leads to deposit formation. Fuel in the spray-impact core, which is the area of

minimum liquid-film thickness, evaporates quickly, limiting deposit formation. At low surface temperatures, the spreading and the spray-impact area are slow-evaporation areas. Within the liquid film, there are different evaporation durations. First, the accumulation zones at the periphery of the spreading and at the periphery of the spray impact areas correspond to slow evaporation zones favoring the formation of deposits (5). The rest of the liquid film is thinner and evaporates faster limiting the risk of deposit formation (6).

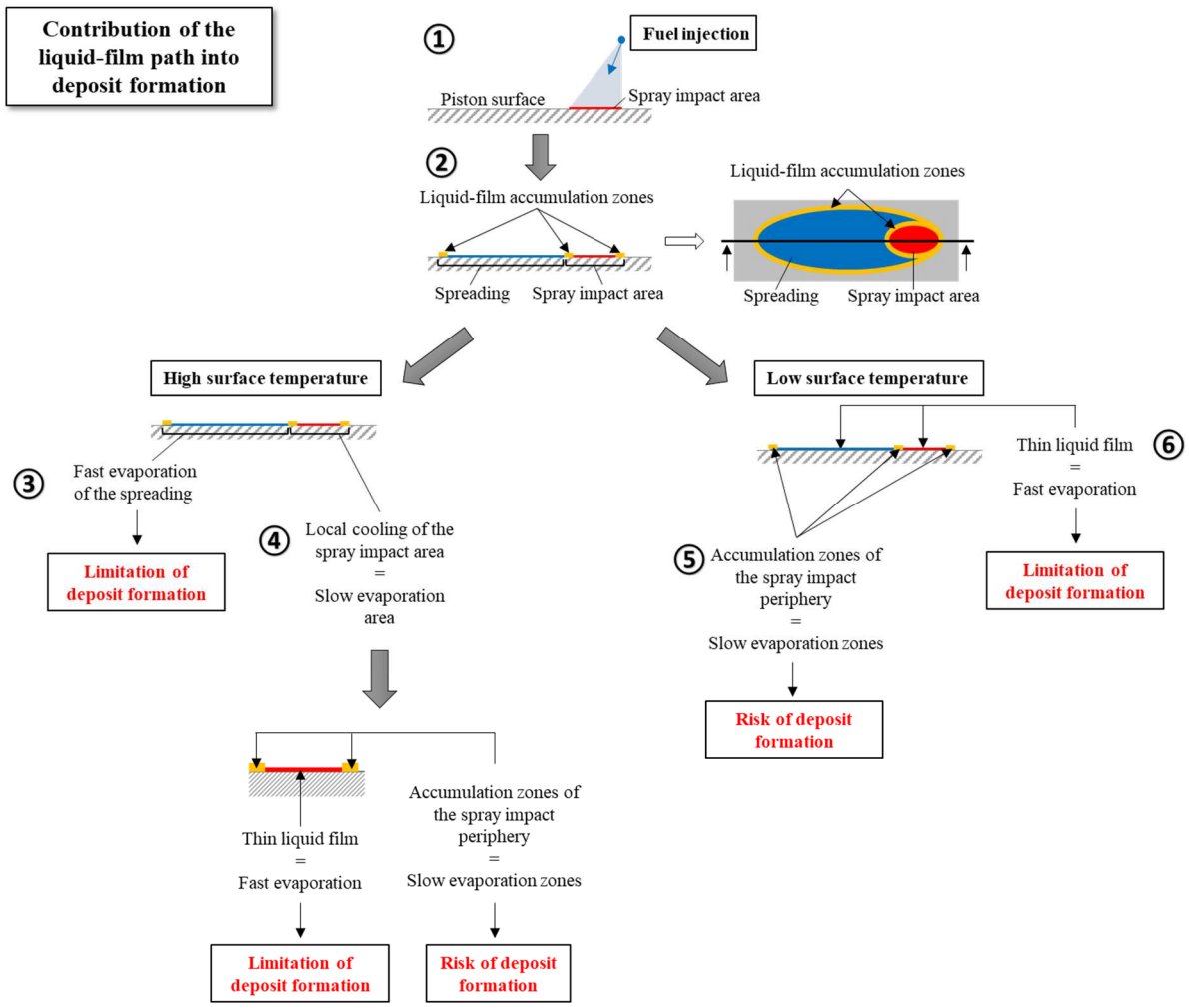

Figure 111: Scheme of the contribution of the liquid-film path in the formation of the deposit.

After analyzing the liquid-film zones and the parameters leading to the liquid-film-path deposit formation, the contribution of the soot path is added. In the following, it is assumed that a liquid film has formed as a result of the impact of the spray on the piston surface. Figure 112 shows the contribution of the soot path to the formation of the deposit. The soot formed during combustion is deposited on the piston surface. Depending on the richness of the mixture, the soot concentration, and thus its contribution to the soot path deposit is determined.

Two cases of rich combustion have been identified. The first case corresponds to the formation of a liquid film on the piston surface (1). As seen previously, depending on the surface temperature , this liquid film evaporates more or less quickly. If the evaporation of the liquid film is slow, this can lead to richer combustion zones near the wall (2). These rich combustions form a lot of soot in accumulation

mode which is deposited on the wall by thermophoresis or inertial deposition (3). At the next injection, a new cycle starts, and the deposited soot is washed away to the periphery of the liquid film (4).

The second case of rich combustion is the consequence of a late injection strategy. Late injection does not provide sufficient time for the fuel and the air to mix (5). This creates rich zones in the gas phase that will form a lot of soot in agglomeration mode. This soot will then deposit on the piston surface by thermophoresis or inertial deposition (6).

In case of a lean fuel/air mixture, the formation of large soot agglomerates is limited (7). The contribution of the soot path mechanisms is therefore also limited.

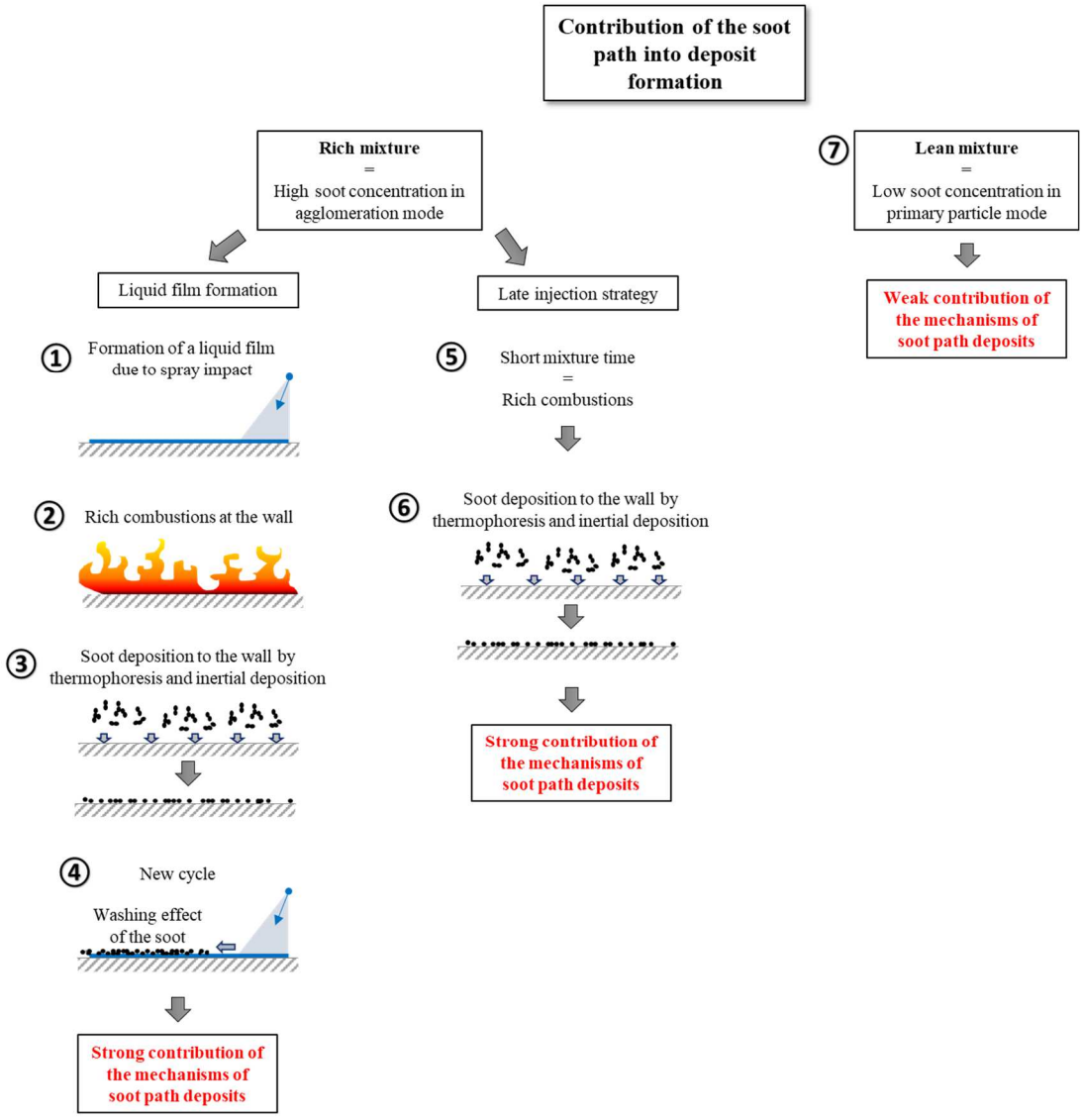

Figure 112: Scheme of the contribution of the soot path in the formation of the deposit.

6 INFLUENCE OF THE SURFACE PROPERTIES ON DEPOSITS FORMATION

The objective of this chapter is to investigate the effect of the piston surface properties on in-cylinder deposits formation. The focus is on the influence of surface temperature, surface roughness, and the piston material on the deposits formation mechanism. First, the methodology for evaluating the effect of the surface parameters is introduced, then the influence of each parameter is investigated and discussed.

6.1 Methodology for evaluating the influence of surface properties on deposits formation

The methodology to evaluate the influence of the piston surface properties on deposits formation is based on the *ex situ* and *in situ* analysis tools presented in chapter 3 and chapter 4 respectively. The *ex situ* analysis corresponds to the macroscopic and microscopic analysis of the piston surface after each experiment. For the macroscopic analysis, deposits color, texture, and patterns are identified. For the microscopic analysis, the morphologies at different scales are characterized. The *in situ* analysis is based on the particle-size distribution and on high-speed visualization of in-cylinder processes. The particle-size distribution is measured via SMPS in the engine exhaust to determine the impact of the parametric variations on the deposits formation via the soot path. Direct visualization is used to observe the presence of liquid films and thus to determine the impact of the surface properties on the deposits formation through the liquid-film path. This last technique also allows us to characterize the kinetics of deposits formation and combustion, *i.e.,* to identify rich mixing zones that can promote the soot path.

First, it is necessary to determine criteria of repeatability for each of these analyses in order to characterize their detection sensitivity. These criteria are determined by repeatability experiments for two different operating conditions. The first operating condition corresponds to a 360 CAD BTDC injection, a cooling water temperature of 20 °C and an initial piston temperature of 133 °C. Two experiments A and B are performed at these conditions and compared to determine the repeatability of the macroscopic and microscopic analyses and the particle-size distribution measurement in the exhaust. The second operating condition (experiments C and D) also corresponds to a 360 CAD BTDC injection, a cooling-water temperature of 20 °C but with an initial piston temperature of 20 °C. Experiments C and D are carried out for these conditions and the results are analyzed for repeatability. The duration of all experiment is 10 minutes.

6.1.1 Repeatability for *ex situ* measurements

The deposits-laden piston surfaces obtained after the experiments A and B are shown in Figure 113. The areas marked in blue correspond to reflections related to the lighting used to take the picture and the red zone corresponds to deposits. Many similarities can be observed for the two experiments using identical conditions. Two brown marks on the periphery and the pattern corresponding to the impact of the six-cone spray are identified. Both features have similar surface, area, and color. This macroscopic analysis shows that there is almost no difference in deposits color and that the areas of deposits are in the same proportions. The color and relative proportion of the deposits areas are selected as macroscopic criteria in the rest of the study.

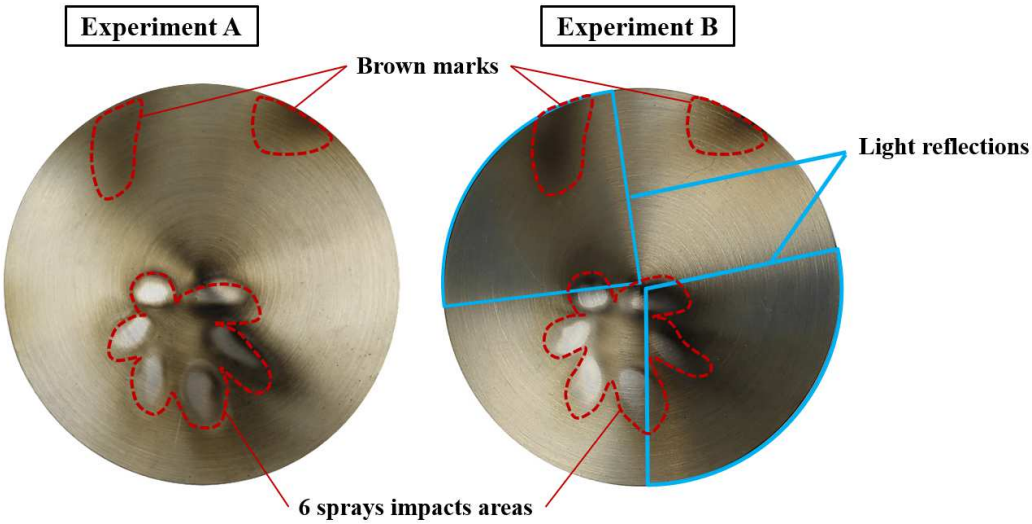

Figure 113: Cylinder surface after repeated experiments under identical conditions (360 CAD BTDC injection, cooling-water temperature: 20 °C, warm start with an initial surface temperature of 133 °C).

Microscopic analyses of the deposits from experiment A and B are performed on three different zones named (a), (b), and (c) in Figure 114. These three zones correspond to the outer zone, the periphery of the spray, and the core zone of the spray, respectively. It should be noted that in the electron microscopy images, some areas are affected by the so-called charge effect[6] that are not further considered in the analysis. For both experiments A and B, zone (a) and zone (b) exhibit particles with an average size below 100 nm. A smooth surface morphology is also observed in both locations. Zone (c) has a lower deposits thickness than the other two zones as machining marks can be distinguished for both experiments. In this zone, the two samples show granular aggregates corresponding to dense local aggregates of particles. In conclusion, for each of the zones, the same deposits morphologies are found in both cases in similar proportions. The deposits morphology and its proportion are therefore considered a relevant criterion for analyzing the influence of surface properties on deposits formation.

[6] Zones of charges: They correspond to an accumulation of electrons during SEM analysis that do not discharge on the surface of the sample. This causes highlighting that hinders the analysis of the sample.

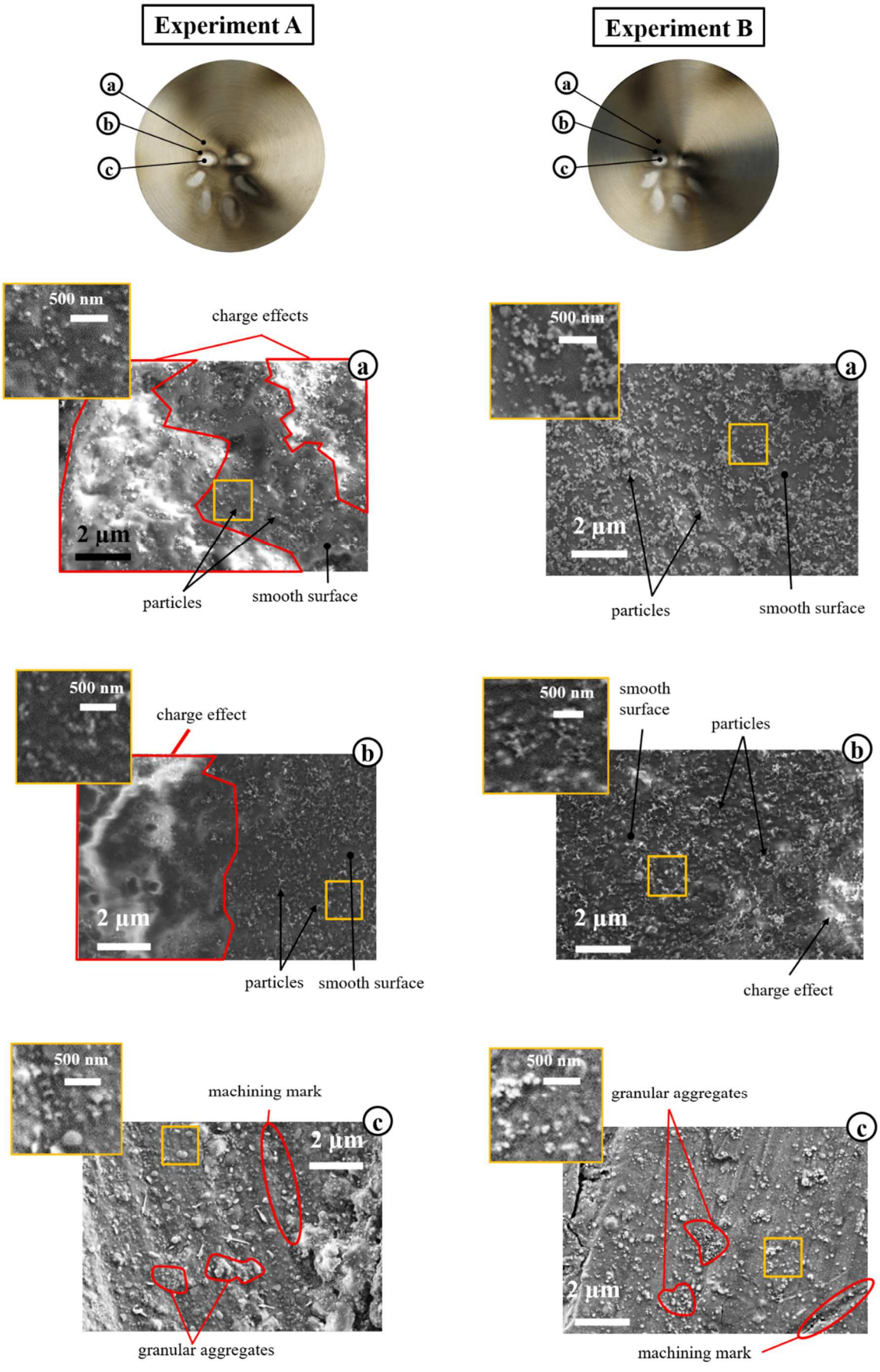

Figure 114: Microscopic observations of samples from experiments A and B by SEM-EDS.

To characterize the repeatability of the particle-size distribution measurement, the DMS 500 is used for both experiments A and B. Measurements are made throughout the 10-min duration of the experiments at an acquisition frequency of 1 Hz. For both experiments, the particle-size distribution shown in Figure 3 is invariant over time. It is therefore possible to average the particle-size distribution over the entire duration of the experiments and compare the resulting particle-size distribution for both experiments (Figure 116). The agglomeration mode is very similar for both experiments, centered around 65 nm and with a particle concentration of 6.4×10^7 cm^{-3} for A and 6.8×10^7 cm^{-3} for B. The primary-particle mode shows some differences between the two experiments. Although it is located around 10 nm for both experiments, the concentration is higher for B (2.5×10^8 cm^{-3}) than for A (1.55×10^8 cm^{-3}). Therefore, the evaluation criteria of the particle-size distribution will be based on significant differences in the position of the nucleation and accumulation peaks as well as on differences in concentrations of more than 1.0×10^8 cm^{-3}.

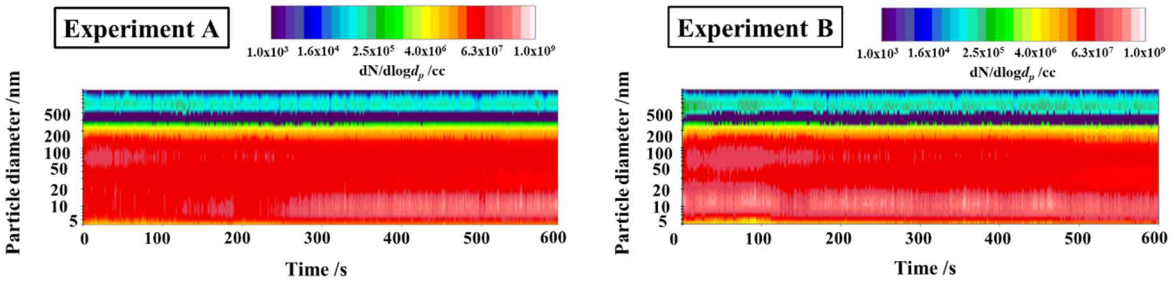

Figure 115: Temporal variation of the soot particle-size distribution in the exhaust for experiments A and B.

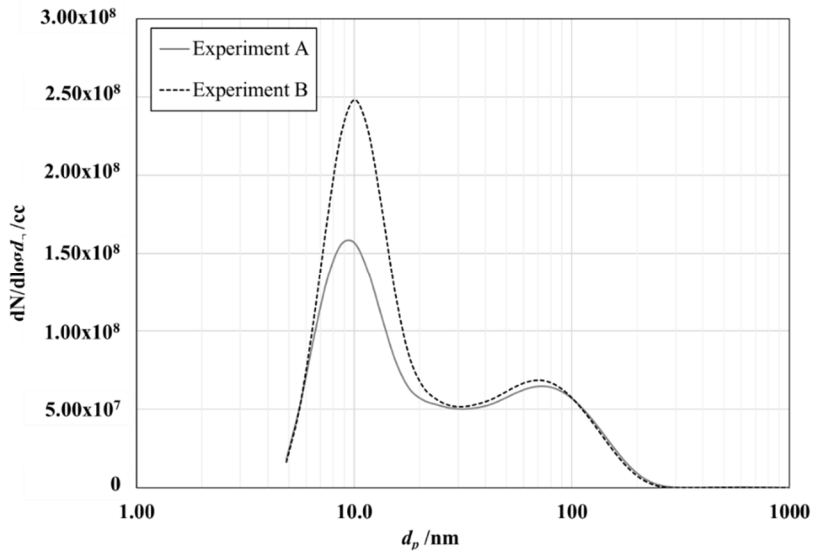

Figure 116: Averaged particle-size distributions for the experiments with early injection and warm start (experiments A and B).

6.1.2 Repeatability for *in situ* measurements

For the images obtained with the high-speed camera, the evaluation criteria are qualitative. The analysis of the images set obtained with experiments C and D shows similar characteristics, *i.e.*, of the liquid film and the same kinetics of deposits formation are observed, after 2 minutes of operation, the progress

of deposits formation is similar. Figure 117 compares the direct visualization of the two pistons at the 62nd cycle of the experiment. It should be noted that the two experiments have different angles of view and lighting. The piston surfaces in both cases have an observable deposits corresponding to the liquid-film spreading formed by the impact of the spray.

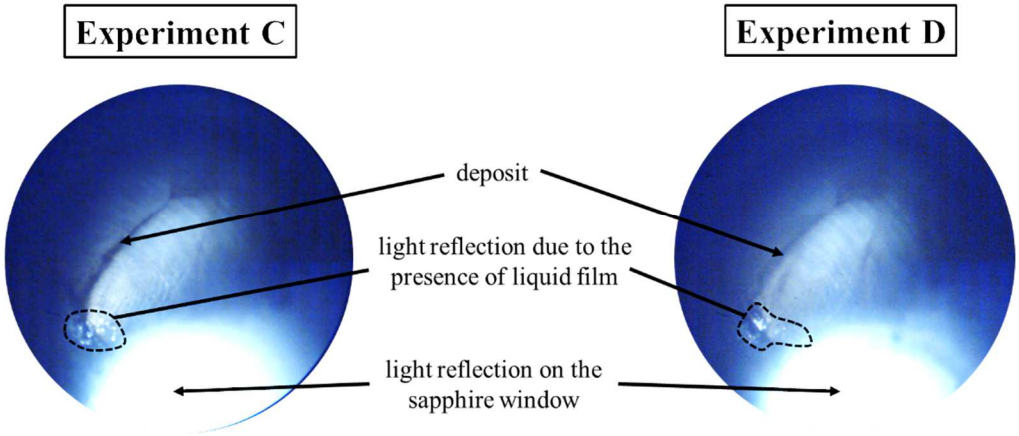

Figure 117: Images obtained by direct visualization of the piston surfaces for experiment C and D at the 62nd cycle (360 CAD BTDC injection, cooling water temperature: 20 °C, cold start).

6.2 Effect of the piston surface temperature on deposits formation

In this section, the influence of the of the piston-surface temperature on deposits formation is studied. As seen previously, the surface temperature can affect both deposits formation paths. It impacts the behavior of the liquid films and incidentally the deposits formation by the liquid-film path. It can also modify the temperature gradient at the walls of the combustion chamber and thus impacts thermophoretic transport and thus deposits formation via the soot path. In the following, first, the experiments matrix is described. Then the piston surface temperatures are characterized for the related operating conditions. Finally, the effect of the surface temperature on the deposit formation by the liquid-film-path and soot-path mechanisms is evaluated.

6.2.1 Presentation of the matrix of experiments

Four methods were used to control the surface temperature of the piston: (1) variation of the piston thickness (10 or 30 mm), (2) addition of air cooling (blower) from the backside of the piston, (3) variation of the cooling-water temperature (20 or 90 °C), and (4) use of the warm-start strategy to increase the initial piston surface temperature. These methods are illustrated in Figure 118.

As presented in chapter 5, two operating points were used to study both formation paths. The matrix of experiments to study the effect of temperature on deposit formation is presented in Table 9. Experiments #1 to #5 were performed to study the impact of surface temperature on the deposits formed by the liquid-film path and correspond to the early injection timing set at 360 CAD BTDC. Experiments #6 and #7 were carried out to study the impact of surface temperature on the deposits formed by the soot path and correspond to the late injection timing set at 60 CAD BTDC. The ignition timing is set to 37 CAD BTDC for all experiments. The duration of the experiments is 10 min. The characterization of the piston surface temperature for the different experiments is presented in the next section. Experiment #3 is considered in this study as the reference experiment to which the parametric variations influence will be compared.

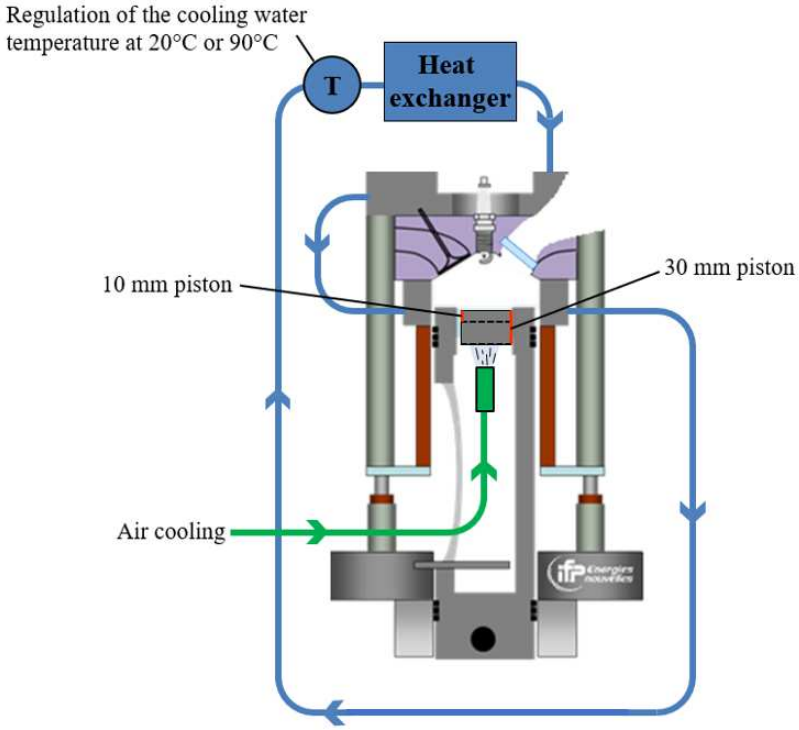

Figure 118: Schematics of the different methods to vary the temperature of the piston surface.

Table 9: Experiment matrix for the early and late injection experiments with the reference experiment #3 in bold black and the parametric variations from experiment #3 in bold red.

Experiment	Injection phasing	Spark timing	Pressure at the TDC	Engine experiment duration	Piston thickness	Blower	Warm start strategy	$T_{Cooling\ water}$
# 1	360 CAD BTDC	37 CAD BTDC	23 bars	10 min	**10 mm**	No	Yes	20°C
# 2	360 CAD BTDC	37 CAD BTDC	23 bars	10 min	**10 mm**	**Yes**	Yes	20°C
# 3 (Ref)	**360 CAD BTDC**	**37 CAD BTDC**	23 bars	**10 min**	**30 mm**	**No**	**Yes**	**20°C**
# 4	360 CAD BTDC	37 CAD BTDC	25 bars	10 min	30 mm	No	**No**	20°C
# 5	360 CAD BTDC	37 CAD BTDC	27 bars	10 min	30 mm	No	Yes	**90°C**
# 6	**60 CAD BTDC**	37 CAD BTDC	20 bars	10 min	30 mm	No	Yes	20°C
# 7	**60 CAD BTDC**	37 CAD BTDC	20 bars	10 min	30 mm	No	Yes	**90°C**

6.2.2 Characterization of the piston surface temperature

The piston surface temperature is measured by thermographic phosphor measurements as presented in section 3.3.1. For these measurements, the engine was operated in PFI mode. In addition, measurements were performed for the experiments performed with a cooling-water temperature of 20 °C. The temperature measurements therefore focus on experiments #1 – #4. It will then be considered that these measurements are representative of the direct-injection experiments, and that the injection strategy, *i.e.*, PFI *vs*. GDI, does not have a significant impact on the method used to vary the piston surface temperature. Therefore, experiments #3 (Ref) and #6 will be assumed to have the same piston thermal behavior.

For experiments #5 and #7 with the cooling water set to 90 °C, the piston temperature was determined from a 3D finite element simulation in ANSYS. To validate the use of this numerical simulation, a simulation was carried out to calculate the final temperature of the reference experiment #3 (Ref) and the result was compared with the measured temperature. The final temperature calculated for experiment #3 (Ref) is 171 °C, which matches the measured temperature of 169 °C. The numerical simulation is

therefore considered valid also for the other operating conditions. The temporal variation of the temperature for experiments #5 and #7 can then be extrapolated combining experiment # 3 and the result obtained with the simulation, 225 °C after 10 minutes of engine operation.

Figure 119 shows the temporal variation of the piston surface temperature for experiments #1 – #7. All temperature traces for the warm-start cases (*i.e.*, all experiments except #4) are similar: A continuous increase of about 20 °C is observed during the 10-min experiment. Experiment #4, as expected, shows a different behavior with a fast increase during the first two minutes of the experiment from 20 to ~130°C. After that, the piston temperature behaves similar to the warm-start cases. Therefore, it seems appropriate for the warm-start experiments to consider a time-averaged temperature, whereas for experiment #5, the temporal variation of the temperature will be considered. The average temperatures of the experiments are 175, 144, 159, and 215°C for the experiments #1, #2, #3 or #6, and #5 or #7, respectively (Figure 120).

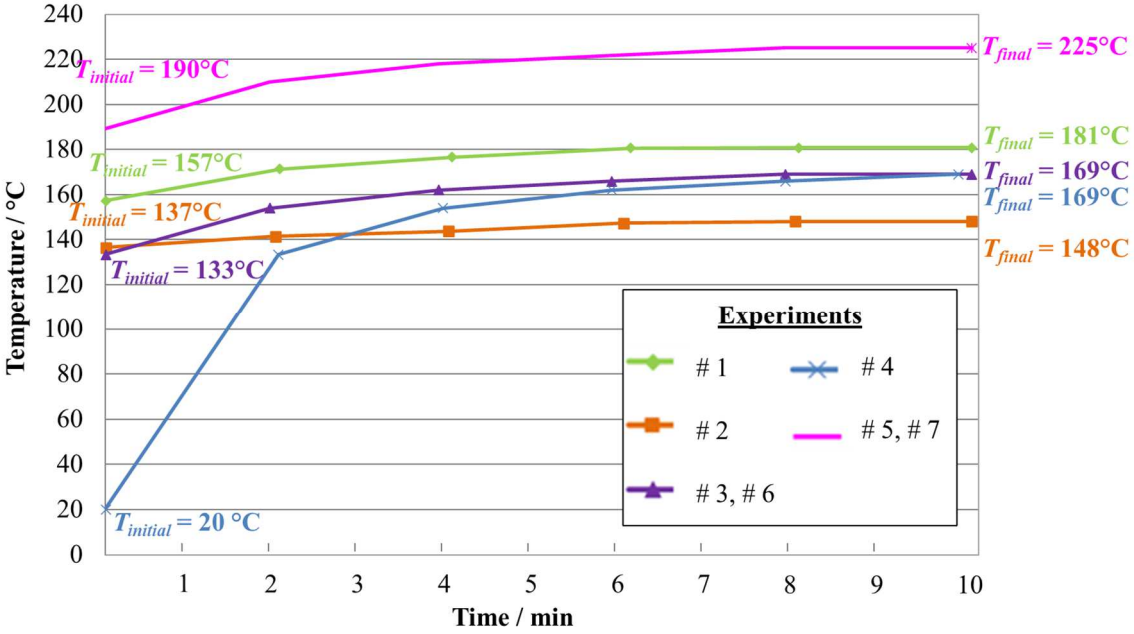

Figure 119: Temporal variation of the piston surface temperature during experiments #1–#7.

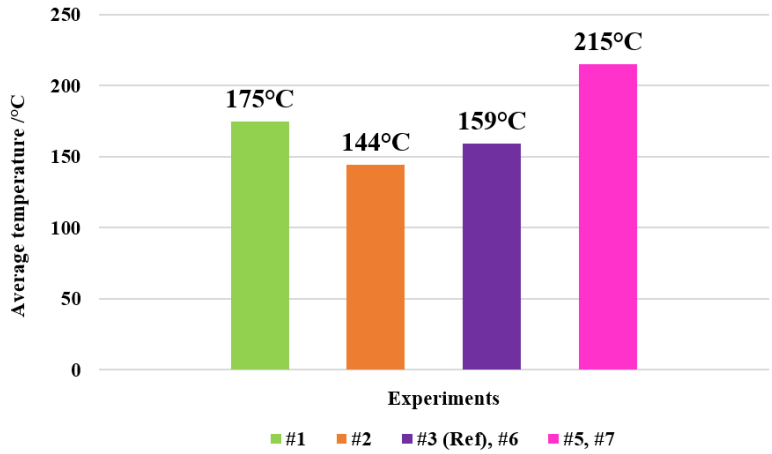

Figure 120: Average piston temperatures for the various warm-start experiments.

Experiments #1, #2, and #3 (Ref) have similar average temperatures. They will provide a fine analysis of the effect of temperature on the formation of the deposits. Experiment #5 has the largest temperature difference of 56 °C compared to the reference experiment #3. For experiment #4, during the first two minutes the temperature increases rapidly and then gradually reaches a temperature identical to experiment #3 (Ref) at 169°C. The average temperature of experiment #3 (Ref) between 2 and 10 min is 151°C. The thermal behavior of the piston over this period is similar to experiments #1, #2, and #3.

6.2.3 Influence of the piston surface temperature on deposits formation

6.2.3.1 Effect of the piston surface temperature on the liquid-film path deposit formation

Early injection conditions experiments are used to study the deposit formation through the liquid-film path for various piston surface temperatures. In chapter 3 and 4 it was shown that for early injection, the deposit morphology corresponds to the reference liquid-film path deposit. The analysis of the piston surfaces is based on the two deposit zones identified in Chapter 4 (Figure 121). The first zone studied is the inner zone that includes the two sub-zones of deposition called spray-impact periphery and spray-impact area. The second zone studied is the outer zone. For these two zones, macroscopic analysis of the deposits is first performed. The deposit area, pattern, color, and texture are compared between the different experiments. Then, a microscopic analysis is performed to confirm the presence of liquid-film path deposit, and to identify whether a temperature variation induces differences in the deposit morphologies. The results from the different experiments are then confronted with the Nukiyama theory to identify the evaporation regimes of the liquid films regarding the temperature. Finally, the influence of temperature on the liquid-film path will be assessed. The pistons sampled after the experiments are shown in Figure 122. The images obtained by SEM-EDS microscopy are presented in Annex B.

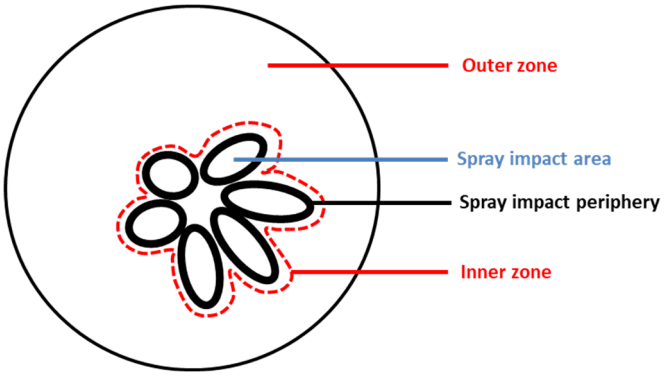

Figure 121: Schematics of the inner and outer areas of piston deposits.

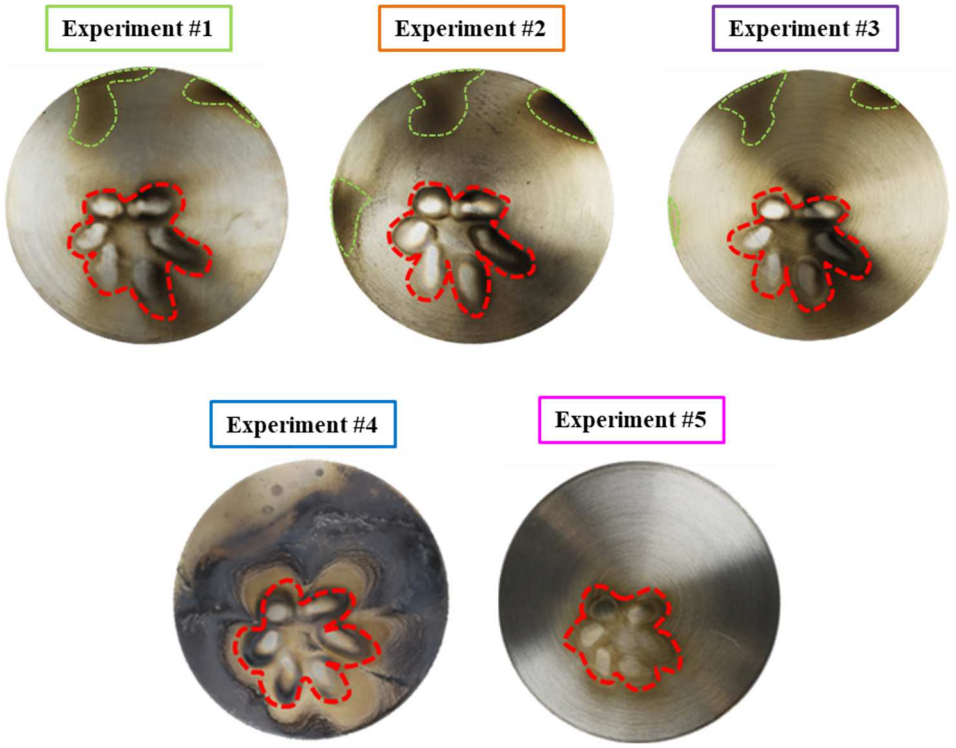

Figure 122: Images of the piston surfaces of experiments #1–#5 with early injection. For each case, the red line marks the inner zone from the external zone and the green lines delimit the brown marks.

In the inner zone, clear (mostly deposit-free) areas corresponding to the spray impact and darker areas corresponding to the periphery of the spray impact are observed for the five experiments but in different proportions. Experiments #1, #2, and #3 (Ref) have the same inner-zone size with the spray impact area being clear, *i.e.*, resembling the color of the aluminum, and the spray-impact periphery being brown. In comparison, experiment #4 (cold start) presents a similar inner zone, with a clear spray impact area but with a larger black spray impact indicating more deposit. For experiment #5 (warm cooling water), the inner zone size is reduced by about 10 % compared to the other four experiments. The spray impact periphery is brown and it is possible to distinguish the machining marks indicating a thin deposit layer. The spray-impact area is clear, like in the other four experiments.

Microscopic analysis (Annex B) showed that for all experiments the spray impact periphery corresponds to the liquid-film path deposit and the spray impact area has a granular surface, where it is not possible to distinguish the deposit corresponding to the liquid-film path. The microscopic analysis does not show any unexpected morphology. These results are consistent with the analysis of the liquid-film path mechanisms in Chapter 4. They confirm the presence of liquid-film deposit in the spray-impact periphery as a liquid-film accumulation zone and the spray impact area with little deposit as a zone of minimum liquid-film thickness.

From all these results it seems that for a high initial temperature of the piston, the deposit formation by the liquid-film path in the inner zone is limited. For a low initial temperature of 20 °C in contrast, the deposit formation of the inner zone is promoted. For piston temperatures between 144 and 175 °C, there is no significant effect of the surface temperature on the formation of liquid-film path deposit in the inner zone.

Regarding the outer zone, experiments #1, #2, and #3 (Ref) show a thin brown deposit for which it is possible to distinguish visually the machining marks. Experiment #1 shows zones with the color of the

aluminum surface, which indicates the absence of deposits. Also, brown marks marked in green in Figure 122 are observed at the periphery of the pistons for experiments #1, #2, and #3. The mechanism responsible for these brown marks observed earlier in Chapter 5 has not been clearly identified. Therefore, the analysis of the effect of surface temperature on these marks is limited. Experiment #4, which was studied in the previous section, has a smooth, matt black deposit area compared to the other four samples. This black area seems rather thick as it is not possible to distinguish the machining marks of the piston surface. The existence of brown marks for experiment #4 cannot be determined because of the black deposit covering the surface of the piston. For experiment #5, no deposit is observed macroscopically. The entire outer zone corresponds to the color of the aluminum surface of the piston.

Microscopic analysis showed that for experiments #1–#4, the outer zone (brown marks excluded) corresponds to the liquid-film path deposit. This result is consistent with the analysis of the liquid-film path deposit formation mechanisms which shows that this outer zone corresponds to the spreading of the liquid film. Figure 123 compares SEM microscopic images of the outer zone of the piston in experiment #5 with the clean piston surface. Machining marks are observed in both cases, confirming the absence of deposit in the outer zone for experiment #5. Abrasion marks and impurities characteristic of the clean surface are also identified in experiment #5.

Lowering the initial surface temperature from 133 to 20 °C has a significant impact on the deposit formation in the outer zone with a significant increase of deposit formation. Changing the average surface temperature from 144 to 175 °C does not have a significant impact on the outer zone deposit formation. By significantly increasing this temperature to 215 °C, the deposit formation in the outer zone is greatly reduced. High surface temperatures seem to limit the formation of brown marks.

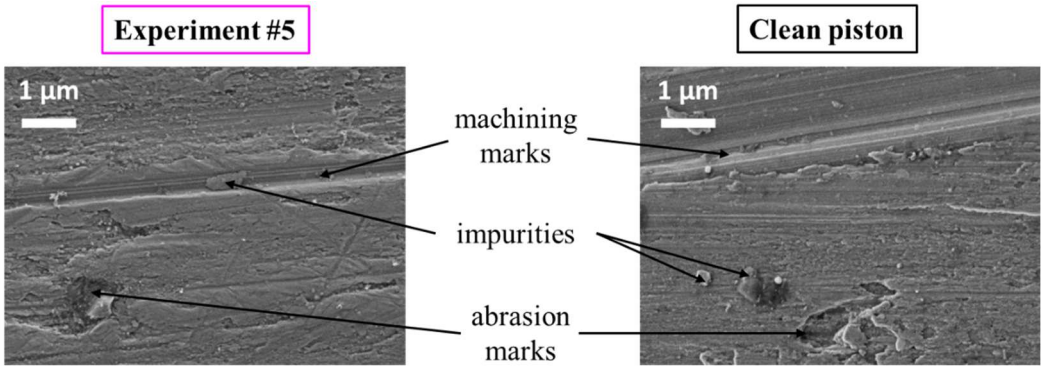

Figure 123 : SEM images of the outer zone of the piston surface in experiment #5 and of a clean piston surface.

Now that the effect of surface temperature on the formation of the deposit by the liquid-film path has been evaluated, the effect of surface temperature on the liquid-film thermal behavior is studied. To determine the liquid film evaporation regimes of experiments #1–#5, the piston temperature ranges of the five experiments are displayed on the Nukiyama curve of the RFG fuel (surrogate of the E10 fuel used in the experiments) in Figure 124.

Experiments #1, #2, and #3 (Ref) are situated on the part of the curve corresponding to the transition from regimes II to III. Experiment #4, due to the large temperature variation of the piston, corresponds to regime I, II, and III. Experiment #5 is in regime III. Considering the temperature variation in the combustion chamber during an engine cycle, the Nukiyama theory shows that the Nukiyama curve horizontally shifts towards the hottest temperatures and the part of the curve corresponding to regimes III and IV is vertically shifted towards much shorter liquid-film lifetimes. Thus, the lifetimes of the liquid films in the experiments are modified with pressure.

As the pressure increases, experiments #1, #2, and #3 (Ref) are more likely to shift towards regime II, *i.e.*, the liquid film evaporates more and more rapidly through the 10-min experiment. Experiment #4 starts in regime I and ends in regime II. It therefore follows very slow evaporation of the liquid film at the beginning of the experiment, which then gradually shifts to faster evaporation in regime II. The pressure effect should be taken into account. In the engine, peak pressure are significantly above 1 bar. Therefore, as mentioned in section 5.2.4.1 of Chapter 5, the evaporation time in regimes III and IV are reduced significantly. The consequence is that experiment #5 is very probably characterized by a fast evaporation of the liquid film.

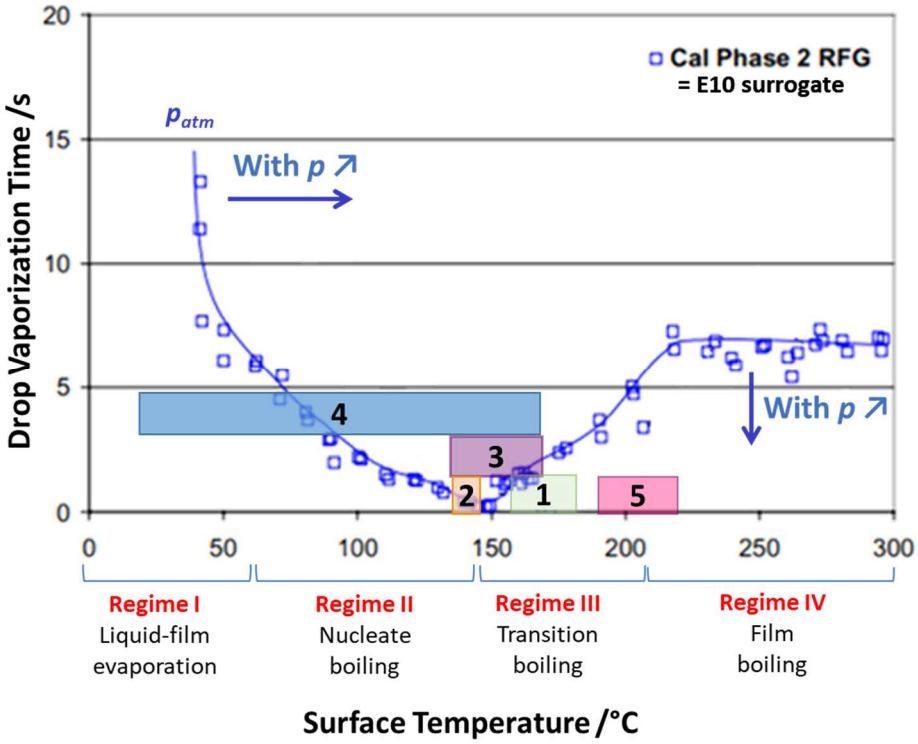

Figure 124: Nukiyama curve of RFG fuel at atmospheric pressure (p_{atm}) displaying the temperature ranges typical for the five early-injection experiments investigated here [107].

As seen in section 5.2.4 of Chapter 5, the mechanism of deposit formation by the liquid-film path is linked to the formation of the liquid film in different zones of the piston surface. These zones are the spray-impact area, the spray-impact periphery, and the outer zone. In each zone, the deposit formation is governed by a different phenomenon which could be impacted by the piston surface temperature. These phenomena are the cooling effect, the liquid-film accumulation and the liquid-film spreading, corresponding to the above mentioned zones.

Spray cooling, the accumulation zones, and the spreading are weakly impacted when the global temperature of the piston surface varies by ±15 °C compared to the reference case at 159 °C. When the temperature of the piston surface increases more significantly (experiment #5 at 225 °C), the spreading zone is strongly reduced and this leads to a 100 % reduction of the deposit formation through the liquid-film path. The spray-impact area is less impacted which means that the cooling effect of the spray can counterbalance the surface temperature increase. For low temperature as in the cold-start case, the deposit formation is increased in every zone as it favors the liquid film formation and elongates its life time.

To resume, increasing significantly the temperature is a way to limit the deposit formation through the liquid film path by reducing the lifetime of the liquid film and reducing the consequences of the spray cooling effect.

6.2.3.2 *Effect of the piston surface temperature on the soot-path deposit formation*

This study focuses on the comparison of the deposits formed for two different temporal average surface temperatures, a low temperature of 159 °C and a high temperature of 215 °C, corresponding to experiments #6 and #7, respectively. The objective is to generate different near-wall temperature gradients to evaluate the impact of the surface temperature on thermophoresis and therefore on deposit formation by the soot path. The investigations focus on the macroscopic and microscopic analysis of the deposits formed on the pistons as well as the analysis of the particle-size distribution in the engine exhaust during the experiments.

The piston-surface samples obtained from experiments #6 and #7 are shown in Figure 125. In both cases, the piston surfaces show black deposits with a matt appearance. A pattern corresponding to the impact of the six-cone spray is observed for both experiments that is different for the two experiments. A black area deposit is also present for both experiments. Its area is about 60 % smaller in experiment #7 than in experiment #6. According to these observations, increasing the surface temperature affects the deposit formation via the soot path.

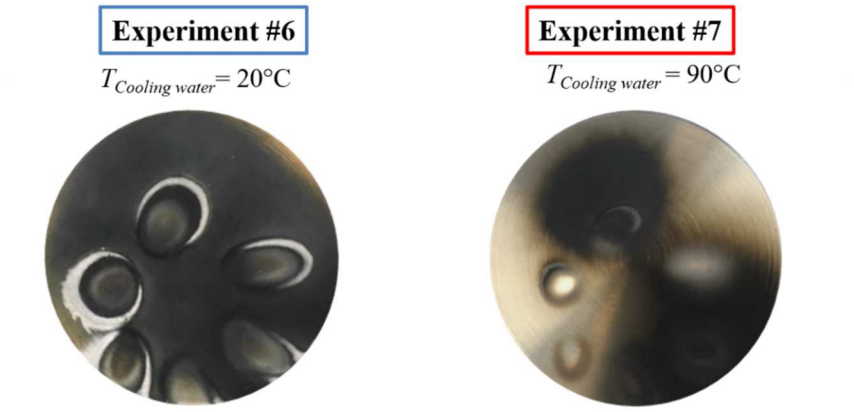

Figure 125: Images of the piston deposits formed at late injection.

To determine whether the surface temperature alters the soot-path mechanism, microscopic analyses are presented in Figure 126. For both experiments, four zones are identified with the microscopic analysis. These zones correspond to the black deposit observed around the spray impact location, the clear area observed at the spray impact, the spray impact zone, and the zone at the center of the six spray impacts, named zone (a), (b), (c), and (d), respectively (Figure 126). Zone (a) shows a particle morphology with an average diameter below 100 nm for both experiments. These particles form a homogeneous layer on the piston surface. Zone (b) shows a smooth surface morphology with particles that appear coated in the smooth surface for both experiments. These particles are larger than those in zone (a) with an average diameter up to 200 nm. This morphology is homogeneous over the whole zone. Zone (c) shows large particles agglomerates of the order of 3 µm in diameter for experiment #6 and of the order of 1 µm in diameter for experiment #7. For both experiments, the particles constituting the agglomerates measure less than 100 nm in diameter. The morphology observed in zone (d) is similar to the morphology of zone (a) and corresponds to a layer of particles, for both experiments. These particles also measure an average diameter below 100 nm.

From these observations, it appears that a variation of the piston surface temperature from 159 to 215 °C has little effect on the morphology of the deposits. Increasing the surface temperature does not seem to change the mechanisms involved in the deposit formation in the case of late injection.

Macroscopic and microscopic analysis showed that increasing the surface temperature from 144 to 215 °C does not have a significant effect on the morphology of the deposit but does have a significant impact on the amount of deposit formed with an approximate 60 % reduction in the soot path deposit.

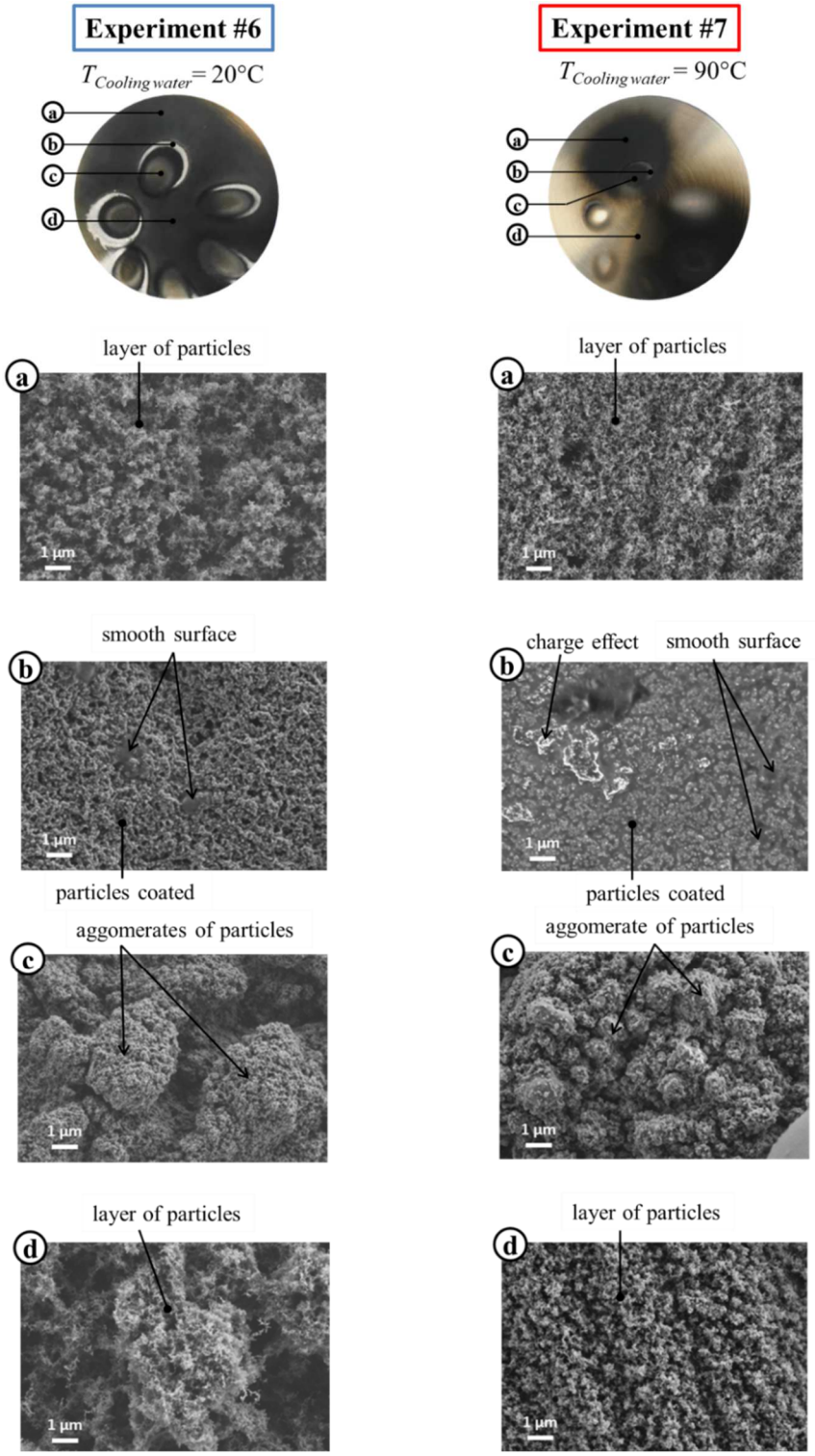

Figure 126: SEM images of deposits for cases #6 and #7.

The objective is now to investigate the role of the soot particle-size distribution found in the exhaust gas on how the surface temperature influences the deposit formation mechanism by the soot path. Based on the analysis presented in Chapter 4, the formation of the soot path deposit by thermophoresis depends on the particle-size distribution and the temperature gradient near the wall. The temporal variation of the particles-size distribution is presented in Figure 127. It is temporally invariant for both experiments. The average particle-size distributions are presented in Figure 128. Experiments #6 and #7 show an agglomerate mode with a peak at 100 nm for 5.0×10^8 cm^{-3} and a peak at 87 nm for 5.8×10^8 cm^{-3}, respectively. In addition, the agglomerate mode is much stronger than the primary-particle mode for both experiments. Their particle-size distributions are therefore similar. We can therefore deduce that the difference in the amount of deposit observed between the two experiments is mainly due to the impact the temperature of the piston surface on the thermophoretic force.

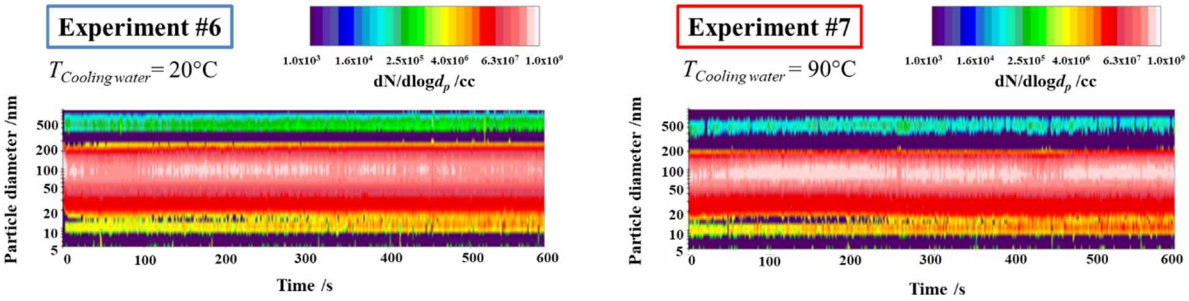

Figure 127: Temporal variation of the particle-size distribution for experiments #6 and #7.

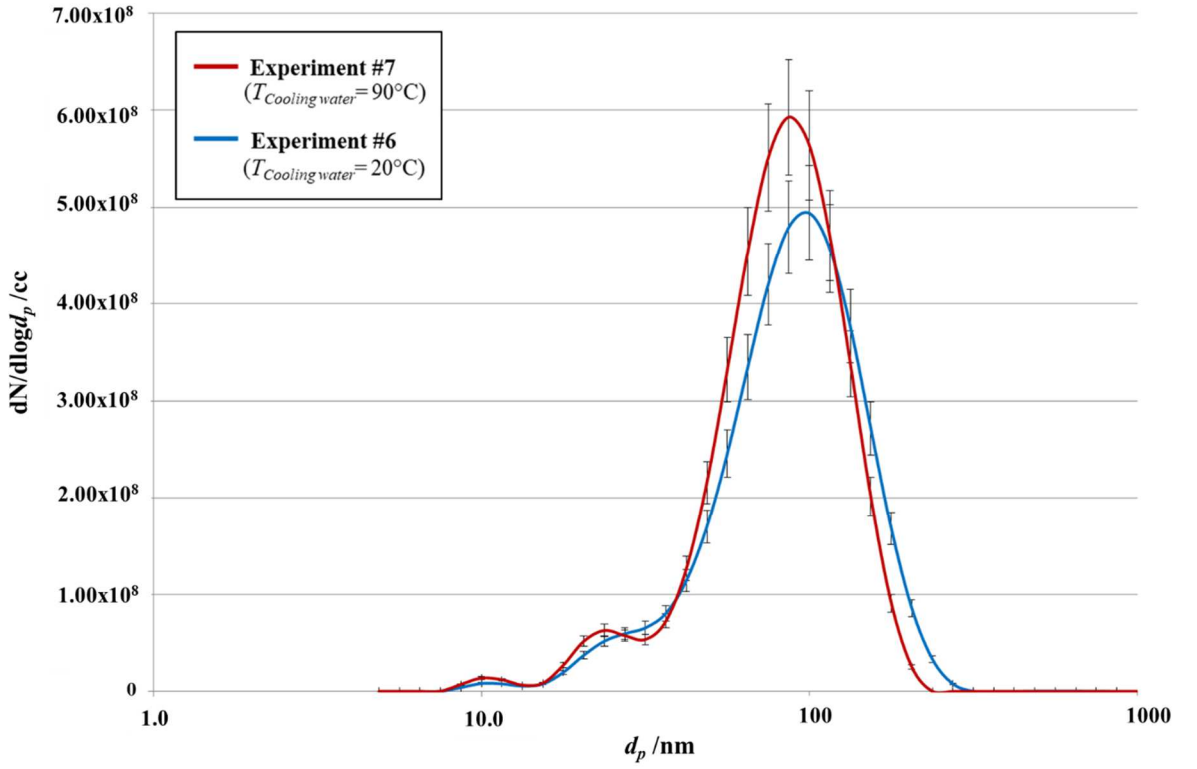

Figure 128: Averaged particle-size distribution for experiments #6 ($T_{\text{cooling water}}$ = 20 °C) and #7 ($T_{\text{cooling water}}$ = 90 °C).

In conclusion, increasing the piston surface temperature affects the deposit formation through the soot-path mechanism. The analysis of the results showed that from 159 to 215°C, the deposit formation was decreased by about 60 %. This result is attributed to a reduction of the thermophoresis effect due a reduction of the temperature gradient.

6.2.3.3 Conclusion on the effect of surface temperature on the formation of deposits by the liquid-film path and the soot path

The variation of the temperature of the piston surface has an impact on the mechanisms of deposit formation by the liquid-film path and the soot path. For the liquid-film path, increasing the initial piston surface temperature from 20 to 190 °C reduces deposit formation in the inner zone and prevents deposit formation in the outer zone. A variation by ±20 °C around the reference point has a minor impact on the liquid-film mechanism. The piston surface should be at the beginning of regime III of the Nukiyama curve of the fuel used when the engine is started to limit the risk of deposit formation via the liquid-film path. For the soot path, increasing the surface temperature from 159 to 215 °C reduces soot deposition by thermophoresis and thus soot-path deposition.

6.3 Influence of the surface roughness on deposits formation

Previous experiments in the literature showed that at ambient pressure and temperature, the deposit formation by the liquid-film path is affected by the roughness of the deposition surface [117]. This section investigates the effect of surface roughness on the formation in engine of the liquid-film path deposit. The first objective of this section is therefore to evaluate the impact of roughness on the quantity of deposit under engine conditions. The second objective is to determine whether a smooth surface (roughness $Ra \approx 0.1$ nm) such as those used in optical access engines is representative of a standard surface ($Ra = 1.2$ µm) for studying deposit formation.

6.3.1 Matrix of the roughness effect experiments

To study the effect of piston surface roughness on deposit formation by the liquid-film mechanism, early-injection experiments are performed. Two different initial conditions are studied: Warm start with an initial piston surface temperature of 133 °C and cold start with an initial piston surface temperature of 20 °C. The objective is to analyze two cases of liquid film formation, *i.e.* a case where the spreading of the liquid film is limited and a case where it is favored, corresponding to the warm and cold start cases, respectively. For the warm-start experiments, three different levels of piston surface roughness were studied: $Ra = 1.2$ µm, which corresponds to a standard roughness typically found for parts inside a combustion chamber; $Ra = 60$ nm, which corresponds to a mirror finish; and $Ra = 0.3$ µm, an intermediate value. For the cold-start case, two experiments were performed with steel pistons with different surface roughness ($Ra = 0.3$ and 1.2 µm). The operating conditions are summarized in Table 10. The pistons are sampled after each experiment. To study the effect of roughness on the formation mechanisms by the liquid-film path, ex-situ macroscopy and microscopy analyses are performed as well as *in situ* direct visualization analysis.

Table 10: Experiment matrix for the roughness experiments.

Cases	*Ra*	Injection phasing	Spark timing	Engine experiment duration	Piston thickness	Warm start strategy	$T_{Cooling\ water}$	$T_{Initial}$	T_{Final}
Warm start	1.2 µm	360 CAD BTDC	37 CAD BTDC	10 min	30 mm	Yes	20°C	133°C	169°C
	0.3 µm	360 CAD BTDC	37 CAD BTDC	10 min	30 mm	Yes	20°C	133°C	169°C
	0.06 µm	360 CAD BTDC	37 CAD BTDC	10 min	30 mm	Yes	20°C	133°C	169°C
Cold start	1.2 µm	360 CAD BTDC	37 CAD BTDC	10 min	30 mm	No	20°C	20°C	169°C
	0.3 µm	360 CAD BTDC	37 CAD BTDC	10 min	30 mm	No	20°C	20°C	169°C

6.3.2 Influence of the surface roughness on deposits formation by the liquid-film path

6.3.2.1 Effect of surface roughness when liquid-film spreading is limited

In the warm start case, the piston surfaces are first analyzed macroscopically and then microscopically. For the three piston surfaces with different roughness, the inner zone corresponding to the impact of the six-cone spray, marked in red in Figure 129, is analyzed. This zone has the same dimension and the same pattern for all three cases. The deposit in the inner zone has a brighter appearance when the roughness decreases from 1.2 µm to 0.06 µm. In addition, the six spray-impact zones appear sharper for the piston with a roughness of *Ra* = 0.06 µm. In comparison, the other pistons have a blurred boundary for these same zones. Outside the inner zone, *i.e.*, inside the outer zone, brown marks are observed for all three pistons. Grey zones are also observed for the pistons with roughness of 0.3 and 0.06 µm. These brown marks and grey zones are also sharper for the case 0.06 µm compared to the other cases.

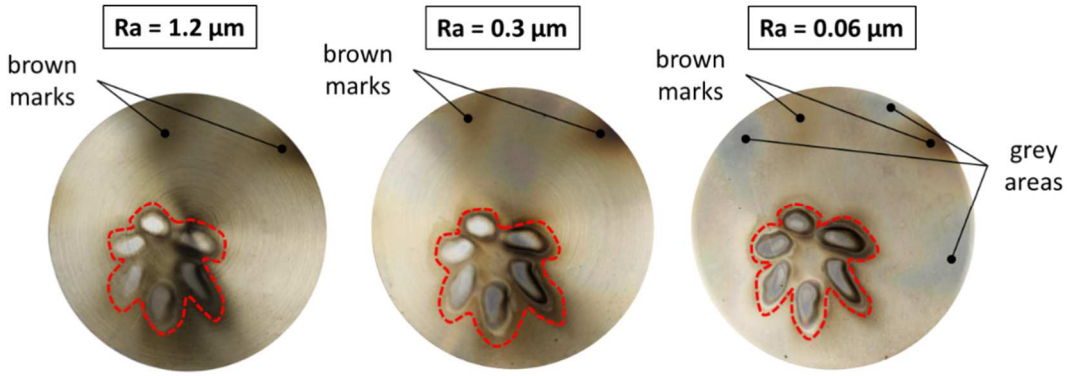

Figure 129: Deposits on steel pistons with three different roughness, the first piston is the reference case.

Microscopic observations comparing different deposition zones between the three pistons are shown in Figure 20. These zones are named (a), (b), and (c) and correspond to the outer zone, the spray impact periphery, and the spray impact area, respectively. For zone (a), all three pistons show the same morphology of smooth surface corresponding to liquid-film path deposit and particles corresponding to soot path deposit. These particles have an average diameter of less than 100 nm for the case *Ra* = 1.2 µm, and of the order of 500 nm for *Ra* = 0.3 µm and *Ra* = 0.06 µm. For zone (b), the pistons with *Ra* = 1.2 and 0.3 µm show similar morphologies of smooth surface and average particle diameter below 100 nm. The piston with *Ra* = 0.06 µm also has a smooth surface and particles of the same dimensions, but it also shows many large agglomerates with sizes between 250 and 500 nm. For zone (c), all three pistons have a granular appearance. Microscopic observation of the grey zones was also carried out for pistons with roughness of 0.3 and 0.06 µm to determine whether they correspond to an absence of deposits. Figure 21 shows the microscopic observation of one of the grey zones for the *Ra* = 0.06 µm piston. The image shows the presence of a deposit, with a smooth surface morphology and particles with an average

diameter of less than 100 nm corresponding to the liquid-film path and the soot path respectively. The same analysis is drawn from the observation of the grey zones of the *Ra* = 0.3 µm piston.

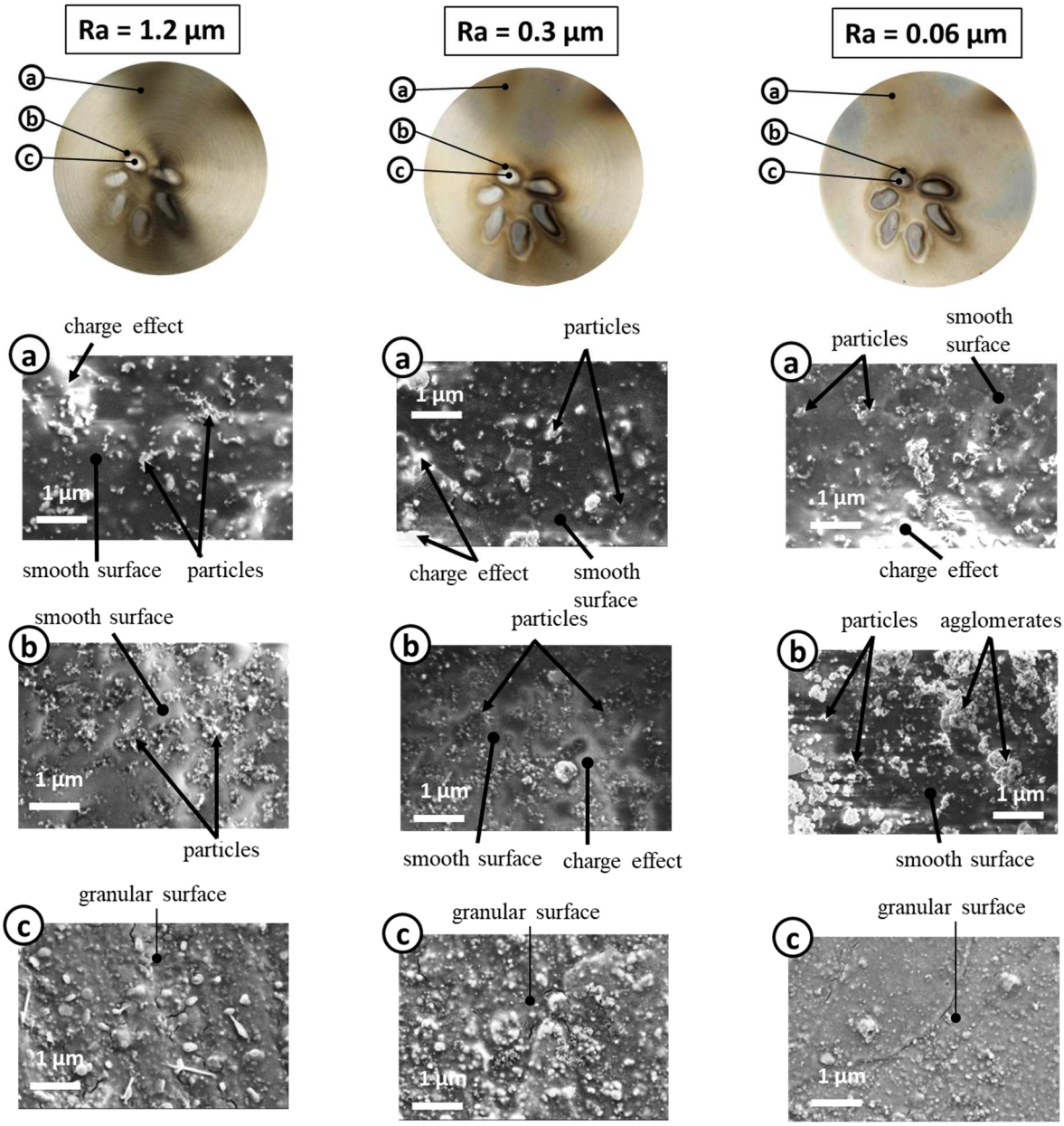

Figure 130: Microscopic observation of the deposits on three pistons with different roughness.

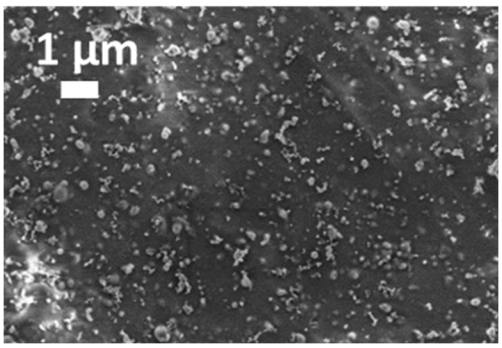

Figure 131: Microscopic observation of one of the grey zones of the piston with a *Ra* = 0.06 µm.

From all these observations, decreasing the roughness from 1.2 to 0.06 µm does not seem to have a significant effect on the mechanisms by which the deposit is formed by the liquid-film path, apart from a sharper effect on the boundaries of the different deposition zones. The deposit morphologies are very similar between the different pistons and correspond to the liquid-film path and soot path deposits, except for the observation of particle aggregates in the two pistons with lower roughness. In conclusion, when the spreading is limited, the roughness does not have an important effect on the mechanisms by which the deposit is formed by the liquid-film path.

6.3.2.2 Effect of surface roughness when liquid-film spreading is promoted

The analysis now focuses on the cold-start operation promoting liquid-film spreading formation for pistons with *Ra* = 1.2 and 0.3 µm. Macroscopic and microscopic analyses of the piston surfaces are presented in Figure 132. The same three deposition zones are observed on the two pistons: A black zone outlined in yellow, a clear zone outlined in red, and six zones outlined in black corresponding to the impact of the six-cone spray. What distinguishes the two pistons are the boundaries between these zones: they appear blurred for *Ra* = 1.2 µm and sharper for *Ra* = 0.3 µm. Moreover, the clear zone is larger for the *Ra* =0.3 µm piston. The deposit of the *Ra* = 0.3 µm piston has a bright appearance compared to the *Ra* =1.2 µm piston.

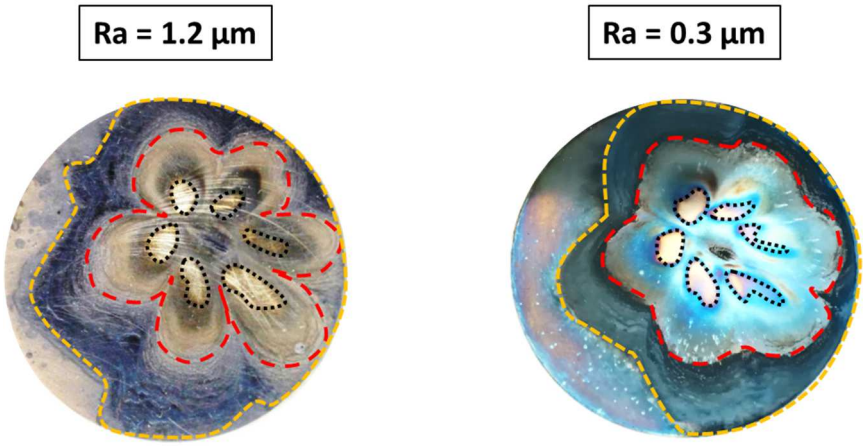

Figure 132: Images of the deposits formed at cold start on two steel pistons with different roughness.

The microscopic images comparing different deposition zones between the two pistons are presented in Figure 133. These zones are named (a), (b), and (c) and correspond to the spray-impact area, the spray-impact periphery, and the black deposit, respectively. For zone (a), the *Ra* =1.2 µm piston shows an average particle diameter of less than 100 nm. These particles are not observed for the other piston with a roughness of 0.3 µm. The observation of machining marks on the surface of the *Ra* = 0.3 µm piston tends to show that less deposit is obtained in zone (a) when the roughness is decreased. For zone (b), the same morphology is observed for both pistons with particles deposited on a smooth surface with an average particle diameter of less than 100 nm. For zone (c), the same smooth surface morphology is observed in both cases. For the *Ra* =1.2 µm case, there are particles with an average particle diameter of less than 100 nm on the surface that do not seem to be present for the *Ra* = 0.3 µm case.

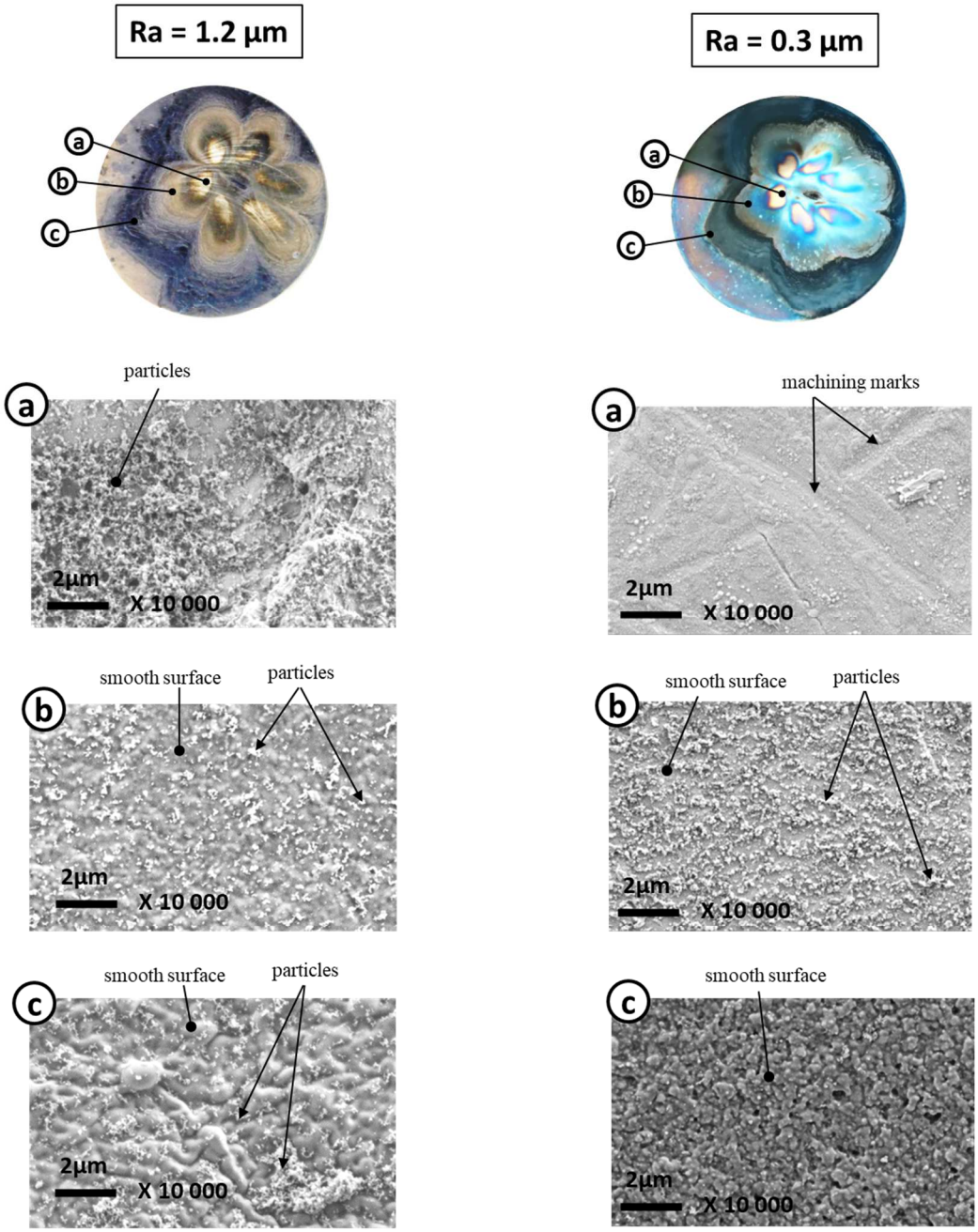

Figure 133: Microscopic analysis of the deposits on two steel pistons with different roughness.

The macroscopic differences observed correspond to a higher brightness of the deposit and a sharper boundary of the deposition zones. Microscopic analysis showed that for both pistons, the liquid-film accumulation zone corresponding to the spray-impact periphery and the spreading zone (zone (b) and (c), respectively) exhibit a morphology corresponding to the liquid-film path. The spray-impact area does not show any liquid-film path related deposit, for both pistons. All these results show that the variation of the roughness from 1.2 to 0.3 µm conserves the formation of deposit by the liquid-film path when the liquid-film spreading is promoted. It is also observed a similar surface area for the deposit formed in the spreading area for both roughness, which could mean that the intensity of the spreading is not affected by the roughness. It can thus be concluded that reducing the roughness does not significantly affect the liquid-film path mechanism of deposit formation.

6.3.2.3 Conclusion on the effect of the surface roughness on liquid-film-path deposit formation

The impact of surface roughness on the deposition mechanisms of the liquid-film path was studied for two operating points, a warm-start case and a cold-start case. For the warm-start case, the reduction of the roughness from 0.3 to 0.06 µm has no significant impact on the deposit formation mechanisms of the liquid-film path. Nevertheless, the boundaries between the deposition zones seem sharper as the roughness decreases. For the cold-start case, the reduction of the roughness from 1.2 to 0.3 µm impacts the pattern corresponding to the spray impact. As for the previous case, the boundaries between the deposition zones appear sharper, which can be attributed to an effect of the roughness on the surface tension of the liquid film on the surface [118]. It would be interesting to study the impact of roughness on the surface tension of liquid films and understand how it impacts the spreading and accumulation areas of the liquid film.

To conclude, the roughness seems to have no significant impact on the formation of engine deposits by the liquid-film path. It therefore seems that roughness is not an effective lever to reduce the formation of deposits by the liquid-film path. This result is interesting in the framework of the use of transparent materials to study deposit formation using optical diagnostics. Based on the negligible effect of roughness found here one may conclude that optical parts, characterized in particular by very low roughness (since optical windows are polished to an optical grade), may be suitable materials that do not seem to cause bias in the deposit formation because of their flat surfaces. This aspect will be investigated in more detail in the next section.

6.4 Influence of surface material on deposits formation

This section presents the study on the influence of the use of various materials on the formation of the liquid-film path deposit. This is pf specific interest in the context of transparent materials that would enable the optical investigation of deposit formation. Two transparent materials of interest are quartz and sapphire. First, they are investigated as thin coatings on aluminum pistons to limit the influence of their thermal properties on the deposit formation. Then, a solid sapphire piston is studied. The aim is to determine whether the deposits formed using transparent materials are representative of the deposits obtained on the aluminum pistons. Such result would be of great interest and would allow the use of optical diagnostics for future investigations on liquid film *in situ* measurement.

6.4.1 Experimental conditions

As shown in section 5.3, the soot-path mechanism depends on the distribution in size and number of the particles, the near-wall temperature gradient, and the turbulence intensity. It seems therefore that materials variations do not have a significant effect on soot deposition on the piston surface assuming that an appropriate strategy is chosen to ensure that the surface temperature is similar. Thus, in this section, the effect of transparent materials is evaluated focusing on the liquid path mechanism.

First, to assess the influence of the materials while limiting the influence of its thermal properties, engine experiments are carried out with aluminum pistons with thin quartz and sapphire coatings[7] and the results are compared to reference experiments with an aluminum piston. Both coatings have a thickness of 1.5 µm. It can then be assumed that the surface temperature is identical between the coated pistons

[7] The coatings of the pistons are obtained by spraying a powder of the desired material.

and the aluminum reference piston. The resulting roughness of these coatings is identical to that of the reference piston, *i.e.*, *Ra* = 1.2 µm.

To determine the effect of the surface temperature of a solid transparent piston on the formation of the liquid-film path deposit, an engine experiment is performed with a full-sapphire piston. Full-quartz pistons were not investigated because the thermal properties of quartz are significantly different from aluminum, and when thermal representativeness is required, sapphire is often chosen to conduct optical engine experiments. To avoid the influence of the roughness, the aluminum reference experiment is carried out with a polished aluminum piston with a roughness of *Ra* = 0.06 µm. This value is considered close enough to the optical roughness of the sapphire window (*Ra* = 0.1 nm).

The thermal behavior of the two solid pistons was characterized. Figure 134 shows the surface temperature variations of full-sapphire and aluminum pistons obtained *in situ* by phosphor thermometry. For the full-sapphire experiment, data beyond 2 minutes cannot be used because the temperature reach values above the calibration limit, around 240 °C. This means that the temperature of the full-sapphire piston is significantly higher compared to the aluminum reference piston. This temperature will be therefore taken into account in the analysis of the deposit formation.

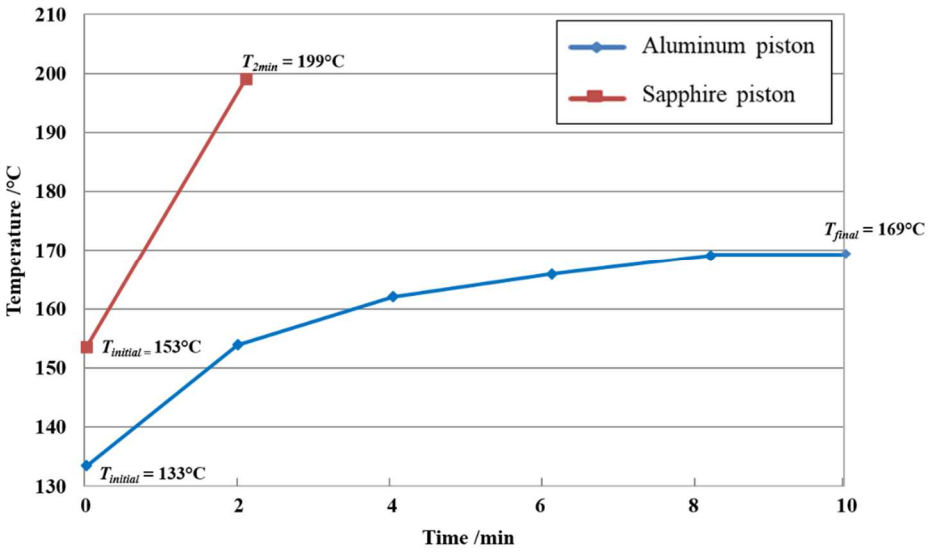

Figure 134: Variation of the aluminum and sapphire piston surface temperature measured by phosphor thermometry during engine operation.

Table 11 shows the matrix of experiments in this study. For all experiments, the early injection is set at 360 CA BTDC with the warm start strategy defined in Chapter 3, and the cooling water temperature set at 20 °C. The warm-start strategy is chosen to limit the effect of temperature when comparing the aluminum piston with the full-sapphire piston.

Table 11: Matrix of experiments

Effect evaluated	Material	*Ra*	Injection phasing	Spark timing	Engine experiment duration	Piston thickness	Warm start strategy	$T_{Cooling\ water}$
Material	Aluminum	1.2 µm	360 CAD BTDC	37 CAD BTDC	10 min	30 mm	Yes	20°C
	Quartz coating	1.2 µm	360 CAD BTDC	37 CAD BTDC	10 min	30 mm	Yes	20°C
	Sapphire coating	1.2 µm	360 CAD BTDC	37 CAD BTDC	10 min	30 mm	Yes	20°C
Full transparent material	Aluminum	0.06 µm	360 CAD BTDC	37 CAD BTDC	10 min	30 mm	Yes	20°C
	Sapphire	0.1 nm	360 CAD BTDC	37 CAD BTDC	10 min	30 mm	Yes	20°C

6.4.2 Analysis of the influence of quartz and sapphire coatings on deposits formation

The deposits obtained with the coated pistons are compared macroscopically and then microscopically with the aluminum piston reference deposit. Figure 135 shows the piston deposits for the three materials. All three pistons show the same pattern with an inner zone deposit outlined in red corresponding to the impact of the six-cone spray and the outer zone deposit in light brown. The same brown marks at the periphery of the pistons are also observed for the three cases.

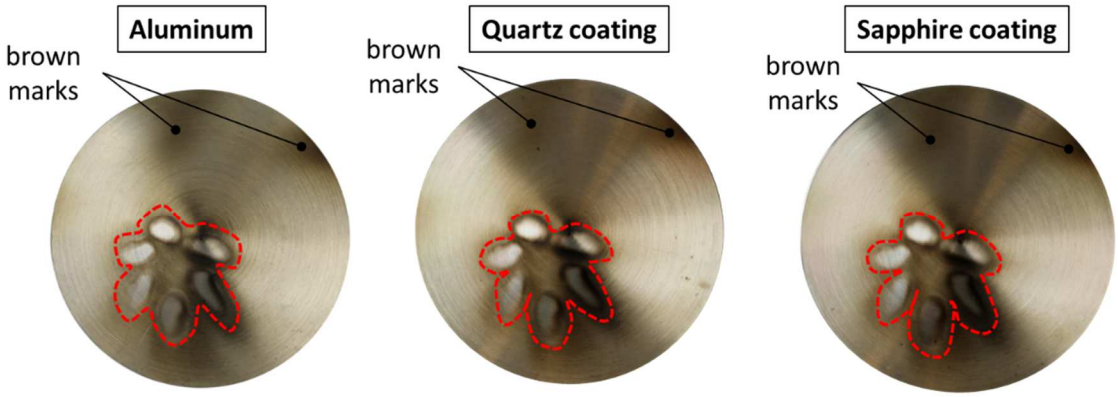

Figure 135: Images of deposits formed on aluminum pistons with quartz and sapphire coating, compared to the reference aluminum piston.

The microscopic observations shown in Figure 136 are made in the same three areas of the piston surfaces corresponding to the outer zone (a), the periphery of the spray impact (b), and the area of the spray impact (c). For zone (a), the three pistons show similar morphologies with smooth surfaces and average particle diameters below 100 nm. Zone (b) also shows for the three pistons smooth surface morphologies and particles of the same dimensions as those observed in zone (a). Area (c) for the aluminum piston has a granular texture corresponding to particles. The electron microscopy measurements of areas (c) of the quartz- and sapphire-coated pistons show charge effects in extended areas, which complicates the interpretation. Nevertheless, it is possible to distinguish particles but it is difficult to determine whether they form a granular texture.

The macroscopic and microscopic similarities between the deposits of the pistons with quartz and sapphire coatings and the deposit of the aluminum piston show that there is no significant effect of the quartz and sapphire coatings on the deposit formation mechanisms of the liquid-film path.

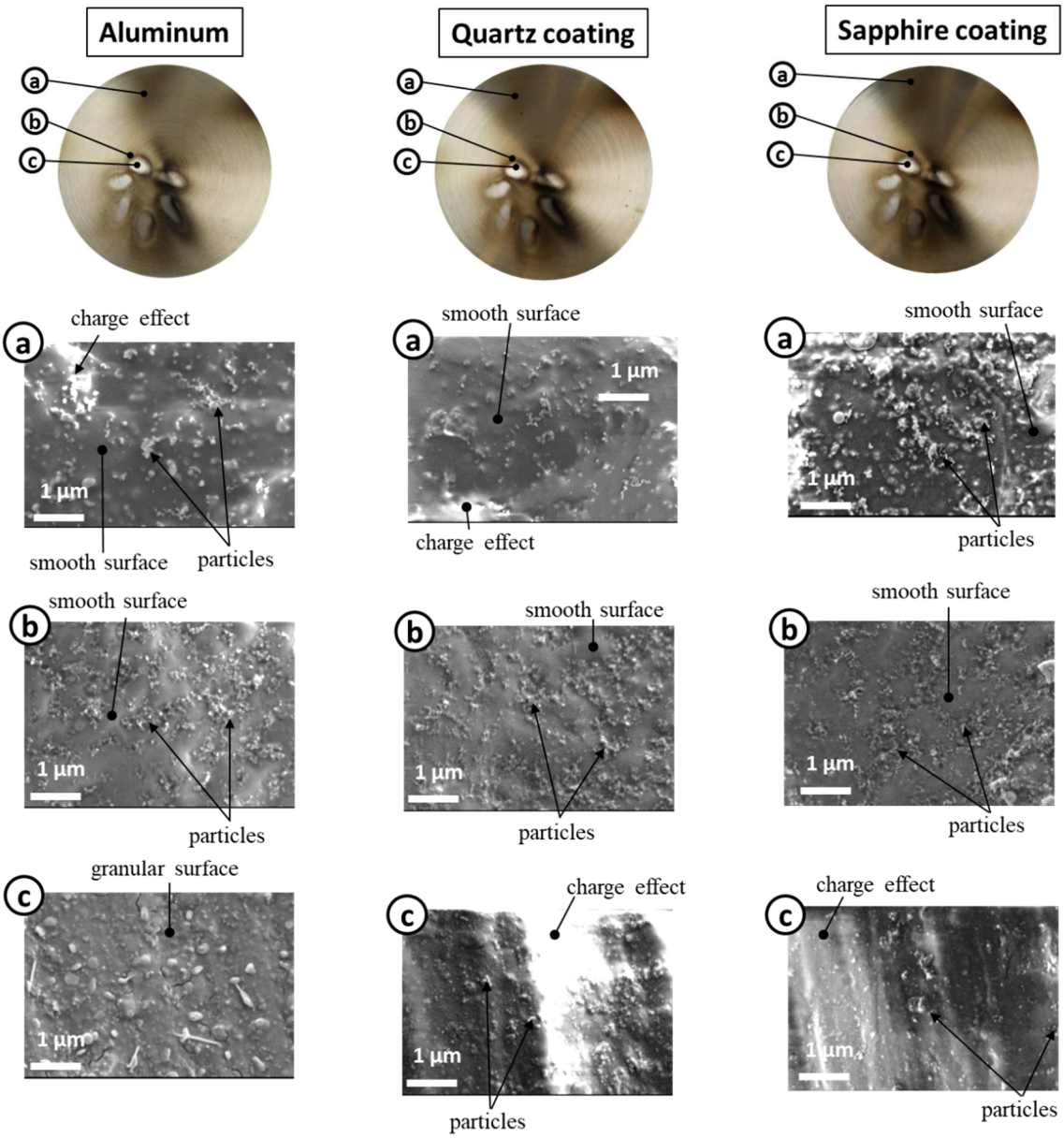

Figure 136: Microscopic observation of the deposits on aluminum piston surfaces without and with quartz and sapphire coating.

6.4.3 Influence of a full-sapphire piston on deposits formation

Macroscopic and microscopic analyses of the full-sapphire piston deposit are compared with the aluminum reference piston with a roughness of Ra = 0.06 µm. The pistons obtained after the engine experiments are shown in Figure 24. The same pattern corresponding to the six-cone spray is observed for both pistons (marked in red). It is also possible to observe the same brown marks for both cases. Nevertheless, small differences can be observed. The deposit of the inner zone appears shiny for the aluminum piston whereas it is matt for the full-sapphire case. The contours of the deposits in the spray impact periphery are sharper in the case of the aluminum. This difference in colors would tend to lead to the result that there is slightly more deposit in the aluminum case in the spray impact periphery, but it is not possible to firmly conclude at this point.

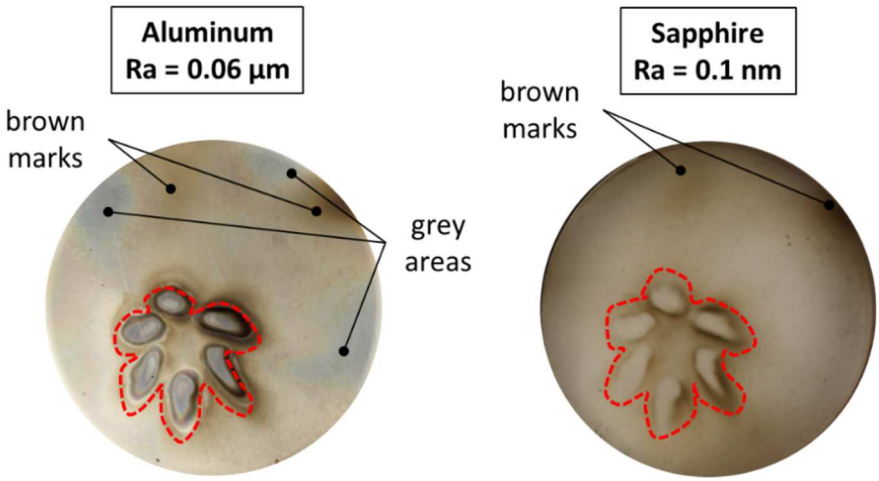

Figure 137: Deposits on an aluminum piston and a full-sapphire piston under otherwise identical operating conditions (warm start).

Microscopic observations of the deposits obtained with the aluminum and the full-sapphire pistons are shown in Figure 138. The usual three zones are observed, namely the outer zone (a), the spray impact periphery (b), and the spray impact area (c). For the zone (a), a similar morphology is observed for both pistons with the presence of a smooth surface and particles with an average diameter lower than 100 nm. For zone (b), the aluminum piston presents a smooth surface and particles also on the order of 100 nm in diameter, whereas the full-sapphire piston surface is entirely covered with particles forming a granular surface. It is difficult to distinguish whether an additional smooth deposit lies under the granular surface. For zone (c), both pistons show a granular surface. For this area it seems that the concentration of particles is higher for the full-sapphire case.

Regarding the macroscopic and microscopic analysis, it seems that the main differences between the full-sapphire and aluminum reference piston are in the area of the spray impact periphery. It is difficult to conclude without the characterization of the exhaust particle-size distribution by SMPS whether the soot-path mechanism is enhanced or the liquid-film trajectory mechanism is reduced. Nevertheless, due to the significant increase in temperature for the full-sapphire case according to Figure 134, it can be expected that liquid-film evaporation is favored, which could explain the predominance of the soot path in the microscopic observations.

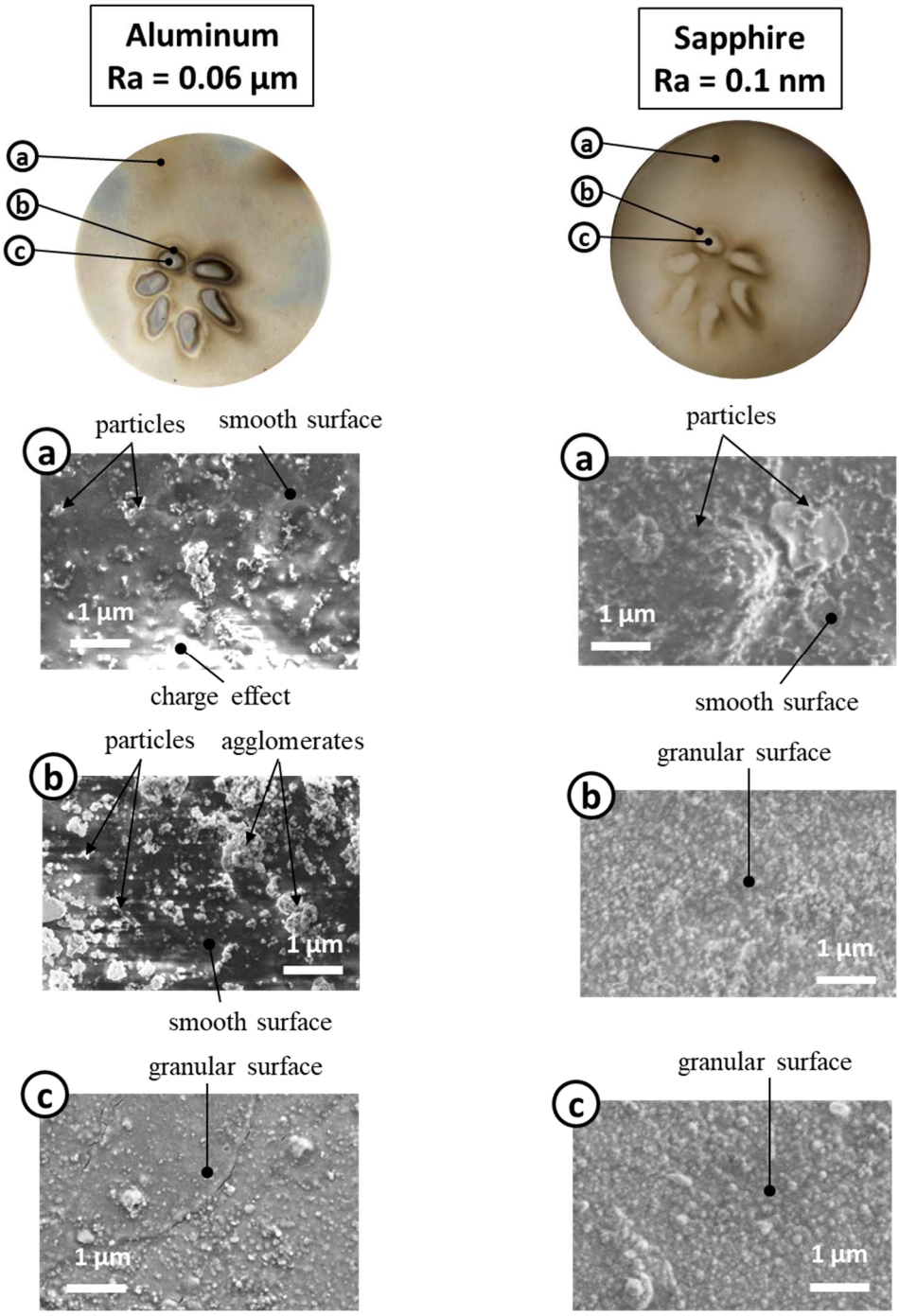

Figure 138: Microscopic images the deposits on an aluminum and a full-sapphire piston.

6.4.4 Conclusions on the materials effect on deposit formation

In this section, quartz and sapphire materials were used, and compared to the aluminum piston reference to determine their influence on the engine deposit formation process. Experiments conducted with quartz and sapphire nanometer-thick coatings indicate that the materials have no (stronger or reduced) catalytic effect on the deposit formation through the liquid-film path mechanism. Experiments conducted with a full-sapphire piston show that a similar mechanism is involved compared to an aluminum reference piston, though the quantity and structure of the obtained deposit present some differences. These are attributed to a higher surface temperature in the full-sapphire case. Therefore, the use of sapphire for

conducting experiments in an optical engine to study deposit formation seems feasible, but particular attention to the thermal behavior of the piston would be required.

6.5 Conclusions on the influence of surface properties on deposits formation

In this chapter, the influence of different piston surface conditions on the formation of deposits has been studied. The objective is first to identify levers to limit or prevent the formation of deposits, and secondly to evaluate the representativeness of transparent materials for the study of deposit formation using optical diagnostics.

First, the effect of surface temperature on the mechanisms of deposition formation by the liquid-film path and the soot path were investigated. Increasing the initial piston temperature from 20 to 190 °C increases the evaporation rate of the liquid film leading to an approximate 10 % reduction in the inner zone deposit and an approximate 100 % reduction in the outer zone deposit. For the soot-path deposition, the increase in surface temperature from 159 to 215 °C reduces the temperature gradient and therefore the thermophoresis effect on the soot deposition mechanism. This reduces the deposit formation by about 60 %. In conclusion, a significant increase in surface temperature reduces the deposit formation by the liquid-film path and the soot path by reducing the liquid-film lifetime and the near-wall temperature gradient, respectively.

Then, the impact of roughness on the formation of the deposit by the liquid-film path was presented. It was observed that the roughness does not have a significant impact on the liquid-film path deposit formation mechanism. The only effect observed concerns the spreading of the liquid film when the roughness is decreased down to Ra = 0.1 nm with the observation of sharper boundaries of the different deposition zones. Therefore, the variation of the roughness is not identified as an interesting lever to reduce the formation of deposits by the liquid-film path in an engine.

Finally, the impact of transparent materials on the formation of the liquid-film path deposit was studied. Two studies were carried out: The first with two aluminum pistons with quartz coating and sapphire coatings to avoid changes of the thermal properties of these materials, the second with a completely transparent piston made of sapphire. The study with the coatings showed that these materials did not have a significant impact on the formation of deposits by the liquid-film path as long as they have the same temperature as the reference case. The study with the fully-transparent sapphire piston shows that the liquid-film path mechanism can be reproduced with some morphological differences on the formed deposits. As the case studied limits the formation of the liquid film due to faster heat-up, further experiments are required to study the impact of the full-sapphire piston surface temperature on the liquid-film spreading.

7 CONCLUSIONS

This thesis on deposit formation in the combustion chamber of spark-ignition engines has provided an improved understanding of their formation pathways. A bibliographical study directed the research work towards the study of two deposit formation mechanisms. The first corresponds to the liquid-film path and the second to the soot path. The liquid-film path is related to the formation of a film of liquid fuel on the walls of the combustion chamber. This film can be formed during injection by the impact of the spray or by condensation on the walls. The soot path is related to the formation of soot during combustion, which is then deposited on the walls or in the liquid film. Supported by the high-temperature and -pressure conditions in the combustion chamber, durable deposits form and further grow for many engine cycles. The study of previous publications also revealed that the deposits can have different colors as well as other macroscopic and microscopic aspects depending on the engine operating parameters, such as a liquid-like or a soot-like appearance of the deposit. In the literature, some parameters have been identified that play in favor or against the formation of deposits in the liquid-film path or the soot path, such as the fuel/air equivalence ratio, the surface temperature, or the presence of high boiling point fuel compounds. The analysis of the deposit properties has highlighted different analytical methods for measuring the physical and chemical properties of the deposits. These include electron microscopy, which provides data on the morphology and elemental composition of the deposit. This initial work has thus made it possible to define the lines of research and the strategy for studying the mechanisms of deposit formation.

In this thesis, a new methodology for determining the origin of deposits between the liquid-film- and the soot-path mechanisms was presented. Preliminary experiments were conducted to determine the impact of the location in the combustion chamber on deposit formation, the effect of engine geometry, and the parameters of interest for studying deposit formation mechanisms. These results showed that the location in the chamber and the engine geometry do not have a great impact on the formation of deposits, i.e., the morphology and chemical composition of the deposit at the walls of the combustion chamber, the piston, and the injector nozzle were very similar. Based on these results, the thesis focused on the deposits formed on the piston and used two direct-injection spark-ignition engines for the experiments. These preliminary studies also highlighted the cooling water temperature and the injection timing as two parameters that can influence the macroscopic and microscopic appearance of the deposits and thus the deposit formation mechanisms.

For further evaluating the deposits formed in the engine, reference deposits were generated under well-controlled conditions in the laboratory. The objective was first to determine if these reference deposits can reproduce engine deposits. The second objective was to evaluate if the reference deposits can calibrate the measurement techniques identified in the literature and then can be used to determine the origin engine deposits. In the first step, reference deposits were formed using a microcoking device to form a deposit from the liquid film path, and using a soot generator and a direct injection spark ignition engine to form a deposit from the soot path. In a second step, two injection timings were identified to promote deposit formation corresponding to the two identified deposit formation paths: an early injection time favoring the liquid-film path, and a late injection time favoring the soot path. The reference and engine deposits were analyzed by electron microscopy, and Raman and infrared spectroscopy. Macroscopic analysis revealed a black, mat deposit corresponding to the soot path reference deposit and a clear, bright deposit for the liquid-film path reference deposit. Microscopic analysis showed a smooth surface mor-

phology for the liquid-film-path reference deposit and particles for the soot-path reference deposit. Spectroscopic analyses were not considered relevant to the analysis of the engine deposits because they do not provide information on the deposition proportion for each pathway. The liquid-film path deposit properties were identified in the engine deposit of the early injection strategy. And the properties of the reference deposit of the soot path were identified in the engine deposit of the late injection strategy. This methodology enabled the study of both pathways of engine deposit formation.

The different mechanisms of deposit formation were further evaluated using two typical injection phasings, i.e. early injection and late injection using a combination of *ex situ* materials analysis and *in situ* analysis of deposit formation. The *in situ* analysis was based on observations with a high-speed camera on a direct-injection spark-ignition engine with optical access to visualize the formation of deposits on the piston. To study the mechanisms related to the soot path, the soot particle-size distribution was analyzed in the exhaust. For the liquid-film path using the early injection strategy, the study highlighted the importance of the piston surface temperature on the liquid-film lifetime and deposit formation. In cold-start conditions, the surface temperature is about 20 °C, the evaporation time is long and favors the formation of the deposit. On the other hand, when the surface temperature at start-up is around 133 °C, the evaporation time is short and the deposit formation is limited. It was found that two other factors influence the lifetime of the liquid film. The first is the presence of accumulation zones at the periphery of the liquid film and at the periphery of the spray impact, which will slow down the evaporation of the liquid film and favor the formation of the deposit by the liquid-film path. The second is the local cooling of the piston surface, which can create colder areas on the piston and slow down evaporation. For the soot path, several mechanisms can explain the deposition of soot on the piston surface depending on the flow inside the combustion chamber. When the flow is laminar, the soot deposits by thermophoresis when it is close enough to the wall where a strong temperature gradient resides. In turbulent flows, the soot particles will either follow the flow to the exhaust or deposit by inertia. Liquid film deposit was observed in the case of late injection and soot path deposit in the case of early injection. The study showed that these mechanisms can interact.

The impact of the piston surface properties on the deposit formation mechanisms was also investigated. First, the effect of surface temperature on the deposit formation mechanisms via the liquid-film path and the soot path was investigated. Increasing the initial piston surface temperature from 20 to 190 °C increases the evaporation rate of the liquid film, resulting in approximately 10 % reduction in deposit formation in the inner region and almost 100 % in the outer region. For soot-path deposition, increasing the surface temperature from 159 to 215 °C reduces the temperature gradient and thus the thermophoresis effect on the soot deposition mechanism. Thus, a significant increase in surface temperature reduces deposit formation via the liquid-film path and the soot path by reducing the liquid-film lifetime and the temperature gradient near the wall, respectively. It was shown that the surface roughness does not significantly influence deposit formation through the liquid-film path. Finally, the impact of transparent materials on the formation of deposits via the liquid-film path was studied. To separate thermal and materials effects, first aluminum pistons coated with thin layers of either with silica or alumina were investigated to maintain the same surface temperatures as with metal pistons. Second, a completely transparent sapphire piston was used where the surface temperature is expected to deviate because of the different heat conduction properties. The study with the coatings showed that these materials did not have a significant impact on the formation of deposits by the liquid-film route. The study with the fully transparent sapphire piston showed that the deposit formation mechanisms of the liquid-film path can be reproduced with some morphological differences in the deposits formed providing an option for fu-

ture experiments with optical detection of deposit formation through transparent sections of the combustion chamber wall. Since the studied case limits the liquid-film formation, additional experiments are needed to investigate the impact of the surface temperature of the solid sapphire piston on the liquid film spreading.

In conclusion, a methodology has been developed in this thesis that enables to study and understand the mechanisms of deposit formation in en engine combustion chamber. This methodology was then applied to evaluate the impact of surface properties on the identified formation mechanisms. The two formation pathways identified in the literature were studied separately. For the liquid-film path, the work showed that the formation of the deposit by the liquid film was conditioned by the evaporation rate of the liquid film. The evaporation rate depends on the temperature of the piston surface and the amount of liquid fuel to be evaporated. In this study, the surface roughness, the use of silica or alumina surface material does not have a significant impact on the formation of the deposit via the liquid-film path. For the soot path, two mechanisms have been identified in the deposition of soot on the surface. These are thermophoresis and inertial deposition. Depending on the turbulent intensity in the cylinder and the temperature gradient in the near wall, one of the two mechanisms dominates. The results showed that an increase in the surface temperature reduced the deposition of soot.

Outlook

One of the questions raised by the thesis is the chemical process of deposit formation by the liquid-film-path mechanism. For the liquid-film path, the relationship between evaporation time and deposit formation has been demonstrated. This work, however, did not yet establish the chemical transformation process between the liquid and solid phases. Real-time measurements of this process would allow seeing the chemical evolution of the liquid fuel towards a deposit. Such measurements could be performed in the laboratory with the microcoking device to chemically characterize the formation of the reference deposit by the liquid-film path. Based on the finding that an all-sapphire piston is representative for an aluminum piston in terms of deposit formation via the liquid-film path, it would be interesting to use optical diagnostics and transparent pistons under real engine conditions in future work to *in situ* analyze deposit formation. One important perspective opened by this thesis is to test laser-induced fluorescence optical diagnostics to measure in real-time the evolution of the deposit formation on the walls of the combustion chamber. Gasoline fuels consist of hundreds of components, some of which fluoresce upon illumination in the ultraviolet, but regarding the deposits formed by the liquid film path, there are no known studies on their fluorescence properties. To validate the implementation of this technique, a preliminary study of the deposit fluorescence will be necessary. A decreasing evolution of the fluorescence intensity measurement from the formation of a liquid fuel film to the formation of a solid deposit during an engine cycle would give interesting information about the evaporation rate of the liquid film. Conversely, an increasing evolution of the fluorescence intensity measurement would give quantitative information on the amount of deposit formed on the walls.

REFERENCES

[1] European Commission, “Climate strategies & targets: 2030 climate & energy framework,” https://ec.europa.eu/clima/policies/strategies/2030_en#tab-0-0.

[2] European Environment Agency, “Greenhouse gas emissions from transport in Europe,” https://www.eea.europa.eu/data-and-maps/indicators/transport-emissions-of-greenhouse-gases-7/assessment.

[3] Bossi, A., Hoffmann, G., and Shi, J., “Optimization of next generation high flow gasoline direct injection,” in: Tschöke, H. and Marohn, R. (eds.), 11. Tagung Einspritzung und Kraftstoffe 2018, Proceedings, Springer Vieweg:251–269, 2019.

[4] Hoffmann, G., Befrui, B., Berndorfer, A., Piock, W.F. et al., “Fuel System Pressure Increase for Enhanced Performance of GDi Multi-Hole Injection Systems,” SAE Int. J. Engines 7(1):519–527, 2014.

[5] Caprotti, R., Bhatti, N., and Nobuyuki, I., “Protecting Diesel Fuel Injection Systems,” SAE Technical Paper 2011-01-1927, 2011.

[6] Ho, R.J., Yusoff, M.Z., and Palanisamy, K., “Trend and future of diesel engine: Development of high efficiency and low emission low temperature combustion diesel engine,” IOP Conf. Ser.: Earth Environ. Sci. 16:12112, 2013.

[7] Hoekman, S.K., Broch, A., Robbins, C., Ceniceros, E. et al., “Review of biodiesel composition, properties, and specifications,” Renewable and Sustainable Energy Reviews 16(1):143–169, 2012.

[8] Omori, T., Tanaka, A., Yamada, K., and Bunne, S., “Biodiesel deposit formation mechanism and improvement of Fuel Injection Equipment (FIE),” SAE Technical Paper 2011-01-1935, 2011.

[9] Kalghatgi, G.T., “Combustion Chamber Deposits in Spark-Ignition Engines: A Literature Review,” SAE Technical Paper 952443, 1995.

[10] Hosogi, T., Kaneko, R., Ito, H., and Sunami, K., “Research of Knocking Deterioration due to Accumulated Carbon Deposits on Piston Surfaces,” SAE Technical Paper 2019-01-1141, 2019.

[11] Güralp, O., Hoffman, M., Assanis, D.N., Filipi, Z. et al., “Thermal Characterization of Combustion Chamber Deposits on the HCCI Engine Piston and Cylinder Head Using Instantaneous Temperature Measurements,” SAE Technical Paper 2009-01-0668, 2009.

[12] Zerda, T.W., Yuan, X., Moore, S.M., and Leon y Leon, C.A., “Surface area, pore size distribution and microstructure of combustion engine deposits,” Carbon 37(12):1999–2009, 1999.

[13] Nagano, S., Yokoo, N., Kitano, K., and Nakata, K., “Effects of High Boiling Point Fuel Additives on Deposits in a Direct Injection Gasoline Engine,” SAE Int. J. Fuels Lubr. 10(3), 2017.

[14] Alves Fortunato, M. and Starck, L., “Oxidation Stability of Diesel-Biodiesel Blends: Impact of Physical-Chemical Properties Over Ageing into Fuel Injection Systems (FIS) and Storage,” SAE Technical Paper 2016-01-2267, 2016.

[15] Ben Amara, A., Lecointe, B., Jeuland, N., Takahashi, T. et al., “Experimental Study of the Impact of Diesel/Biodiesel Blends Oxidation on the Fuel Injection System,” SAE Int. J. Fuels Lubr. 7(3):849–860, 2014.

[16] Birgel, A., Ladommatos, N., Aleiferis, P., Zülch, S. et al., “Deposit Formation in the Holes of Diesel Injector Nozzles: A Critical Review,” SAE Technical Paper 2008-01-238, 2008.

[17] Arondel, M., Rodeschini, H., Lopes, M., and Dequenne, B., “Fuel Additives for Reduction of Internal Diesel Injectors Deposits (IDID, “lacquering”): A Critical and Priority Route,” SAE Technical Paper 2012-01-1687, 2012.

[18] Shu, G., Dong, L., and Liang, X., “A review of experimental studies on deposits in the combustion chambers of internal combustion engines,” International Journal of Engine Research 13(4):357–369, 2012.

[19] Cheng, S.-w.S., “The Impacts of Engine Operating Conditions and Fuel Compositions on the Formation of Combustion Chamber Deposits,” SAE Technical Paper 2000-01-2025, 2000.

[20] Lepperhoff, G. and Houben, M., “Mechanisms of Deposit Formation in Internal Combustion Engines and Heat Exchangers,” SAE Technical Paper 931032, 1993.

[21] Diaby, M., Sablier, M., Le Negrate, A., El Fassi, M. et al., “Understanding carbonaceous deposit formation resulting from engine oil degradation,” Carbon 47(2):355–366, 2009.

[22] Watkinson, A.P. and Wilson, D.I., “Chemical reaction fouling: A review,” Experimental Thermal and Fluid Science 14(4):361–374, 1997.

[23] Sarnecki, J., Gawron, B., and Głąb, J., “Hydroperoxides Formation in Jet Fuels Coming from Different Production Processes in Simulated Fuel System of Modern Aircraft,” Journal of KONBiN 43(1):277–299, 2017.

[24] Zhou, J., Pei, Y., Peng, Z., Zhang, Y. et al., “Characteristics of near-nozzle spray development from a fouled GDI injector,” Fuel 219:17–29, 2018.

[25] Zhang, W., Ding, H., Shuai, S., Zheng, B. et al., “Effect of Fuel Detergent on Injector Deposit Formation and Engine Emissions in a Gasoline Direct Injection (GDI) Engine,” SAE Technical Paper 2017-01-2247, 2017.

[26] Wen, Y., Wang, Y., Fu, C., Deng, W. et al., “The Impact of Injector Deposits on Spray and Particulate Emission of Advanced Gasoline Direct Injection Vehicle,” SAE Technical Paper 2016-01-2284, 2016.

[27] Caprotti, R., Fowler, W., Lepperhoff, G., and Houben, M., “Diesel Additive Technology Effects on Injector Hole Erosion/corrosion, Injector Fouling and Particulate Traps,” SAE Technical Paper 932739, 1993.

[28] Nishiwaki, K. and Hafnan, M., “The Determination of Thermal Properties of Engine Combustion Chamber Deposits,” SAE Technical Paper 2000-01-1215, 2000.

[29] Quader, A.A. and Dasch, C.J., “Spark Plug Fouling: A Quick Engine Test,” SAE Technical Paper 92006, 1992.

[30] Shayler, P.J., Dixon, J., and Isaacs, R.M., “The Use of Vehicle Drive Cycles to Assess Spark Plug Fouling Performance,” SAE Technical Paper 940101, 1994.

[31] Mogi, K., Ohno, E., and Nakamura, N., “Spark Plug Fouling: Behavior and Countermeasure,” SAE Technical Paper 922093, 1992.

[32] Ishiguro, H., Kanao, K., Okabe, S., and Hashizume, K., “Super Carbon Fouling Resistive Small Size Spark Plug,” SAE Technical Paper 2005-01-1158, 2005.

[33] Glawar, A.F.G., Ziman, P.R., Wu, K., Natarajan, V. et al., “Understanding the Adverse Effects of Inlet Valve Deposits on SI Engine Operation, through a Novel Technique to Create Surrogate Deposits,” SAE Technical Paper 2018-01-1742, 2018.

[34] Taniguchi, B.Y., Peyla, R.J., Parsons, G.M., Hoekman, S.K. et al., “Injector Deposits — The Tip of Intake System Deposit Problems,” SAE Technical Paper 861534, 1986.

[35] Price, R.J., Martin, D.P., Dickens, N., and Bohr, P., “The Impact of Inlet Valve Deposits on PFI Gasoline SI Engines – Quantified Effects on Fuel Consumption,” SAE Technical Paper 2007-01-0004, 2007.

[36] Noma, K., Noda, T., Isomura, H., Ashida, T. et al., “A Study of Injector Deposits, Combustion Chamber Deposits (CCD) and Intake Valve Deposits (IVD) in Direct Injection Spark Ignition (DISI) Engines II,” SAE Technical Paper 2003-01-3162, 2003.

[37] Harpster, M.O., Matas, S.E., Fry, J.H., and Litzinger, T.A., “An Experimental Study of Fuel Composition and Combustion Chamber Deposit Effects on Emissions from a Spark Ignition Engine,” SAE Technical Paper 950740, 1995.

[38] Jung, H.S., Kim, S.H., Lee, S.M., Park, S.I. et al., “The Effect of Combustion Chamber Deposits on Octane Requirement Increase in a Spark Ignition Engine,” SAE Technical Paper 2008-01-1761, 2008.

[39] Tondelli, G., Carriero, M., and Pedicillo, A., “Combustion Chamber Deposits: Fuel and Lubricant Effects on Exhaust Hydrocarbon Emissions Measured by Fast FID Analyzer,” SAE Technical Paper 2000-01-2024, 2000.

[40] Ishii, H., Emi, M., Yamada, Y., Kimura, S. et al., “Heat Loss to The Combustion Chamber Wall with Deposit Adhering to The Wall Surface in D.I. Diesel Engine First Report: Influence of Deposit on Instantaneous Heat Flux into The Piston Surfaces,” SAE Technical Paper 2001-01-1811, 2001.

[41] Hopwood, A.B., Chynoweth, S., and Kalghatgi, G.T., “A Technique to Measure Thermal Diffusivity and Thickness of Combustion Chamber Deposits In-Situ,” SAE Technical Paper 982590, 1998.

[42] Okada, Y., Miyashita, S., Izumi, Y., and Hayakawa, Y., “Study of Low-Speed Pre-Ignition in Boosted Spark Ignition Engine,” SAE Int. J. Engines 7(2):584–594, 2014.

[43] Daly, D.T., Bannon, S.A., Fog, D.A., and Harold, S.M., “Mechanism of Combustion Chamber Deposit Formation,” SAE Technical Paper 941889, 1994.

[44] Edwards, J.C. and Choate, P.J., “Average Molecular Structure of Gasoline Engine Combustion Chamber Deposits Obtained by Solid-State 13 C, 31 P, and 1 H Nuclear Magnetic Resonance Spectroscopy,” SAE Technical Paper 932811, 1993.

[45] Kelemen, S.R., Siskin, M., Avery, N.L., Rose, K.D. et al., “Gasoline Type and Engine Effects on Equilibrium Combustion Chamber Deposits (CCD),” SAE Technical Paper 2001-01-3583, 2001.

[46] Stevens, E. and Steeper, R., “Piston Wetting in an Optical DISI Engine: Fuel Films, Pool Fires, and Soot Generation,” SAE Technical Paper 2001-01-1203, 2001.

[47] Miyashita, K., Tsukamoto, T., Fukuda, Y., Kondo, K. et al., “High-Speed UV and Visible Laser Shadowgraphy of GDI In-Cylinder Pool Fire,” SAE Technical Paper 2016-01-2165, 2016.

[48] Laget, O., Malbec, L.-M., Kashdan, J., Dronniou, N. et al., “Experimental and Numerical Investigations on the Mechanisms Leading to the Accumulation of Particulate Matter in Lubricant Oil,” SAE Int. J. Engines 9(4):2030-2043, 2016.

[49] Kondo, K., Takahashi, J., and Aizawa, T., “Morphology Analysis of Wall-Deposited Diesel Soot Particles via Transmission Electron Microscope,” SAE Int. J. Fuels Lubr. 7(3):683–692, 2014.

[50] Suhre, B.R. and Foster, D.E., “In-Cylinder Soot Deposition Rates Due to Thermophoresis in a Direct Injection Diesel Engine,” SAE Technical Paper 921629, 1992.

[51] Brugière, E., “Le spectromètre thermophorétique circulaire, un nouvel instrument pour mesurer la thermophorèse : application aux agrégats de suies de morphologie fractale,” INSA de Rouen, 2012.

[52] Alain Mailliat (ed.), “Les milieux aérosols et leurs représentations,” EDP Sciences, 2010.

[53] Mao, N., “Nonwoven fabric filters,” Advances in Technical Nonwovens(Elsevier):273–310, 2016.

[54] Ashida, T., Takei, Y., and Hosi, H., “Effects of Fuel Properties on SIDI Fuel Injector Deposit,” SAE Technical Paper 2001-01-3694, 2001.

[55] Xu, H., Wang, C., Ma, X., Sarangi, A.K. et al., “Fuel injector deposits in direct-injection spark-ignition engines,” Progress in Energy and Combustion Science 50:63–80, 2015.

[56] Uehara, T., Takei, Y., Hoshi, H., Shiratani, K. et al., “Study on Combustion Chamber Deposit Formation Mechanism -Influence of Fuel Components and Gasoline Detergents-,” SAE Int. J. Fuels Lubr. 106(4):741–759, 1997.

[57] Taniguchi, S., Yoshida, K., and Tsukasaki, Y., “Feasibility Study of Ethanol Applications to A Direct Injection Gasoline Engine,” SAE Technical Paper 2007-01-2037, 2007.

[58] Schwahn, H., Lutz, U., and Kramer, U., “Deposit Formation of Flex Fuel Engines Operated on Ethanol and Gasoline Blends,” SAE Int. J. Fuels Lubr. 3(2):22–37, 2010.

[59] Ramadhas, A.S., Singh, V.P., Subramanian, M., Acharya, G.K. et al., “Impact of Fuel Additives on Intake Valve Deposits, Combustion Chamber Deposits and Emissions,” SAE Technical Paper 2011-01-1980, 2011.

[60] Pullen, J. and Saeed, K., “An overview of biodiesel oxidation stability,” Renewable and Sustainable Energy Reviews 16(8):5924–5950, 2012.

[61] Bacha, K., “Etude de l’Interaction entre le Carburant Diesel et les Composants du Système d’Injection Diesel,” Université de haute alsace, 2016.

[62] Bacha, K., Ben-Amara, A., Vannier, A., Alves-Fortunato, M. et al., “Oxidation Stability of Diesel/Biodiesel Fuels Measured by a PetroOxy Device and Characterization of Oxidation Products,” Energy Fuels 29(7):4345–4355, 2015.

[63] Bacha, K., Ben Amara, A., Alves Fortunato, M., Wund, P. et al., “Original Experimental Approach for Assessing Transport Fuel Stability,” Journal of visualized experiments : JoVE(116), 2016.

[64] Arifin, “Diesel and Bio-diesel Fuel Deposits on a Hot Wall Surface,” Gunma University, 2009.

[65] Bouilly, J., Mohammadi, A., Iida, Y., Hashimoto, H. et al., “Biodiesel Stability and its Effects on Diesel Fuel Injection Equipment,” SAE Technical Paper 2012-01-0860, 2012.

[66] Jain, S. and Sharma, M.P., “Thermal stability of biodiesel and its blends: A review,” Renewable and Sustainable Energy Reviews 15(1):438–448, 2011.

[67] Tang, J., Pischinger, S., Lamping, M., Körfer, T. et al., “Coking Phenomena in Nozzle Orifices of Dl-Diesel Engines,” SAE Int. J. Fuels Lubr. 2(1):259–272, 2009.

[68] d’Ambrosio, S. and Ferrari, A., “Diesel Injector Coking: Optical-Chemical Analysis of Deposits and Influence on Injected Flow-Rate, Fuel Spray and Engine Performance,” J. Eng. Gas Turbines Power 134(6):62801, 2012.

[69] Argueyrolles, B., Dehoux, S., Gastaldi, P., Grosjean, L. et al., “Influence of injector nozzle design and cavitation on coking phenomenon,” SAE Technical Paper 2007-01-1896, 2007.

[70] Barker, J., Cook, S., and Richards, P., “Sodium Contamination of Diesel Fuel, its Interaction with Fuel Additives and the Resultant Effects on Filter Plugging and Injector Fouling,” SAE Int. J. Fuels Lubr. 6(3):826–838, 2013.

[71] Risberg, P.A. and Alfredsson, S., “The Effect of Zinc and Other Metal Carboxylates on Nozzle Fouling,” SAE Technical Paper 2016-01-0837, 2016.

[72] Kelemen, S.R., Siskin, M., Homan, H.S., Pugmire, R.J. et al., “Fuel, Lubricant and Additive Effects on Combustion Chamber Deposits,” SAE Technical Paper 982715, 1998.

[73] Diaby, M., “Compréhension des mécanismes de formation de dépôts en fond de première gorge de piston de moteurs Diesel,” Ecole Polytechnique, 2009.

[74] Tsukasaki, Y., Yasuda, A., Ito, S., and Nohira, H., “Study of Mileage-Related Formaldehyde Emission from Methanol Fueled Vehicles,” JOURNAL OF FUELS & LUBRICANTS, SAE Transactions Vol. 99, Section 4: pp. 283-288, 1990.

[75] Nakic, D.J., Assanis, D.N., and White, R.A., “Effect of Elevated Piston Temperature on Combustion Chamber Deposit Growth,” SAE Technical Paper 940948, 1994.

[76] Furuhata, T., Ohmori, T., and Arai, M., “Evaporation Deposits of Diesel and Bio-diesel Fuels on a Hot Surface,” SAE International 2011-01-1933, 2011.

[77] “Proceedings of the FISITA 2012 World Automotive Congress,” Lecture Notes in Electrical Engineering, Springer Berlin Heidelberg, Berlin, Heidelberg, ISBN 978-3-642-33749-9, 2013.

[78] Singh, S.K., Agarwal, A.K., and Sharma, M., “Experimental investigations of heavy metal addition in lubricating oil and soot deposition in an EGR operated engine,” Applied Thermal Engineering 26(2-3):259–266, 2006.

[79] Zerda, T.W., Yuan, X., and Moore, S.M., “Effects of fuel additives on the microstructure of combustion engine deposits,” Carbon 39(10):1589–1597, 2001.

[80] Kalghatgi, G.T., “Combustion Chamber Deposit Flaking and Startability Problems in Three Different Engines,” SAE Technical Paper 2003-01-3187, 2003.

[81] Zerda, T.W., Yuan, X., and Moore, S.M., “Effects of fuel additives on the microstructure of combustion engine deposits,” Carbon 39(10):1589–1597, 2001.

[82] Venkataraman, R. and Eser, S., “Characterization of deposits formed on diesel injectors in field test and from thermal oxidative degradation of n-hexadecane in a laboratory reactor,” Chemistry Central journal 2:25, 2008.

[83] Esaki, Y., Ishiguro, T., Suzuki, N., and Nakada, M., “Mechanism of Intake-Valve Deposit Formation Part 1: Characterization of Deposits,” SAE Technical Paper 900151, 1990.

[84] Rounthwaite, N.J., Williams, R., McGivery, C., Jiang, J. et al., “A Chemical and Morphological Study of Diesel Injector Nozzle Deposits - Insights into their Formation and Growth Mechanisms,” SAE Int. J. Fuels Lubr. 10(1):106–114, 2017.

[85] Costa, J., Sarkisov, L., Seaton, N., and Cracknell, R., “Adsorption-based Structural Characterization of Intake Valve Deposits,” SAE Technical Paper 2011-01-0901, 2011.

[86] Pinto da Costa, J.M.C., Cracknell, R.F., Sarkisov, L., and Seaton, N.A., “Structural characterization of carbonaceous combustion-chamber deposits,” Carbon 47(14):3322–3331, 2009.

[87] Studzinski, W.M., Liiva, P.M., Choate, P.J., Acker, W.P. et al., “A Computational and Experimental Study of Combustion Chamber Deposit Effects on NOx Emissions,” SAE Technical Paper 932815, 1993.

[88] Overbye, V.D., Bennethum, J.E., Uyehara, O.A., and Myers, P.S., “Unsteady Heat Transfer in Engines,” SAE Technical Paper 610041, 1961.

[89] Anderson, C.L., Uyehara, O.A., and Myers, P.S., “An In Situ Determination of the Thermal Properties of Gombustion-Chamber Deposits,” SAE Technical Paper 820071, 1982.

[90] Hayes, T.K., White, R.A., and Peters, J.E., “The In-Situ Measurement of the Thermal Diffusivity of Combustion Chamber Deposits in Spark Ignition Engines,” SAE Technical Paper 920513, 1992.

[91] Güralp, O., Hoffman, M., Assanis, D.N., Filipi, Z. et al., “Characterizing the Effect of Combustion Chamber Deposits on a Gasoline HCCI Engine,” SAE Technical Paper 2006-01-3277, 2006.

[92] “L’aluminium,” Techniques de l'ingénieur, 2005.

[93] Suryantoro, M.T., Sugiarto, B., and Mulyadi, F., “Growth and characterization of deposits in the combustion chamber of a diesel engine fueled with B50 and Indonesian biodiesel fuel (IBF),” Biofuel Res. J. 3(4):521–527, 2016.

[94] Stojilovic, N., “Why Can’t We See Hydrogen in X-ray Photoelectron Spectroscopy?,” J. Chem. Educ. 89(10):1331–1332, 2012.

[95] Raphet, B., “États de surface - Mesure,” Techniques de l'ingénieur, 2006.

[96] Uy, D., Ford, M.A., Jayne, D.T., O'Neill, A.E. et al., “Characterization of gasoline soot and comparison to diesel soot: Morphology, chemistry, and wear,” Tribology International 80:198–209.

[97] Jing, “CAST Principle,” http://www.sootgenerator.com/CAST_principle.htm.

[98] AVL, “AVL Smoke Meter: A filter-type smoke meter for the measurement of soot content,” https://www.avl.com/ko/-/avl-smoke-meter.

[99] SIA (ed.), “Investigation of particle formation mechanisms in GDI engines during transient heating operation,” Strasbourg, France, 2013.

[100] The Bernasek Lab, “ATR-FTIR,” http://chemists.princeton.edu/bernasek/atr-ftir.

[101] Sadezky, A., Muckenhuber, H., Grothe, H., Niessner, R. et al., “Raman microspectroscopy of soot and related carbonaceous materials: Spectral analysis and structural information,” Carbon 43(8):1731–1742, 2005.

[102] Aldén, M., Omrane, A., Richter, M., and Särner, G., “Thermographic phosphors for thermometry: A survey of combustion applications,” Progress in Energy and Combustion Science 37(4):422–461, 2011.

[103] Borman, G. and Nishiwaki, K., “Internal-combustion engine heat transfer,” Progress in Energy and Combustion Science 13(1):1–46, 1987.

[104] Tree, D.R. and Svensson, K.I., “Soot processes in compression ignition engines,” Progress in Energy and Combustion Science 33(3):272–309, 2007.

[105] Shiro, N., “Memories of my research on boiling,” International Journal of Heat and Mass Transfer 27(7):955–957, 1984.

[106] Habchi, C., “A Comprehensive Model for Liquid Film Boiling in Internal Combustion Engines,” Oil Gas Sci. Technol. – Rev. IFP 65(2):331–343, 2010.

[107] Stanglmaier, R.H., Roberts, C.E., and Moses, C.A., “Vaporization of Individual Fuel Drops on a Heated Surface: A Study of Fuel-Wall Interactions within Direct-Injected Gasoline (DIG) Engines,” SAE Technical Paper 2002-01-0838, 2002.

[108] California Air Resources Board, “California RFG Fact Sheet 1: California Reformulated Gasoline - An Overview,”

[109] Geiler, J.N., Grzeszik, R., Quaing, S., Manz, A. et al., “Development of laser-induced fluorescence to quantify in-cylinder fuel wall films,” International Journal of Engine Research 19(1):134–147, 2017.

[110] Pan, H., Xu, M., Hung, D., Lv, H. et al., “Experimental Investigation of Fuel Film Characteristics of Ethanol Impinging Spray at Ultra-Low Temperature,” SAE Technical Paper 2017-01-0851, 2017.

[111] Contino, M., Allocca, L., Montanaro, A., Cardone, G. et al., “Dynamic Thermal Behavior of a GDI Spray Impacting on a Heated Thin Foil by Phase-Averaged Infrared Thermography,” SAE Int. J. Adv. & Curr. Prac. in Mobility 2(2):512-519, 2020.

[112] Maricq, M.M. and Xu, N., “The effective density and fractal dimension of soot particles from premixed flames and motor vehicle exhaust,” Journal of Aerosol Science, 35(10), 1251-1274. Journal of Aerosol Science 35(10):1251–1274, 2004.

[113] Fan, X., Che, Z., Wang, T., and Lu, Z., “Numerical investigation of boundary layer flow and wall heat transfer in a gasoline direct-injection engine,” International Journal of Heat and Mass Transfer 120:1189–1199, 2018.

[114] He, C. and Ahmadi, G., “Particle Deposition with Thermophoresis in Laminar and Turbulent Duct Flows,” Aerosol Science and Technology 29(6):525–546, 1998.

[115] Pilla, G. and Francqueville, L. de (eds.), “Investigation of particle formation processes in a GDI engine in catalyst heating operation,” Baden-Baden, 22-23 May 2011, 2011.

[116] Ma, P.C., Ewan, T., Jainski, C., Lu, L. et al., “Development and Analysis of Wall Models for Internal Combustion Engine Simulations Using High-speed Micro-PIV Measurements,” Flow Turbulence Combust 98(1):283–309, 2017.

[117] Furuhata, T., Ohmori, T., and Arai, M., “Evaporation Deposits of Diesel and Bio-diesel Fuels on a Hot Surface,” SAE Technical Paper 2011-01-1933, 2011.

[118] Sébastien MOULINET, “Rugosité et dynamique d’une ligne de contact sur un substrat désordonné,” Université Paris-Diderot - Paris VII, 2003.

ANNEX

A/ Determination of surface temperature from phosphor thermometry

To derive temperature from phosphor thermometry surface measurement, the time-resolved signal decay from 100 measurements is acquired at the valve overlap representing a total duration of 1 s corresponding to measurements at 100 Hz. This duration is short enough to assume that the temperature does not vary during detection. For a greater stability of the post-processing, the analysis is based on an average of 100 raw curves. The objective is to determine the decay rate and convert it to temperature using the prerecorded calibration. The decay rate is determined via the 'luminescence intensity by time' method according to the following steps:

- Step 1: Description of the exponential signal decrease

$$I(t) = A\mathrm{e}^{-\frac{t}{\tau}}$$

- Step 2: Multiplication by time

$$F(t) = t \times I(t) = At\mathrm{e}^{-\frac{t}{\tau}}$$

- Step 3: Derivation of the equation and search for the maximum

$$\frac{dF(t)}{dt} = A\mathrm{e}^{-\frac{t}{\tau}} - A\frac{t}{\tau}e^{-\frac{t}{\tau}} = 0 \;\leftrightarrow\; A\mathrm{e}^{-\frac{t}{\tau}} = A\frac{t}{\tau}\mathrm{e}^{-\frac{t}{\tau}} \leftrightarrow \frac{t}{\tau} = 1 \leftrightarrow t = \tau$$

B/ SEM microscopy of the deposits for cases 1–5 for early injection for the following zones: (a) outer zone, (b) spray impact periphery, and (c) spray impact area.

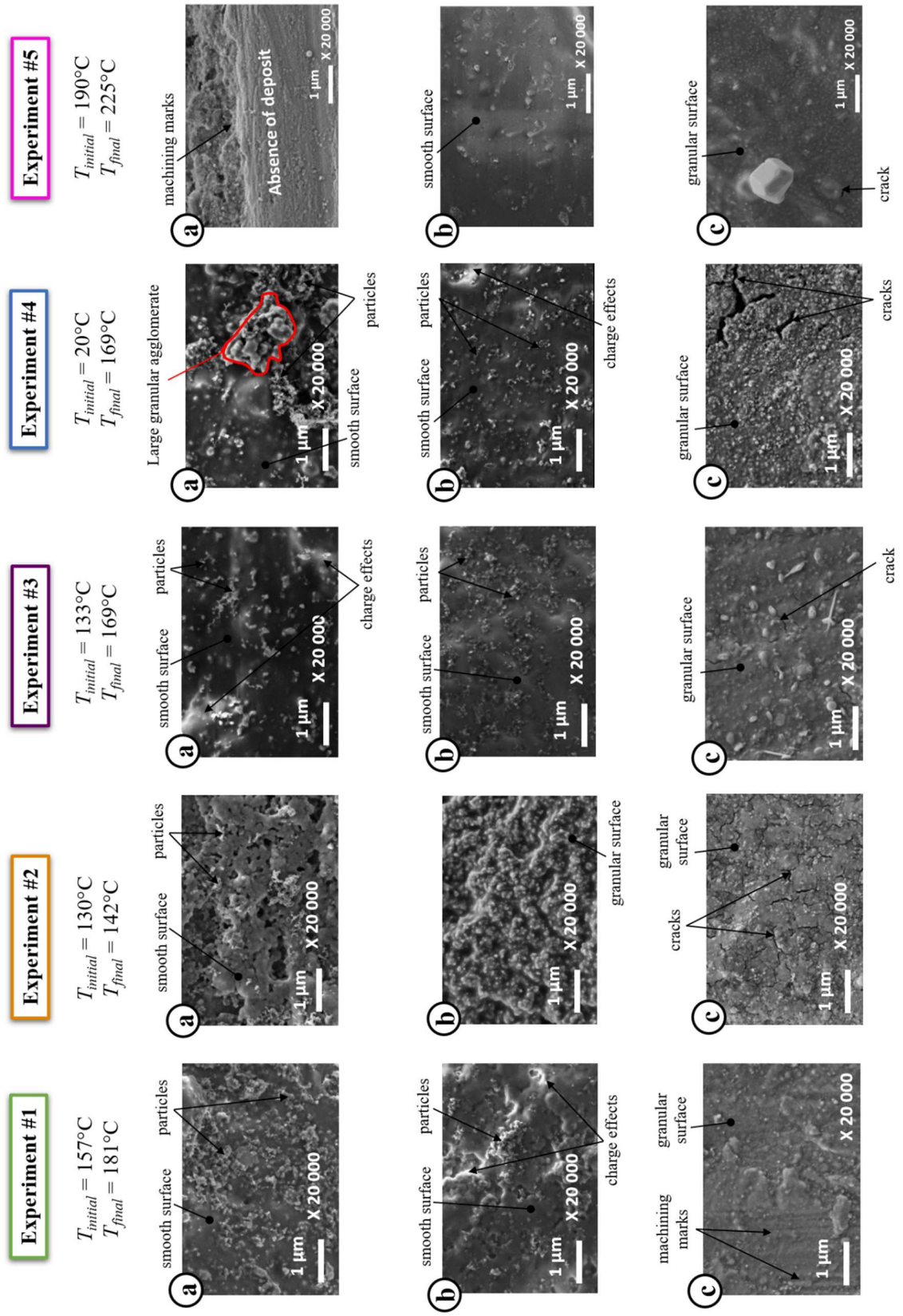

C/ Synthèse du manuscrit en français

1. Introduction

Les nouvelles réglementations sur les émissions dans le secteur du transport routier, telles que les normes Euro, ont entraîné des changements dans la technologie des moteurs. Les fournisseurs de carburant ont également développé de nouvelles formulations de carburant, et ont introduit une grande variété de biocarburants sur le marché. Ces évolutions ont créé de nouvelles contraintes pour le carburant, entraînant la formation de dépôts dans la chambre de combustion des moteurs. Ces dépôts ont un impact sur l'efficacité et la durée de vie du moteur, ils augmentent la consommation de carburant et contribuent aux émissions polluantes. En parallèle, la nouvelle réglementation demande de contrôler la durabilité des performances des moteurs. C'est pourquoi il est nécessaire de s'attaquer au problème des dépôts dans les moteurs.

La problématique de la formation de dépôts dans l'industrie du raffinage et dans les systèmes d'alimentation en carburant des voitures a été largement étudiée et discutée dans la littérature. Cependant, le processus de formation de dépôts à ces endroits n'est pas représentatif des conditions de la chambre de combustion en termes de pression, de température et de produits de combustion. La littérature disponible sur les dépôts dans les chambres de combustion correspond principalement à des analyses ex-situ des dépôts visant à déterminer leurs compositions chimiques [1]. Ces études ex-situ ont montré que la formation des dépôts est un processus complexe. De plus, les dépôts présentent différentes caractéristiques physiques et chimiques en fonction des conditions de fonctionnement telles que le phasage injection [2]. Les dépôts obtenus sont formés par la présence des suies, du carburant liquide, ou de l'huile moteur [3, 4]. Néanmoins, les paramètres qui jouent un rôle dans les mécanismes de formation des dépôts sont encore mal compris, en particulier, la synergie qui pourrait exister entre l'injection de carburant et la formation de suies. Aussi, la formation de dépôts dans un moteur réel est un processus long. Ainsi, les caractérisations chimiques ex-situ des dépôts nécessitent une masse d'échantillon importante et donc des expériences moteur longues (~100h). Ces processus industriels de formation de dépôts dans des moteurs réels sont principalement utilisés pour évaluer les propriétés des carburants à former des dépôts mais ne sont pas utilisés pour réaliser des études fondamentales sur leurs mécanismes de formation. Il n'existe pas de méthodologie expérimentale établie pour étudier les mécanismes de formation de dépôts dans la chambre de combustion d'un moteur.

L'objectif de ce travail est de développer une telle méthodologie et de l'utiliser pour fournir une meilleure compréhension du processus de formation des dépôts. La méthodologie est basée sur des dépôts de référence contrôlés en laboratoire qui reproduisent les dépôts du moteur à partir de films liquides de carburant et de suies. L'impact de l'huile moteur dans la formation des dépôts n'est pas considéré dans ce travail. Les données issues de la caractérisation physico-chimique de ces dépôts de référence vont permettre d'identifier les paramètres moteurs favorisant la formation de dépôts moteur liés au chemin du film liquide ou au chemin de la suie. Cette méthodologie est ensuite appliquée à la compréhension des mécanismes de formation des dépôts tout au long des cycles du moteur pour le chemin de formation du film liquide et le chemin de formation de la suie. Les travaux sont réalisés sur des moteurs de recherche à allumage commandée monocylindres à injection directe avec accès optique. La caractérisation des dépôts est effectuée en utilisant des analyses ex-situ telles que la microscopie électronique et des diagnostics in-situ tels que la visualisation directe par une caméra à haute vitesse.

2. Synthèse de l’état de l’art sur les dépôts moteurs

Les dépôts moteurs peuvent se former à différents endroits dans la chambre de combustion. Ils contribuent à la dégradation de la combustion et à l'augmentation des émissions polluantes, ce qui peut entraîner une augmentation de la consommation de carburant et une réduction de la puissance du moteur. Différentes hypothèses de mécanismes de formation de dépôts ont été décrites dans la littérature, impliquant la formation d'un film liquide sur la surface et le dépôt de suies formées pendant la combustion qui se dépose sur la surface de la chambre de combustion ou sur le film de carburant liquide formé. Plusieurs facteurs ont été identifiés comme contribuant à la formation de dépôts. Tout d'abord, certaines propriétés du combustible peuvent être des facteurs prédominants, comme la présence de certains additifs ou la présence d'espèces à point d'ébullition élevé. La température de surface est également un facteur important dans la formation des dépôts. En effet, lorsque la température de la surface augmente, la formation des dépôts diminue. Les paramètres du moteur, tels que la présence d'un système de recirculation des gaz d'échappement (EGR), le type de carburant, le rapport d'équivalence carburant/air, influencent la formation des dépôts. Diverses techniques d'analyse ont été identifiées dans la revue de la littérature. L'observation microscopique a été identifiée comme une technique d'analyse non-destructive pour déterminer la morphologie des dépôts sur les moteurs. L'analyse élémentaire couplée à la microscopie électronique est intéressante pour identifier les éléments présents dans les dépôts, qui sont principalement le carbone et l'oxygène. Des techniques telles que la porosimétrie et la thermogravimétrie sont prometteuses pour caractériser les dépôts mais sont destructives.

En conclusion, plusieurs paramètres importants influencent la formation des dépôts. Il s'agit notamment des conditions de fonctionnement du moteur, de la température de la surface de la chambre de combustion et des propriétés du carburant. D'autres phénomènes physiques sont impliqués, tels que la physique du spray pendant l'injection ou l'aérodynamique à l'intérieur du cylindre. Pour mieux comprendre comment ces paramètres et phénomènes affectent la formation des dépôts, il est pertinent d'utiliser des méthodes d'analyse in situ. Par conséquent, un moteur optique semble approprié pour cette thèse. Comme un moteur optique n'utilise pas d'huile de lubrification, la formation de dépôts due au carburant et à la combustion peut être séparée des autres facteurs. Cette thèse se concentre sur le carburant essence conventionnel afin de limiter les effets des propriétés du carburant. La thèse est construite en trois sujets de recherche :

- Le premier sujet de cette thèse **(3.a.)** analyse macroscopiquement les dépôts formés à différents endroits de la chambre de combustion pour déterminer leurs similitudes ou leurs différences en fonction des paramètres de fonctionnement du moteur. Une méthodologie d'identification des origines des dépôts est présentée afin de déterminer si le film liquide ou le chemin de la suie est dominant. Deux dispositifs seront utilisés pour former des dépôts de référence à partir de ces deux voies et les dépôts de référence seront comparés aux dépôts obtenus dans la chambre de combustion du moteur. L'objectif est d'évaluer l'applicabilité des dépôts de référence comme modèle pour les dépôts du moteur.
- Le deuxième sujet de la thèse **(3.b.)** décrit l'étude des mécanismes de formation des dépôts. Cette étude est motivée par l'absence d'une méthode expérimentale en temps réel dans la recherche pour étudier les mécanismes de formation des dépôts. Cette étude est donc basée sur l'utilisation de l'analyse in situ par visualisation directe, l'analyse de la distribution des particules avec un analyseur de particules, et l'utilisation de la méthode précédente pour distinguer les voies de dépôt et quantifier leur contribution.

- Le troisième et dernier thème de cette thèse **(3.c.)** est consacré à l'étude des variations paramétriques sur la formation des dépôts. L'effet de la température de surface sera étudié par visualisation di-rect. L'effet de la rugosité sur la formation des dépôts sera également évalué. Et pour documenter et aider à la mise en place de diagnostics optiques pour mesurer les propriétés des dépôts, l'effet des matériaux transparents sur la formation des dépôts sera étudié.

3. Résultats

a. Etablissement de la méthode d'étude des dépôts dans les moteurs

L'objectif de cette partie est de définir et d'évaluer une méthode permettant de distinguer et de quantifier les différentes voies de formation des dépôts dans les moteurs, à savoir le chemin de formation du film liquide et le chemin de formation des suies. Cette méthode est basée sur l'analyse ex-situ de dépôts de référence et de dépôts moteur à injection commandée. Tout d'abord, les dépôts de référence sont analysés pour déterminer leurs propriétés physiques et chimiques, avec un intérêt particulier pour les analyses macroscopiques et microscopiques. Les caractéristiques des dépôts de référence ont été déterminées macroscopiquement et microscopiquement. Le dépôt de référence correspondant au chemin de formation du film liquide a une couleur transparente et un aspect brillant avec une morphologie de surface lisse. Le dépôt correspondant au chemin de formation des suies a une couleur noire et un aspect mat avec une morphologie de particules. Ensuite, les dépôts provenant de différentes expériences sur les moteurs sont analysés macroscopiquement et microscopiquement. L'objectif est de déterminer l'effet de différents paramètres du moteur sur les propriétés des dépôts. Le premier paramètre étudié est l'effet de l'emplacement dans la chambre de combustion sur les propriétés des dépôts. L'objectif est d'identifier la partie de la chambre de combustion la plus pertinente pour une étude plus approfondie. Les résultats ont montré que l'emplacement dans la chambre de combustion n'a pas d'impact significatif sur l'aspect et la morphologie des dépôts. Le dépôt sur le piston présente une configuration particulière attribuée à l'impact du spray sur la surface. Cette zone de la chambre de combustion est retenue dans la suite de l'étude. Le deuxième paramètre étudié est l'impact de la géométrie de deux moteurs sur les propriétés des dépôts afin de déterminer la possibilité d'étudier les dépôts indépendamment de la géométrie du moteur. Cette étude a montré que les dépôts peuvent être étudiés indépendamment des deux moteurs utilisés dans l'étude. Le troisième et dernier paramètre est la détermination de l'effet du phasage injection sur les propriétés des dépôts. Les propriétés de ces dépôts formés à partir de différents phasages injection sont comparées à des dépôts de référence. Deux temps d'injection ont été choisis : le premier est l'injection précoce à 360 CAD BTDC qui forme des dépôts avec une morphologie correspondant essentiellement au trajet du film liquide ; le second est l'injection tardive à 60 CAD BTDC qui contribue largement à la formation de dépôts avec une morphologie correspondant au trajet de la suie. Ces deux temps d'injection permettront d'étudier les mécanismes des deux voies de formation des dépôts.

En plus des analyses macroscopiques et microscopiques, des analyses spectroscopiques FTIR-ATR et Raman ont été évaluées. L'objectif était de déterminer la capacité de ces techniques à identifier les signatures chimiques correspondant aux dépôts des moteurs de référence. La spectroscopie FTIR-ATR a permis d'identifier la présence d'un dépôt formé à partir du chemin du film liquide pour les cas d'injection précoce et tardive, mais pas pour le chemin de la suie. La technique ne fournit pas d'information sur la proportion de dépôt pour chaque voie. L'utilisation de la spectroscopie FTIR-ATR est donc exclue pour les travaux suivants réalisés au cours de cette thèse. Pour l'analyse Raman, aucune information n'a pu être extraite pour le dépôt de référence pour la voie du film liquide et aucune corrélation n'a

été trouvée entre la morphologie et les informations dérivées de l'analyse des pics. Par conséquent, cette technique ne permet pas d'établir une corrélation entre la structure du carbone et la morphologie. L'utilisation de la spectroscopie Raman est donc également exclue ci-après. La méthode utilisée pour déterminer l'origine des dépôts sur les moteurs ne fournit que des informations qualitatives.

b. Mécanismes de formation des dépôts dans les moteurs

La stratégie a consisté à isoler les deux chemins de formation des dépôts pour étudier leurs mécanismes séparément. L'injection tôt a été utilisée pour étudier les mécanismes de formation du film liquide et l'injection tardive pour étudier les mécanismes de formation de la suie. Les mécanismes identifiés pour chacune des voies de formation ont ensuite été comparés pour chacune des stratégies d'injection.

Chemin de formation par le film liquide

Pour le chemin de formation du film liquide, deux dépôts ont été formés lors de deux expériences moteurs différentes pour des températures initiales de surface à 20°C et 133°C, correspondant respectivement à un démarrage à froid et à un démarrage à chaud. Les analyses ex-situ et in-situ des dépôts obtenus, comparées aux données de la littérature, ont mis en évidence des mécanismes expliquant la formation des dépôts. Lors de l'injection, l'impact du spray sur la surface du piston conduit à la formation d'un film liquide. De ce film liquide, on distingue deux zones : La zone d'étalement et la zone d'impact du spray. La première zone correspond à l'étalement du film liquide qui se forme dans la zone extérieure de la surface du piston. La zone extérieure dépend de la température de la surface. A haute température, le film liquide s'évapore rapidement, et la formation de dépôts est limitée. Pour le cas du démarrage à chaud, aucun étalement n'est observé avec la caméra haute vitesse. Cependant, l'analyse microscopique de la zone extérieure a montré la présence d'un dépôt par rapport au trajet du film liquide. Il est probable que le liquide se soit étalé puis se soit évaporé immédiatement, ne permettant pas la formation d'une couche épaisse de dépôt par rapport à la zone noire observée pour le cas du démarrage à froid. Pour le cas du démarrage à froid, un étalement est clairement observé. Sa trajectoire diminue à mesure que la température de surface du piston augmente, et le dépôt de la zone noire se forme à la périphérie du film liquide, qui se déplace vers le centre du piston. La visualisation in-situ a montré que le dépôt noir de la zone extérieure se forme à partir du bord du piston et progresse vers le centre sur plusieurs cycles. Les zones brunes observées sur les zones externes de la surface des pistons pour les deux conditions de fonctionnement correspondent aux zones où le carburant s'évapore rapidement ce qui explique la présence d'une couche de dépôt plus fine que pour la zone noire observée pour le cas du démarrage à froid. De plus, des marques brunes ont été identifiées sur la zone extérieure pour le cas du démarrage à chaud, plus précisément à la périphérie du piston. Ces marques sont plus foncées que le reste de la zone brune et indiquent une plus grande épaisseur de dépôt. Leur morphologie indique l'implication d'un mécanisme lié au film liquide mais les résultats présentés dans ce chapitre ne permettent pas d'expliquer leur présence.

La deuxième zone correspond au film liquide formé dans la zone interne du piston. Deux zones distinctes de film liquide sont identifiées ici : La zone centrale d'impact du spray et la zone périphérique du piston d'impact du spray. La littérature a montré que le film liquide a une épaisseur minimale dans la zone centrale de pulvérisation et présente une accumulation de combustible liquide à la périphérie de l'impact de pulvérisation. En outre, l'analyse SEM-EDS a montré une densité de dépôt plus faible dans la zone du cœur du jet que dans la périphérie de l'impact du jet. Ceci est attribué à une évaporation rapide

à partir de la zone centrale de la pulvérisation conduisant à une formation limitée de dépôts et à une évaporation plus lente à la périphérie de l'impact de la pulvérisation conduisant à une formation de dépôts.

Chemin de formation par les suies

Différents mécanismes de transport des suies peuvent se produire dans la chambre de combustion. Une fois formée, les suies sont transportées par l'écoulement. En fonction du nombre de Reynolds de l'écoulement, c'est-à-dire de l'intensité de la turbulence, différents mécanismes vont entraîner le transport des particules de suie. Si la turbulence est faible et que la suie est proche de la paroi où il y a un gradient de température, la thermophorèse est très probable pour transporter la suie vers la paroi. Si la turbulence est forte, comme dans le cas de la course d'expansion, plusieurs possibilités sont envisagées. Si la suie a un faible rapport masse aérodynamique/traînée par rapport à l'intensité de la turbulence, elle continuera probablement à suivre le flux vers l'échappement. Si la suie a un rapport masse aérodynamique/traînée élevé, elle peut être éjectée d'un tourbillon en raison de son inertie. Dans ce cas, si la suie heurte une paroi de la chambre de combustion, elle a de fortes chances de s'y déposer ; c'est le mécanisme de dépôt inertiel.

Synthèse sur les mécanismes de formation des dépôts

L'objectif de cette section est de proposer un mécanisme global de formation des dépôts impliquant les mécanismes du chemin du film liquide et du chemin de la suie.

La figure 1 montre la contribution du film liquide à la formation du dépôt. Au moment de l'injection, une faible distance entre le piston et la buse de l'injecteur peut conduire à l'impact du spray (1). Cet impact conduit à la formation d'un film liquide, qui peut s'étendre sur la surface du piston et qui peut conduire à la formation de zones d'accumulation (2). De ce film liquide, on peut distinguer deux zones, la zone d'impact du spray et la zone d'étalement. Dans ces zones, le carburant s'évapore à des vitesses différentes selon l'épaisseur du film et la température de la surface.

A haute température, l'étalement s'évapore très rapidement, ce qui limite la formation de dépôts (3). Le carburant dans la zone d'impact du spray s'évapore plus lentement que dans la zone d'étalement car l'impact du spray provoque un refroidissement local (4). Dans la zone d'impact du spray, on distingue deux autres zones, la périphérie de l'impact du spray et le cœur de l'impact du spray. Le carburant dans la périphérie de l'impact de pulvérisation, qui est une zone d'accumulation, s'évapore lentement et entraîne la formation de dépôts. Le carburant dans le cœur de l'impact de pulvérisation, qui est la zone d'épaisseur minimale du film liquide, s'évapore rapidement, ce qui limite la formation de dépôts. À basse température de surface, l'étalement et la zone d'impact du spray sont des zones d'évaporation lente. Au sein du film liquide, les durées d'évaporation sont différentes. Tout d'abord, les zones d'accumulation à la périphérie de l'étalement et à la périphérie des zones d'impact du spray correspondent à des zones d'évaporation lente favorisant la formation de dépôts (5). Le reste du film liquide est plus fin et s'évapore plus rapidement limitant le risque de formation de dépôts (6).

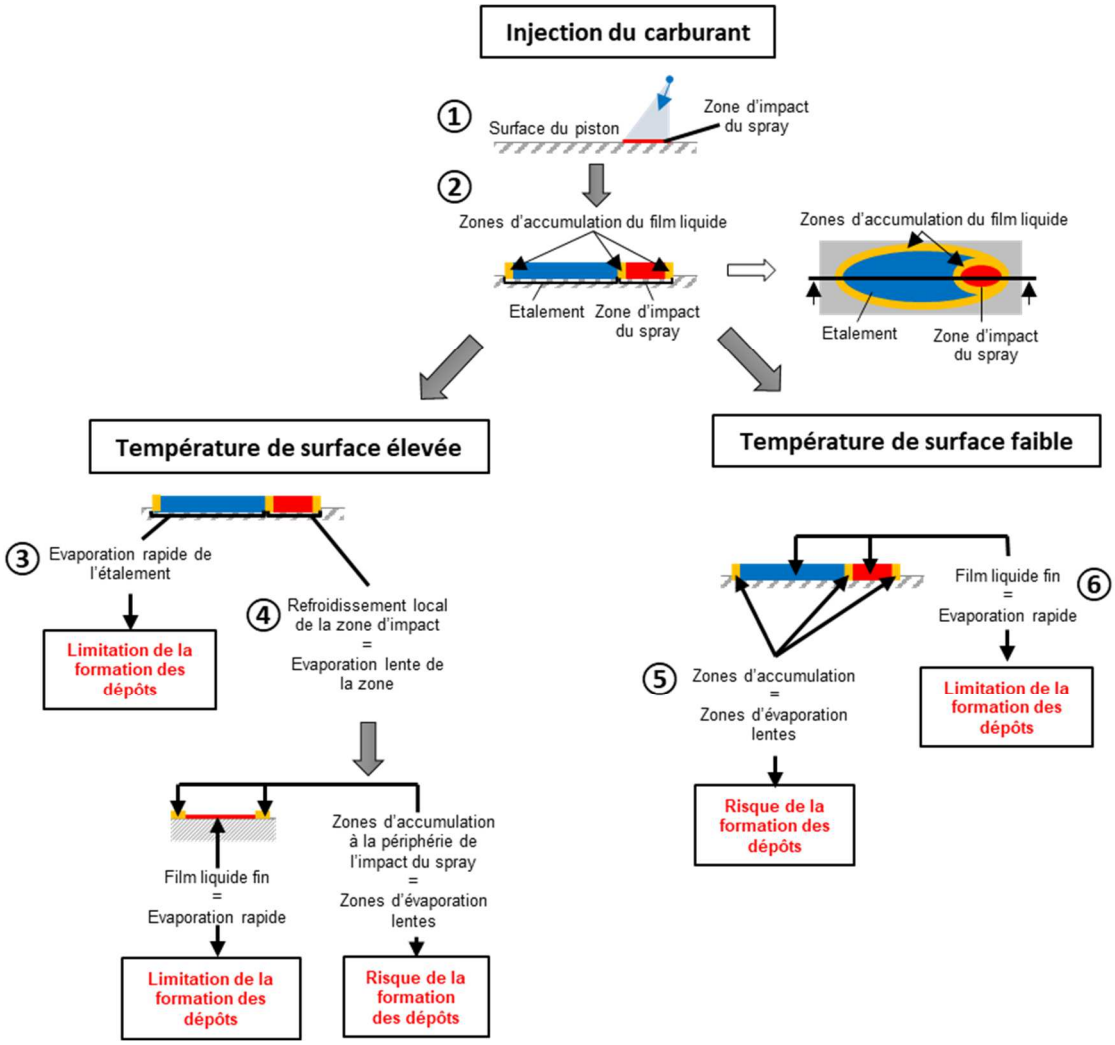

Figure 1: Schéma de la contribution du chemin de formation du dépôt par un film liquide dans la formation des dépôts.

Après avoir analysé les zones de film liquide et les paramètres conduisant à la formation des dépôts par le chemin du film liquide, on ajoute la contribution du chemin des suies. Dans la suite, on suppose qu'un film liquide s'est formé suite à l'impact du spray sur la surface du piston. La figure 2 montre la contribution du chemin de formation des dépôts par les suies. Les suies formées lors de la combustion se déposent sur la surface du piston. En fonction de la richesse du mélange, la concentration en suies, et donc leur contribution au dépôt, est déterminée.

Deux cas de combustion riche ont été identifiés. Le premier cas correspond à la formation d'un film liquide sur la surface du piston (1). Comme vu précédemment, en fonction de la température de surface, ce film liquide s'évapore plus ou moins rapidement. Si l'évaporation du film liquide est lente, cela peut conduire à des zones de combustion plus riches près de la paroi (2). Ces combustions riches forment beaucoup de suies en mode accumulation qui se déposent sur la paroi par thermophorèse ou déposition inertielle (3). A l'injection suivante, un nouveau cycle commence, et les suies déposées sont emportée à la périphérie du film liquide (4).

Le deuxième cas de combustion riche est la conséquence d'une stratégie d'injection tardive. L'injection tardive ne laisse pas suffisamment de temps au carburant et à l'air pour se mélanger (5). Cela crée des

zones riches dans la phase gazeuse qui vont former beaucoup de suie en mode agglomération. Cette suie va ensuite se déposer sur la surface du piston par thermophorèse ou par dépôt inertiel (6).

Dans le cas d'un mélange carburant/air pauvre, la formation de gros agglomérats de suie est limitée (7). La contribution des mécanismes de cheminement des suies est donc également limitée.

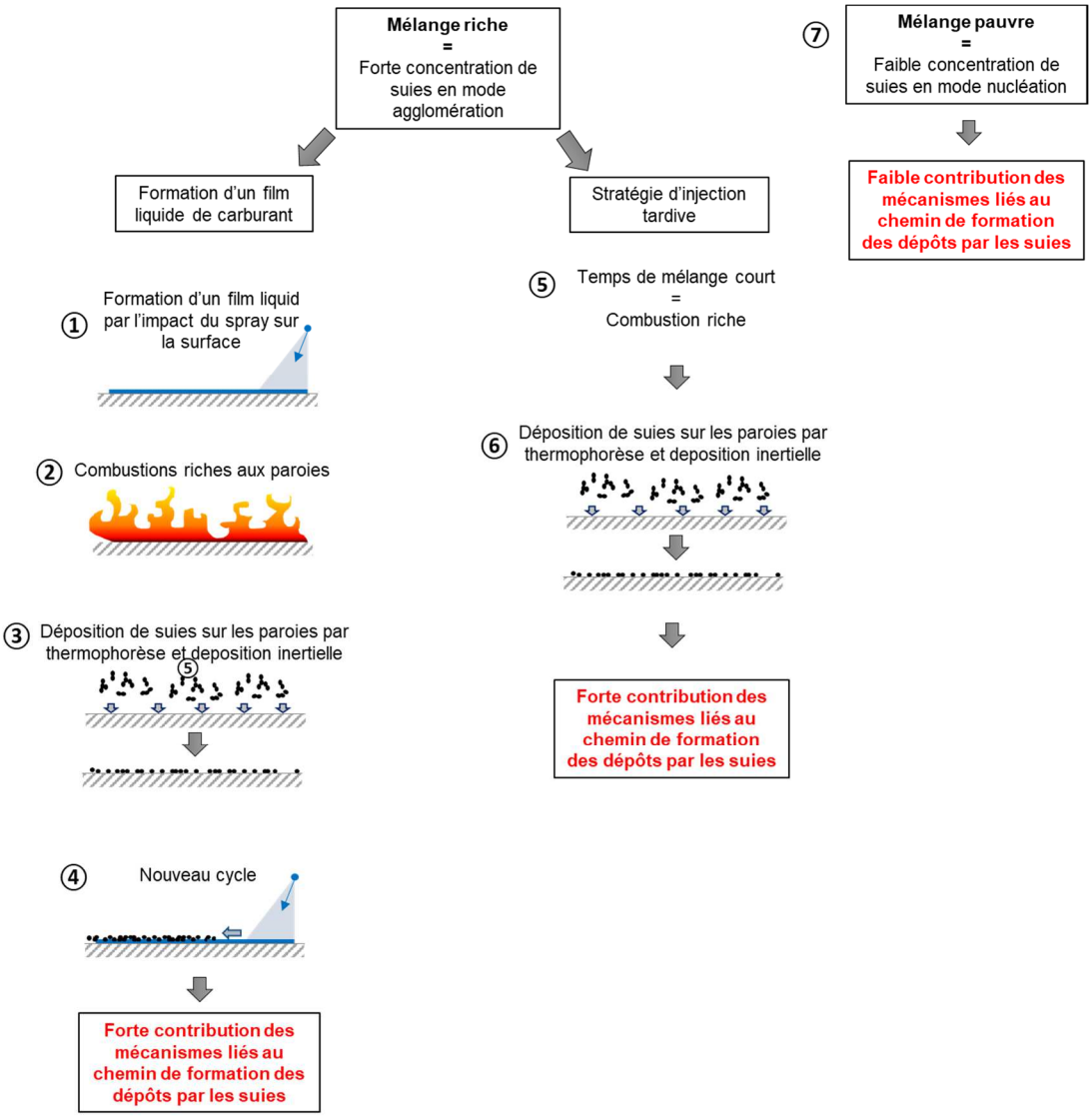

Figure 2 : Schéma de la contribution du chemin de la suie dans la formation du dépôt.

c. Influence des propriétés de la surface sur la formation des dépôts

L'objectif de cette partie est d'étudier l'effet des propriétés de la surface du piston sur la formation de dépôts dans le cylindre. L'accent est mis sur l'influence de la température de surface, de la rugosité de surface du piston et de matériaux transparents sur le mécanisme de formation des dépôts. L'objectif est d'une part d'identifier des leviers pour limiter ou empêcher la formation de dépôts, et d'autre part d'évaluer la représentativité des matériaux transparents pour l'étude de la formation de dépôts à l'aide de diagnostics optiques. La méthodologie pour évaluer l'influence des propriétés de la surface du piston sur la formation des dépôts est basée sur les outils d'analyse ex situ et in situ présentés dans les

parties 3.b et 3.c respectivement. L'analyse ex situ correspond à l'analyse macroscopique et microscopique de la surface du piston après chaque expérience. Pour l'analyse macroscopique, la couleur, la texture et les motifs des dépôts sont identifiés. Pour l'analyse microscopique, les morphologies à différentes échelles sont caractérisées. L'analyse in situ est basée sur la distribution de la taille des particules et sur la visualisation à grande vitesse des processus dans le cylindre. La distribution granulométrique est mesurée par SMPS dans l'échappement du moteur afin de déterminer l'impact des variations paramétriques sur la formation des dépôts via le chemin de la suie. La visualisation directe est utilisée pour observer la présence de films liquides et ainsi déterminer l'impact des propriétés de surface sur la formation de dépôts via le chemin des films liquides. Cette dernière technique nous permet également de caractériser la cinétique de formation des dépôts et de combustion, c'est-à-dire d'identifier les zones de mélange riches pouvant favoriser le chemin de la suie.

Dans un premier temps, l'effet de la température de surface sur les mécanismes de formation des dépôts par la voie du film liquide et par la voie de la suie a été étudié. L'augmentation de la température initiale du piston de 20 à 190 °C augmente la vitesse d'évaporation du film liquide, ce qui entraîne une réduction d'environ 10 % du dépôt dans la zone intérieure et d'environ 100 % dans la zone extérieure. Pour le dépôt par chemin de suie, l'augmentation de la température de surface de 159 à 215 °C réduit le gradient de température et donc l'effet de thermophorèse sur le mécanisme de dépôt de la suie. Cela réduit la formation de dépôts d'environ 60 %. En conclusion, une augmentation significative de la température de surface réduit la formation de dépôts par le chemin du film liquide et le chemin de la suie en réduisant la durée de vie du film liquide et le gradient de température près de la paroi, respectivement.

Ensuite, l'impact de la rugosité sur la formation du dépôt par le chemin du film liquide a été étudié. Il a été observé que la rugosité n'a pas d'impact significatif sur le mécanisme de formation du dépôt par le chemin liquide-film. Le seul effet observé concerne l'étalement du film liquide lorsque la rugosité est réduite jusqu'à Ra = 0.1 nm avec l'observation de limites plus nettes des différentes zones de dépôt. Par conséquent, la variation de la rugosité n'est pas identifiée comme un levier intéressant pour réduire la formation de dépôts par le trajet liquide-film dans un moteur.

Enfin, l'impact des matériaux transparents sur la formation du dépôt par le chemin du film liquide a été étudié. Deux études ont été réalisées : La première avec deux pistons en aluminium avec un revêtement en quartz et un revêtement en saphir pour éviter les changements des propriétés thermiques de ces matériaux, la seconde avec un piston complètement transparent en saphir. L'étude avec les revêtements a montré que ces matériaux n'avaient pas d'impact significatif sur la formation de dépôts par la voie du film liquide tant qu'ils ont la même température que le cas de référence. L'étude avec le piston en saphir totalement transparent montre que le mécanisme du trajet du film liquide peut être reproduit avec quelques différences morphologiques sur les dépôts formés. Comme le cas étudié limite la formation du film liquide en raison d'une montée en température plus rapide, des expériences supplémentaires sont nécessaires pour étudier l'impact de la température de la surface du piston en saphir complet sur l'étalement du film liquide.

4. Conclusions et Perspectives

a. Conclusions

Dans cette thèse, une nouvelle méthodologie pour déterminer l'origine des dépôts entre les mécanismes du film liquide et du chemin de la suie a été présentée. Des expériences préliminaires ont été

menées pour déterminer l'impact de l'emplacement dans la chambre de combustion sur la formation des dépôts, l'effet de la géométrie du moteur et les paramètres d'intérêt pour l'étude des mécanismes de formation des dépôts. Ces résultats ont montré que l'emplacement dans la chambre et la géométrie du moteur n'ont pas un grand impact sur la formation des dépôts, c'est-à-dire que la morphologie et la composition chimique du dépôt au niveau des parois de la chambre de combustion, du piston et de la buse de l'injecteur étaient très similaires. Sur la base de ces résultats, la thèse s'est concentrée sur les dépôts formés sur le piston et a utilisé deux moteurs à injection directe et à allumage commandé pour les expériences. Ces études préliminaires ont également mis en évidence la température de l'eau de refroidissement et le timing d'injection comme deux paramètres pouvant influencer l'aspect macroscopique et microscopique des dépôts et donc les mécanismes de formation des dépôts.

Pour évaluer plus précisément les dépôts formés dans le moteur, des dépôts de référence ont été générés dans des conditions bien contrôlées en laboratoire. L'objectif était d'abord de déterminer si ces dépôts de référence peuvent reproduire les dépôts du moteur. Le deuxième objectif était d'évaluer si les dépôts de référence peuvent calibrer les techniques de mesure identifiées dans la littérature et peuvent ensuite être utilisés pour déterminer l'origine des dépôts du moteur. Dans un premier temps, des dépôts de référence ont été formés en utilisant un dispositif de microcokéfaction pour former un dépôt à partir du chemin du film liquide, et en utilisant un générateur de suie et un moteur à allumage par étincelle à injection directe pour former un dépôt à partir du chemin de la suie. Dans un deuxième temps, deux temps d'injection ont été identifiés pour favoriser la formation de dépôts correspondant aux deux voies de formation de dépôts identifiées : un temps d'injection précoce favorisant la voie du film liquide, et un temps d'injection tardif favorisant la voie de la suie. Les dépôts de référence et du moteur ont été analysés par microscopie électronique et par spectroscopie Raman et infrarouge. L'analyse macroscopique a révélé un dépôt noir et mat correspondant au dépôt de référence du trajet de la suie et un dépôt clair et brillant pour le dépôt de référence du trajet du film liquide. L'analyse microscopique a montré une morphologie de surface lisse pour le dépôt de référence du trajet du film liquide et des particules pour le dépôt de référence du trajet de la suie. Les analyses spectroscopiques n'ont pas été considérées comme pertinentes pour l'analyse des dépôts du moteur car elles ne fournissent pas d'informations sur la proportion de dépôt pour chaque voie. Les propriétés du dépôt de la trajectoire du film liquide ont été identifiées dans le dépôt du moteur de la stratégie d'injection précoce. Et les propriétés du dépôt de référence du chemin de la suie ont été identifiées dans le dépôt du moteur de la stratégie d'injection tardive. Cette méthodologie a permis d'étudier les deux voies de formation des dépôts dans le moteur.

Les différents mécanismes de formation des dépôts ont été évalués en utilisant deux phases d'injection typiques, à savoir l'injection précoce et l'injection tardive, en combinant l'analyse ex situ des matériaux et l'analyse in situ de la formation des dépôts. L'analyse in situ était basée sur des observations effectuées à l'aide d'une caméra à grande vitesse sur un moteur à injection directe et à allumage par étincelle, avec un accès optique permettant de visualiser la formation de dépôts sur le piston. Pour étudier les mécanismes liés au parcours de la suie, la distribution granulométrique de la suie a été analysée dans l'échappement. Pour le trajet du film liquide utilisant la stratégie d'injection précoce, l'étude a mis en évidence l'importance de la température de surface du piston sur la durée de vie du film liquide et la formation de dépôts. Dans des conditions de démarrage à froid, la température de surface est d'environ 20 °C, le temps d'évaporation est long et favorise la formation du dépôt. En revanche, lorsque la température de surface au démarrage est d'environ 133 °C, le temps d'évaporation est court et la formation du dépôt est limitée. Il a été constaté que deux autres facteurs influencent la durée de vie du film liquide. Le premier est la présence de zones d'accumulation à la périphérie du film liquide et à la périphérie de l'impact du spray, qui vont ralentir l'évaporation du film liquide et favoriser la formation du dépôt par le

trajet liquide-film. Le second est le refroidissement local de la surface du piston, qui peut créer des zones plus froides sur le piston et ralentir l'évaporation. Pour le chemin de la suie, plusieurs mécanismes peuvent expliquer le dépôt de la suie sur la surface du piston en fonction de l'écoulement à l'intérieur de la chambre de combustion. Lorsque l'écoulement est laminaire, la suie se dépose par thermophorèse lorsqu'elle est suffisamment proche de la paroi où se trouve un fort gradient de température. Dans les écoulements turbulents, les particules de suie vont soit suivre l'écoulement jusqu'à l'échappement, soit se déposer par inertie. Le dépôt par film liquide a été observé dans le cas d'une injection tardive et le dépôt par chemin de suie dans le cas d'une injection précoce. L'étude a montré que ces mécanismes peuvent interagir.

L'impact des propriétés de la surface du piston sur les mécanismes de formation des dépôts a également été étudié. Tout d'abord, l'effet de la température de surface sur les mécanismes de formation de dépôts par le biais du film liquide et du chemin de la suie a été étudié. L'augmentation de la température initiale de la surface du piston de 20 à 190 °C augmente le taux d'évaporation du film liquide, ce qui entraîne une réduction d'environ 10 % de la formation de dépôts dans la région intérieure et de presque 100 % dans la région extérieure. Pour le dépôt par chemin de suie, l'augmentation de la température de surface de 159 à 215 °C réduit le gradient de température et donc l'effet de thermophorèse sur le mécanisme de dépôt de la suie. Ainsi, une augmentation significative de la température de surface réduit la formation de dépôts via le chemin du film liquide et le chemin de la suie en réduisant la durée de vie du film liquide et le gradient de température près de la paroi, respectivement. Il a été démontré que la rugosité de la surface n'a pas d'influence significative sur la formation de dépôts par le chemin du film liquide. Enfin, l'impact des matériaux transparents sur la formation de dépôts via le trajet du film liquide a été étudié. Afin de séparer les effets thermiques et les effets des matériaux, des pistons en aluminium recouverts de fines couches de silice ou d'alumine ont été testés pour maintenir les mêmes températures de surface que pour les pistons métalliques. Ensuite, un piston en saphir complètement transparent a été utilisé pour lequel la température de surface devrait varier en raison des différentes propriétés de conduction thermique. L'étude avec les revêtements a montré que ces matériaux n'avaient pas d'impact significatif sur la formation de dépôts par la voie du film liquide. L'étude avec le piston en saphir entièrement transparent a montré que les mécanismes de formation de dépôts par la voie du film liquide peuvent être reproduits avec quelques différences morphologiques dans les dépôts formés, ce qui offre une option pour de futures expériences de détection optique de la formation de dépôts à travers des sections transparentes de la paroi de la chambre de combustion. Comme le cas étudié limite la formation du film liquide, des expériences supplémentaires sont nécessaires pour étudier l'impact de la température de surface du piston en saphir solide sur l'étalement du film liquide.

En conclusion, une méthodologie a été développée dans cette thèse qui permet d'étudier et de comprendre les mécanismes de formation de dépôts dans la chambre de combustion d'un moteur. Cette méthodologie a ensuite été appliquée pour évaluer l'impact des propriétés de surface sur les mécanismes de formation identifiés. Les deux voies de formation identifiées dans la littérature ont été étudiées séparément. Pour la voie liquide-film, les travaux ont montré que la formation du dépôt par le film liquide était conditionnée par le taux d'évaporation du film liquide. Le taux d'évaporation dépend de la température de la surface du piston et de la quantité de carburant liquide à évaporer. Dans cette étude, la rugosité de la surface, l'utilisation d'un matériau de surface en silice ou en alumine n'a pas d'impact significatif sur la formation du dépôt via le chemin du film liquide. Pour le chemin de la suie, deux mécanismes ont été identifiés dans le dépôt de la suie sur la surface. Il s'agit de la thermophorèse et du dépôt inertiel. Selon l'intensité de la turbulence dans le cylindre et le gradient de température dans la

paroi proche, l'un des deux mécanismes domine. Les résultats montrent qu'une augmentation de la température de surface réduit le dépôt de suie.

b. Perspectives

Une des questions soulevées par la thèse est le processus chimique de formation du dépôt par le mécanisme du chemin liquide-film. Pour le trajet liquide-film, la relation entre le temps d'évaporation et la formation du dépôt a été démontrée. Cependant, ce travail n'a pas encore établi le processus de transformation chimique entre les phases liquide et solide. Des mesures en temps réel de ce processus permettraient de voir l'évolution chimique du combustible liquide vers un dépôt. De telles mesures pourraient être réalisées en laboratoire avec le dispositif de microcokéfaction pour caractériser chimiquement la formation du dépôt de référence par la voie liquide-film. Sur la base du constat qu'un piston tout saphir est représentatif d'un piston en aluminium en termes de formation de dépôt par le chemin du film liquide, il serait intéressant d'utiliser des diagnostics optiques et des pistons transparents dans des conditions réelles de moteur dans des travaux futurs pour analyser in situ la formation de dépôt. Une perspective importante ouverte par cette thèse est de tester le diagnostic optique par fluorescence induite par laser pour mesurer en temps réel l'évolution de la formation de dépôts sur les parois de la chambre de combustion. Les carburants à essence sont constitués de centaines de composants, dont certains sont fluorescents lorsqu'ils sont éclairés dans l'ultraviolet, mais en ce qui concerne les dépôts formés par le chemin du film liquide, il n'existe aucune étude connue sur leurs propriétés de fluorescence. Pour valider la mise en œuvre de cette technique, une étude préliminaire de la fluorescence des dépôts sera nécessaire. Une évolution décroissante de la mesure de l'intensité de fluorescence depuis la formation d'un film de carburant liquide jusqu'à la formation d'un dépôt solide au cours d'un cycle moteur donnerait des informations intéressantes sur la vitesse d'évaporation du film liquide. Inversement, une évolution croissante de la mesure de l'intensité de fluorescence donnerait des informations quantitatives sur la quantité de dépôt formé sur les parois.

5. Références

[1] Shu, G., Dong, L., and Liang, X., “A review of experimental studies on deposits in the combustion chambers of internal combustion engines,” International Journal of Engine Research 13(4):357–369, 2012.

[2] Cheng, S.-w.S., “The Impacts of Engine Operating Conditions and Fuel Compositions on the Formation of Combustion Chamber Deposits,” SAE Technical Paper 2000-01-2025, 2000.

[3] Lepperhoff, G. and Houben, M., “Mechanisms of Deposit Formation in Internal Combustion Engines and Heat Exchangers,” SAE Technical Paper 931032, 1993.

[4] Diaby, M., Sablier, M., Le Negrate, A., El Fassi, M. et al., “Understanding carbonaceous deposit formation resulting from engine oil degradation,” Carbon 47(2):355–366, 2009.